

IRE Transactions on ANTENNAS and PROPAGATION



Volume AP-7

JANUARY, 1959

Number 1

Published Quarterly

TABLE OF CONTENTS

CONTRIBUTIONS

Propagation of a Ground Wave Pulse Around a Finitely Conducting Spherical Earth from a Damped Sinusoidal Source Current,	<i>J. R. Johler and L. C. Walters</i>	1
On the Measurement of Virtual Height,	<i>I. Kay</i>	11
Back-Scattering Measurements with a Space-Separation Method,	<i>H. J. Schmitt</i>	15
Scattering of a Surface Wave by a Discontinuity in Reactance,	<i>Alan F. Kay</i>	22
Spherically Symmetric Lenses,	<i>Alan F. Kay</i>	32
On the Design of Some Rhombic Antenna Arrays,	<i>A. A. de Carvalho Fernandes</i>	39
Radiation Field of an Elliptical Helical Antenna,	<i>J. Y. Wong and S. C. Loh</i>	46
The Rectangular Loop Antenna as a Dipole,	<i>Ronald King</i>	53
Properties of Slotted Dielectric Interfaces,	<i>R. E. Collin</i>	62
Traveling-Wave Cylindrical Antenna Design—A Graphical Synthesis Method,	<i>Peter Foldes</i>	74
Theoretical Research on Tropospheric Scatter Propagation in the United States, 1954–1957,	<i>Harold Staras and Albert D. Wheelon</i>	80
URSI Report on Antennas and Waveguides, and Annotated Bibliography,	<i>H. V. Cottony, R. S. Elliott, E. C. Jordan, V. H. Rumsey, K. M. Siegel, J. R. Wait, and O. C. Woodyard</i>	87

COMMUNICATIONS

Preliminary Results of Measurements on Doppler Shift of Satellite Emissions,	<i>P. R. Arendt</i>	99
Suppressed Sidelobe Antenna of 32 Elements,	<i>G. Reber</i>	101
Measuring the Capacitance Per Unit Length of Two Infinite Cones of Arbitrary Cross Section,	<i>J. D. Dyson</i>	102
The Exact Solution of the Field Intensities from a Linear Radiating Source,	<i>Sheldon S. Sandler</i>	104
Correction to "Determination of a Current Distribution over a Cone Surface Which Will Produce a Prescribed Radiation Pattern",	<i>H. Unz</i>	104
Fall Meeting of International Scientific Radio Union October 20–22, 1958, Pennsylvania State University,		105
Abstracts of Papers from the Region Three Technical Meeting,		113
Contributors,		115

PUBLISHED BY THE

Professional Group on Antennas and Propagation

Administrative Committee

R. L. Mattingly, *Chairman*

Arthur Dorne, *Vice-Chairman*

S. Bowhill

J. W. Findlay

F. T. Haddock, Jr.

J. W. Herbstreit

E. C. Jordan

S. M. King

R. K. Moore

K. S. Kelleher, *Secretary*

W. H. Radford

K. M. Siegel

O. G. Villard, Jr.

Ex-Officio Members

J. I. Bohnert

D. C. Ports

H. G. Booker

Honorary Member

L. C. Van Atta

IRE TRANSACTIONS® PGAP IS A PUBLICATION DEVOTED TO
EXPERIMENTAL AND THEORETICAL PAPERS ON RADIO ANTENNAS,
ON GUIDED OR UNGUIDED PROPAGATION OF RADIO WAVES, AND
ON ALLIED FIELDS OF RADIO PHYSICS SUCH AS RADIO ASTRONOMY

MANUSCRIPTS should be submitted to John B. Smyth, Editor, Smyth Research Associates, 3555 Aero Court, San Diego 11, Calif. Manuscripts should be original typewritten copy, double spaced, plus one carbon copy. References should appear as footnotes and include author's name, title, journal, volume, initial and final page numbers, and date. Each paper must have a summary of not more than 200 words. News items concerning PGAP members and group activities should be sent to the News Editor, Mr. Arthur Dorne, Dorne and Margolin, Inc., 30 Sylvester Street, Westbury, L.I., N.Y.

ILLUSTRATIONS should be submitted as follows: All line drawings (graphs, charts, block diagrams, cutaways, etc.) should be inked uniformly and ready for reproduction. If commercially printed grids are used in graph drawings, author should be sure printer's ink is of a color that will reproduce. All half-tone illustrations (photographs, wash, airbrush, or pencil renderings, etc.) should be clean and ready to reproduce. Photographs should be glossy prints. Call-outs or labels should be marked on a registered tissue overlay, not on the illustration itself. No illustration should be larger than 8 x 10 inches.

Copies can be purchased from
THE INSTITUTE OF RADIO ENGINEERS
1 East 79 St., New York 21, N.Y.

PRICE PER COPY: members of the Professional Group on Antennas and Propagation, \$2.50; members of the IRE, \$3.75; nonmembers, \$7.50.

ANNUAL SUBSCRIPTION PRICE: PGAP members, included in PGAP fee of \$4.00; IRE members, \$8.50; Colleges and public libraries, \$10.00; non-members, \$17.00.

IRE TRANSACTIONS ON ANTENNAS AND PROPAGATION
Copyright © 1959, by The Institute of Radio Engineers, Inc.

Printed in U.S.A.

Entered as second-class matter, at the post office at Menasha, Wisconsin, under the act of August 24, 1912. Acceptance for mailing at a special rate of postage is provided for in the act of February 28, 1925, embodied in Paragraph 4, Section 412, P. L. & R., authorized October 26, 1927.

669423

5856-30
TK7800
I-2
V.APM

contributions

Propagation of a Ground Wave Pulse Around a Finitely Conducting Spherical Earth from a Damped Sinusoidal Source Current*

J. R. JOHLER† AND L. C. WALTERS†

Summary—The form of the transient electromagnetic ground wave which has been propagated over a finitely conducting spherical earth from a source current dipole can be calculated by a direct quadrature evaluation of the Fourier integral. The method is illustrated in this paper by a calculation of the transient field radiated by the particular case of the damped sinusoidal source current dipole. At short distances from the source, the earth was assumed to be a plane and the displacement currents in the earth were neglected. The pulse was then calculated by a direct evaluation of the Fourier integral and the integration was verified by special operational methods (inverse Laplace transformation). The form of this pulse was then predicted at great distance from the source by a direct evaluation of the Fourier integral in which the displacement currents in the earth and the earth's curvature were introduced into the Fourier transform. The form of the transient signal was found to be dispersed by the propagation medium. The most noteworthy attribute of this dispersion is a stretching of the period of the wave so that the form of the source is somewhat obscured by the filtering action of the medium.

INTRODUCTION

IN RECENT YEARS, the interest in the change with distance in the form or shape of various propagated radio-frequency transients, especially at low frequencies, can be attributed to the use of pulse tech-

* Manuscript received by the PGAP, April 21, 1958; revised manuscript received, October 23, 1958. The basic theoretical study in this paper was in large measure completed in 1953 by NBS Radio Navigation Project 1404-30-6815 sponsored by Rome Air Development Center, Rome, N. Y. The theory was further enhanced and reduced to computational form in 1957 and 1958 on NBS Project 8830-11-8835 sponsored by AFCRC, Bedford, Mass. Part of the computational work was completed in 1958 in connection with NBS Project 8830-12-8833 sponsored by the U. S. Coast Guard, Washington, D. C.

† Natl. Bureau of Standards, Boulder Labs., Boulder, Colo.

niques in radio navigation systems and the interest in sferics which radiate from thunderstorms. The prediction of these propagated transients at various distances, employing idealized source models, constitutes the theoretical problem.

This paper introduces a vertically polarized point source current or Hertz¹ dipole, the amplitude of which varies in time as a damped sinusoid. The step function and the impulse function are limiting cases of this general type of source. More complicated sources can be simulated by superposition of this basic type.

THEORY

The propagated pulse, at a distance, d , and a time, t , which is described in this paper as a space-time function, $E(t, d)$, is built upon a source, $F_s(t)$, for which the transform, $f_s(\omega)$, may be written:

$$f_s(\omega) = \int_{-\infty}^{\infty} \exp(-i\omega t) F_s(t) dt, \quad (1)$$

where $\omega = 2\pi f$, f = frequency, cycles.

The transfer function which characterizes the propagation medium, $E(\omega, d)$, and the source integral (1) together describe a Fourier transform, $f(\omega, d)$,

$$f(\omega, d) = f_s(\omega) E(\omega, d). \quad (2)$$

¹ H. Hertz, "Die Kräfte Elektrischer Schwingungen Behandelt Nach der Maxwell'schen Theorie," *Ann. Phys. Chem. (Leipzig)*, vol. 36, pp. 1-22; 1889.

The function, $E(\omega, d)$, can be interpreted as the amplitude, $|E(\omega, d)|$, and the phase lag, $\text{Arg } E(\omega, d)$, of a "continuous wave" signal, *i.e.*, a sinusoidal wave of constant amplitude, uninterrupted in time, and propagated around the surface of the earth from a Hertzian dipole source current. The product of such a function and the transform, $f_s(\omega)$, of the particular source under consideration, $F_s(t)$, (1), therefore describes the Fourier transform of a pulse. The propagated transient, $E(t, d)$, can then be formally represented in space and time as a Fourier integral,

$$E(t, d) = \frac{1}{2\pi} \int_{-\infty}^{\infty} \exp(i\omega t) f_s(\omega) E(\omega, d) d\omega. \quad (3)$$

Primary interest is concerned with the real part of the space-time function, $\text{Re } E(t, d)$, since this represents the instantaneous signal observed in an "infinite bandwidth" receiver. The amplitude envelope, $|E(t, d)|$, and the phase envelope, $\phi(t, d)$, where

$$E(t, d) = |E(t, d)| \exp\{i[\phi(t, d) - \omega t]\}, \quad (4)$$

are only of secondary interest since these waveforms would ordinarily be recovered at the output of the receiver with some sort of envelope detection.

The source currents, $F_s(t)$, employed in this paper may be represented in complex form for the cosine source,

$$\begin{aligned} \text{Re } F_s(t) &= \text{Re } \exp(-\nu t) \\ &= \exp(-c_1 t) \cos \omega_{ct}, \quad (0 < t < \infty) \\ &= 0, \quad (t < 0) \end{aligned} \quad (5a)$$

or for the sine source,

$$\begin{aligned} -\text{Im } F_s(t) &= \text{Re } i \exp(-\nu t) \\ &= \exp(-c_1 t) \sin \omega_{ct}, \quad (0 < t < \infty) \\ &= 0, \quad (t < 0) \end{aligned} \quad (5b)$$

where

$$\nu = c_1 + i\omega_c. \quad (5c)$$

The transform, $E(\omega, d)$, which represents the propagation medium, can be described as an amplitude and phase transfer characteristic for a pulse as follows:

$$\begin{aligned} E(\omega, d) &= |E(\omega, d)| \\ &\cdot \exp\left\{-i\left[\phi_c(\omega, d) - \frac{\pi}{2} + a\omega\right]\right\} \end{aligned} \quad (6)$$

where

$$a = \frac{\eta_1 d}{c}, \quad (6a)$$

and where η_1 is the index of refraction of air at the surface of the earth ($\eta_1 \sim 1.000338$) and c is the speed of light [$c \sim 2.997925 \times 10^8$ meters/second].

It is convenient to write

$$E(\omega, d) \exp(i\omega t)$$

$$= |E(\omega, d)| \exp\left\{i\left[\omega t' - \phi_c(\omega, d) + \frac{\pi}{2}\right]\right\} \quad (7)$$

where the local time, t' , is

$$t' = t - a. \quad (8)$$

The primary propagation time, (6a), is thus included in the local time and $\phi_c(\omega, d)$ is the secondary phase or phase correction² resulting from the influence of the earth on the propagation mechanism. The time, $t' = 0$, thus describes the earliest time at which the pulse signal could be observed.

The neglect of the earth's curvature and the displacement currents in the earth at short distances make possible the employment of the operational calculus to give an immediate and somewhat useful solution to the problem. Employing the symbol, s , as used in the operational method,

$$s = i\omega, \quad (9)$$

the Laplace transform of the Norton³ surface wave⁴ is as follows:⁵

$$E(s, d) = C \left\{ f_0(s) + \frac{1}{a(s + \nu)} + \frac{1}{a^2 s(s + \nu)} \right\} \quad (10)$$

$$f_0(s, d) = \frac{s}{s + \nu} - \frac{s^2}{s + \nu} \sqrt{\pi\alpha} \exp(s^2\alpha) \text{erfc}(s\sqrt{\alpha}) \quad (11)$$

where

$$C = 2 \frac{I_0 l a^2}{4\pi\kappa d^3} = \frac{2(10^{-7})}{d}$$

($I_0 l = 1$ ampere-meter, the dipole momentum). (12)

$$\kappa = \frac{\eta_1^2}{c^2 \mu_0}, \quad \text{a constant,}$$

² J. R. Johler, W. J. Kellar, and L. C. Walters, "Phase of the Low Radio-Frequency Ground Wave," NBS Circular 573, pp. 1-6; June 27, 1956.

³ K. A. Norton, "The propagation of radio waves over the surface of the earth and in the upper atmosphere," PROC. IRE, vol. 25, pp. 1203-1236; September, 1937. See especially (57), p. 1212. See also K. A. Norton, "The propagation of radio waves over the surface of the earth in the upper atmosphere," PROC. IRE, vol. 24, pp. 1367-1387; October, 1936. Also, K. A. Norton, "The physical reality of space and surface waves in the radiation field of radio antennas," PROC. IRE, vol. 25, pp. 1192-1202; September, 1937.

⁴ A. Sommerfeld, "Über Die Ausbreitung der Wellen in der Drahtlosen Telegraphie," Ann. Phys., vol. 28, pp. 665-736; March, 1909.

⁵ The complementary error function, $\text{erfc}(z)$ is defined,

$$\text{erfc}(z) = \frac{2}{\sqrt{\pi}} \int_z^{\infty} \exp(-u^2) du.$$

where, μ_0 is the permeability of space, $\mu_0 = 4\pi(10^{-7})$, and⁶

$$\alpha = \frac{\eta_1^3 d}{2\sigma\mu_0 c^3}, \quad (13)$$

in which σ is the conductivity of the earth ($\sigma = 0.005$ mho/meter for typical land).

The inverse Laplace transform of the Norton surface wave may then be written:⁷

$$E(t', d) = \nu C \exp(-\nu t') \left\{ -1 - \nu \sqrt{\pi \alpha} \exp(\nu^2 \alpha) \cdot \left[\operatorname{erfc}(-\nu \sqrt{\alpha}) - \operatorname{erfc}\left(\frac{t'}{2\alpha} - \nu \sqrt{\alpha}\right) \right] + \frac{1}{\alpha v} - \frac{1}{a^2 \nu^2} \right\} + \left[\frac{t'}{2\alpha} + \nu \right] C \exp\left[\frac{-t'^2}{4\alpha}\right] + \nu C \left[\frac{1}{a^2 \nu^2} \right]. \quad (14)$$

The introduction of the displacement currents ($\epsilon_2 \neq 0$) and the earth's curvature, Fig. 1, complicates the func-

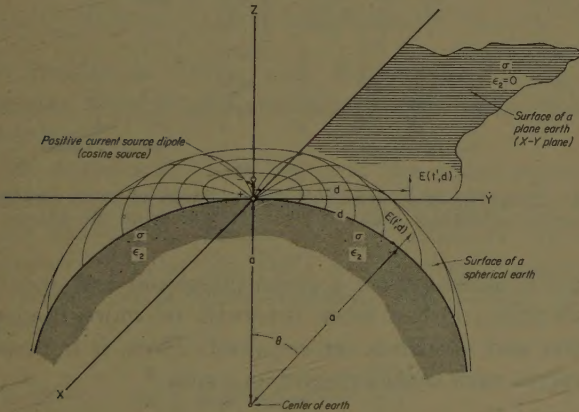


Fig. 1—Orientation of the source dipole and the earth with respect to coordinate systems.

tion $f_0(s)$. The transformation may be formally written as follows:

$$E(t', d) = F_0(t', d) + F_{i,e}(t', d) \quad (15)$$

$$F_0(t', d) = C \mathcal{L}^{-1} f_0(s). \quad (16)$$

The function, $F_0(t', d)$, is of primary importance in this paper since the contributions from the induction and electrostatic fields, $F_{i,e}(t', d)$, are quite minute at

⁶ The index of refraction, η_1 , of the earth's atmosphere is constant at the surface value with respect to altitude for purposes of the surface wave transformation at short distances. The effect of the vertical lapse of the index of refraction at great distances is introduced as the factor, β , (29), ($\beta \sim 0.75$).

⁷ J. R. Johler, "Transient radiofrequency ground waves over the surface of a finitely conducting plane earth," *J. Res. NBS*, vol. 60, pp. 281-285; April, 1958. See also, J. R. Johler, "Propagation of the radiofrequency ground wave transient over finitely conducting plane earth," *Geofis. pura e appl. (Milan)*, vol. 37, pp. 116-126; February, 1957.

great distances. The function, $F_0(t', d)$, may be re-written in the Fourier integral, (3), notation employing the variable ω instead of the operational symbol s ,

$$F_0(t', d) = \frac{1}{2\pi} \int_{-\infty}^{\infty} \exp(i\omega t') E(\omega, d) \cdot \int_{-\infty}^{\infty} F_s(t) \exp(-i\omega t) dt d\omega \quad (17)$$

or, with the aid of (5a) and (5b), and evaluating the inner integral of (17),

$$E(t', d) = \frac{1}{2\pi} \int_0^{\infty} |E(\omega, d)| \left\{ \left[\frac{\cos\left[\omega t' - \phi_c + \tan^{-1} \frac{-(\omega_c + \omega)}{c_1}\right]}{\sqrt{c_1^2 + (\omega_c + \omega)^2}} \right. \right. \\ \left. \left. + \frac{\cos\left[-\omega t' + \phi_c' + \tan^{-1} \frac{-(\omega_c - \omega)}{c_1}\right]}{\sqrt{c_1^2 + (\omega_c - \omega)^2}} \right] \right. \\ \left. + i \left[\frac{\sin\left[\omega t' - \phi_c' + \tan^{-1} \frac{-(\omega_c + \omega)}{c_1}\right]}{\sqrt{c_1^2 + (\omega_c + \omega)^2}} \right. \right. \\ \left. \left. + \sin\left[-\omega t' + \phi_c' + \tan^{-1} \frac{-(\omega_c - \omega)}{c_1}\right] \right] \right\} d\omega, \quad (18)$$

where

$$\phi_c' = \phi_c - \frac{\pi}{2}. \quad (18a)$$

It immediately becomes obvious that the real part of the amplitude time function (18), $\operatorname{Re} E(t', d)$, is the desired function for the cosine source (5a), and the imaginary part, $-\operatorname{Im} E(t', d) = \operatorname{Re} [iE(t', d)]$, is the desired function for the sine source (5b). Thus the problem has been reduced to the evaluation of a real integral,

$$E(t', d) = \int_0^{\infty} F_t(\omega, d) d\omega \\ = \operatorname{Re} \int_{-\infty}^{\infty} f(\omega, d) \exp(i\omega t) d\omega. \quad (19)$$

The transform of the pulse is asymmetrical as a result of the source function. The Fourier spectrum, $f_x(\omega, d)$, Fig. 2, can be determined for the transform, $f(\omega, d)$, the amplitude spectrum,

$$|f_x(\omega, d)| = |f(\omega, d) + f(-\omega, d)| \quad (\omega \geq 0), \quad (20)$$

and the phase spectrum,

$$\phi_x(\omega, d) = \operatorname{Arg} [f(\omega, d) + f(-\omega, d)], \quad (\omega \geq 0). \quad (20a)$$

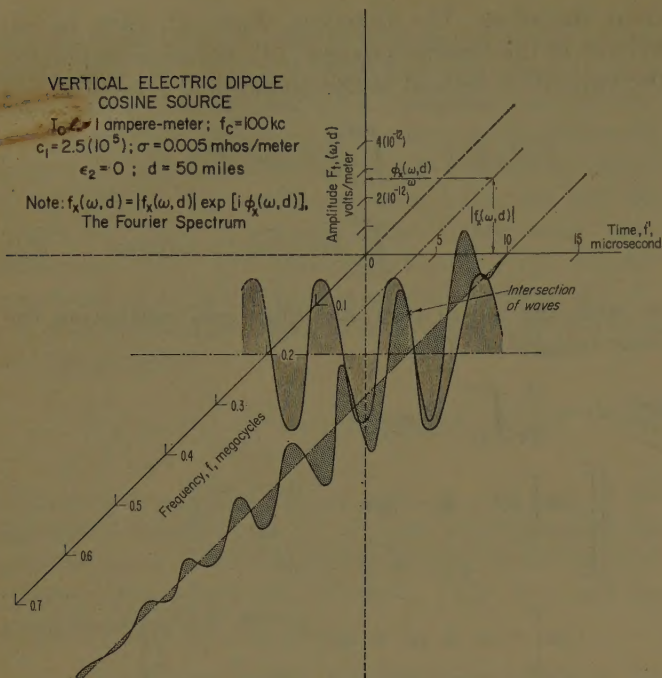


Fig. 2—Integrand of Fourier integral or image of pulse in the frequency-amplitude plane at small distance from the source, illustrating the relation of the integrand to the Fourier spectrum waves.

The integrand, $F_t(\omega, d)$, Figs. 2, 3, in the frequency-amplitude plane, is rather severely mutilated at great distances by the conduction and displacement currents in the earth and the effect of the earth's curvature. This is quite advantageous from a computational point of view, since the convergence of the integral at higher frequencies is rapid, and, as a matter of fact, analog methods such as a planimeter integration could be employed to evaluate the amplitude-time function, $E(t', d)$. However, numerical mastery of the problem is achieved by a reduction of the computation to a digital process.

The integral, $E(t', d)$, which involves the limits zero and infinity is rewritten as the sum of integrals with finite limits as follows:

$$\int_0^\infty F_t(\omega, d) d\omega = \int_0^{b_1} F_t(\omega, d) d\omega + \int_{b_1}^{b_2} F_t(\omega, d) d\omega + \int_{b_2}^{b_3} F_t(\omega, d) d\omega + \dots, \quad (21)$$

where enough terms are taken so that any remainder error is small. Each finite integral is evaluated by Gaussian quadrature.^{8,9} The limits of each finite integral are somewhat arbitrary, but are chosen consistent with the required accuracy and the availability of Gaussian quadrature weights and abscissas.⁹ If the range of inte-

⁸ Z. Kopal, "Numerical Analysis," John Wiley and Sons, Inc., New York, N. Y., p. 367; 1955.

⁹ P. Davis and P. Rabinowitz, "Abscissas and weights for Gaussian quadratures of high order," *J. Res. NBS*, vol. 56, pp. 35-37; January, 1956.

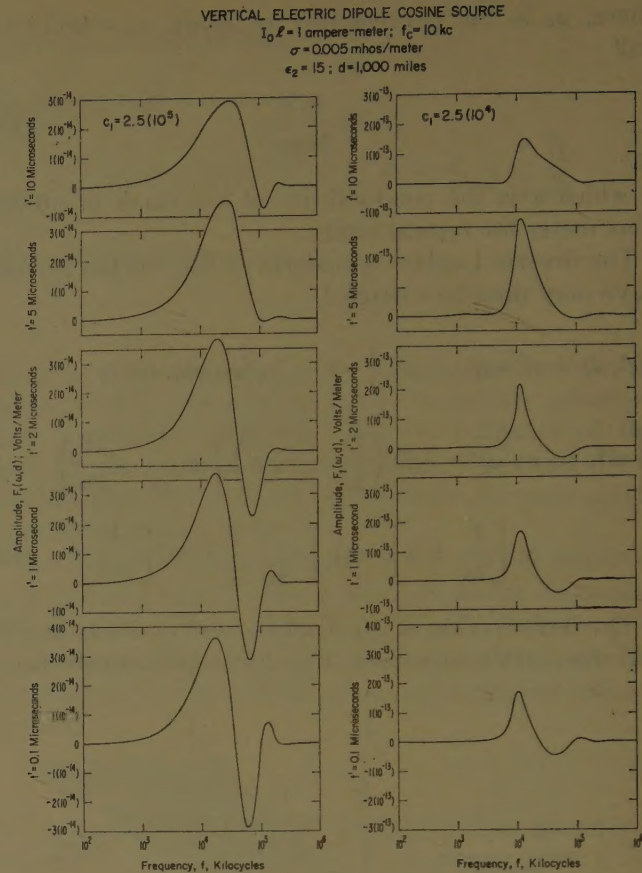


Fig. 3—Integrand of Fourier integral or image of pulse in the frequency-amplitude plane at great distance from the source.

gration is increased for a given integrand and accuracy specification, either more intervals or more Gaussian weights and abscissas are required. Thus, it is possible to express each finite integral as a sum:⁸

$$\int_{b_n}^{b_{n+1}} F_t(\omega, d) d\omega = \sum_{m=1}^M W_m F_t(\omega_m, d) + \epsilon(M), \quad (22)$$

where $\epsilon(M)$ is an error term which can, in general, be made arbitrarily small by increasing M , and where

$$m = 1, 2, 3, \dots, M. \quad (22a)$$

$$\omega_m = \frac{1}{2}[b_{n+1} - b_n]x_m + \frac{1}{2}[b_{n+1} + b_n]. \quad (22b)$$

The x_m 's are the Gaussian abscissas and M determines the number of values of $F_t(\omega, d)$ to be used in the quadrature. The Gaussian weights and abscissas can be determined from the following considerations:

$$\int_{-1}^1 f(x) dx = \sum_{m=1}^M H_m f(x_m) \quad (23)$$

$$W_m = \frac{1}{2}[b_{n+1} - b_n]H_m. \quad (24)$$

The x_m 's are the roots of the Legendre polynomial defined by

$$\frac{d^m}{dx^m} (x^2 - 1)^m = 2^m m! P_m(x) \quad (25)$$

$$\begin{aligned}
 P_0(x) &= 1 \\
 P_1(x) &= x \\
 P_2(x) &= \frac{3}{2}x^2 - \frac{1}{2} \\
 P_3(x) &= \frac{5}{2}x^3 - \frac{3}{2}x \\
 P_4(x) &= \frac{35}{8}x^4 - \frac{15}{4}x^2 + \frac{3}{8} \\
 &\dots
 \end{aligned} \tag{26}$$

Polynomials of higher degree are determined by use of the recursion formula.

$$(m+1)P_{m+1}(x) + mP_{m-1}(x) = (2m+1)xP_m(x). \tag{27}$$

Upon determination of the roots, the weight coefficients, H_m , of the corresponding quadrature formula are evaluated as follows:

$$H_m = \frac{2}{(1-x_m^2)[P_m'(x_m)]^2}. \tag{28}$$

The results of Davis and Rabinowitz⁹ (forty-eight Gaussian weights and abscissas) were employed in the quadrature.

The amplitude $|E(\omega, d)|$ and the phase correction, $\phi_e(\omega, d)$, for the ground wave were calculated by means of the convergent residue series (s series) of Watson,¹⁰ Bremmer,^{11,12} van der Pol¹¹ and Norton,¹³ employing the conventional time function, $\exp(-i\omega t)$ as follows:^{2,14}

$$\begin{aligned}
 E^*(\omega, d) &= -i\omega C \left[2\pi\beta^{2/3}(k_1\alpha')^{1/3} \frac{d}{\alpha'} \right]^{1/2} \\
 &\sum_{s=0}^{\infty} \frac{\exp \left\{ i \left[(k_1\alpha')^{1/3}\tau_s \beta^{2/3} \frac{d}{\alpha'} + \frac{\beta d}{2\alpha'} + \frac{\pi}{4} \right] \right\}}{\left[2\tau_s - \frac{1}{\delta_e^2} \right]} \tag{29}
 \end{aligned}$$

in which

$$s = 1, 2, 3, \dots$$

α' = the radius of the earth [$\alpha' \sim 6.36739(10^6)$] meters,

¹⁰ G. N. Watson, "The diffraction of electric waves by the earth and the transmission of electric waves round the earth," *Proc. Roy. Soc. (London)*, vol. 95, p. 83; October, 1918; p. 546; July, 1919.

¹¹ B. van der Pol and H. Bremmer, "The diffraction of electromagnetic waves from an electrical point source round a finitely conducting sphere, with applications to radiotelegraphy and the theory of the rainbow," *Phil. Mag.*, vol. 24, pt. I, p. 141, July, 1937; pt. II, p. 825, November, 1937; *Supp. J. Science*, vol. 25, p. 817; June, 1938.

¹² H. Bremmer, "Terrestrial Radio Waves; Theory of Propagation," Elsevier Publishing Co., New York, N. Y., pp. 11-50; 1949.

¹³ K. A. Norton, "The calculation of the ground wave field in intensity over a finitely conducting spherical earth," *Proc. IRE*, vol. 29, pp. 623-639; December, 1941.

¹⁴ J. R. Wait and H. H. Howe, "Amplitude and Phase Curves for Ground Wave Propagation in the Band 200 Cycles per Second to 500 Kilocycles," NBS Circular 574, pp. 1-17; May, 1956.

$$E^*(\omega, d) = |E(\omega, d)| \exp i \left[\phi_e - \frac{\pi}{2} \right], \tag{30}$$

$$k_1 = \frac{\omega}{c} \eta_1, \tag{31}$$

$$k_2^2 = \frac{\omega^2}{c^2} \left[\epsilon_2 + i \frac{\sigma \mu_0 c^2}{\omega} \right], \tag{32}$$

$$\delta_e = \frac{i \frac{k_2^2}{k_1^2} \beta^{1/3}}{(k_1 \alpha')^{1/3} \left[\frac{k_2^2}{k_1^2} - 1 \right]^{1/2}}, \tag{33}$$

and τ_s comprises the roots (see Appendix) of Riccati's differential equation:¹⁵

$$\frac{d\delta_e}{d\tau_s} - 2\delta_e^2 \tau_s + 1 = 0. \tag{34}$$

The amplitude and phase transfer characteristic of the ground wave is illustrated (Figs. 4, 5) in this paper for a conductivity, $\sigma = 0.005$ mho per meter, and a dielectric constant, $\epsilon_2 = 15$. It should be noted that at short distances, the induction and electrostatic fields enhance the amplitude and phase at low frequencies. The earth's curvature and the conduction and displacement currents in the earth enhance the phase and attenuate the signal rather severely at high frequencies and great distances. The convergence of the infinite integral (21) is primarily a result of the exponential high frequency attenuation (29),

$$\exp \left\{ -\text{Im} \left[(k_1 \alpha')^{1/3} \tau_s \beta^{2/3} \frac{d}{\alpha'} \right] \right\}.$$

THE SOURCE

The cosine source used in this paper employs an abrupt initial current (Figs. 7, 9, 11). The radiated field therefore propagates an impulse type of function which is superposed upon the sinusoid. This may be explained quite simply for the case of an infinite conducting earth:

$$E(s) = 1 \quad (\nu = 0, \alpha = 0) \tag{35}$$

then

$$E(t', d) = \mathcal{L}^{-1}E(s) = \delta(t'). \tag{35a}$$

$\delta(t')$ is the Dirac impulse function which can be defined in relation to the step function, $u(t)$, as follows:

$$\int_0^t \delta(t) dt = u(t), \tag{36}$$

where

$$u(t) = 1, \quad t > 0 \tag{37}$$

$$u(t) = 0, \quad t < 0. \tag{37a}$$

¹⁵ Bremmer, *op. cit.*, p. 45.

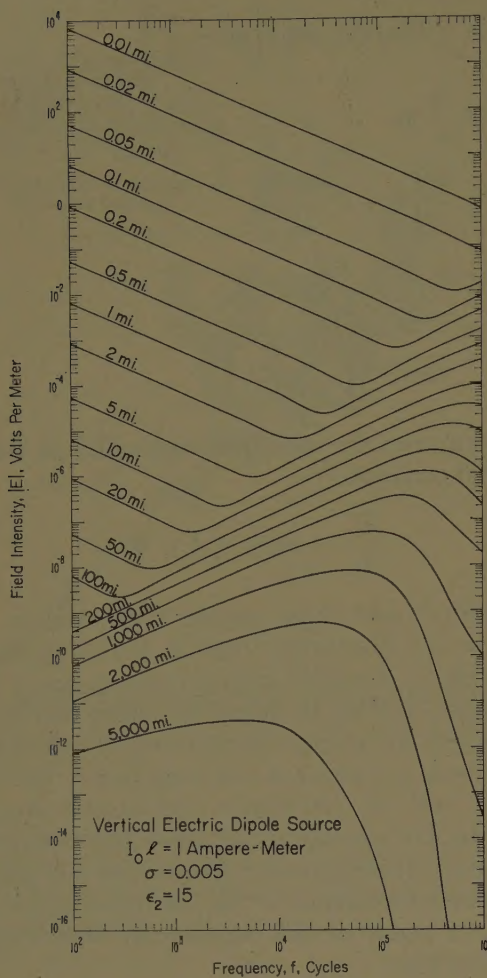


Fig. 4—Amplitude transfer characteristic of the ground wave.

The step function response of the ground wave at considerable distance from the source is a modified impulse function. Indeed, this is merely a limiting case of (14), $c_1 = 0$, $\nu = 0$, or,

$$E(t', d) = \frac{t'}{2\alpha} C \exp\left[\frac{-t'^2}{2\alpha}\right]. \quad (38)$$

This is consistent with the step function response derived by Wait.¹⁶ It should be noted that the amplitude and duration of the impulse becomes finite as a result of the introduction of the finite conductivity of the earth into the propagation mechanism.

The step function response resulting from the impulsive radiated field of the cosine current source is implicit in the calculations of this paper. The sine current source on the other hand does not imply such an additional radiation field.

¹⁶ J. R. Wait, "Transient fields of a vertical dipole over a homogeneous curved ground," *Can. J. Res.*, vol. 34, pp. 27-35; January, 1956. See also J. R. Wait, "The transient behaviour of the electromagnetic ground wave over a spherical earth," *IRE TRANS. ON ANTENNAS AND PROPAGATION*, vol. AP-5, pp. 198-202; April, 1957. Also J. R. Wait, "A note on the propagation of the transient ground wave," *Can. J. Phys.*, vol. 35, pp. 1146-1151; September, 1957.

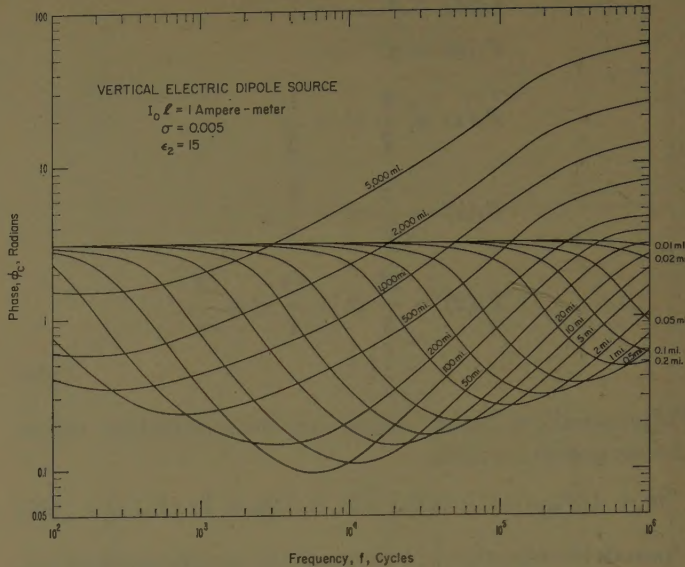


Fig. 5—Phase transfer characteristic of the ground wave.

It is quite possible to introduce the cosine current source less abruptly by redefining the source function, $F_s(t)$, as follows:

$$F_s(t) = \exp(-\nu t) - \exp(-\xi t) \quad (39)$$

where

$$\xi = c_2 + i\omega_c. \quad (39a)$$

ν has been described previously (5c) and c_2 is assigned a large positive value ($c_2 \gg c_1$). In accord with the superposition principle, this merely involves the sum of two waves calculated as previously described (14), (18). The space-time function, $E'(t', d)$, may be written as follows (Figs. 9, 11):

$$E' = E'(t', d) = E_\eta(t', d) - E_\xi(t', d). \quad (40)$$

RESULTS OF THE COMPUTATION

The detailed structure of the transient for various combinations of characteristic frequency, f_c , and damping, c_1 , for both sine and cosine source functions was determined at great distance (Figs. 6-11, pp. 7-9). The transient waves with characteristic period, f_c , of 100 kc, and a damping, c_1 , of $2.5(10^6)$ (Figs. 6, 7), and at a distance, d (Fig. 1), of 50 miles were calculated by both the operational formula (14) and the direct evaluation of the Fourier integral (18). In both cases, the earth was assumed to be a plane, and the displacement currents in the earth were neglected. Close agreement was found between the two methods, in Figs. 6, 7.

The displacement currents in the earth and the effect of the earth's curvature were then introduced by the calculation of the theory (29) of Watson, Bremmer, van der Pol, and Norton (29) at great distances (Figs. 4-11). The dispersion of the pulse at great distance was evident from the calculation. The most noteworthy attribute of

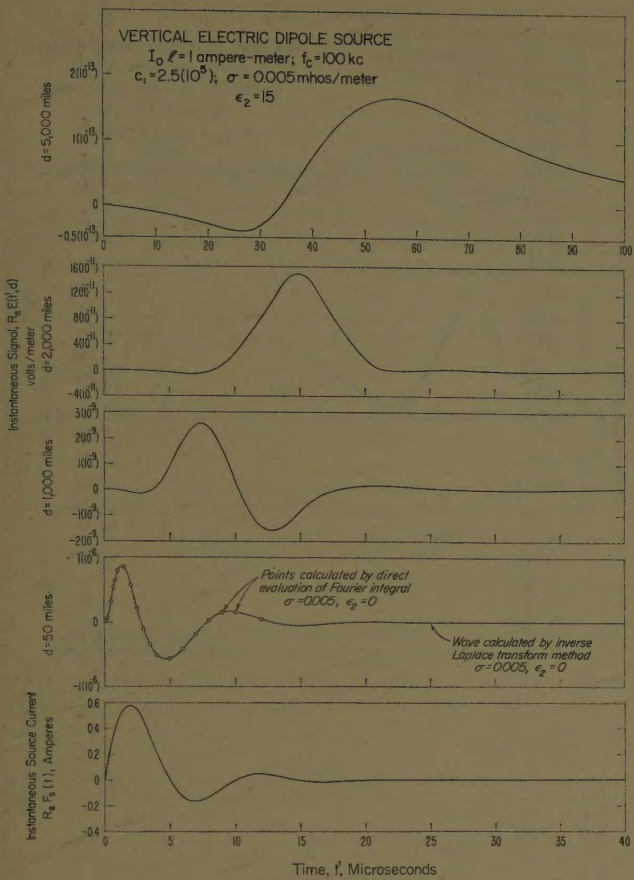


Fig. 6—Instantaneous signal and corresponding damped sine wave source current of a propagated ground wave pulse, illustrating close agreement at short distance between the form of the wave predicted by the operational formulas (inverse Laplace transform) and the form of the wave predicted by the direct evaluation of the Fourier integral.

this dispersion was an increase in the period of the pulse. The form of the source was somewhat obscured by the filtering action of the medium.

THE STEP, DELTA, AND GENERALIZED SOURCE FUNCTIONS

The special case of the step function response of the ground wave has already been discussed (38) in connection with the damped cosine source. This formulation (38) can be readily extended to the spherical earth theory with the following result:

$$E(t', d) = \frac{1}{\pi} \int_0^\infty |E(\omega, d)| \left\{ \frac{1}{\omega} \sin \left[\omega t' - \phi_e' \right] \right\} d\omega. \quad (41)$$

The special case of an impulse source function or "delta function,"

$$F_s(t) = \delta(t) \quad (42)$$

reduces to the following simple formula:

$$E(t', d) = \frac{1}{\pi} \int_0^\infty |E(\omega, d)| \{ \cos [\omega t' - \phi_e'] \} d\omega \quad (43)$$

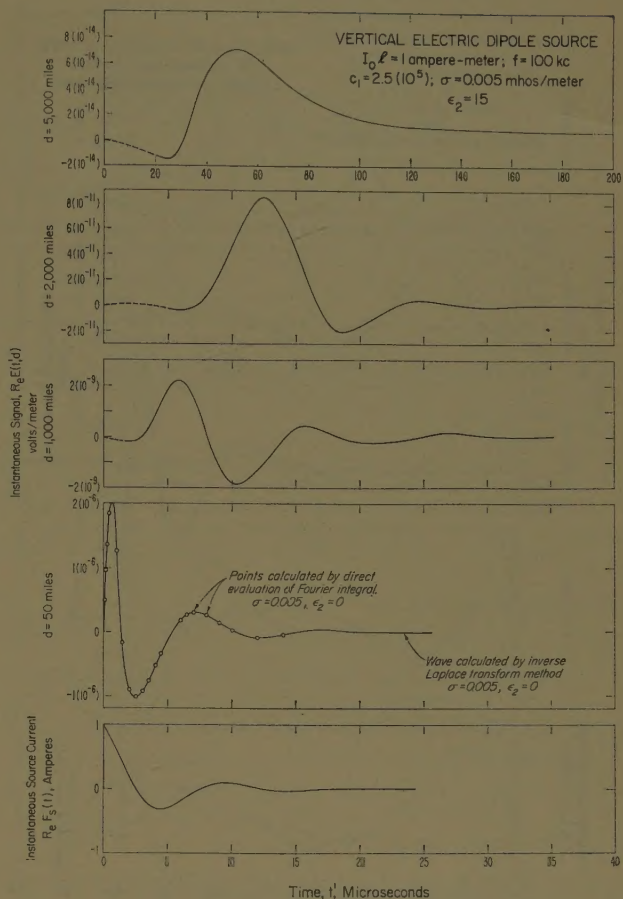


Fig. 7—Instantaneous signal and corresponding damped cosine wave source current of a propagated ground wave pulse, illustrating agreement at short distances between operational methods and the direct evaluation of the Fourier integral.

where each of the above formulas is readily evaluated by the previously described quadrature (22). The results can be checked against the operational methods based on the plane earth theory (14), which yields the following result for the impulse source function or delta function.¹⁶

$$E(t', d) = \left\{ \frac{1}{2\alpha} - \left[\frac{t'}{2\alpha} \right]^2 \right\} C \exp \left[\frac{-t'^2}{4\alpha} \right]. \quad (44)$$

During the past several years some very interesting papers have appeared which describe the propagation of a "delta" or impulse source function over the surface of the earth. Whereas it is questionable whether such a source function represents anything in nature, this is an important theoretical problem nonetheless, and presumably the more complicated source functions could be synthesized by application of the superposition principle.

The results of Levy and Keller¹⁷ account for the earth's curvature but neglect the displacement currents

¹⁷ B. R. Levy and J. B. Keller, "Propagation of electromagnetic pulses around the earth," IRE TRANS. ON ANTENNAS AND PROPAGATION, vol. AP-6, pp. 56-61; January, 1958.

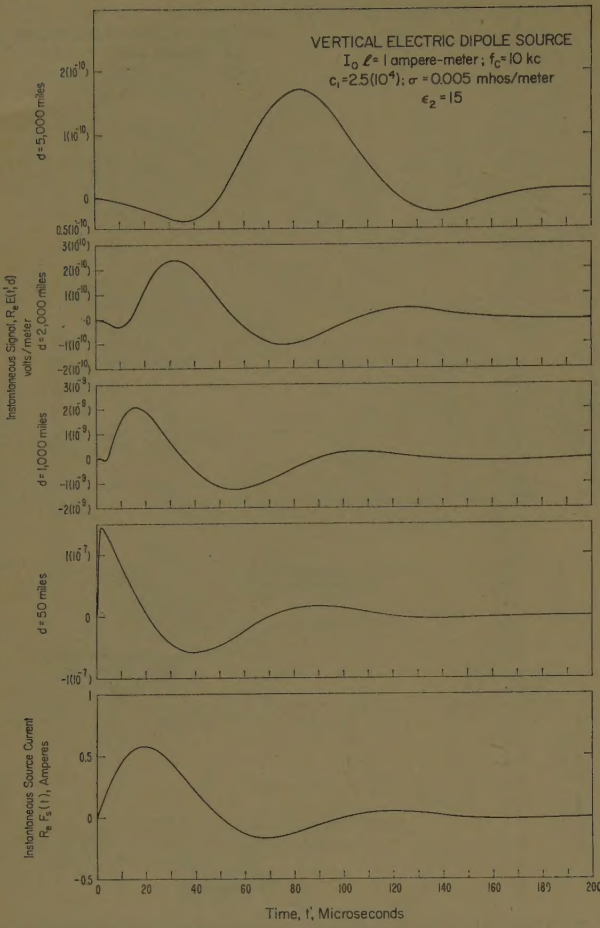


Fig. 8—Instantaneous signal and corresponding damped sine wave source current of a propagated ground wave pulse.

in the earth by the assumption of an infinite conductivity. These authors then approximate the "lossy" case by taking only the first term in the infinite series which represents the roots of Riccati's differential equation (34) (see Appendix). In contrast, the results of Pekeris and Alterman¹⁸ completely neglect the conduction currents in the earth and consider only the displacement currents, and further assume that the earth is a plane, which is reasonable only at short distances. On the other hand, Wait,¹⁶ has developed a method for the solution of this problem which not only considers displacement currents and conduction currents, but also the earth's curvature.

It seems to be quite possible to get an exact solution to this problem by the method described in this paper (43), especially since the delta or impulse source function is a much simpler one than the sinusoid with which this paper is primarily concerned.

The source functions which represent natural phenomena will not in general have the precise mathematical form of a damped sinusoid. Since the application of the superposition principle is not always practical,

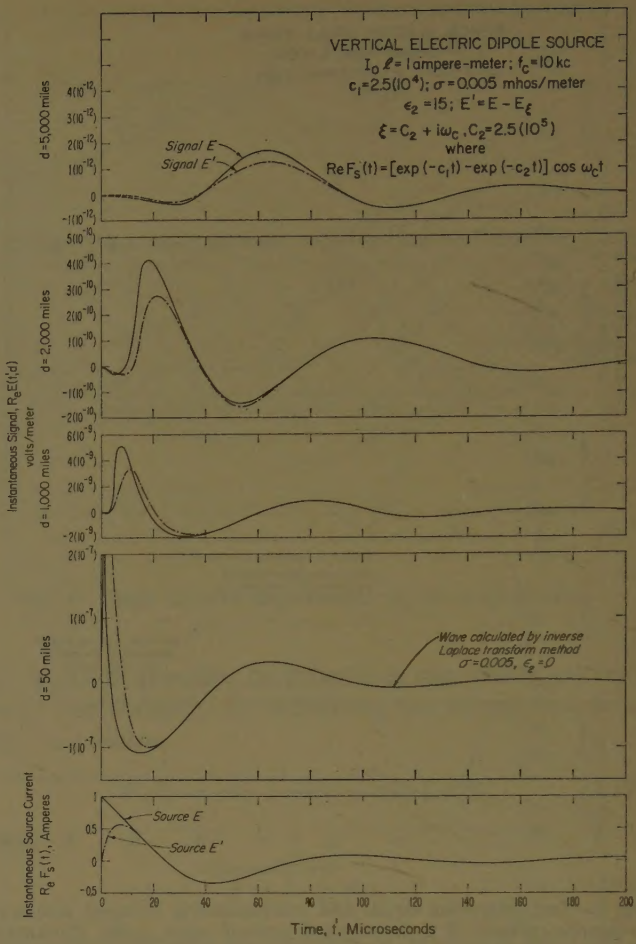


Fig. 9—Instantaneous signal and corresponding damped cosine wave source current of a propagated ground wave pulse, illustrating the introduction of a less abrupt initial source current.

another approach to the general problem is appropriate. Indeed, it is quite possible to extend the theory to complicated waveforms. Consider an experiment in which the signal, $\text{Re } E(t', d)$ is observed and recorded at some distance, d_1 , from the source. The theory is then required to predict the form of the signal recorded at some other distance, d_2 . The theory is also required to determine the form of the source, $F_s(t)$.

The spectrum (18), (20), (20a) can be determined directly from the observed signal, $\text{Re } E(t', d)$:

$$f_x(\omega, d) = \int_0^\infty \exp(-i\omega t') \text{Re } E(t', d) dt'. \quad (45)$$

The infinite integral can, as before, be split into the sum of finite integrals subject to the previously described (21) conditions of convergence,

$$f_x(\omega, d) = \int_0^{t_1'} F(\omega, t') dt' + \int_{t_1'}^{t_2} F(\omega, t') dt' + \dots + \int_{t_n'}^{t_{n+1}} F(\omega, t') dt' + \dots, \quad (46)$$

¹⁸ C. L. Pekeris and Z. Alterman, "Radiation from an impulsive current in a vertical antenna placed on a dielectric ground," *J. Appl. Phys.*, vol. 28, pp. 1317-1323; November, 1957.

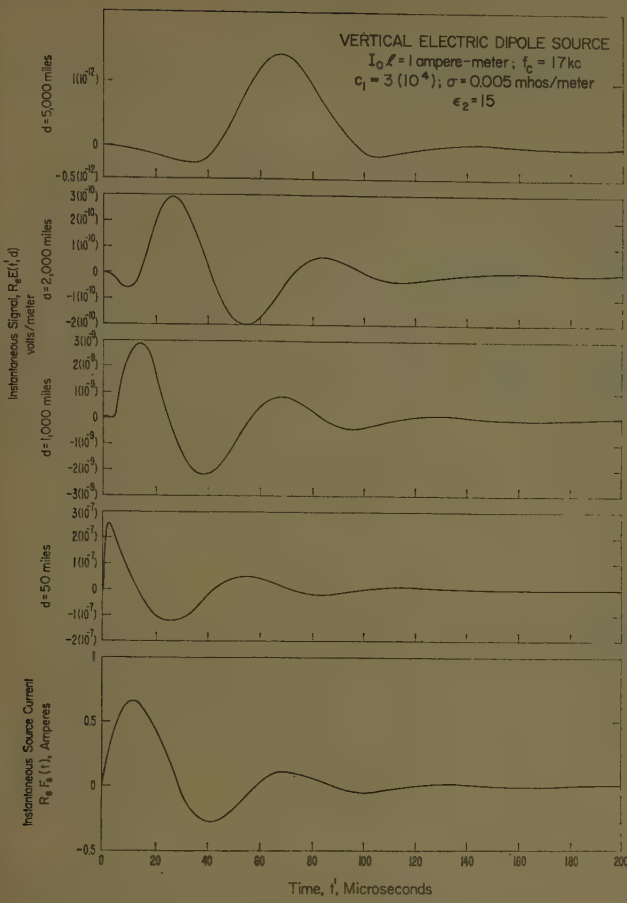


Fig. 10—Instantaneous signal and corresponding damped sine wave source current of a propagated ground wave pulse.

$$\int_{t'_n}^{t'_{n+1}} F(\omega, t') dt' = \sum_{m=1}^M W_m F(\omega, t'_m), \quad (47)$$

$$m = 1, 2, 3, \dots, M, \quad (47a)$$

$$t'_m = \frac{1}{2}(t'_{n+1} - t'_n)x_m + \frac{1}{2}(t'_{n+1} + t'_n). \quad (47b)$$

The spectrum of the source, $f_{x,s}(\omega)$, can then be determined,

$$f_{x,s}(\omega) = \frac{f_x(\omega, d)}{E(\omega, d)}. \quad (48)$$

Since the real part of the signal, $\text{Re } E(t', d)$, was employed in the analysis (45), the source function, $\text{Re } F_s(t)$, can be described as an integral with a symmetrical integrand,

$$F_s(t) = \frac{1}{2\pi} \int_{-\infty}^{\infty} \exp(i\omega t) f_{x,s}(\omega) d\omega, \quad (49)$$

or

$$F_s(t) = \frac{1}{\pi} \int_0^{\infty} |f_{x,s}(\omega)| \{ \cos [\omega t + \phi_{x,s}(\omega)] \} d\omega. \quad (50)$$

Also

$$f_x(\omega, d_2) = \frac{f_x(\omega, d_1)}{E(\omega, d_1)} E(\omega, d_2), \quad (51)$$

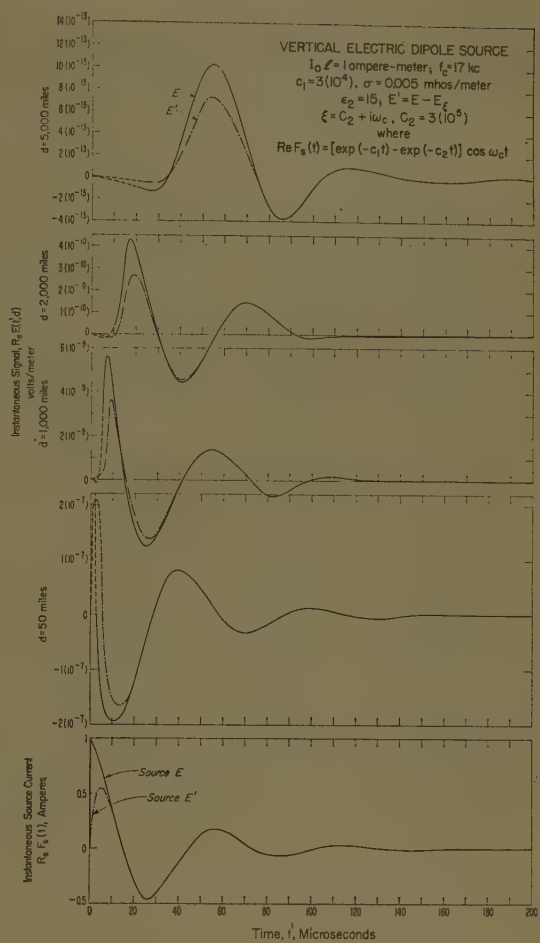


Fig. 11—Instantaneous signal and corresponding damped cosine wave source current of a propagated ground wave pulse, illustrating the introduction of a less abrupt initial source current.

and

$$E(t', d_2) = \frac{1}{\pi} \int_{-\infty}^{\infty} |f_x(\omega, d_2)| \cos [\omega t' + \phi_x(\omega, d_2)] d\omega. \quad (52)$$

The integrals (50), (52) can be evaluated by previously described quadrature (22).

The recovery of the form of the source (50) is not always practical at great distance, since the ground wave is rather severely attenuated at high frequencies (Fig. 4). The limit of resolution for which the source can be recovered at a given distance is experimental, *i.e.*, the resolution is dependent upon the accuracy with which the signal, $\text{Re } E(t', d)$, can be observed and the accuracy with which the constants which characterize the propagation medium can be determined. But this is merely another way of stating that the form of the source is somewhat obscured by the propagation medium at great distances.

CONCLUSIONS

The form of the transient ground wave signal which has been propagated to great distance from a current source has been theoretically determined. More complicated signals can be formed by superposition and the

simple signals such as the step function can be formed as limiting cases of the more general sinusoid. Complicated waveforms at a given distance from the source can be

$$\begin{aligned}\tau_s &= \tau_{s,0} - \delta - \frac{2}{3} \tau_{s,0} \delta^3 + \frac{1}{2} \delta^4 - \frac{4}{5} \tau_{s,0}^2 \delta^5 + \frac{14}{9} \tau_{s,0} \delta^6 - \frac{1}{7} (5 + 8\tau_{s,0}^3) \delta^7 + \frac{58}{15} \tau_{s,0}^2 \delta^8 - \left(\frac{328}{81} \tau_{s,0} + \frac{16}{9} \tau_{s,0}^4 \right) \delta^9 \\ &\quad + \left(\frac{423}{315} + \frac{1552}{175} \tau_{s,0}^3 \right) \delta^{10} - \left(\frac{7576}{495} \tau_{s,0}^2 + \frac{32}{11} \tau_{s,0}^5 \right) \delta^{11} + \dots \quad |\delta^2 \tau| < \frac{1}{2} \\ \tau_s &= \tau_{s,\infty} - \left[\frac{1}{2\tau_{s,\infty}} \right] \frac{1}{\delta} - \left[\frac{1}{8\tau_{s,\infty}^3} \right] \frac{1}{\delta^2} - \left[\frac{1}{12\tau_{s,\infty}^2} + \frac{1}{16\tau_{s,\infty}^5} \right] \frac{1}{\delta^3} - \left[\frac{7}{96\tau_{s,\infty}^4} + \frac{5}{128\tau_{s,\infty}^7} \right] \frac{1}{\delta^4} \\ &\quad - \left[\frac{1}{40\tau_{s,\infty}^3} + \frac{21}{320\tau_{s,\infty}^6} + \frac{7}{256\tau_{s,\infty}^9} \right] \frac{1}{\delta^5} - \left[\frac{29}{720\tau_{s,\infty}^5} + \frac{77}{1280\tau_{s,\infty}^8} + \frac{21}{1024\tau_{s,\infty}^{11}} \right] \frac{1}{\delta^6} \\ &\quad - \left[\frac{1}{112\tau_{s,\infty}^4} + \frac{19}{360\tau_{s,\infty}^7} + \frac{143}{2560\tau_{s,\infty}^{10}} + \frac{33}{2048\tau_{s,\infty}^{13}} \right] \frac{1}{\delta^7} \\ &\quad - \left[\frac{97}{4480\tau_{s,\infty}^6} + \frac{163}{2560\tau_{s,\infty}^9} + \frac{429}{8192\tau_{s,\infty}^{12}} + \frac{429}{32768\tau_{s,\infty}^{15}} \right] \frac{1}{\delta^8} \\ &\quad - \left[\frac{1}{288\tau_{s,\infty}^5} + \frac{13661}{362880\tau_{s,\infty}^8} + \frac{6769}{92160\tau_{s,\infty}^{11}} + \frac{2431}{49152\tau_{s,\infty}^{14}} + \frac{715}{65536\tau_{s,\infty}^{17}} \right] \frac{1}{\delta^9} \\ &\quad - \left[\frac{2309}{201600\tau_{s,\infty}^7} + \frac{820573}{14515200\tau_{s,\infty}^{10}} + \frac{37961}{460800\tau_{s,\infty}^{13}} + \frac{46189}{983040\tau_{s,\infty}^{16}} + \frac{2431}{262144\tau_{s,\infty}^{19}} \right] \frac{1}{\delta^{10}} + \dots \quad |\delta^2 \tau| > \frac{1}{2}.\end{aligned}$$

evaluated in practical experiments by a Fourier transformation employing numerical integration of the observed or real part of the signal. The signal can then be predicted at some other distance from the source by an inverse Fourier transformation employing similar numerical integration. The source can in principle be recovered from the observed signal, but at great distance it is somewhat obscured by the propagation medium.

The technique for the direct evaluation of the Fourier integral for the case of the ground wave suggests applications to other problems, such as the propagation of a transient through a filter or the propagation of the transient sky wave.

APPENDIX

The roots of Riccati's differential equation (34) can be found as follows:

The poles and zeros $|\tau_{s,\infty}|$ and $|\tau_{s,0}|$ have been tabulated,¹⁹ where

$$\tau_{s,\infty} = |\tau_{s,\infty}| \exp \left[i \frac{\pi}{3} \right] \text{ and } \tau_{s,0} = |\tau_{s,0}| \exp \left[i \frac{\pi}{3} \right].$$

ACKNOWLEDGMENT

The authors herewith acknowledge the helpful suggestions of G. Hefley of NBS and E. L. Lewis of NFCRC, and the able assistance of C. M. Lilley in carrying out the electronic computer operations.

¹⁹ Johler, *et al.*, *op. cit.*, p. 33, table 44.

On the Measurement of Virtual Height*

I. KAY†

Summary—A time dependent definition of the virtual height of a reflected wave train is suggested. This definition is such that its accuracy increases as the width of the incident pulse increases. Moreover, it is theoretically possible to obtain an estimate of the virtual height with as small an error as desired, no matter what the nature of the reflecting medium.

Suppose an incident pulse having width W and a carrier frequency ω_0 produces a reflected wave which, when measured at a fixed point $x=0$ in space, is $R(\omega_0, w, t)$. The suggested definition of the virtual height $h'(\omega_0)$ is

$$h'(\omega_0) = \lim_{w \rightarrow \infty} c \left\{ \frac{\int_{-\infty}^{\infty} t |R(\omega_0, w, t)|^2 dt}{\int_{-\infty}^{\infty} |R(\omega_0, w, t)|^2 dt} \right. \\ \left. - \frac{\int_{-\infty}^{\infty} t |I(\omega_0, w, t)|^2 dt}{\int_{-\infty}^{\infty} |I(\omega_0, w, t)|^2 dt} \right\},$$

where c is the free space velocity of light. This relation for $h'(\omega_0)$ holds for any physically reasonable incident wave train and is independent of its envelope shape.

An example is given of a reflected wave whose virtual height cannot be determined by inspection in the usual manner. The expression given here for the virtual height provides the correct result.

INTRODUCTION

MUCH of the data obtained from radio sounding investigations of the upper atmosphere is given in terms of the virtual height reached by a narrow pulse-modulated wave transmitted from the earth. A virtual height record, which is a record of the group delay time of the test pulse multiplied by the free space velocity of light, is generally made from measurements of the time required roughly for the wave packet to go out from and return to the antenna from which it was radiated.

Some ambiguity in the measurement of the delay time of the pulse will always occur in a standard experiment. The reason for this ambiguity lies in the difficulty of prescribing a fixed point of reference on the pulse envelope so that the movement of the wave group can be described as the movement of a single entity. The difficulty, of course, occurs because the pulse envelope must undergo a certain amount of distortion in its travel back and forth, including some spreading of its energy over a longer time interval than that which determined its initial width.

Still, in many cases the amount of distortion suffered by the pulse is small.¹ When such a case is under consideration the ambiguity in the virtual height measure-

* Manuscript received by the PGAP, December 26, 1957. The research reported here was sponsored by the Dept. of Defense under Contract No. DA49-170-sc-2253.

† New York University, Inst. of Mathematical Sciences, New York 3, N. Y.

¹ O. E. H. Rybeck, "A theoretical survey of the possibilities of determining the distribution of the free electrons in the upper atmosphere," *Trans. Chalmers Univ. Tech., Gothenburg, Sweden*, no. 3, pp. 1-74; 1942.

ment should be correspondingly small. It may be useful, however, to remark that in any case the ambiguity caused by the distortion of a test pulse in a radio sounding experiment is not inherent in this kind of measurement. It is due, rather, to the imprecise concept of group delay time used in the interpretation of the data supplied by the experiment. In the present paper an attempt will be made to overcome the difficulty by referring to the precise definition of group delay time instead of the heuristic idea of it.

The precise definition of virtual height is generally given as the free space velocity of light times the derivative, with respect to frequency of the phase of the complex reflection coefficient characteristic of the medium being investigated.^{1,2} To be more explicit: imagine a CW of unit amplitude and frequency ω incident on the medium. The complex number $|r(\omega)| \exp\{j\phi(\omega)\}$, giving the amplitude $|r(\omega)|$ and the phase $\phi(\omega)$ of the reflected wave, is the reflection coefficient of the medium; the virtual height of a pulse at a frequency ω_0 for this medium will be

$$h' = cd\phi/d\omega|_{\omega=\omega_0}, \quad (1)$$

where c is the free space velocity of light.

If this precise definition of virtual height is used, a second criticism of the standard measurement technique comes to mind. Due to the so-called uncertainty principle relating a transient waveform and its frequency spectrum, a very narrow pulse will have a spectrum which is rather evenly distributed over a broad frequency band; consequently, the idea of the group delay time of the pulse loses its intuitive meaning. The group delay time, then, will not necessarily be given correctly in terms of the phase derivative of the reflection coefficient, at least according to the arguments ordinarily found in literature.¹⁻³ In fact, in order to obtain a sensible definition of group delay time, one must deal with a wave packet having a narrow-band frequency spectrum, that is, a wave packet considerably spread out in time. Therefore, it seems reasonable that in order to improve the accuracy and to remove the ambiguity of virtual height measurements, one should use as broad a pulse as possible in radio sounding experiments.

It is the purpose of this paper to suggest the kind of measurement appropriate to the use of a broad test pulse instead of a narrow one. The analysis shows that, theoretically at least, the ambiguity in such a measure-

² J. Shmoys, "Limitations on the calculation of expected virtual height for specific ionospheric distributions," *J. Geophys. Res.*, vol. 57, pp. 95-111; 1952.

³ J. A. Stratton, "Electromagnetic Theory," McGraw-Hill Book Co., Inc., New York, N. Y., pp. 330-333; 1941.

ment can be made arbitrarily small for all carrier frequencies no matter what the dispersive properties of the reflecting medium may be. In particular, the h' -curves obtained at the present time from radio soundings of the ionosphere exhibit a great deal of ambiguity when the carrier frequency is near the penetration or critical frequency of a layer. Thus the use of a broad test pulse with the interpretation of virtual height suggested here offers the possibility for improving the accuracy of measurements at frequencies in the neighborhood of the critical frequency, for example.

DEFINITIONS

The proposed modification of the method for obtaining the virtual height is based on the following considerations.

Suppose, at a point $x=0$ in free space below the medium to be investigated, the incident pulse is given by a real function of time t

$$I(\omega_0, w, t) = I(t/w) \cos \omega_0 t, \quad (2)$$

where $I(t/w)$ represents a more or less arbitrary pulse envelope with a maximum at $t=0$. The constant w , assumed positive, roughly fixes the width of the pulse in the sense that as w becomes large $I(t/w)$ remains near its value at $t=0$ for a large range of t . For example, we might have

$$I(t/w) = \exp(-t^2/2w^2), \quad (3)$$

a Gaussian envelope with standard deviation w or

$$I(t/w) = \begin{cases} 1 & \text{for } -w/2 < t < w/2 \\ 0 & \text{for } |t| > w/2, \end{cases} \quad (4)$$

a square pulse of width w .

If we define the Fourier transform

$$i(\omega) = \int_{-\infty}^{\infty} I(\tau) \exp(j\omega\tau) d\tau, \quad i(\omega) = |i(\omega)| \exp\{j\theta(\omega)\}$$

$$I(\tau) = \frac{1}{2\pi} \int_{-\infty}^{\infty} i(\omega) \exp(-j\omega\tau) d\omega, \quad (5)$$

then the Fourier transform of the incident pulse (2) is the function

$$i(\omega_0, w, \omega) = \int_{-\infty}^{\infty} I(\omega_0, w, t) \exp(j\omega t) dt$$

$$= (w/2)[i\{w(\omega + \omega_0)\} + i\{w(\omega_0 - \omega)\}]. \quad (6)$$

In terms of the reflection coefficient $r(\omega)$ the Fourier transform of the reflected wave packet $R(\omega_0, w, t)$ is $r(\omega) i(\omega_0, w, \omega)$ and we have

$$R(\omega_0, w, t) = \frac{1}{2\pi} \int_{-\infty}^{\infty} r(\omega) i(\omega_0, w, \omega) \exp(-j\omega t) d\omega. \quad (7)$$

It will be shown later that under these conditions:

$$\lim_{w \rightarrow \infty} \int_{-\infty}^{\infty} |R(\omega_0, w, t)|^2 dt / \int_{-\infty}^{\infty} |I(\omega_0, w, t)|^2 dt = |r(\omega_0)|^2$$

and

$$\lim_{w \rightarrow \infty} c \left\{ \int_{-\infty}^{\infty} t |R(\omega_0, w, t)|^2 dt / \int_{-\infty}^{\infty} |R(\omega_0, w, t)|^2 dt \right. \\ \left. - \int_{-\infty}^{\infty} t |I(\omega_0, w, t)|^2 dt / \int_{-\infty}^{\infty} |I(\omega_0, w, t)|^2 dt \right\} \\ = cd\phi(\omega)/d\omega |_{\omega=\omega_0} = h'(\omega_0) \quad [\text{by (1)}]. \quad (8)$$

The relations (8) indicate that, except for quantities of infinitesimal order as w becomes large, the amplitude of the reflection coefficient and the virtual height of the incident pulse can be expressed in terms of the power, and the centroid of the power in the incident and reflected wave packets. The error committed in using (8) with large but finite w would seem to depend on $\omega_0 w$ as well as on the ratio of w to the effective width of the reflecting medium.

In the case of a narrow incident pulse which produces a narrow reflected pulse, the measurement of virtual height obtained by the standard technique (consisting of a direct physical observation of the delay time) will give the same result as the approximation based on (8) where the actual finite value of w is used instead of $w \rightarrow \infty$. Thus, the approximation suggested by (8) will always be at least as accurate as the standard method for measuring virtual height and should be more accurate when a broad incident pulse is used instead of a narrow one.

EXAMPLE OF A DISPERSED REFLECTED PULSE

It is easy to find reflection coefficients in connection with a given incident pulse of any desired width such that an inspection of the corresponding reflected wave packet will reveal no clue to the virtual height as defined by (1). If the incident pulse is sufficiently broad, however, the computation suggested by (8) will always give the virtual height even in this case.

Consider for example, a reflection coefficient

$$r(\omega) = j\alpha \exp(2j\omega L)/(\omega + j\alpha), \quad (9)$$

where α and L are real positive constants. The amplitude of $r(\omega)$ is

$$|r(\omega)| = \alpha/(\omega^2 + \alpha^2)^{1/2}; \quad (10)$$

the phase of $r(\omega)$ is

$$\phi(\omega) = -\tan^{-1}(\alpha/\omega) + \pi/2 + 2\omega L, \quad (11)$$

and thus the virtual height, according to (1), is

$$h'(\omega_0) = c\alpha/(\omega_0^2 + \alpha^2) + 2cL. \quad (12)$$

Let us choose for the incident pulse

$$I(\omega_0, w, \omega) = I(t/w) \cos \omega_0 t, \quad (13)$$

where

$$I(t/w) = \begin{cases} 1, & \text{for } |t| < w \\ 0, & \text{for } |t| > w \end{cases}. \quad (14)$$

The reflected wave packet is given by the expression

$$R(\omega_0, w, t) = \begin{cases} 0, & t < 2L - w \\ \sin \theta [\exp \{ \alpha(2L - w - t) \} \sin (\omega_0 w - \theta) + \sin \{ \omega_0(t - 2L) + \theta \}], & 2L - w < t < 2L + w \\ \sin \theta [\exp \{ \alpha(2L + w - t) \} \sin (\omega_0 w + \theta) + \exp \{ \alpha(2L - w - t) \} \sin (\omega_0 w - \theta)], & 2L + w < t, \end{cases} \quad (15)$$

where $\sin \theta = \alpha / (\alpha^2 + \omega_0^2)^{1/2}$.

The envelope of $R(\omega_0, w, t)$ has essentially the same shape for any value of the carrier frequency ω_0 . Thus, there is no obvious way to obtain the virtual height (12) from $R(\omega_0, w, t)$ by inspection. (See Fig. 1.)

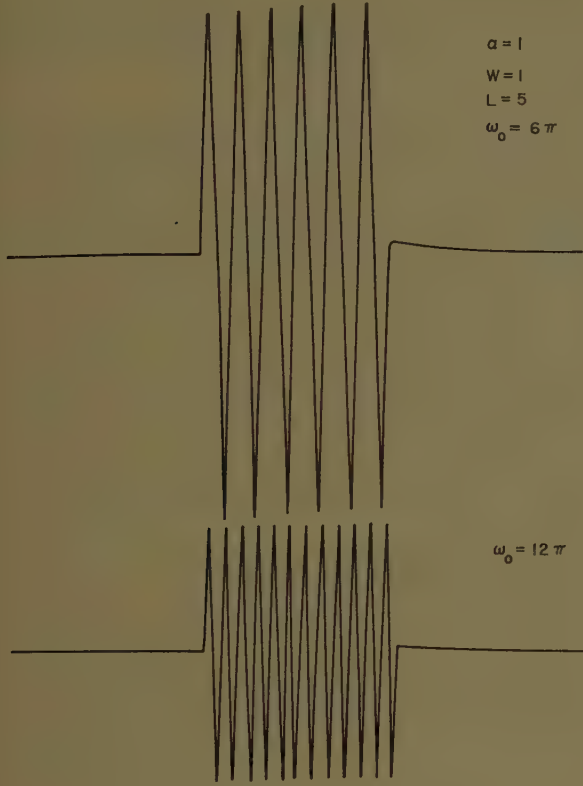


Fig. 1—Reflected pulse $R(\omega_0, w, t)$ vs time t .

We can apply (8) to compute the virtual height, however. We have:

$$i(\omega) = \int_{-1}^1 \exp(j\omega t) dt = 2 \sin \omega / \omega \quad (16)$$

so that by (6)

$$i(\omega_0, w, \omega) = \sin \{ w(\omega + \omega_0) \} / (\omega + \omega_0) + \sin \{ w(\omega - \omega_0) \} / (\omega - \omega_0). \quad (17)$$

We also have:

$$\begin{aligned} \int_{-\infty}^{\infty} |I(\omega_0, w, t)|^2 dt &= w + o(w) \\ \int_{-\infty}^{\infty} |R(\omega_0, w, t)|^2 dt &= w\alpha^2 / (\alpha^2 + \omega_0^2) + o(w) \\ \int_{-\infty}^{\infty} t |R(\omega_0, w, t)|^2 dt &= w\alpha^3 / (\omega_0^2 + \alpha^2)^2 + 2wL\alpha^2 / (\alpha^2 + \omega_0^2) + o(w). \end{aligned} \quad (18)$$

The general results (8) are thus verified in this special case. The error actually depends on $\omega_0 w$ and αw but not particularly on L , as a more detailed calculation will show. The quantity L , according to (15), is just the distance of the edge of the reflecting medium divided by c , the free space velocity of light. The quantity α may be regarded as a measure of the width of the reflecting medium since $r(\omega)$ becomes zero if α approaches zero.

PROOF OF (8)

Relations and definitions (5)–(7) are necessary for the proof of (8). A standard argument which is employed in the proof of the Fourier integral theorem will be used to demonstrate a preliminary result we shall require.

Theorem A

Let $f(\omega)$ be continuous and uniformly bounded for all real ω , and assume

$$\int_{-\infty}^{\infty} |I(\tau)|^2 d\tau = \frac{1}{2\pi} \int_{-\infty}^{\infty} |i(\omega)|^2 d\omega < \infty.$$

Then

$$\begin{aligned} \int_{-\infty}^{\infty} f(\omega) |i(\omega_0, w, \omega)|^2 d\omega &= \frac{w}{4} \{ f(\omega_0) + f(-\omega_0) \} \int_{-\infty}^{\infty} |i(\omega)|^2 d\omega + o(w). \end{aligned}$$

Proof

By (6) we have

$$\begin{aligned} |i(\omega_0, w, \omega)|^2 &= \frac{w}{4} [|i\{w(\omega + \omega_0)\}|^2 + |i\{w(\omega - \omega_0)\}|^2 \\ &\quad + i\{w(\omega + \omega_0)\} i^* \{w(\omega - \omega_0)\} \\ &\quad + i^* \{w(\omega + \omega_0)\} i\{w(\omega - \omega_0)\}]. \end{aligned} \quad (19)$$

First we consider the first two terms on the right of (19) at the same time. We have

$$\begin{aligned} \int_{-\infty}^{\infty} \{f(\omega) - f(\pm \omega_0)\} |i\{w(\omega \pm \omega_0)\}|^2 d\omega &= \frac{1}{w} \int_{-\infty}^{\infty} \{f(\sigma/w \pm \omega_0) - f(\pm \omega_0)\} |i(\sigma)|^2 d\sigma \\ &= \frac{1}{w} \int_{-\sqrt{w}}^{\sqrt{w}} \{f(\sigma/w \pm \omega_0) - f(\pm \omega_0)\} |i(\sigma)|^2 d\sigma \\ &\quad + \frac{1}{w} \left[\int_{\sqrt{w}}^{\infty} + \int_{-\infty}^{-\sqrt{w}} \right] \{f(\sigma/w \pm \omega_0) \\ &\quad - f(\pm \omega_0)\} |i(\sigma)|^2 d\sigma. \end{aligned} \quad (20)$$

Consider the first term on the right of (20). We have

$$\begin{aligned} \frac{1}{w} \int_{-\sqrt{w}}^{\sqrt{w}} |f(\sigma/w \pm \omega_0) - f(\pm \omega_0)| |i(\sigma)|^2 d\sigma \\ \leq \frac{\epsilon}{w} \int_{-\infty}^{\infty} |i(\sigma)|^2 d\sigma \quad (21) \end{aligned}$$

for w large enough, by the continuity of $f(\omega)$ and ω_0 . The last two terms on the right of (20) are evidently equal to $(1/w)o(1)$. Since ϵ in (21) can be made as small as we please for large w , we have finally

$$\begin{aligned} \int_{-\infty}^{\infty} f(\omega) |i\{w(\omega \pm \omega_0)\}|^2 d\omega \\ = (1/w)f(\pm \omega_0) \int_{-\infty}^{\infty} |i(\sigma)|^2 d\sigma + (1/w)o(1). \quad (22) \end{aligned}$$

Now we consider the last two terms on the right of (19) one at a time. We have

$$\begin{aligned} & \int_{-\infty}^{\infty} f(\omega) i\{w(\omega + \omega_0)\} i^*\{w(\omega - \omega_0)\} d\omega \\ &= (1/w) \int_{-\infty}^{\infty} f(\sigma/w + \omega_0) i^*(\sigma) i(\sigma + 2\omega_0 w) d\sigma \\ &= (1/w) \int_{-\sqrt{w}}^{\sqrt{w}} f(\sigma/w + \omega_0) i^*(\sigma) i(\sigma + 2\omega_0 w) d\sigma \\ &+ (1/w) \left[\int_{\sqrt{w}}^{\infty} + \int_{-\infty}^{-\sqrt{w}} \right] \\ & \quad \cdot f(\sigma/w + \omega_0) i^*(\sigma) i(\sigma + 2\omega_0 w) d\sigma. \quad (23) \end{aligned}$$

By Schwartz's inequality the first term of the right side of (23) is of order

$$(1/w) \left[\int_{-\infty}^{\infty} |i(\sigma)|^2 d\sigma \right]^{1/2} \cdot \left[\int_{2\omega_0 w - \sqrt{w}}^{2\omega_0 w + \sqrt{w}} |i(\sigma)|^2 d\sigma \right]^{1/2} = (1/w)o(1).$$

The second and third terms on the right side of (23) can also be estimated by Schwartz's inequality:

$$(1/w) \int_{\sqrt{w}}^{\infty} f(\sigma/w + \omega_0) i^*(\sigma) i(\sigma + 2\omega_0 w) d\sigma$$

$$\leq (1/w) \left[\int_{\sqrt{w}}^{\infty} |i(\sigma)|^2 d\sigma \int_{\sqrt{w}}^{\infty} |f(\sigma/w + \omega_0)|^2 \right. \\ \left. \cdot |i(\sigma + 2\omega_0 w)|^2 d\sigma \right]^{1/2} = (1/w)o(1),$$

and, of course, we have the same result for the other term. Combining these results with (22) we arrive at Theorem A.

From Plancherel's theorem for the Fourier transform (7) and the fact that $|r(\omega)|$ is an even function of ω , we obtain the first part of (8). To obtain the second part we start with Plancherel's theorem applied to the first moment of a function. Thus, if $f(\omega)$ is the Fourier transform of $F(t)$ we note that

$$\int_{-\infty}^{\infty} t |F(t)|^2 dt = \frac{-j}{2\pi} \int_{-\infty}^{\infty} f'(\omega) f^*(\omega) d\omega. \quad (24)$$

Applying (24) to the numerator of the first term on the left of the second equation in (8) we have

$$\begin{aligned} & \int_{-\infty}^{\infty} t |R(\omega_0, w, t)|^2 dt \\ &= \frac{-j}{2\pi} \int_{-\infty}^{\infty} \frac{d}{d\omega} \{r(\omega) i(\omega_0, w, \omega)\} \cdot r^*(\omega) i^*(\omega_0, w, \omega) d\omega \\ &= \frac{1}{2\pi} \int_{-\infty}^{\infty} \frac{d}{d\omega} \{\phi(\omega) + \theta(\omega_0, w, \omega)\} |i(\omega_0, w, \omega)|^2 |r(\omega)|^2 d\omega \\ &+ \frac{1}{2\pi} \int_{-\infty}^{\infty} \frac{d}{d\omega} \{ |r(\omega)| |i(\omega_0, w, \omega)| \} \\ & \quad \cdot \{ |r(\omega)| |i(\omega_0, w, \omega)| \} d\omega \\ &= \frac{1}{2\pi} \int_{-\infty}^{\infty} \frac{d}{d\omega} \{\phi(\omega) + \theta(\omega_0, w, \omega)\} |i(\omega_0, w, \omega)|^2 |r(\omega)|^2 d\omega, \end{aligned}$$

for

$$\begin{aligned} & \int_{-\infty}^{\infty} \frac{d}{d\omega} \{ |r(\omega)| |i(\omega_0, w, \omega)| \} \{ |r(\omega)| |i(\omega_0, w, \omega)| \} d\omega \\ &= \frac{1}{2} \int_{-\infty}^{\infty} \frac{d}{d\omega} \{ |r(\omega)|^2 |i(\omega_0, w, \omega)|^2 \} d\omega = 0. \quad (25) \end{aligned}$$

A similar consideration applies to the numerator of the second term on the left of the second equation in (8). Combining these results with an application of Theorem A, we obtain the second relation in (8).

Back-Scattering Measurements with a Space-Separation Method*

H. J. SCHMITT†

Summary—A method for the experimental determination of the back-scattering cross section of arbitrarily shaped obstacles is suggested, which, in a manner analogous to the Michelson interferometer in optics, makes use of a semitransparent mirror in order to separate the incident wave and the reflected wave. A measurement setup is described, and possible sources of error are discussed. The accuracy of measurements is investigated by comparing the measured values of the back-scattering cross section of circular metallic disks with the results obtained from the exact theory.

INTRODUCTION

THE investigation of the back-scattering cross section of arbitrarily shaped reflecting objects involves a determination of the field strength of the wave scattered in the opposite direction to the incident wave a large distance away from the scattering object. The incident wave is generally assumed to be a plane wave. A rigorous theoretical treatment of the back-scattering behavior is limited to objects with a particular kind of symmetry because of numerous mathematical difficulties. Various mathematically simpler approximation methods have been developed, however, which can be applied to more complicated diffraction problems.

The accuracy of these approximate solutions can only be checked by comparing the results with suitable experiments. The question of accurate experimental methods is therefore of importance, and several different methods for measuring the back-scattering cross section have been suggested, particularly in the range of microwaves.¹ For example, the intensity of the back-scattered wave can be determined by a measurement of the standing-wave ratio between the source and the object, resulting from the superposition of the scattered wave and the incident wave.² It is most advantageous to measure the small amount of energy scattered back directly by separating the scattered wave from the incident wave. This can be done in several ways: in a manner analogous to the technical application in radar, a separation in time can be achieved by transmitting very short pulses;³ a separation with regard to frequency may be had by making use of the Doppler effect if the obstacle is put

into fast motion;⁴ a separation is also possible by a direct cancellation of the amount of signal in the receiver due to the incident wave.⁵

All these methods have one feature in common: they contain as essential parts typical elements of high-frequency technique, either in the form of a field probe, a demodulator, a mixing device, or closed waveguides. The sensitivity and accuracy of these methods therefore depend critically on the features of these elements and on their careful construction, which may become difficult in the region of very short wavelengths.

In this report, a very simple method for the measurement of back-scattering cross sections is suggested which depends on a separation of the incident signal from the scattered signal but does not use typical waveguide elements for this purpose. Therefore, the effectiveness is not restricted towards higher frequencies. A measurement setup will be described and tested by measurements of the back-scattering cross section of circular metallic disks at 1 cm and 3 cm wavelength.

METHOD OF MEASUREMENTS

The principle of the measurement procedure makes use of a separation in space of the back-scattered signal from the incident signal. It is plotted schematically in Fig. 1.

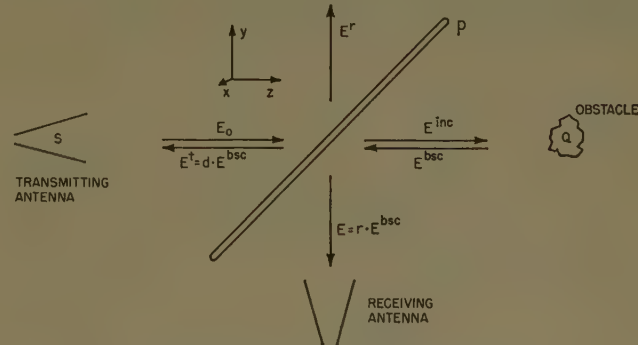


Fig. 1—Separation of incident and back-scattered waves by a semitransparent mirror.

A beam of electromagnetic waves is radiated from the source *S* towards the scattering object *Q*. Between object and source the beam has to cross a semitransparent mirror *p*, the surface of which is inclined at an angle of about 45 degrees against the direction of incidence. The incident wave, coming from the $-z$ direction, is split into

* H. Scharfman and D. D. King, "Antenna scattering measurements by modulation of the scatterer," PROC. IRE, vol. 42, pp. 854-858; May, 1954.

† R. W. P. King and T. T. Wu, "The Reflection of Electromagnetic Waves from Surfaces of Complex Shape," Cruft Lab., Harvard University, Cambridge, Mass., Sci. Rep. No. 12; November, 1957.

‡ D. D. King, "Measurement and interpretation of antenna scattering," PROC. IRE, vol. 37, pp. 770-777; July, 1949.

§ C. H. H. Tang, "Electromagnetic Back-Scattering from Thin Circular Disks by a Microwave Pulse Method," Cruft Lab., Harvard University, Cambridge, Mass., Sci. Rep. No. 15; March, 1958.

two parts while hitting the mirror: a reflected wave (E') traveling in the positive y direction, where it is assumed to be completely absorbed, and a transmitted wave E^{inc} traveling in the direction towards the scattering object. Part of the energy of this wave is scattered back towards the source E^{bs} . The scattered wave hits the back of the mirror and will be partly transmitted (E') and partly reflected (E). The reflected part of the scattered wave travels in the direction of the negative y axis—that is, opposite to the primarily reflected wave. Here it is received by a directional antenna and can be measured by any suitable device.

The semitransparent mirror can be placed anywhere along the z axis between the source and the scattering object. Generally, it will be useful to arrange it about halfway between source and object in order to avoid any coupling between source and mirror or between object and mirror.

On the total way from the source to the receiving antenna the reflected part of the scattered wave is once transmitted *through* the mirror (transmission factor d) and once reflected *by* the mirror (reflection factor r). Neglecting losses in the mirror material, the received intensity is ultimately

$$|E|^2 = \text{const} \cdot r^2 \cdot d^2 = \text{const} \cdot r^2 (1 - r^2). \quad (1)$$

For symmetry reason the received intensity reaches a maximum if

$$r^2 = d^2 = \frac{1}{2}. \quad (2)$$

Simultaneously, while fulfilling (2), the received intensity in the first approximation is independent of fluctuations in the transmitter frequency, since, if

$$r = r(\lambda),$$

the expression

$$\frac{\partial |E|^2}{\partial \lambda} = \frac{\partial |E|^2}{\partial r} \cdot \frac{\partial r}{\partial \lambda}$$

becomes zero because of

$$\frac{\partial |E|^2}{\partial r} = 0.$$

This fact is of definite importance since small frequency variations are difficult to avoid and may disturb considerably measurements involving the cancellation of the incident signal.

A semitransparent mirror with small electric losses can easily be realized in the region of short electromagnetic waves and in the region of optics by a homogeneous plane dielectric sheet of matched thickness l and dielectric constant ϵ . If, for example, the electric vector is perpendicular to the plane of incidence, the transmission factor is given by⁶

⁶ C. G. Montgomery, "Technique of Microwave Measurements," McGraw-Hill Book Co., Inc., New York, N. Y., p. 584; 1947.

$$d = \frac{4\sqrt{q}e^{-i\beta l}}{(\sqrt{q} + 1)^2 - (\sqrt{q} - 1)^2 e^{-2i\beta l}}, \quad (3)$$

where

$$q = \frac{\epsilon - \sin^2 \phi}{1 - \sin^2 \phi},$$

and

$$\beta = \frac{2\pi}{\lambda} \sqrt{\epsilon - \sin^2 \phi}$$

with ϕ = angle of incidence.

Multiplying (3) with the conjugate complex value yields, for the transmitted energy,

$$d^2 = 1 - r^2$$

$$= \frac{1}{1 + \frac{1}{8} \left(\frac{1}{\sqrt{q}} - \sqrt{q} \right)^2 \left(1 - \cos \frac{4\pi}{\lambda} \sqrt{\epsilon - \sin^2 \phi} l \right)}. \quad (4)$$

For different values of ϵ , the square of the transmission factor is plotted in Fig. 2 as a function of the thickness of the dielectric sheet. Obviously, the dielectric constant must have a certain minimal value in order to reach $r^2 = d^2 = \frac{1}{2}$. A more instructive view may be gained from Fig. 3. For an angle of incidence of 45 degrees, the curves $d^2 = \text{const} = 0.5$ are plotted as a function of ϵ and l/λ . The hatched region inside the fingers corresponds to values of $d^2 < 0.5$, and, for the other region, $0.5 < d^2 \leq 1$. Particularly for $\epsilon < 3.4$, d^2 is always larger than 0.5.

Two factors recommend operation in the lowest mode, that is, with the smallest possible thickness of the dielectric sheet. First, for loss tangents of the dielectric medium that are not too high, the absorption can be neglected and, second, the assumption made for the derivation of (4), *i. e.*, that a plane wave is incident on the mirror, is not generally fulfilled in the experiment. The incident wave can be described rather by a spherical wave originating from the source. Corresponding to the dimensions of the scattering object, only a certain sector of this spherical wave is actually used in the measurement. Border rays of this sector hit the mirror under somewhat different angles and have to travel different distances within the dielectric. A mutual phase shift between different rays within the sector is thereby produced. The phase distortion depends on the thickness of the sheet and is smallest for the lowest order.

The effectiveness of this measurement principle obviously depends on how far a direct coupling between the transmitting and receiving antennas on the one side and scattering object and receiving antenna on the other side can be avoided. It depends also on the degree to which the reception of scattered radiation from objects other than the original scatterer—for example, surrounding walls or the side edges of the mirror—can be suppressed. A sufficient decoupling of the two antennas necessarily requires the use of directional antennas,

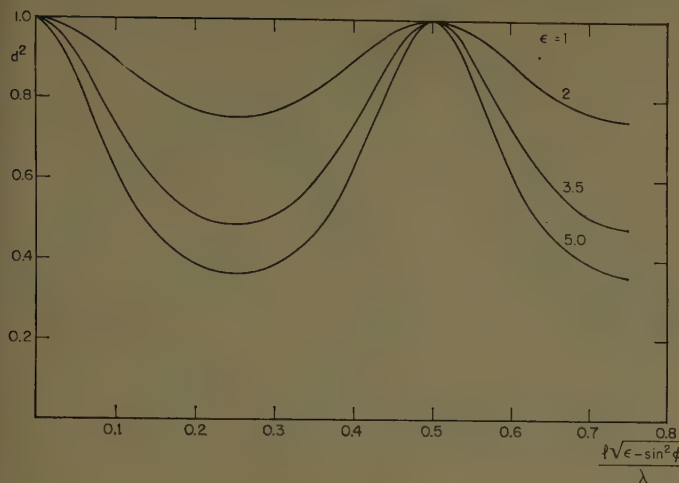


Fig. 2—Transmission coefficient of a plane dielectric sheet as a function of the thickness (angle of incidence $\phi=45$ degrees, electric vector perpendicular to the plane of incidence).

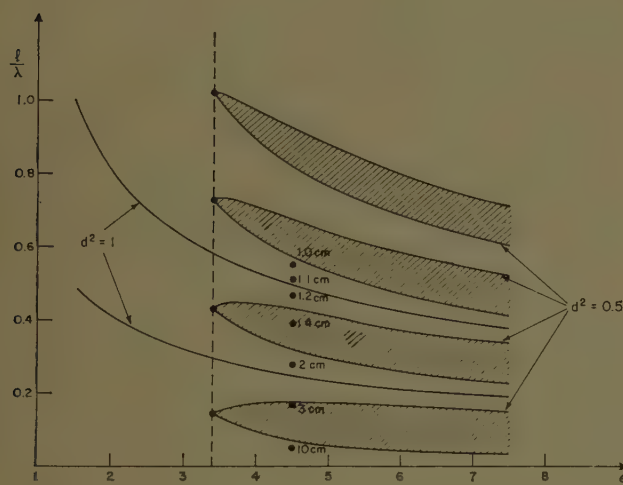


Fig. 3—Curves of constant transmission coefficients for a plane dielectric sheet ($\phi=45$ degrees). Points mark wavelength for a sheet thickness of 0.55 cm.

thereby restricting application to the region of microwaves and eventually still higher frequencies for which a sufficiently narrow beam can be achieved. It must be kept in mind, however, that the radiation pattern of these directional antennas may contain numerous sidelobes. But since the position of the receiving antenna along the negative y axis is arbitrary, in almost any case a position can be determined which is in a minimum of the radiation pattern of the transmitting antenna. And since the position of the scattering object along the z axis is oblique, as long as it is situated in the far-zone field of both the transmitting and receiving antennas, a position can generally be found for which it is in a minimum of the pattern of the receiving antenna. Thereby, a direct coupling can be adequately suppressed.

In order to avoid any undesired scattered radiation, a reflection-free support must be provided for the object under investigation. For objects having a plane of symmetry in which the electric field tangential to this plane vanishes, an image-screen technique can be used¹ in

which the measurement setup is reduced to a half-space by putting a large metallic ground screen in the plane of symmetry. Although the space-separation method is not restricted to the ground screen technique, use of an image plane, where possible, is helpful, since electronic instruments such as the generator and the receiver can be put under the screen, *i.e.*, outside the field of incident and scattered waves.

Using this technique and a sufficiently large mirror, the problem of undesired scattered radiation is simply to avoid a reflection of the two waves E^{inc} and E^r at the edges of the image plane. Eventually, if the equipment is set up in a closed room, care must be taken to minimize reflections at the surrounding walls. Both disturbances can be made small if a sufficiently large ground screen is used and the surrounding walls are covered with absorbers. Furthermore, a small reflection of E^{inc} , for example, can be compensated by a corresponding reflection of E^r in the other arm of the setup. Particularly in indoor measurements, it is necessary to make use of this possibility, since it is very difficult to minimize reflection to less than 2 per cent by means of the usual absorbers in the microwave region. As in the case of the cancellation method,⁵ it should be noted that the scattering object in the measurement space now has two effects: on the one hand, a wave is scattered from the object, and, on the other, the formerly existing compensation between the two arms of the setup is disturbed by the withdrawal of the scattered intensity from the incident wave. With the rough assumption that all waves are plane and the scattering object a nontransparent plane surface with purely geometrical reflection, a simple estimate of both effects yields, for the amplitude of the received signal,⁷

$$E = \text{const} (r_1 e^{i\psi_1} e^{iky} + r_2 e^{i\psi_2} e^{iky}), \quad (5)$$

where

$$\begin{aligned} r_1 e^{i\psi_1} &= \text{reflection factor of the scattering surface,} \\ r_2 e^{i\psi_2} &= \text{reflection factor of the surrounding walls.} \end{aligned}$$

Since the back-scattering cross section of any object is defined by

$$\sigma = 4\pi\rho^2 \frac{P^{bsc}}{P^{inc}} = 4\pi\rho^2 \frac{|E^{bsc}|^2}{|E^{inc}|^2}, \quad (6)$$

where ρ is the distance between receiving antenna and scattering object, only the square of the absolute value of the amplitude is of interest.

$$|E|^2 = \text{const} (r_1^2 + r_2^2 + 2r_1 r_2 \cos(\psi_1 - \psi_2)), \quad (7)$$

The second and third terms represent disturbances in the accuracy of the measurements. If the objects under investigation are metallic plates with linear dimensions that are large compared to the wavelength, the assump-

⁷ The reflection factor of the semitransparent mirror obviously is unimportant here, since both parts have once been reflected and once transmitted through the mirror.

tions made are in good approximation to the actual situation. In this case, ($r_1=1$, $r_2 \ll 1$), the maximum relative error is, with $\cos(\psi_1 - \psi_2) = \pm 1$,

$$\frac{\Delta |E|^2}{|E|^2} = \pm 2r_2; \quad (8)$$

that is, for an assumed reflection factor of 2 per cent, the measured value of the back-scattering cross section is accurate within 4 per cent.

For a quantitative determination of σ , it is feasible to compare the measured signal with the signal received from an object with a known back-scattering cross section. There is, however, the possibility of an absolute measurement of σ if the transmission factor of the mirror is known. For this purpose the reflected part of the scattered wave, $|E|^2 = r^2 \cdot |E^{bss}|^2$, is determined first and then the receiving antenna is fixed on the opposite arm of the setup in equal optical distance to the source as the scattering object. The received amplitude E^r is equal to the amplitude of the incident field at the position of the object times a constant and known factor

$$|E^r|^2 = \frac{r^2}{d^2} |E^{inc}|^2. \quad (9)$$

With this relation, the back-scattering cross section is

$$\sigma = 4\pi\rho^2 \frac{|E^{bss}|^2}{|E^{inc}|^2} = 4\pi\rho^2 \frac{|E|^2}{|E^r|^2} \cdot \frac{1}{d^2}. \quad (10)$$

MEASUREMENT SETUP

An indoor measurement setup was constructed embodying the space-separation principle, and the ground screen technique, with its special advantages, was used to determine the back-scattering behavior of symmetrical objects at 3-cm and 1-cm wavelength. The entire assembly is shown in Fig. 4.

The essential part of the equipment consists of an aluminum ground screen 1.25 by 2.50 m in size, which is firmly mounted on a wooden frame. In the center of one of the narrow sides is fixed the transmitting horn antenna, dimensioned for either 3-cm or 1-cm wavelength. The semitransparent mirror is mounted in the middle of the image plane, extending across the whole screen and inclined at an angle of 45 degrees against the direction of incidence of the emitted wave. In the direction of the primarily transmitted and reflected waves, the ground screen was enlarged by additional metal sheets of about 1-m length joined on the main screen. The edges of these pieces are polygon-shaped on the outside. Along the rim of the whole screen (hatched region), absorber material is attached, extending about 60 cm above the metallic plane. The polygon structure avoids a direct geometrical reflection on the surface of the absorbers in the direction towards the receiver and therefore decreases the disturbing scatter signal. The receiving antenna, also a horn, is situated on one of the wide sides of the ground screen. In the center of the

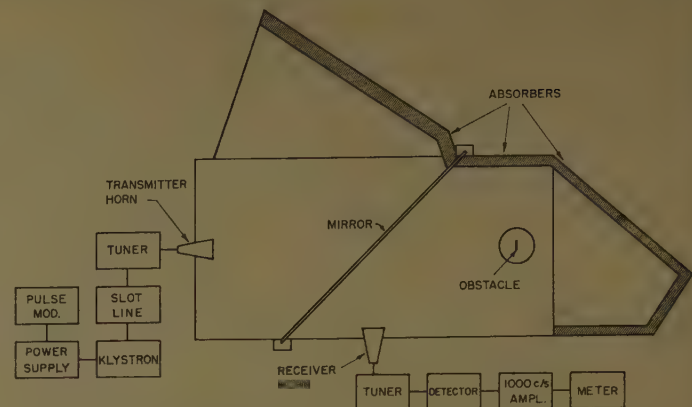


Fig. 4—Schematic diagram of experimental setup.

narrow side, opposite to the source, a circular hole with a diameter of 20 cm is cut into the screen making it possible to insert fitting aluminum disks on which either the measurement sample can be mounted or a probe supported to investigate the field distribution.

The klystron generators for 1-cm and 3-cm wavelength (types 2K33 and 2K25, respectively), as well as the receiving apparatus, are standard equipment and are located underneath the ground screen. The quadratic characteristic of the crystal detector has been checked at the particular wavelengths by measuring the sinusoidal field distribution in a waveguide.

As a semitransparent mirror, a very homogeneous glass plate with a thickness of 5.56 mm and the dimensions 90×180 cm was used. Two wooden beams with cut-in slots were mounted vertically on the framework of the ground screen, providing a firm support for the glass mirror. The dielectric constant of the glass material was measured at 3-cm wavelength in a waveguide. The dielectric constant was found to be $\epsilon=4.5$ and the loss tangent $\tan \delta=0.005$. For the particular thickness and dielectric constant of the glass plate, the wavelength corresponding to the scale of the ordinate is plotted in Fig. 3 (circles). It can be seen that, with $\lambda=3.34$ cm and 1.23 cm, the transmission factor is very close to $d^2=0.5$. Since no absolute measurements of back-scattering cross section were intended, d^2 was not measured more precisely.

The absorption material around the ground screen consists of enmeshed graphitized animal hair ("Eccosorb"). The average reflection factor of this material for vertically incident waves was found to be about 10 per cent and tended to increase slightly at oblique incidence. Owing to the inclined position of the absorbers with respect to the wavefronts, the geometrically reflected energy is almost completely suppressed and only scattered radiation from the irregular surface actually comes into the measurement room. At 1-cm wavelength, the amplitude of this scattered wave corresponds to a reflection factor of 3 per cent, while at 3 cm, this value is about 2 per cent (see Fig. 6). The signal in the receiver due to this remaining reflection may be fully cancelled by proper adjustment of the absorbers in the other arm

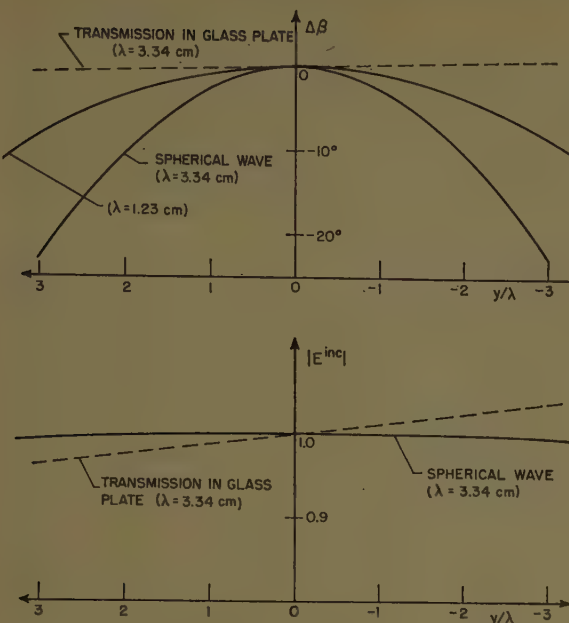


Fig. 5—Phase error and amplitude of the incident wave at the location of the obstacles.

of the measurement equipment, so that without the sample the received signal is below the noise level of the receiving apparatus. A systematic error is thereby introduced which, under the foregoing assumption, is at most in the order of magnitude of 6 per cent for a wavelength of 1 cm, and 4 per cent for a wavelength of 3 cm.

Transmitting and receiving antennas at a wavelength of 3 cm are two horns of equal dimensions with apertures of $17.5 \times 17.5 \text{ cm}^2$ (including the image formed by the metallic screen). The beamwidth is approximately

$$\alpha = \frac{\lambda}{D} \sim 10^\circ \quad (D = \text{length of the edges of the horn}).$$

For measurements at 1-cm wavelength, the aperture of the transmitting horn was $12 \times 12 \text{ cm}^2$ and that of the receiving horn $10 \times 10 \text{ cm}^2$; the beamwidths were 6.5 and 8 degrees, respectively. At a distance of $s = 230 \text{ cm}$ between the sample and the apex of the horns, and at an optical distance of 180 cm between sample and receiving horn, the far-zone condition

$$s \geq \frac{2D^2}{\lambda}$$

is sufficiently fulfilled.

Under the assumption that a spherical wave with a wavelength of 3.34 cm originates at the apex of the transmitter horn, the field distribution in the region of the sample, perpendicular to the direction of propagation, has been computed (Fig. 5, unbroken line). It must be remembered, however, that the glass mirror causes an additional field distortion. Applying simple ray optics, the effect of the mirror on the amplitude and phase of the field in the region of the sample also has been computed for the given dimensions of the dielectric sheet (dashed lines). Regarding the phase, the deviation of the

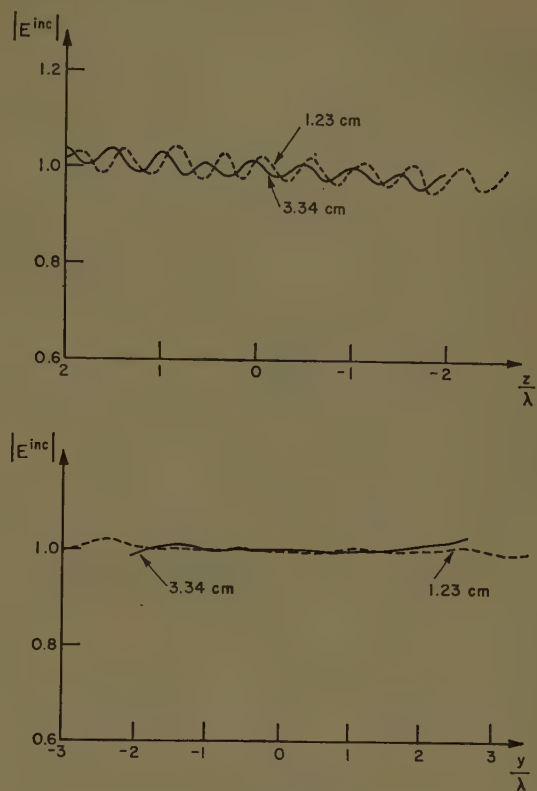


Fig. 6—Measured amplitude of the incident wave in the region of the obstacles.

actual field from a plane-wave distribution is mainly due to the spherical-wave nature of the transmitted signal. Regarding amplitude, the main deviations are due to the dependence of the reflection and transmission factor of the glass plate on the angle of incidence. At 1-cm wavelength, the phase distortion naturally is smaller, since the optical distance between source and sample is much larger.

In order to measure the amplitude of the electric field in the region of the sample, an inset has been constructed exactly fitting into the hole in the ground screen. The inset itself contains an eccentrically located smaller hole, also containing an inset, from which an eccentrically placed probe extends 5 mm above the ground screen. The probe can be rotated around the axis of the small inset. By this rotation and rotation of the large inset, the field in a circular region having a diameter of 14 cm can be investigated. The measured field strength along the y and z axes is plotted in Fig. 6. While the field along the y axis is nearly constant in the region of measurement, a superposition of E^{inc} with a weak wave reflected by the absorbers is indicated in the field distribution along the z axis.

MEASUREMENT OF THE BACK-SCATTERING CROSS SECTION OF CIRCULAR METALLIC DISKS

For a practical test and application of the measurement setup, the back-scattering cross sections of circular metallic disks (radius a) have been measured, and the experimental results have been compared with the

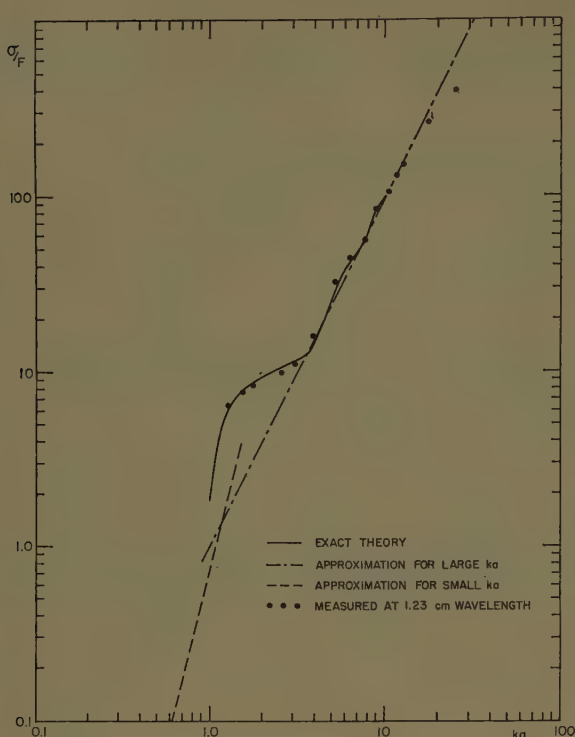


Fig. 7—Back-scattering cross section of plane conducting circular disks.

results of the exact theory of Andrejewski.⁸

The rigorous solution of the diffraction problem by Andrejewski yields, for the Hertz vector of the scattered wave in the far zone (for a vertically incident plane wave),

$$\begin{aligned} \Pi_x^{sc} &= \left\{ \frac{\epsilon_0 E^{inc}}{k^2} \bar{V}_0(\cos \theta; ka; 0) + kU_1(ka)[\bar{\phi}_0(\cos \theta; ka) \right. \\ &\quad \left. + \cos 2\phi \bar{\phi}_2(\cos \theta; ka)] \right\} \frac{e^{-j(k\rho - \omega t)}}{k\rho} \\ \Pi_y^{sc} &= kU_1(ka) \sin 2\phi \bar{\phi}_2(\cos \theta; ka) \frac{e^{-j(k\rho - \omega t)}}{k\rho}, \end{aligned} \quad (11)$$

where $\bar{V}_0(\cos \theta; ka; 0)$, $U_1(ka)$, and $\bar{\phi}_2(\cos \theta; ka)$ represent complex functions defined by Andrejewski,⁸ and θ, ϕ are the usual spherical coordinates. These expressions simplify in the special case of the field along the z axis ($\phi=0, \theta=0$), since in this case $\bar{\phi}_2(1, ka) \equiv 0$

$$\begin{aligned} E_x^{bsc} &= \frac{k^2}{\epsilon_0} \Pi_x^{bsc} \\ &= \left(E^{inc} \bar{V}_0(1; ka; 0) + \frac{k^3}{\epsilon_0} U_1(ka) \bar{\phi}_0(1; ka) \right) \frac{e^{-j(k\rho - \omega t)}}{k\rho} \end{aligned}$$

$$H_y^{bsc} = \frac{E_x^{bsc}}{z_0} \left(\text{with } z_0 = \sqrt{\frac{\mu_0}{\epsilon_0}} = 377 \Omega \right), \quad (12)$$

$$E_z^{bsc} = E_y^{bsc} = H_z^{bsc} = H_x^{bsc} = 0.$$

⁸ W. Andrejewski, "Die Beugung elektromagnetischer Wellen an der leitenden Kreisscheibe und an der kreisförmigen Öffnung im leitenden ebenen Schirm," thesis, Technische Hochschule, Aachen, Ger.; 1952.

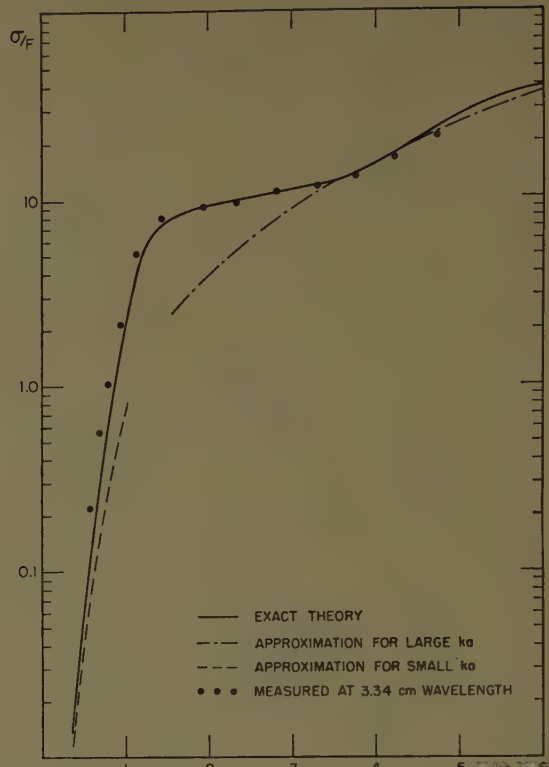


Fig. 8—Back-scattering cross section of plane conducting circular disks.

It follows with

$$U_1 = -\frac{\epsilon_0}{k^3} E^{inc} \cdot U$$

that the back-scattering cross section according to (6) is given by

$$\begin{aligned} \sigma &= 4\pi\rho^2 \left| \frac{E^{bsc}}{E^{inc}} \right|^2 \\ &= \frac{4\pi a^2}{k^2 a^2} \left| \bar{V}_0(1; ka; 0) - U(ka) \bar{\phi}_0(1; ka) \right|^2. \end{aligned} \quad (13)$$

Or, if F is the surface of the metallic disk

$$\frac{\sigma}{F} = \frac{4}{(ka)^2} \left| \bar{V}_0 - U \bar{\phi}_0 \right|^2. \quad (14)$$

The functions $\bar{V}_0(1; ka; 0)$, $\bar{\phi}_0(1; ka)$, and $U(ka)$ are given numerically by Andrejewski for a value of $ka=10$. In addition to this, fourteen values in the range of $0 < ka \leq 10$ have been newly computed by means of their defining equations. The numerical results are compiled in the Appendix. The calculated curves of the back-scattering cross section are contained in Figs. 7 and 8 as unbroken lines.

Of special interest for a comparison with the exact solution is the approximation for very small ka values as well as the Kirchhoff approximation for very large ka . In the case of small radii, the far-zone field can be represented by the field of an electric dipole of a moment⁸

$$m_x = -\frac{16}{3} \epsilon_0 E^{inc} \cdot a^3. \quad (15)$$

With the Poynting vector defined as

$$P^{bsc} = \frac{8}{9} \frac{k^4 a^6}{\pi^2 \rho^2 \cdot z_0} E^{inc^2}, \quad (16)$$

it follows, for the back-scattering cross section, that

$$\frac{\sigma}{F} = \frac{64}{9} \frac{(ka)^4}{\pi^2}. \quad (17)$$

The approximate solution of the diffraction of a plane wave by a circular disk with a radius large compared to the wavelength has been given by Severin.⁹ The field on the z axis in front of the metallic disk is found to be

$$E^{bsc} = E^{inc} \left(e^{jka} - \frac{z}{\sqrt{a^2 + z^2}} e^{j\sqrt{a^2 + z^2}} \right). \quad (18)$$

The expansion of this expression for large distances z yields

$$E^{bsc} = j \frac{ka}{2} E^{inc} e^{jka} \frac{a}{z}. \quad (19)$$

Therefore, the back-scattering cross section of large metallic disks is simply given by

$$\frac{\sigma}{F} = (ka)^2. \quad (20)$$

The evaluation of both approximations (Figs. 7 and 8, dashed line for $ka \ll 1$, dashed-pointed line $ka \gg 1$) shows a good agreement with the results of rigorous solution in the respective regions, $ka < 0.5$ and $ka > 3.5$.

For the experimental investigation, a number of samples have been made and the back-scattering cross section has been measured in the region $1.28 \leq ka \leq 25$ at 1.23-cm wavelength, and in the region $0.6 \leq ka \leq 4.75$ at 3.34-cm wavelength. For small diameters of the disks ($2a \leq 1.5$ cm) samples are milled out of 0.5-mm sheet brass, with a strip-type extension which is inserted into a matched slot on the ground screen to provide a support for the samples [Fig. 9(a)]. Larger samples are worked out of full material on a lathe and have the form of the quarter-discus sketched in Fig. 9(b). The base is about 2 mm thick and contains a 0.09-inch thread to support the sample. The thickness at the edge is less than 0.5 mm, and great care was taken to get very flat surfaces of the disks.

The results of the measurements are plotted in Fig. 7 (for $\lambda = 1.23$ cm) and Fig. 8 ($\lambda = 3.34$ cm), together with the rigorously calculated curve and the approximate solutions for large and small values of ka . In the experiment, the theoretical values of the back-scattering cross section for disks with $ka = 10.5$ (Fig. 7) and $ka = 2.82$ (Fig. 8) served as standards, and all numerical values of σ were obtained by relating the measured signals to the measured intensities of the scattered wave for these disks.

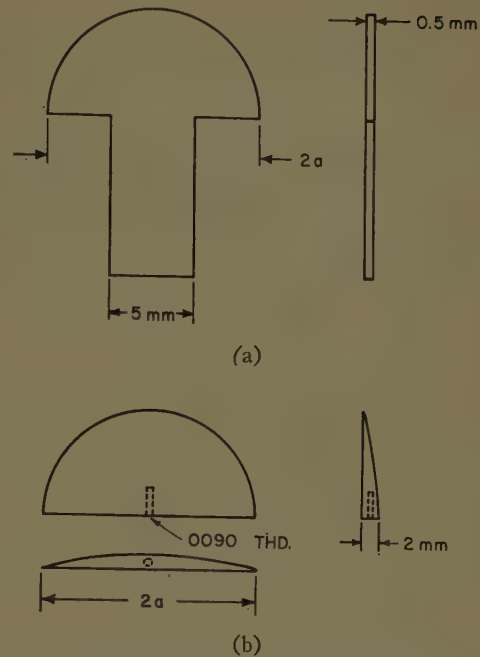


Fig. 9—(a) Shape of obstacles for $2a \leq 1.5$ cm.
(b) Shape of obstacles for $2a \geq 2$ cm.

In the region from $ka \geq 0.75$ to $ka \leq 17.5$, experimental and theoretical results are in nearly complete agreement. For larger values of ka ($ka > 17.5$), a noticeable discrepancy between measurement and theory occurs, due to the structure of the incident field which no longer can be considered a plane wave. A value of $ka = 17.5$ corresponds to a radius of 2.8 wavelengths. The phase error at the edge of the scattering object is about -7 degrees, assuming a spherical wave and a distance of $s = 230$ cm at 1.23-cm wavelength. The phase error rapidly increases with an increase in the dimensions of the disk, so that agreement cannot be expected for larger disks. As expected, the measured signal, i.e., the back-scattering cross section, is too small.

The deviation from the measured values at very small disks, however, is entirely due to the disturbing reflection from the surrounding absorber walls. The assumptions made while deriving the estimate of error (8) are no longer valid, since the small circular disks radiate in the form of a dipole in any direction. With P^{bsc} the Poynting vector of the scattered wave in the direction of the source and r the reflection factor of the mirror, the intensity

$$I_1 = r^2 P^{bsc} \cdot \overline{D^2} \quad (21)$$

will be received by the receiving horn, where $\overline{D^2}$ is the absorption cross section of the antenna, which is assumed to be perfectly matched. On the other hand, a total amount of energy⁸

$$I_2 = \oint P^{sc} df = \frac{128}{27} \frac{(ka)^4 \cdot a^2}{2\pi z_0} E^{inc^2} \quad (22)$$

is withdrawn from the wave, E^{inc} . Therefore, the compensation between both arms of the setup is disturbed,

⁹ H. Severin, "Beugung elektromagnetischer Zentimeterwellen an metallischen Kreisscheiben," *Z. angew. Physik*, vol. 2, pp. 499-505; December, 1950.

giving rise to a signal in the receiver with the maximum intensity

$$r^2 \cdot r_2^2 \cdot I_2,$$

where r_2 is the reflection factor of the surrounding wall. Inserting P^{bsc} (16) and comparing I_1 and I_2 yields, as a necessary condition for an exact measurement of σ at very small values of ka ,

$$\frac{8}{3} \pi r_2^2 \ll \frac{\overline{D^2}}{\rho^2}.$$

A more quantitative determination of the error in this case would involve a knowledge of the wave itself rather than the intensities. Within the order of magnitude, however, a comparison of the energies will give correct results. With $\overline{D^2} \sim D^2$ and the given dimensions ($D = 17.5$ cm, $\rho = 150$ cm, and $r_2 = 0.02$), the maximum error which should be expected is of the order of 25 per cent. This value corresponds fairly well with the actually observed deviation. It should be noted that this systematic error occurs in all methods depending on a direct compensation of the incident wave, in which the disturbing reflection of surrounding walls could not be avoided.

CONCLUSION

The smallest back-scattering cross section measured here is $0.01 \lambda^2$. No full use of the sensitivity of the method has yet been made due to low-power generators and (unnecessary) reflections from the surrounding

laboratory wall. The systematic limit, however, is only given by the beamwidth of transmitting and receiving antennas and their decoupling. It is estimated that this limit will be reached at back-scattering signals, which are at least a factor 10 or 100 smaller than the smallest measured here.

APPENDIX

The functions $\bar{V}(1; ka; 0)$, $\bar{\phi}_0(1; ka)$, and $\bar{U}_1(ka)$ are defined in Andrejewski's work.⁸ Numerical values have been additionally computed in Table I.

TABLE I

ka	$U(ka) = \frac{k^2}{\epsilon_0 E^{inc}} U_1(ka)$	$\bar{V}_0(1; ka; 0)$	$\bar{\phi}_0(1; ka)$
0.5	$1.224 - j0.067$	$0.313 + j0.102$	$0.300 + j0.098$
1.0	$1.792 - j0.949$	$0.594 + j0.421$	$0.494 + j0.356$
1.5	$0.347 - j2.251$	$0.831 + j0.987$	$0.508 + j0.672$
2.0	$-0.731 - j1.564$	$1.033 + j1.835$	$0.322 + j0.916$
2.5	$-1.084 - j1.033$	$1.238 + j2.978$	$-0.031 + j0.969$
3.0	$-1.260 - j0.637$	$1.487 + j4.392$	$-0.456 + j0.770$
3.5	$-1.474 - j0.497$	$1.748 + j6.039$	$-0.840 + j0.334$
4.0	$-1.757 + j0.456$	$2.046 + j7.900$	$-1.028 + j0.247$
5.0	$-0.608 + j2.237$	$2.519 + j12.349$	$-0.628 - j1.277$
6.0	$1.408 + j1.440$	$2.999 + j17.884$	$0.532 - j1.235$
7.0	$2.212 - j0.034$	$3.510 + j24.406$	$1.383 - j0.034$
8.0	$1.479 - j2.402$	$3.977 + j31.812$	$0.965 + j1.449$
9.0	$-1.444 - j2.209$	$4.525 + j40.400$	$-0.460 + j1.638$
10.0	$-2.583 - j0.363$	$5.024 + j49.916$	$-1.619 + j0.257$

ACKNOWLEDGMENT

The author wishes to express his thanks to Prof. R. W. P. King for his support of this work.

Scattering of a Surface Wave by a Discontinuity in Reactance*

ALAN F. KAY†

Summary—The following two-dimensional scattering problem is solved exactly by a Wiener-Hopf procedure. The incident field is a TM surface wave traveling in the positive x direction and guided by a reactive surface in the plane $z=0$. The surface has normal reactance X_0 if $x < 0$, and X_1 if $x > 0$. X_0 and X_1 are assumed positive and real. The discontinuity produces reflected and transmitted surface waves and a radiated field. Closed form expressions are found for the magnitudes of these fields. The reflected, radiated, and transmitted power flows, relative to that of the incident field, are plotted in universal curves. Conservation of energy is verified exactly.

* Manuscript received by the PGAP, December 24, 1957; revised manuscript received, August 25, 1958.

† Tech. Res. Group, New York, N. Y.

INTRODUCTION

PROBLEMS related to the guidance of surface waves over a reactive surface occur in antenna and transmission line theory and in some models of propagation over the earth. Before proceeding, it is well to say what is meant by a reactive surface in this paper. For a given monochromatic source one may define at any boundary point P , between two media A and B , the normal surface impedance looking into medium A as the ratio of tangential and mutually orthogonal components of E and H at P . More specifically, if a local rectangular coordinate system is chosen so that the unit vector i_z

coincides with the outward normal to medium A at P , then the normal surface impedance at P looking into medium A is a vector with two components Z and Z' , defined by

$$\frac{E_x}{H_y} = -Z \quad \frac{E_y}{H_x} = Z'.$$

In the general case, Z and Z' are functions of both P and the incident field. In this paper we are concerned only with a two-dimensional problem in which the field is TM , so that only the definition of Z plays a role. Moreover, we restrict our attention to flat surfaces of a special type in which Z is independent of both the particular field which is incident on the surface and the particular point on the surface. Despite these severe restrictions, such surfaces exist at least approximately and are of considerable importance. It is not hard to show that an interface between free space and a medium with electromagnetic parameters μ , ϵ , and σ has to first approximation a normal surface impedance of

$$Z_1 = \sqrt{\frac{i\mu\omega}{\sigma + i\omega\epsilon}}$$

provided that, as in the case of the earth, Z_1 is small in magnitude compared to the characteristic impedance $\sqrt{\mu_0/\epsilon_0}$ of free space [11]. Here and elsewhere, we assume a time dependence of $e^{-i\omega t}$. From the point of view of geometrical optics, one sees that a body of low impedance such as the earth constrains all rays just within its surface to be nearly normal to the surface regardless of the exterior angle of incidence. The impedance concept has been very useful in treating problems of propagation over the earth [11].

In this paper we are specifically concerned with lossless or reactive surfaces. In this case, we may define X by

$$X = i\sqrt{\frac{\epsilon_0}{\mu_0}} Z$$

as the normal surface reactance, normalized to free space, and X will be real. By a reactive surface in this paper we mean, therefore, one which imposes a boundary condition on any incident field which can be characterized by a single number, the reactance X . Such a surface may be realized approximately by corrugating a perfect conductor with rectangular grooves, spaced a distance D apart with groove depth d and groove width g [9], [10]. If D is small compared to the wavelength λ , then

$$X \simeq \frac{g}{D} \tan\left(\frac{2\pi d}{\lambda}\right).$$

One should note that such a surface is anisotropic, i.e., $Z' \neq Z$, and in any experiment where the three-dimensional nature of the world becomes important, the

present theory must be used with caution. It is also noteworthy that both inductive and capacitive surfaces may be made, depending on whether the integer part of $4d/\lambda$ is even or odd, respectively.

The dielectric clad ground plane, on the other hand, is an example of a surface whose normal impedance depends on the incident field unless the dielectric constant is large. In particular for an incident plane wave the reactance depends strongly on incidence angle even if the dielectric is thin compared to the wavelength [9]. The "fakir's bed," which is a regular array of metal pins normal to a flat metal surface, is a further example.

In experiments performed at Technical Research Group, (TRG, Inc.) with a fakir's bed, we have found that for all pin heights L , in the range $0 < L < 0.4\lambda$, with a pin spacing of 0.2λ and pin diameter of 0.05λ , the normal surface reactance clearly depends on the angle of incidence of an incident plane wave. The dependence in this case has also been verified theoretically. Even with such surfaces as the dielectric clad ground plane and fakir's bed, however, we feel that the theory in this paper is useful for semiquantitative studies of surface waves.

In this paper we assume that a surface wave is traveling over an infinite plane reactive surface, and we solve exactly for what happens when an abrupt discontinuity occurs in the value of the reactance. The material presented here was obtained under sponsorship of the AFCRC and appeared in a recent report [3], which also contained several applications of the results. It is hoped that descriptions of the applications will also be published when they have been more fully investigated experimentally.

A special case of this problem, namely zero reactance on the transmitted side of the discontinuity, was previously solved independently by Bazer [1] and Senior [4]. Our method, and indeed, much of our notation, follows Bazer. Bazer was apparently unaware, however, of the great simplification which follows from neglecting phase and considering only the generally more important quantities, the magnitudes of the reflected and transmitted surface waves and of the radiated field. This simplification was first pointed out to the author by J. Lurye of TRG. Lurye, several years ago, in unpublished notes, worked out the detailed solution of Bazer's paper and obtained an energy balance in that case. Our paper may be considered, therefore, a direct generalization of Lurye's work.

Weill [8] has also considered the general problem and obtained formulas for the transmitted, reflected, and radiated fields, which are similar to (25), (26), and (31) here. Aside from notation and other minor differences in these formulas, his formula for the radiated field has several misprints. Weill's [8] expansion¹ for the transmission coefficient for "loosely bound surface waves," (small X_0, X_1 case, in our notation), is also in error.

¹ See especially p. 246.

The chief original contributions of the present paper are the explicit formulas for the reflected, transmitted, and radiated field magnitudes, in which all contour integrals have been explicitly evaluated. The resulting formulas are suitable for simple computation, and numerical results obtained from them are presented here graphically.

WIENER-HOPF SOLUTION OF A STEP DISCONTINUITY
IN THE NORMAL REACTANCE OF A PLANE
BOUNDING A HALF-SPACE (SEE FIG. 1)

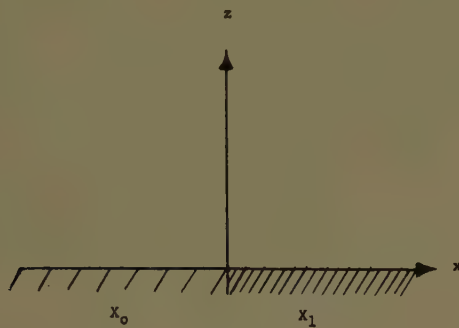


Fig. 1.

Suppose a TM surface wave traveling in the positive x direction is guided by a reactive surface of normal reactance X_0 . The only component of H in this incident field is the y component, normal to the paper, and it may be written in the form

$$h_{inc}(x, z) = e^{im_0x - kX_0z}, \quad z \geq 0, \quad m_0 = k\sqrt{1 + X_0^2}. \quad (1)$$

For $x > 0$ the normal reactance is assumed to change abruptly to a value X_1 . This discontinuity in the reactance at the origin causes a scattered field $h_s(x, z)$ which generally consists of transmitted and reflected surface waves and a radiation field. If we assume a slight conductivity in space, then $h_s(x, z)$ is exponentially small at great distances from the origin, and we may write it in the form

$$h_s(x, z) = (1/2\pi) \int_{-\infty}^{\infty} H(u) e^{i(ux + wz)} du \quad (2)$$

where

$$w = \sqrt{k^2 - u^2} \quad \text{or} \quad i\sqrt{u^2 - k^2}. \quad (3)$$

To properly define the branch of the square root, we have written w in (3) so that if the conductivity vanishes and if u is real, the square roots must be positive [1], [2]. Now²

$$\frac{\partial h_s(x, z)}{\partial z} = (1/2\pi) \int_{-\infty}^{\infty} iwH(u) e^{i(ux + wz)} du. \quad (4)$$

It follows from the definition of normal reactance that

$$\begin{aligned} \frac{\partial}{\partial z} (h_s(x, 0) + h_{inc}(x, 0)) \\ = -kX_0(h_s(x, 0) + h_{inc}(x, 0)), \quad x < 0 \\ \frac{\partial}{\partial z} (h_s(x, 0) + h_{inc}(x, 0)) \\ = -kX_1(h_s(x, 0) + h_{inc}(x, 0)), \quad x > 0. \end{aligned} \quad (5)$$

We now define functions $f^-(u)$ and $g^+(u)$ as follows:

$$\begin{aligned} (ikX_0 - w)H(u) &= f^-(u) \\ (ikX_1 - w)H(u) + \frac{k(X_1 - X_0)}{u - m_0} &= g^+(u). \end{aligned} \quad (6)$$

Using (2), (4), and (5) we may write (6) as

$$\begin{aligned} f^-(u) &= i \int_0^{\infty} \left[kX_0 h_s(x, 0) + \frac{\partial}{\partial z} h_s(x, 0) \right] e^{-iux} dx \\ g^+(u) &= i \int_{-\infty}^0 \left(kX_1 h_s(x, 0) + \frac{\partial}{\partial z} h_s(x, 0) \right) e^{-iux} dx. \end{aligned} \quad (7)$$

From (7) it follows that $f^-(u)$ is analytic in the lower half-plane and $g^+(u)$ is analytic in the upper half-plane. In the strip $-\text{Im } k < u < \text{Im } k$, where $\text{Im } k$ is the imaginary part of k , both functions are analytic. From (7),

$$\frac{\sigma_1(u)}{\sigma_0(u)} f^-(u) + \frac{k(X_1 - X_0)}{u - m_0} = g^+(u), \quad (8)$$

where, in analogy with the definition (3.13) of [1],

$$\begin{aligned} \sigma_1(u) &= 1 - \frac{a_1}{\sqrt{u^2 - k^2}} = \frac{\sigma_1^+(u)}{\sigma_1^-(u)} \\ \sigma_0(u) &= 1 - \frac{a_0}{\sqrt{u^2 - k^2}} = \frac{\sigma_0^+(u)}{\sigma_0^-(u)} \end{aligned} \quad (9)$$

where

$$a_1 = kX_1, \quad a_0 = kX_0, \quad (10)$$

and the new functions in (9), $\sigma_j^{\pm}(u)$, $j = 0$ or 1, are the Wiener-Hopf factors³ defined by (4.6) of [1] as:

$$\sigma_j^{\pm}(u) = \exp \left\{ (-1/2\pi i) \int_{-\infty \mp i\beta}^{\infty \mp i\beta} \frac{\log \left(1 - \frac{a_j}{\sqrt{z^2 - k^2}} \right) dz}{u - z} \right\}, \quad 0 < \beta < \text{Im } k. \quad (11)$$

In view of (9) we may write (8) as

$$\begin{aligned} \frac{\sigma_0^-(u)}{\sigma_1^-(u)} f^-(u) + \frac{k(X_1 - X_0)\sigma_0^+(m_0)}{(u - m_0)\sigma_1^+(m_0)} \\ = \frac{-k(X_1 - X_0)}{(u - m_0)} \left[\frac{\sigma_0^+(u)}{\sigma_1^+(u)} - \frac{\sigma_0^+(m_0)}{\sigma_1^+(m_0)} \right] + \frac{g^+(u)\sigma_0^+(u)}{\sigma_1^+(u)}. \end{aligned} \quad (12)$$

² See p. 12 of Bazer [1].

³ The Wiener-Hopf factorization procedure is also described in the more readily accessible reference [12].

The left member of (12) is analytic in the lower half-plane, the right member in the upper half-plane. There is an overlapping strip of analyticity, for the $\sigma_j^\pm(u)$ are analytic and not zero in this strip and in the indicated half-plane, whether $j=0$ or 1. It can also be shown, following the argument of [1], that both members of (12) are bounded by a constant for large $|u|$. By the Liouville Theorem, we have then,

$$f^-(u) = \frac{k(X_1 - X_0)\sigma_0^+(m_0)\sigma_1^-(u)}{(m_0 - u)\sigma_0^+(m_0)\sigma_1^-(u)}$$

$$g^+(u) = \frac{k(X_1 - X_0)}{(u - m_0)} \left[1 - \frac{\sigma_1^+(u)\sigma_0^+(m_0)}{\sigma_0^+(u)\sigma_1^+(m_0)} \right]. \quad (13)$$

From (2) and (7) we obtain the general solution for the scattered field,

$$h_s(x, z) = \frac{k(X_0 - X_1)}{2\pi i} \int_{-\infty}^{\infty} \frac{\sigma_0^+(m_0)\sigma_1^-(u)e^{i(ux+wz)}du}{\sigma_1^+(m_0)\sigma_0^-(u)(u - m_0)(kX_0 - \sqrt{u^2 - k^2})}. \quad (14)$$

Let us now seek expressions for the radiation field, and the transmitted and reflected surface waves, by evaluating (14) asymptotically at large distances from the origin. Before doing so we need additional properties of the functions $\sigma_j^\pm(u)$. From the definition we see that

$$\sigma_j^+(u) = \frac{1}{\sigma_j^-(u)} \quad j = 0 \text{ or } 1 \quad (15)$$

We, therefore, need consider in detail only $\sigma_j^-(u)$. We drop the subscript for the time being in order to deal with both cases simultaneously. We observe that since the integral in (11) is analytic (except for branch points at $\pm k$ and logarithmic singularities at $z = \pm m$), and since the integrand is $0(1/|z|^2)$ for large $|z|$, we may deform the given integration contour to a new contour, II+I, shown in Fig. 2.

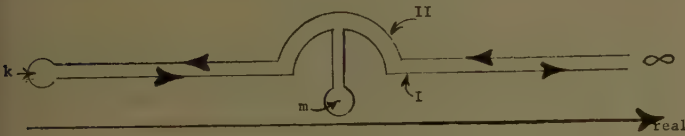


Fig. 2.

Without changing the value of $\sigma^-(u)$, this contour may be deformed slightly at any point except at $z=k$ and $z=m$ where the singularities of the integrand occur. This shows that $\sigma^-(u)$ is analytic and nonzero (though multivalued) everywhere except possibly at k and m . And hence, in view of (15), $\sigma^+(u)$ is regular and nonzero everywhere except possibly at $u=-k$ or $-m$. It is important to know the singularities at these points. From (9) we may write

$$\sigma^-(u) = \frac{\sigma^+(u)\sqrt{u^2 - k^2}}{\sqrt{u^2 - k^2} - a}. \quad (16)$$

Since $\sigma^+(u)$ is regular and not zero at $u=k$, we see that $\sigma^-(u)$ has a branch point and zero of order one-half at $u=k$. Again since $\sigma^+(u)$ is regular and nonzero at $u=m$, we see that $\sigma^-(u)$ has a simple pole at $u=m$ with residue

$$\text{res } \sigma^-(u) = \frac{2\pi i a^2}{m} \sigma^+(m). \quad (17)$$

Likewise $\sigma^+(u)$ has a branch point and singularity of order minus one-half at $u=-k$, and a zero at $u=-m$:

$$\lim_{u \rightarrow -m} \frac{\sigma^+(u)}{u + m} = \frac{-m\sigma^+(-m)}{a^2}. \quad (18)$$

Another useful relation follows from (9) and (15):

$$\sigma^-(u) = \frac{\sigma^+(u)}{\sigma(u)} = \frac{1}{\sigma(u)\sigma^+(-u)}. \quad (19)$$

Hence

$$\sigma^-(u)\sigma^+(-u) = \frac{1}{\sigma(u)}. \quad (20)$$

A. Transmitted Surface Wave

For x large and positive, we may deform the contour in (14) to a line I) parallel to the original contour which was along the real axis, 2) slightly in the upper half-plane, and 3) indented below at the singularities of the integrand which occur at $u=k$, m_0 , and m_1 , where

$$m_0 = k\sqrt{1 + X_0^2}, \quad m_1 = k\sqrt{1 + X_1^2}. \quad (20a)$$

The contribution of this contour other than in the immediate neighborhood of the singularities is negligible because of the rapid damping of the exponential term $\exp(iux + iwz)$ for large x . Provided neither X_0 nor X_1 is zero, the contribution in the neighborhood of $u=k$ corresponds to a radiation field with decay of the order e^{ikx}/x for large x . This follows from the fact that the integrand is bounded at the branch point $u=k$ so that the integral is dominated by some integral of the form

$$M \int_{\text{Im } k}^{\infty} e^{-xv} dv = 0 \left(\frac{e^{-\text{Im } kx}}{x} \right), \quad (21)$$

where v is the imaginary part of u . It is worth noting that the radiation far field, which in general decays like $r^{-1/2}$ in a two-dimensional problem, has therefore a null in the direction parallel to the positive x axis. This will be demonstrated again when we obtain the expression for the radiation field (69).

At $u=m_0$ and m_1 we have simple poles. The residue of the pole at $u=m_0$ may be calculated as follows. We note that

$$\frac{\sigma_0^+(m_0)}{\sigma_0^-(u)(kX_0 - \sqrt{u^2 - k^2})} = \frac{-\sigma_0^+(m_0)}{\sigma_0^-(u)\sigma(u)\sqrt{u^2 - k^2}}. \quad (22)$$

In view of (9), as $u \rightarrow m_0$, the factor in (22) approaches $-1/kX_0$. The residue at $u = m_0$ of (14) is thus

$$\left[\frac{X_1 - X_0}{X_0} \right] \frac{\sigma_1^-(m_0)}{\sigma_1^+(m_0)} e^{im_0x - kX_0z} = \frac{(X_1 - X_0) e^{im_0x - kX_0z}}{X_0 \sigma_1(m_0)}. \quad (23)$$

Since from (9)

$$\sigma_1(m_0) = 1 - X_1/X_0, \quad (24)$$

we see that this surface wave exactly cancels that of the incident field. Of course, since no wave with vertical attenuation constant kX_0 can propagate over a boundary with normal reactance X_1 not equal to X_0 , it is physically necessary to have such total cancellation. We may look upon this result, therefore, as a check on our work. From (14) and (17) we find the residue at $u = m_1$ to be

$$h_t(x, z) = \left[\frac{\sigma_0^+(m_0) \sigma_1^+(m_1) (kX_1)^2 e^{im_1x - kX_1z}}{\sigma_1^+(m_0) \sigma_0^-(m_1) m_1 (m_1 - m_0)} \right]. \quad (25)$$

Since we have shown that (25) is the dominant term in the field at large positive values of x , with z fixed, the subscript t is used to indicate the "transmitted" field. It is clearly a pure surface wave. As a check on this

C. The Radiation Field

The radiation field may be determined from (14) by a stationary phase evaluation of the integral.

Setting

$$x = r \cos \theta, \quad z = r \sin \theta, \quad (27)$$

the stationary phase point occurs at

$$u = k \cos \theta, \quad w = k \sin \theta, \quad \sqrt{u^2 - k^2} = -ik \sin \theta. \quad (28)$$

In the neighborhood of this point

$$ux + wz = kr - \frac{r(u - k \cos \theta)^2}{2k \sin^2 \theta} + 0(u - k \cos \theta)^3, \quad (29)$$

and with the usual stationary phase assumptions,

$$h_s(x, z) \sim \frac{k(X_0 - X_1)}{2\pi i} \sqrt{\frac{\pi 2k \sin^2 \theta}{ir}} \frac{\sigma_0^+(m_0) \sigma_1^-(k \cos \theta)}{\sigma_1^+(m_0) \sigma_0^-(k \cos \theta)} \frac{e^{ikr}}{(k \cos \theta - m_0)(kX_0 + ik \sin \theta)} \text{ as } r \rightarrow \infty. \quad (30)$$

Thus, the radiation field, indicated by a subscript R is

$$h_R(x, z) = \left[\frac{(X_0 - X_1) \sigma_1^-(m_0) \sigma_1^-(k \cos \theta) \sin \theta e^{ikr}}{[\cos \theta - \sqrt{1 + X_0^2}](X_0 + i \sin \theta) \sigma_0^-(m_0) \sigma_0^-(k \cos \theta) \sqrt{-2i\pi kr}} \right]. \quad (31)$$

formula, by substituting $\sigma_0^+(m_1)/\sigma_0^-(m_1)$ for $\sigma_0^-(m_1)$, it is not hard to show that if X_1 approaches X_0 ,

$$h_t(x, z) \rightarrow e^{im_0x - kX_0z}, \quad X_1 \rightarrow X_0,$$

as it should.

B. Reflected Wave

If x is large and negative, (14) may be evaluated by deforming the contour to a line, 1) parallel to the original contour (which was along the real axis), 2) slightly in the lower half plane, and 3) indented above at the singularities of the integrand which occur at $u = -k$ and $u = -m_0$. As in the case of the transmitted wave, the singularity at k gives rise to the radiation field which is negligible in the limit of the lossless case, in comparison to the contribution from the singularity at $u = -m_0$. The latter, we shall now show, gives rise to the reflected surface wave.

The residue at $u = -m_0$ is

$$h_r(x, z) = \frac{k(X_0 - X_1)(kX_0) \sigma_0^+(m_0) \sigma_1^-(m_0)}{2(k\sqrt{1 + X_0^2})^2 \sigma_1^+(m_0) \sigma_0^-(m_0)} e^{-im_0x - kX_0z} \quad (26)$$

Allowing for the change in notation, and the fact that Bazer's θ is $\pi - \theta$ here, we find that (31) with X_1 set equal to zero, agrees with (8),⁴ of Bazer [1], as it should.

D. Evaluation of Reflected, Transmitted, and Radiated Fields

To evaluate the scattered fields, $h_r(x, z)$, $h_t(x, z)$, and $h_R(x, z)$, it is desirable to obtain closed form expressions for $\sigma^-(u)$. While this does not appear to be entirely possible, we can find expressions suitable for computation. More important, simple closed form expressions will be obtained for $|\sigma^-(u)|$, and these are all that is required for a complete description of power flow. The method is based upon the fact that the derivative with respect to a of the exponent in $\sigma^-(u)$ in (11) is explicitly integrable with respect to z . We first note that if a is sufficiently small,

$$\left| \log \left(1 - \frac{a}{\sqrt{z^2 - k^2}} \right) \right| < \frac{2a}{|\sqrt{z^2 - k^2}|}. \quad (32)$$

Hence for any fixed real u , it follows from (11) and (32) that

$$\lim_{a \rightarrow 0} \sigma_j^\pm(u) = 1. \quad (33)$$

Now $\sigma^-(u)$ may be expressed as an integral along the contour of Fig. 2 as follows:

⁴ See p. 13.

and this is the reflected surface wave, indicated by a subscript r .

$$\sigma^-(u) = \exp \left\{ \frac{I - J}{-2\pi i} \right\}, \quad (34)$$

where

$$I = \int_{\Gamma k}^{\infty} \frac{\log \left(1 - \frac{a}{\sqrt{z^2 - k^2}} \right)}{u - z} dz, \quad (35)$$

$$J = \int_{\Pi k}^{\infty} \frac{\log \left(1 + \frac{a}{\sqrt{z^2 - k^2}} \right)}{u - z} dz.$$

Differentiation yields

$$\frac{\partial I}{\partial a} = \int_{\Gamma k}^{\infty} \frac{dz}{(\sqrt{z^2 - k^2} - a)(z - u)}, \quad (36)$$

$$\frac{\partial J}{\partial a} = \int_{\Pi k}^{\infty} \frac{dz}{(\sqrt{z^2 - k^2} + a)(u - z)}.$$

By means of Cauchy's Theorem, we may eliminate the need for the contour I and write

$$\frac{\partial I}{\partial a} = \int_{\Pi k}^{\infty} \frac{dz}{(\sqrt{z^2 - k^2} - a)(z - u)} + \frac{2\pi i a}{(m - u)m}, \quad (37)$$

where the last term is the residue obtained from crossing the pole at $z = m$. Thus

$$K = \frac{\partial(I - J)}{\partial a}$$

$$= 2 \int_{\Pi k}^{\infty} \frac{\sqrt{z^2 - k^2}}{(z^2 - m^2)(z - u)} dz + \frac{2\pi i a}{(m - u)m}, \quad (38)$$

where K is defined by (38). From (33), (34), and (38),

$$\sigma^-(u) = \exp \left\{ - \int_0^a \frac{K da}{2\pi i} \right\}. \quad (39)$$

We may evaluate the integral in (38) explicitly. To do so it is first desirable to evaluate for real k and M

$$L(t) = \int_k^M \frac{\sqrt{z^2 - k^2}}{z - t} dz, \quad k < t < M, \quad (40)$$

where the contour is indented above at $z = t$. For in terms of this simpler integral we have

$$K = 2 \lim_{M \rightarrow \infty} (AL(m) + BL(-m) + CL(u))$$

$$+ \frac{2\pi i a}{(m - u)m} \quad (41)$$

where A , B , and C are the coefficients of the partial fraction expansion of

$$\frac{1}{(z^2 - m^2)(z - u)} = \frac{A}{z - m} + \frac{B}{z + m} + \frac{C}{z - u}. \quad (42)$$

From (42),

$$A = \frac{1}{2m(m - u)}, \quad B = \frac{1}{2m(m + u)}, \quad C = \frac{1}{u^2 - m^2} \quad (43)$$

and

$$A + B + C = 0$$

$$A(m - u) = B(m + u)$$

$$-muA + muB - m^2C = 1. \quad (44)$$

If by setting $z - t = u$, we write $L(t)$ in the form

$$L(t) = \int_{k-t}^{M-t} \frac{\sqrt{u^2 + 2iu + t^2 - k^2}}{u} du, \quad (45)$$

we may evaluate $L(t)$ by means of standard integral tables (e.g., Pierce,⁵). However, we must be careful to handle the singularity at $u = 0$ properly. Since the indentation is above the origin, this is accomplished if we take

$$L(t) = \lim_{\epsilon \rightarrow 0^+} \left[\int_{k-t}^{-\epsilon} + \int_{\epsilon}^{M-t} \right]$$

$$\frac{\sqrt{u^2 + 2ut + t^2 - k^2}}{u} du - \pi i \sqrt{t^2 - k^2}. \quad (46)$$

Use of the tables then yields

$$L(t) = \sqrt{M^2 - k^2} + t \log \left(\frac{M + \sqrt{M^2 - k^2}}{k} \right) - \pi i \sqrt{t^2 - k^2}$$

$$- \sqrt{t^2 - k^2} \log \left\{ \frac{\sqrt{M^2 - k^2} + \sqrt{t^2 - k^2} + \frac{t}{\sqrt{t^2 - k^2}}}{\frac{k}{\sqrt{t^2 - k^2}}} \right\}. \quad (47)$$

Because of the first two of the relations (44), the first two terms on the right of (47) do not contribute in the summation in (41). That is

$$K = 2(AL_1(m) + BL_1(-m) + CL_1(u)) + \frac{2\pi i a}{(m - u)m}, \quad (48)$$

where $L_1(t)$ is obtained by dropping the first two terms of $L(t)$ in (47) and letting $M \rightarrow \infty$. We obtain

$$L_1(t) = -\sqrt{t^2 - k^2} \left[\log \left(\frac{\sqrt{t^2 - k^2} + t}{k} \right) + \pi i \right]. \quad (49)$$

This relation holds only for $k < t < \infty$. If $-\infty < t < k$, we must determine the correct branch of the logarithm by analytic continuation. As t decreases from $+\infty$ to $-\infty$, following the correct indentations at $\pm k$, the function $\sqrt{t^2 - k^2} + t$ traces a curve shown in the complex plane in Fig. 3. When t is less than $-k$, the logarithm of $t + \sqrt{t^2 - k^2}$ has an imaginary part of $-\pi i$. Thus

⁵ B. O. Pierce, "Short Table of Integrals," Ginn and Co., Boston, Mass., p. 26; 1929.

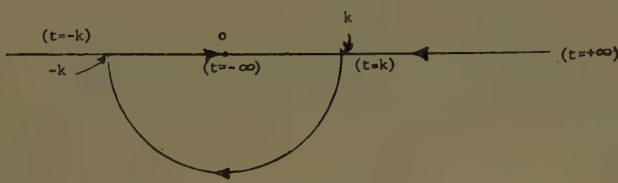


Fig. 3.

$$L_1(t) = -\sqrt{t^2 - k^2} \left[\log \left| \frac{t + \sqrt{t^2 - k^2}}{k} \right| \right], \quad -\infty < t < -k, \quad (50)$$

and

$$L_1(t) = i\sqrt{k^2 - t^2} \left[\log \left(\frac{t - i\sqrt{k^2 - t^2}}{k} \right) + \pi i \right], \quad t^2 < k^2, \quad (51)$$

where the principal branch of the logarithm (with imaginary part between 0 and $-\pi$) is implied. It is perhaps worth noting, that if we set

$$t = k \sin \theta, \quad (52)$$

then

$$L_1(t) = -k(\pi/2 + \theta) \cos \theta, \quad t^2 < k^2. \quad (53)$$

From (43), (48), (50), and (51), we obtain

$$\begin{aligned} K &= \frac{-a}{m(m-u)} \left[\log \left(\frac{m+a}{k} \right) - \pi i \right] \\ &\quad - \frac{a}{m(m+u)} \log \left(\frac{m-a}{k} \right) \\ &\quad - \frac{2\sqrt{u^2 - k^2}}{u^2 - m^2} \left[\log \left(\frac{\sqrt{u^2 - k^2} + u}{k} \right) + \pi i \right] \\ &= \frac{-2au}{m(m^2 - u^2)} \log \left(\frac{m+a}{k} \right) + \frac{\pi ia}{m(m+u)} \\ &\quad - \frac{2\sqrt{u^2 - k^2}}{u^2 - m^2} \left[\log \left(\frac{\sqrt{u^2 - k^2} + u}{k} \right) + \pi i \right]. \end{aligned} \quad (54)$$

Eq. (54) holds for all u if we stipulate the branch of the logarithm of $(\sqrt{u^2 - k^2} + u)/k$, as the one whose imaginary part lies between 0 and $-\pi$. From (39) and (54)

$$\begin{aligned} \sigma^-(u) &= \exp \left\{ \frac{u}{\pi i} I_0 - \frac{I_1}{2} \right. \\ &\quad \left. + \frac{\sqrt{u^2 - k^2}}{\pi i} \left[\log \left(\frac{\sqrt{u^2 - k^2} + u}{k} \right) + \pi i \right] I_2 \right\}, \end{aligned} \quad (55)$$

where

$$\begin{aligned} I_0 &= \int_0^a \frac{y \log \left[\frac{p+y}{k} \right] dy}{p(p^2 - u^2)} \\ &= \int_0^{\sinh^{-1}(a/k)} \frac{kt \sinh t dt}{k^2 \cosh^2 t - u^2}, \end{aligned} \quad (56)$$

where we have set

$$p = \sqrt{k^2 + y^2}, \quad (57)$$

and

$$I_1 = \int_0^a \frac{y dy}{p(p-u)} = \log \left[\frac{u - \sqrt{k^2 + a^2}}{u - k} \right], \quad (58)$$

$$\begin{aligned} I_2 &= \int_0^a \frac{dy}{u^2 - k^2 - y^2} \\ &= \frac{1}{2\sqrt{u^2 - k^2}} \log \left(\frac{\sqrt{u^2 - k^2} + a}{\sqrt{u^2 - k^2} - a} \right). \end{aligned} \quad (59)$$

[Note: The integrations in (58) and (59) may be readily verified by differentiating both members with respect to a . The second form of (56) follows from the substitution $\log [(p+y)/k] = t$.]

These integrals hold in the limit for real u and real a , provided the branch of the logarithm is chosen so that

$$\lim_{a \rightarrow 0} I_1 = \lim_{a \rightarrow 0} I_2 = 0, \text{ all } u. \quad (60)$$

It is desirable now to express $\sigma^-(u)$ in a form which clearly shows the real and imaginary quantities in the exponent. In the following equations we assume that the imaginary part of k has vanished. We first observe that for real u and k if $k^2 < u^2 < k^2 + a^2$,

$$I_2 = \frac{1}{2\sqrt{u^2 - k^2}} \left(\log \left(\frac{a + \sqrt{u^2 - k^2}}{a - \sqrt{u^2 - k^2}} \right) + \pi i \right) \quad (61)$$

and if, $u^2 < k^2$,

$$\begin{aligned} \text{Im } I_2 &= \text{Im} \left(-\frac{1}{2i\sqrt{k^2 - u^2}} \right. \\ &\quad \left. \cdot \log \left(\frac{a - i\sqrt{k^2 - u^2}}{-a - i\sqrt{k^2 - u^2}} \right) \right) = 0. \end{aligned} \quad (62)$$

We also note that I_0 is real unless $k^2 < u^2 < k^2 + a^2$, in which case

$$\begin{aligned} I_0 &= PV \int_0^a \frac{y \log \left(\frac{p+y}{k} \right) dy}{p(p^2 - u^2)} \\ &\quad - \frac{\pi i}{2|u|} \log \left(\frac{|u| + \sqrt{u^2 - k^2}}{k} \right), \end{aligned} \quad (63)$$

where PV means the principal value of the integral. Thus

$$\text{Im } I_0 = \begin{cases} 0, & u^2 < k^2 \text{ or } u^2 > k^2 + a^2 \\ \frac{-\pi}{2|u|} \log \left(\frac{|u| + \sqrt{u^2 - k^2}}{k} \right), & k^2 < u^2 < k^2 + a^2, \end{cases}$$

$$\text{Re } I_0 = PV \int_0^a \frac{y \log \left(\frac{\sqrt{k^2 + y^2} + y}{k} \right) dy}{\sqrt{k^2 + y^2}(k^2 + y^2 - u^2)}. \quad (64)$$

We have, finally, the following expression for $\sigma^-(u)$.

$$\begin{aligned}
 \sigma^-(u) &= \left(\frac{u - k}{u - \sqrt{k^2 + a^2}} \right)^{1/2} \exp \left\{ \frac{u \operatorname{Re} I_0}{\pi i} + \frac{1}{2\pi i} \left[\log \left(\frac{\sqrt{u^2 - k^2} + u}{k} \right) + \pi i \right] \left[\log \left(\frac{\sqrt{u^2 - k^2} + a}{\sqrt{u^2 - k^2} - a} \right) \right] \right\}, \\
 &\quad \text{if } u > \sqrt{k^2 + a^2}; \\
 &= \left(\frac{u - k}{u - \sqrt{k^2 + a^2}} \right)^{1/2} \exp \left\{ \frac{u}{\pi i} \left(\operatorname{Re} I_0 - \frac{\pi i}{2u} \log \left| \frac{u + \sqrt{u^2 - k^2}}{k} \right| \right) \right. \\
 &\quad \left. + \frac{1}{2\pi i} \left[\log \left(\frac{\sqrt{u^2 - k^2} + u}{k} \right) + \pi i \right] \left[\log \left(\frac{a + \sqrt{u^2 - k^2}}{a - \sqrt{u^2 - k^2}} \right) + \pi i \right] \right\}, \text{ if } k < u < \sqrt{k^2 + a^2}; \\
 &= \left(\frac{u - k}{u - \sqrt{k^2 + a^2}} \right)^{1/2} \exp \left\{ \frac{u \operatorname{Re} I_0}{\pi i} + \frac{1}{2\pi i} \left[\log \left(\frac{u - i\sqrt{k^2 - u^2}}{k} \right) + \pi i \right] \left[\log \left(\frac{a - i\sqrt{k^2 - u^2}}{a + i\sqrt{k^2 - u^2}} \right) + \pi i \right] \right\}, \\
 &\quad \text{if } u^2 < k^2; \\
 &= \left(\frac{u - k}{u - \sqrt{k^2 + a^2}} \right)^{1/2} \exp \left\{ \frac{u}{\pi i} \left(\operatorname{Re} I_0 + \frac{\pi i}{2u} \log \left| \frac{-u + \sqrt{u^2 - k^2}}{k} \right| \right) \right. \\
 &\quad \left. + \frac{1}{2\pi i} \left[\log \left| \frac{u + \sqrt{u^2 - k^2}}{k} \right| \right] \left[\log \left(\frac{\sqrt{u^2 - k^2} + a}{a - \sqrt{u^2 - k^2}} \right) + \pi i \right] \right\}, \text{ if } -\sqrt{k^2 + a^2} < u < -k; \\
 &= \left(\frac{u - k}{u - \sqrt{k^2 + a^2}} \right)^{1/2} \exp \left\{ \frac{u \operatorname{Re} I_0}{\pi i} + \frac{1}{2\pi i} \left[\log \left| \frac{u + \sqrt{u^2 - k^2}}{k} \right| \right] \left[\log \left(\frac{\sqrt{u^2 - k^2} + a}{\sqrt{u^2 - k^2} - a} \right) \right] \right\}, \\
 &\quad \text{if } -\sqrt{k^2 + a^2} > u. \quad (65)
 \end{aligned}$$

As a check on this result, it is not hard to verify (20). A further check results from the verification that $\sigma^-(u)$ has a zero of order one half at $u = k$ and a simple pole at $u = \sqrt{k^2 + a^2}$.

We obtain considerable simplification if we consider the magnitude of $\sigma^-(u)$. Taking the square of the magnitude of (65) yields

$$|\sigma^-(u)|^2 = \begin{cases} \left| \frac{u - k}{u - \sqrt{k^2 + a^2}} \right| \left| \frac{\sqrt{u^2 - k^2} + a}{\sqrt{u^2 - k^2} - a} \right|, & u > k, \\ \left| \frac{u - k}{u - \sqrt{k^2 + a^2}} \right|, & u < k. \end{cases} \quad (66)$$

Using (66), (15), and (25), we find after some manipulation

$$|\mathbf{h}_t(x, z)|^2 = \frac{4X_1^2\sqrt{1 + X_0^2}e^{-2kX_1z}}{\sqrt{1 + X_1^2}(X_1 + X_0)^2}. \quad (67)$$

Again using (66) and (26), we find

$$|\mathbf{h}_r(x, z)|^2 = \frac{X_0^2(X_0 - X_1)^2e^{-2kX_0z}}{(1 + X_0^2)(\sqrt{1 + X_0^2} + \sqrt{1 + X_1^2})^2}, \quad (68)$$

whereas, from (31) and (66),

Apart from a proportionality constant depending on the units, the power flows of the incident, reflected, and transmitted surface waves are given respectively by

$$k\sqrt{1 + X_0^2} \int_0^\infty e^{-2kX_0z} dz = \frac{\sqrt{1 + X_0^2}}{2X_0}, \quad (70)$$

$$\begin{aligned}
 k\sqrt{1 + X_0^2} \int_0^\infty |\mathbf{h}_r(x, z)|^2 dz \\
 = \frac{X_0(X_0 - X_1)^2}{2\sqrt{1 + X_0^2}(\sqrt{1 + X_0^2} + \sqrt{1 + X_1^2})^2}, \quad (71)
 \end{aligned}$$

and

$$k\sqrt{1 + X_1^2} \int_0^\infty |\mathbf{h}_t(x, z)|^2 dz = \frac{2X_1\sqrt{1 + X_0^2}}{(X_1 + X_0)^2}. \quad (72)$$

The power reflection coefficient R is the ratio of (71) to (70):

$$R = \frac{X_0^2(X_0 - X_1)^2}{(1 + X_0^2)(\sqrt{1 + X_0^2} + \sqrt{1 + X_1^2})^2}; \quad (73)$$

and the power transmission coefficient T is the ratio of (72) to (70):

$$T = \frac{4X_0X_1}{(X_1 + X_0)^2} = 1 - \left(\frac{X_1 - X_0}{X_1 + X_0} \right)^2. \quad (74)$$

$$|\mathbf{h}_R(x, z)|^2 = \frac{(X_0 - X_1)^2\sqrt{1 + X_0^2} \sin^2 \theta}{(\sqrt{1 + X_0^2} + \sqrt{1 + X_1^2})\pi kr(\sqrt{1 + X_1^2} - \cos \theta)(X_0^2 + \sin^2 \theta)(\sqrt{1 + X_0^2} - \cos \theta)}. \quad (69)$$

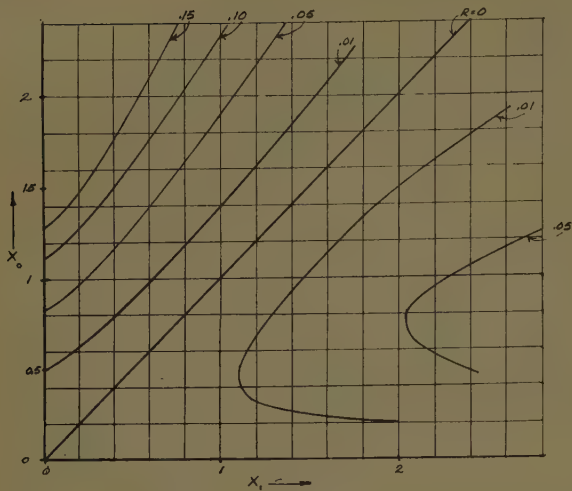


Fig. 4—Reflection coefficient at a discontinuity in normal reactance from X_0 to X_1

$$R = \frac{X_0^2(X_0 - X_1)^2}{(1 + X_0^2)(\sqrt{1 + X_0^2} + \sqrt{1 + X_1^2})^2},$$

Universal curves for R and T vs X_0 and X_1 are given in Figs. 4 and 5. The total radiated power is

$$k \int_0^\pi |h_R(x, z)|^2 r d\theta = \frac{(X_0 - X_1)^2 \sqrt{1 + X_0^2} I}{\pi (\sqrt{1 + X_1^2} + \sqrt{1 + X_0^2})}, \quad (75)$$

where

$$I = \int_0^\pi \frac{\sin^2 \theta d\theta}{(\sqrt{1 + X_1^2} - \cos \theta)(\sqrt{1 + X_0^2} - \cos \theta)(X_0^2 + \sin^2 \theta)}. \quad (76)$$

Where the radiation power coefficient P is the total power radiated divided by the power in the incident surface wave, conservation of energy requires

$$P = 1 - R - T.$$

E. Energy Balance

We now verify conservation of energy as an independent check on our results. We may make the substitution in (76) of

$$Z = e^{i\theta}, \quad dZ = iZ d\theta, \quad \frac{Z + 1/Z}{2} = \cos \theta,$$

$$\frac{Z - 1/Z}{2i} = \sin \theta \quad (77)$$

to yield a contour integral around the unit circle

$$I = \frac{i}{8} \oint \frac{Z(Z^2 - 1)^2 dZ}{\left(\frac{Z^2 + 1}{2} - \sqrt{1 + X_1^2} Z\right) \left(\frac{Z^2 + 1}{2} - \sqrt{1 + X_0^2} Z\right) \left(X_0^2 Z^2 - \frac{(Z^2 - 1)^2}{4}\right)}. \quad (78)$$

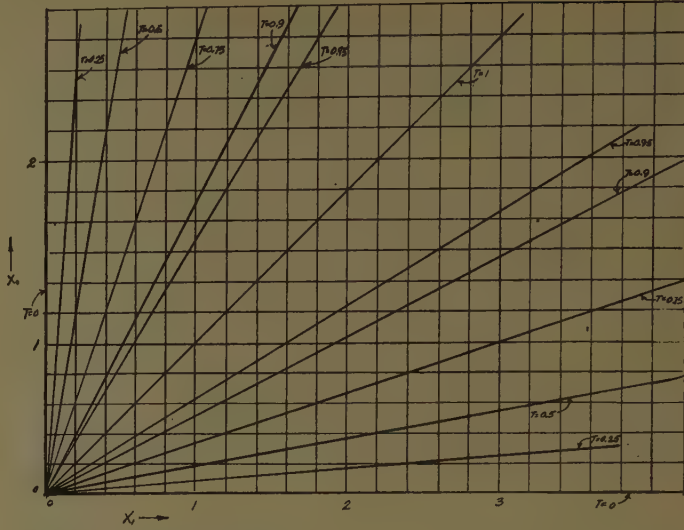


Fig. 5—Transmission coefficient at a discontinuity in normal reactance from X_0 to X_1

$$T = \frac{4X_0 X_1}{(X_0 + X_1)^2}.$$

We factor the denominator of (78) in order to evaluate I by the residue theorem. We find that

$$I = 2i \oint \frac{Z(Z^2 - 1)^2 dZ}{(Z - a)(Z - A)(Z - b)^2(Z - B)^2(Z + b)(Z + B)},$$

where

$$a = \sqrt{1 + X_1^2} - X_1$$

$$A = \sqrt{1 + X_1^2} + X_1$$

$$b = \sqrt{1 + X_0^2} - X_0$$

$$B = \sqrt{1 + X_0^2} + X_0. \quad (80)$$

The poles a , b , and $-b$ lie within the unit circle, whereas A , B , and $-B$ lie exterior to the unit circle. If we write I as the sum of the three residues at the poles within the unit circle, we have

$$I = I_a + I_{-b} + I_b, \quad (81)$$

where the subscripts indicate the pole in question. We find by a straightforward calculation

$$I_a = \frac{\pi X_1}{(X_0^2 - X_1^2)(\sqrt{1 + X_1^2} - \sqrt{1 + X_0^2})}, \quad (82)$$

$$I_{-b} = \frac{-\pi X_0}{4(\sqrt{1 + X_0^2} + \sqrt{1 + X_1^2})(1 + X_0^2)}. \quad (83)$$

$$I_b = 4\pi \frac{\partial}{\partial Z} \left[\frac{Z(Z^2 - 1)^2}{(Z^2 - 2\sqrt{1 + X_1^2} + 1)(Z^2 + 2\sqrt{1 + X_0^2} + 1)(Z - B)^2} \right]_{Z=b}. \quad (84)$$

Since $Z = b$ is a double pole, we have

Using

$$b^2 + 1 = 2b\sqrt{1 + X_0^2}, \quad b^2 - 1 = -2X_0b, \quad (85)$$

we find after considerable manipulation that

$$I_b = \frac{\pi}{2X_0(1 + X_0^2)(\sqrt{1 + X_0^2} - \sqrt{1 + X_1^2})^2} \left[\left(1 + \frac{X_0^2}{2}\right)(\sqrt{1 + X_1^2} - \sqrt{1 + X_0^2}) + X_0^2\sqrt{1 + X_0^2} \right]. \quad (86)$$

Combining (81)–(83), and (86), yields

$$I = \frac{\pi(\sqrt{1 + X_1^2} + \sqrt{1 + X_0^2})}{(X_0^2 - X_1^2)^2(1 + X_0^2)X_0} \left[\frac{X_0^2}{4}(\sqrt{1 + X_1^2} + \sqrt{1 + X_0^2})^2 + \frac{X_1^2 - X_0^2}{2} - X_1X_0(1 + X_0^2) - \frac{X_0^2}{4}(\sqrt{1 + X_1^2} - \sqrt{1 + X_0^2})^2 \right]. \quad (87)$$

From (75) and (87), we have the total radiated power

$$\frac{1}{X_0\sqrt{1 + X_0^2}(X_0 + X_1)^2} \left[\frac{X_0^2}{4}(\sqrt{1 + X_1^2} + \sqrt{1 + X_0^2})^2 + \frac{X_1^2 - X_0^2}{2} - X_1X_0(1 + X_0^2) - \frac{X_0^2}{4}(\sqrt{1 + X_1^2} - \sqrt{1 + X_0^2})^2 \right]. \quad (88)$$

From (70)–(72), the incident power minus the sum of the transmitted and reflected power is

$$\frac{1}{X_0(X_1 + X_0)^2\sqrt{1 + X_0^2}} \left[\frac{1}{2}(1 + X_0^2)(X_1 + X_0)^2 - 2X_0X_1(1 + X_0^2) - \frac{X_0^2}{2}(\sqrt{1 + X_0^2} - \sqrt{1 + X_1^2})^2 \right]. \quad (89)$$

A little manipulation shows that (88) and (89) are equal, as required.

BIBLIOGRAPHY

- [1] J. Bazer, "Propagation of plane electromagnetic waves past a shoreline," Ph.D. dissertation, Dept. of Math., New York University, N. Y.; August, 1952.
- [2] A. F. Kay, "The Excitation of Surface Waves in Multilayered Media," Tech. Res. Group, New York, N. Y.; October, 1954.
- [3] A. F. Kay, "Scattering of a Surface Wave by a Discontinuity in Normal Reactance with Applications to Antenna Problems," Tech. Res. Group, New York, N. Y., Sci. Rep. No. 7, Contract AF19(604)-1307; September 18, 1957.
- [4] T. B. A. Senior, "Diffraction by a semi-infinite metallic sheet," *Proc. Roy. Soc. (London) A*, vol. 213, pp. 436–458; July 22, 1952.
- [5] J. R. Wait, "Mixed path ground wave propagation—short distance," *Bull. Natl. Bur. Standards*, vol. 57, res. paper 2687; July, 1956.
_____, "Mixed path ground wave propagation—larger distances," *Bull. Natl. Bur. Standards*, vol. 59, res. paper 2687; July, 1957.
- [6] J. Robieux, "Radiation Performance of End-Fire Surface Wave Antennas," Compagnie Generale de Telegraphie Sans Fil, Paris, France; November 14, 1957.
- [7] J. Robieux, "Background Research on Surface Wave Discontinuities," Compagnie Generale de Telegraphie Sans Fil, Paris, France; May 20, 1957.
- [8] G. Weill, "Etude d'un probleme de diffraction des ondes électromagnétiques de surface. Application à la théorie de l'antenne dielectrique," *Ann. Radioelect.*, vol. 10, pp. 228–255; July, 1955.
- [9] A. L. Cullen, "The excitation of plane surface waves," *Proc. IEE*, monograph no. 93, pp. 225–234; February 15, 1954.
- [10] W. M. G. Fernando and H. E. M. Barlow, "An investigation of the properties of radial cylindrical surface waves launched over flat reactive surfaces," *Proc. IEE*, pt. B, vol. 103, pp. 307–318; May, 1956.
- [11] J. R. Wait and A. M. Conda, "Pattern of an Antenna on a Curved Lossy Surface," *Natl. Bur. Standards*, Boulder, Colo., Rep. No. 5562; February, 1958.
- [12] E. Titchmarsh, "Introduction to the Theory of Fourier Integrals," Oxford University Press, London, Eng.; 1948.

Spherically Symmetric Lenses*

ALAN F. KAY†

Summary—A design procedure is given for finding the index variation of a spherically (or cylindrically) symmetric lens which will produce, with some restrictions, any desired shaped beam pattern. Applications are made to a broad beam Luneberg lens, a bistatic Luneberg reflector, and a bistatic Eaton-Lippmann lens, and other examples are worked out. The practical importance of the index singularity at the center of lenses of the Eaton-Lippmann type is treated.

INTRODUCTION

THE Luneberg lens is but one of a number of spherical lenses which have been studied in the past.¹ The important property of spherically symmetric lenses is their inherent perfect wide angle or scanning ability. The beam may emerge at various angles as in the Eaton lenses,^{1,2} or the focal point may be interior to the lens as in the lenses of Brown.³ The Luneberg lens and most lenses of microwave interest have unit index on the surface. However, these lenses have been generalized by Brown³ to other spherically symmetric lenses having arbitrary index on the outer surface.

Recently, interest has been demonstrated in a shaped beam modification of the Luneberg lens.⁴ This lens has a broader pencil beam than a Luneberg of the same diameter, since the emergent phase front is not plane but rather spherical of slight curvature. Since the rays are not collimated, we may think of this lens design as being of the "shaped beam" type. Geometrical optics should give a reasonable first approximation to the actual patterns achieved by these lenses just as it does for the shaped beam metal reflectors described by Silver.⁵ Since this type of analysis leads to patterns that are frequency independent, one application of the shaped beam lens is for "pencil beams" with constant beam-width over a broad band. As DeSize points out,⁴ this permits broad-band, wide-angle coverage with a multi-

* Manuscript received by the PGAP, May 7, 1958; revised manuscript received, August 25, 1958. This paper was sponsored by AFCRC Antenna Lab. under Contract No. AF19(604)-4054.

† Tech. Res. Group, New York, N. Y.

¹ J. E. Eaton, "An Extension of the Luneberg-Type Lenses," Naval Res. Lab., Washington, D. C., Rep. No. 4110; February 16, 1953.

² K. Kelleher, "Variable-index lenses producing conical wavefronts," presented at URSI Symp. on Electromagnetic Wave Theory, Univ. of Michigan, Ann Arbor, Mich. For abstract, see IRE TRANS. ON ANTENNAS AND PROPAGATION, vol. AP-4, p. 586; July, 1956.

³ J. Brown, "Microwave wide angle scanner," Wireless Engr., vol. 30, pp. 250-255; October, 1953.

⁴ L. K. DeSize, "An investigation of the feasibility of obtaining a constant beam width Luneberg lens," in "Abstracts of the Seventh Annual Symposium on the USAF Antenna Research and Development Program," Univ. of Illinois, Urbana, Ill., Astia Doc. No. AD-138500; October, 1957.

⁵ S. Silver, "Microwave Antenna Theory and Design," M.I.T. Rad. Lab. Ser., McGraw-Hill Book Co., Inc., New York, N. Y., pp. 497-502; 1949.

plicity of fixed feeds without either failure of coverage at the high-frequency end of the band or wasteful overlap at the low-frequency end.

This paper is concerned with the improved design of shaped beam lenses of several types. In all cases the lenses themselves have circular symmetry so that the index $n(r)$ is a function of the normalized radial distance r , which is defined as the radial coordinate divided by the lens radius a . All results, for lenses of unit radius, apply to lenses of arbitrary radius a by replacing r by r/a .

The theory applies to three types of lenses of current practical interest and is developed for all three types in a parallel exposition. Lenses of Type I have a point source on the surface. The Luneberg lens is an example. Lenses of Type II have a point source at infinity; a ray from the incident plane wave passes through the lens, reflects from a metallic coating on the surface, and then passes through the lens a second time before emerging. The metallic coating covers only a portion of the lens, of course, so that this description applies only to some of the rays. An example of this type of lens is the Luneberg reflector, which is a Luneberg lens with a metallic reflector covering part of the surface. The final type considered, Type III, has a point source at infinity but has no reflecting coating on the surface. The Eaton-Lippmann lens, which is perhaps not so well known, is an example. It appears that Eaton¹ first described this lens whose index variation is

$$n^2(r) = \frac{2}{r} - 1. \quad (1)$$

Eaton pointed out that with a point source on the surface, this lens acts like a flat metal plate reflector tangent to the lens at the point antipodal to the source. Lippmann⁶ observed that this lens also returns a "plane wave" in the direction of an incident plane wave, in the sense that every ray entering the lens ultimately emerges in the direction of its origin.

Unfortunately, when the vector nature of the fields is taken into account, one finds that regardless of the incident polarization, the back-scattering cross section of a spherical Eaton-Lippmann lens is actually zero rather than the large value one would expect from scalar theory. This unusual situation is quite distinct from the Luneberg reflector where vector and scalar theories yield much the same results. A two-dimensional Eaton-Lippmann lens does, on the other hand, have a back-

⁶ B. A. Lippmann, "An Elementary Discussion of the Luneberg Lens," Tech. Res. Group, New York, N. Y., Interim Tech. Rep. No. 1, Contract No. AF19(604)-1015; 1954.

scattering cross section that is large for its size. Such a lens can be realized in a parallel plate region if in (1) r refers to the radial coordinate of cylindrical coordinates.

The Luneberg reflector has application in radar echo enhancement because of its large back-scattering cross section in directions in which the metal surface is in the shadow zone. A cylindrical Eaton-Lippmann lens of finite length may also have a similar application if a large return is required only in or near the azimuth plane, *i.e.*, for an incident wave front nearly parallel to the lens axis. In this case the Eaton-Lippmann lens has the advantage over the Luneberg reflector of complete azimuth coverage. Moreover, an Eaton-Lippmann lens returns circular polarization in the same sense as that of the incident signal, while a Luneberg reflector returns circular polarization of the opposite sense. The former, therefore, gives a larger received signal at the terminals of a circular polarized radar antenna.

The three lenses: Luneberg lens, Luneberg reflector, and Eaton-Lippmann lens may be considered prototypes of each of the three classes. In each case, applications now exist for lenses similar to the prototypes but having broader beams. We have already mentioned an application of the broad-beam Luneberg lens.

The broad-beam Luneberg reflector or broad-beam Eaton-Lippmann lens is useful when a large "bistatic cross section" is desired. By this, we mean that if a radar signal illuminates such a lens, it is desired that a large return occur in all directions θ with respect to the back-scattering direction out to a maximum direction θ_l ; that is, the scattering pattern should be something like

$$F(\theta) = \begin{cases} 1, & 0 < \theta < \theta_l \\ 0, & \theta_l < \theta < \pi. \end{cases} \quad (2)$$

Here θ is the polar angle in a spherical or cylindrical coordinate system with polar axis in the back-scattering direction. In the case of the spherical lens, because of the symmetry of the lens, the pattern is independent of the azimuthal angle and is thus a function of θ alone.

We assume that $F(\theta)$ is a given shaped beam pattern and that it is desired to find the index variation $n(r)$ for a lens (of any of the three types) which will produce this pattern. We assume that there exists an index $n(r)$ which will produce this pattern and for which the variable

$$\xi = \xi(r) = rn(r) \quad (3)$$

is a monotone function of r such that

$$\xi(0) = 0, \quad \xi(1) = 1. \quad (4)$$

While it is possible to relax these assumptions and to replace them by mathematically weaker restrictions, present needs do not seem to justify the additional mathematical complexity. In the case of lenses of Type

I, the primary pattern of the feed $F_0(\theta)$ is prespecified, as well as the shaped beam pattern $F(\theta)$. The index $n(r)$ which is obtained depends on both patterns. Actual formulas for the index are given implicitly in terms of $F(\theta)$ in such a manner that for many cases of interest, the index may be found with a slide rule, with sufficient accuracy for practical purposes, in less than an hour's time. The broad-beam Luneberg lens, the bistatic Luneberg reflector, and the bistatic Eaton-Lippmann lens are worked out in detail and the resulting indexes are presented graphically. Another interesting case, the conical beam lens, is also worked out as an example.

In certain tactical situations, systems analyses lead to optimum scattering patterns more sophisticated than that given by (2). The method may be readily applied to such cases.

If the beam shape asked for is too "extreme," the index found by this method will yield the desired beam shape on the basis of geometrical optics, but will fail to produce the desired pattern in practice, *i.e.*, when diffraction effects are also taken into account. The outstanding example of this defect is the case where $F(\theta)$ is specified as a delta function, which, depending on the lens type, gives rise in this method to the Luneberg lens, the Luneberg reflector, or the Eaton-Lippmann lens. These lenses, of course, do not have delta function patterns, but do have the highest gain patterns they possibly can. Their emerging rays are collimated. Experience with analogous problems, such as the breakdown of performance of shaped beam metallic reflectors in the neighborhood of the \csc^2 singularity, should serve as a guide for shaped beam lenses. In any case, the pattern which will actually be obtained for a given index lens may be more accurately predicted by evaluating a diffraction integral as described in Silver⁵ or Braun.⁷

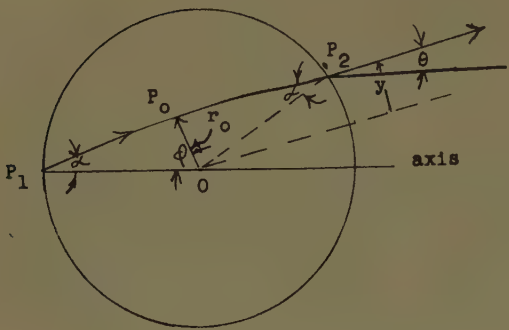
DESIGN OF SHAPED BEAM LENSES

Consider the three types of lenses shown in Fig. 1. In Type I, a point source is located at P_1 with primary pattern $F_0(\alpha)$. The ray at angle α to the lens axis from P_1 reaches a point P_0 of minimum distance r_0 to the lens center. The ray emerges from the lens at P_2 at angle θ to the axis.

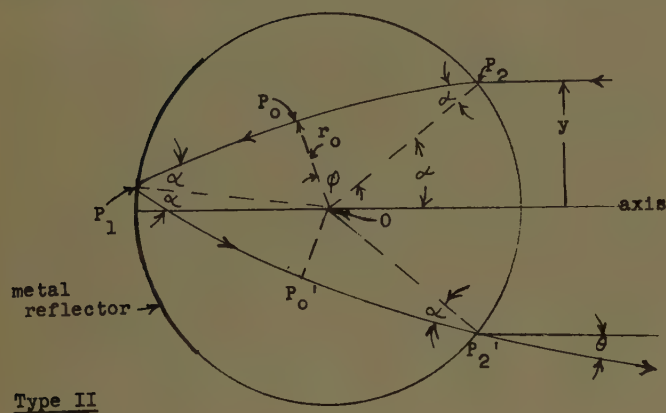
In the Type II and Type III lenses, a typical ray is initially parallel to the axis at a distance y from it and strikes the lens at P_2 . The point of minimum approach to the origin is P_0 . In the Type II lens, the ray reaches the lens surface at P_1 where it is reflected back into the lens by a metallic reflector. It then traverses the ray path segment $\overline{P_1P_0'P_2'}$ which is the symmetric image of $\overline{P_1P_0P_2}$ with respect to $\overline{OP_1}$, and emerges at angle θ with respect to the axis. In the Type III lens, there is no metallic reflector; the lens itself bends the ray

⁵ E. H. Braun, "Radiation characteristics of the spherical Luneberg lens," IRE TRANS. ON ANTENNAS AND PROPAGATION, vol. AP-4, pp. 132-138; April, 1956.

Type I



Type II



Type III

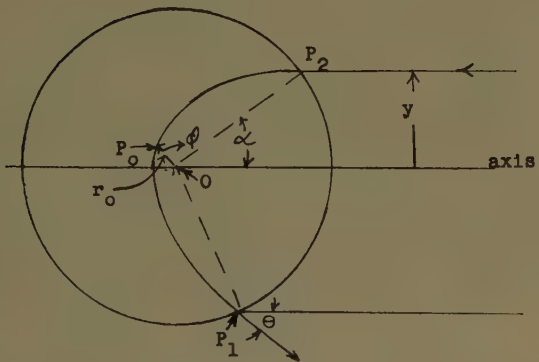


Fig. 1.

around to emerge at P_1 at angle θ to the axis. In all three cases, by symmetry, the ray path segments $\overline{P_0P_2}$ and $\overline{P_0P_1}$ are the images of each other in the line $\overline{OP_0}$.

We desire to find an index $n(r)$ in all three cases which will produce a given shaped beam pattern $F(\theta)$, subject to the conditions of (4). We assume that there exists an index $n(r)$ such that $rn(r)$ is a monotone function of r , which will produce the required pattern.

We have the following relationships among the angles of Fig. 1:

$$\phi = \begin{cases} \frac{\pi - \alpha - \theta}{2}, & \text{Type I} \\ \frac{2\pi - 2\alpha - \theta}{4}, & \text{Type II} \\ \frac{2\pi - 2\alpha - \theta}{2}, & \text{Type III}, \end{cases} \quad (5)$$

where the angle ϕ is given by⁸

$$\phi = y \int_{r_0}^1 \frac{dr}{r \sqrt{r^2 n^2(r) - y^2}} \quad (6)$$

and

$$y = \sin \alpha. \quad (7)$$

The fact that the lenses produce patterns $F(\theta)$ imposes conditions on $n(r)$. Let us determine these conditions first for two-dimensional or cylindrical lenses. In the case of Type I lenses, by geometrical optics,⁹ the energy in the ray bundle consisting of all rays leaving the source between angles α and $\alpha + d\alpha$ is transported in the ray bundle consisting of all rays emerging from the lens at angles between θ and $\theta + d\theta$. Thus

$$Pf(\alpha)d\alpha = F(\theta)d\theta, \quad \text{Type I.} \quad (8)$$

The constant P is a convenient normalizing factor which is determined by conservation of energy. In the case of lenses of Types II and III the analogous equation to (8) is

$$Pdy = F(\theta)d\theta, \quad \text{Types II and III.} \quad (9)$$

If we assume that the rays at $y=0$ and $y=1$, respectively, emerge at angles θ_0 and θ_1 , we have by integration

$$\begin{aligned} P \int_0^{\pi/2} F_0(\alpha)d\alpha &= \int_{\theta_0}^{\theta_1} F(\theta)d\theta, \quad \text{Type I,} \\ P &= \int_{\theta_0}^{\theta_1} F(\theta)d\theta, \quad \text{Types II and III.} \end{aligned} \quad (10)$$

Eq. (10) is a statement of conservation of energy and serves to define P . Indefinite integrals for (8) and (9) yield

$$P \int_0^{\sin^{-1}y} F_0(\beta)d\beta = \int_{\theta_0}^{\theta} F(\Psi)d\Psi, \quad \text{Type I, (11)}$$

$$Py = \int_{\theta_0}^{\theta} F(\Psi)d\Psi, \quad \text{Types II and III.} \quad (12)$$

Eqs. (11) and (12) define θ as an implicit function of y in each case, and thus (5) and (7) define ϕ as a function of y : $\phi = \phi(y)$. The function $\phi(y)$ is not always expressible analytically, but with the pattern $F(\theta)$ given [and, in case I also $F_0(\alpha)$ given], $\phi(y)$ may be tabulated numerically using (5), (7), and (11) or (12); therefore, $\phi(y)$ can be considered known.

We may now solve for $n(r)$ in (6) by a standard procedure.³ We first set

$$\xi = rn(r), \quad f(\xi)d\xi = dr/r \quad (13)$$

where $f(\xi)$ is, as yet, an unknown function. From (6)

⁸ This relationship is well-known, and is given, for example, in A. F. Kay, "The impossibility of certain desirable Luneberg lens modifications," IRE TRANS. ON ANTENNAS AND PROPAGATION, vol. AP-4, pp. 87-88; January, 1956.

⁹ S. Silver, "Microwave Antenna Theory and Design," M.I.T. Rad. Lab. Ser., McGraw-Hill Book Co., Inc., New York, N. Y., pp. 112-114; 1949.

$$\phi(y) = y \int_y^1 \frac{f(\xi) d\xi}{\sqrt{\xi^2 - y^2}}. \quad (14)$$

To solve (14) for $f(\xi)$, we multiply both sides by $1/\sqrt{y^2 - t^2}$, where t is a new variable satisfying $0 \leq t \leq 1$. We then integrate the variable y from t to 1. On the right side of (14), we exchange the order of integration of y and ξ . We use Abel's identity,¹⁰

$$\int_t^1 \frac{y dy}{\sqrt{y^2 - t^2} \sqrt{\xi^2 - y^2}} = \frac{\pi}{2}, \quad (15)$$

to reduce the y integral. We obtain finally

$$\int_t^1 \frac{\phi(y) dy}{\sqrt{y^2 - t^2}} = \frac{\pi}{2} \int_t^1 f(\xi) d\xi. \quad (16)$$

In view of (2) and (13) we may write (16) as

$$\int_t^1 \frac{\phi(y) dy}{\sqrt{y^2 - \xi^2}} = -\frac{\pi}{2} \log r, \quad \xi = rn(r). \quad (17)$$

Eq. (17) gives $n(r)$ implicitly as a function of r . For the special cases considered below, the integral in (17) can be integrated explicitly, and in some cases $n(r)$ may be expressed explicitly. In the general case, the left member of (17) is evaluated numerically for a representative number of values of ξ in the interval $0 < \xi < 1$, and a graph or table of values of r vs ξ is made. $n(r)$ is then determined from

$$n(r) = \frac{\xi(r)}{r}. \quad (18)$$

A. Wide-Beam and Bistatic Lenses

If we define $F(\theta)$ by (2) and for the sake of illustration set

$$F_0(\alpha) = \cos \alpha \quad (19)$$

for the Type I lens, we are seeking for the three lenses: a broad-beam Luneberg lens (Type I), a bistatic Luneberg reflector (Type II), and a bistatic Eaton-Lippmann lens (Type III). We find from (10), that,

$$P = \theta_l, \quad \text{Types I, II, and III.} \quad (20)$$

From (11) and (12)

$$\theta = \theta_l y, \quad \text{Types I, II, and III.} \quad (21)$$

Thus from (5),

$$\phi(y) = \begin{cases} \frac{\pi - \sin^{-1} y - \theta_l y}{2}, & \text{Type I} \\ \frac{2\pi - 2 \sin^{-1} y - \theta_l y}{4}, & \text{Type II} \\ \frac{2\pi - 2 \sin^{-1} y - \theta_l y}{2}, & \text{Type III.} \end{cases} \quad (22)$$

¹⁰ G. Doetsch, "Laplace-Transformation," Dover Publications, Inc., New York, N. Y., pp. 293-294; 1943.

From (17) we may then write

$$\log r = \begin{cases} \frac{\theta_l}{\pi} h_0(\xi) - h_1(\xi), & \text{Type I} \\ \frac{\theta_l}{2\pi} h_0(\xi) - h_1(\xi), & \text{Type II} \\ \frac{\theta_l}{\pi} h_0(\xi) - 2h_1(\xi), & \text{Type III,} \end{cases} \quad (23)$$

where

$$h_0(\xi) = \int_\xi^1 \frac{y dy}{\sqrt{y^2 - \xi^2}} = \sqrt{1 - \xi^2} \quad (24)$$

and

$$\begin{aligned} h_1(\xi) &= \frac{1}{\pi} \int_\xi^1 \frac{(\pi - \sin^{-1} y) dy}{\sqrt{y^2 - \xi^2}} \\ &= \frac{1}{2} \log \left\{ \frac{1 + \sqrt{1 - \xi^2}}{\xi^2} \right\}. \end{aligned} \quad (25)$$

The evaluation of the integral in (25) is described in the Appendix. From (23)-(25) we find, therefore, that

$$r = \begin{cases} \frac{\xi}{\sqrt{1 + \sqrt{1 - \xi^2}}} e^{(\theta_l/\pi)\sqrt{1 - \xi^2}}, & \text{Type I} \\ \frac{\xi}{\sqrt{1 + \sqrt{1 - \xi^2}}} e^{(\theta_l/2\pi)\sqrt{1 - \xi^2}}, & \text{Type II} \\ \frac{\xi^2}{1 + \sqrt{1 - \xi^2}} e^{(\theta_l/\pi)\sqrt{1 - \xi^2}}, & \text{Type III.} \end{cases} \quad (26)$$

We observe that a broad-beam lens of Type I with beam-width, say θ_b , becomes, if it is covered with a reflecting surface, a broad-beam reflector of Type II with beam-width $2\theta_b$. This is a generalization of the fact that the Luneberg lens and the Luneberg reflector have the same index. For the broad-beam type lenses, the generalization is only true if $F_0(\alpha) = \cos \alpha$.

If θ_l is zero, we may solve explicitly for ξ in all cases. Then using (18) we obtain

$$n(r) = \begin{cases} \sqrt{2 - r^2}, & \text{Type I and II} \\ \sqrt{\frac{2}{r} - 1}, & \text{Type III.} \end{cases} \quad (27)$$

These correspond to the Luneberg lens and the Eaton-Lippmann lens, respectively, as they should.

If θ_l is small, a little manipulation shows that, to first order in θ

$$n(r) = \sqrt{2 - r^2} \left(1 - \frac{u(1 - r^2)^2}{(2 - r^2)} \right), \quad u \ll 1, \quad (28)$$

where

$$u = \frac{2\theta_l}{\pi}, \quad \text{Type I; } u = \frac{\theta_l}{\pi}, \quad \text{Type II,} \quad (29)$$

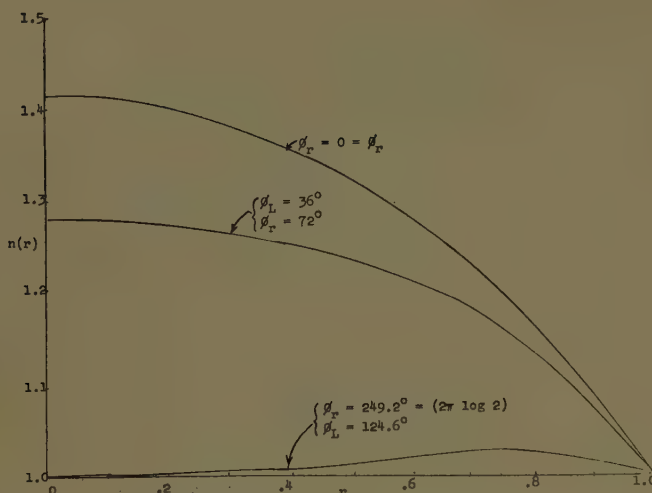


Fig. 2—Cylindrical bistatic Luneberg reflector, Type II, cylindrical broad beam Luneberg lens, ($F_0(\alpha) = \cos \alpha$), Type I.

ϕ_r = Full beamwidth of reflector.
 ϕ_L = Full beamwidth of lens.

and

$$n(r) = \sqrt{\frac{2}{r} - 1} \left(1 - \frac{\theta_l}{\pi} \frac{(1-r)^2}{(2-r)} \right), \quad \theta_l \ll \pi, \text{ Type III.} \quad (30)$$

If θ_l is less than $\pi/5$ in Types II and III or less than $\pi/10$ in Type I, these approximations are accurate to within 1 per cent.

For general values of θ_l , (26) must be solved numerically by tabulating r vs ξ for fixed θ_l and computing $n(r)$ by means of (18). Results are shown in Figs. 2 and 3. One of the difficulties of the method is illustrated in this case. If the half beamwidth of the broad-beam Luneberg lens exceeds $62.3^\circ = (\pi/2) \log 2$ radians, then the index which is required for the beam shaping turns out to be less than unity for part of the lens. Even larger beamwidths in this case lead to functions $r(\xi)$ which are not monotonic but look like Fig. 4. No inverse function $\xi(r)$ exists in the interval $0 \leq r \leq 1$ except one for which $\xi(1) = \xi_0 < 1$. Hence by (18), $n(1)$ is less than 1. In a case such as this, no lens with $r n(r)$ a monotone function of r and $n(1) = 1$ can do the job required.

B. Conical Beam Lenses

If we define $F(\theta)$ as a Dirac delta function,

$$F(\theta) = \delta(\theta - \theta'), \quad (31)$$

the beam produced will be shaped like a conical shell in the three-dimensional case (unless θ' is zero, in which case it will be a pencil beam). We observe from (11) and (12) that θ is a constant equal to θ' . From (5), (7), and (17)

$$\log r = \begin{cases} \theta' h_2(\xi) - h_1(\xi) & \text{Type I} \\ \frac{\theta'}{2} h_2(\xi) - h_1(\xi) & \text{Type II} \\ \theta' h_2(\xi) - 2h_1(\xi) & \text{Type III,} \end{cases} \quad (32)$$

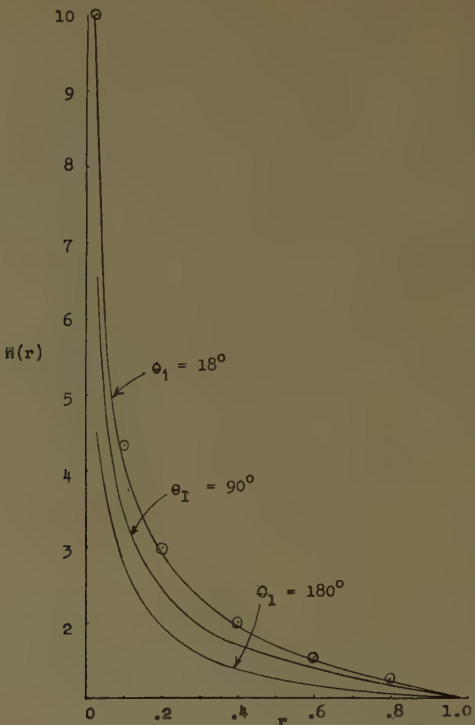


Fig. 3—Cylindrical bistatic lens, Type III, half beamwidth = θ_l , Eaton-Lippmann: $\theta_1 = 0$.

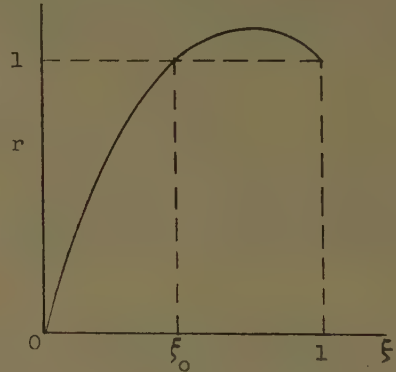


Fig. 4.

where $h_1(\xi)$ is defined by (25) and

$$h_2(\xi) = \frac{1}{\pi} \int_{\xi}^1 \frac{dy}{\sqrt{y^2 - \xi^2}} = \frac{1}{\pi} \log \left\{ \frac{1 + \sqrt{1 - \xi^2}}{\xi} \right\}. \quad (33)$$

We obtain from (32),

$$r = \begin{cases} \xi^{1-\theta'/\pi} \{ 1 + \sqrt{1 - \xi^2} \}^{\theta'/\pi-1/2}, & \text{Type I} \\ \xi^{1-\theta'/2\pi} \{ 1 + \sqrt{1 - \xi^2} \}^{\theta'/2\pi-1/2}, & \text{Type II} \\ \xi^{2-\theta'/\pi} \{ 1 + \sqrt{1 - \xi^2} \}^{\theta'/\pi-1}, & \text{Type III.} \end{cases} \quad (34)$$

In case $\theta' = 0$, these three lenses reduce to the Luneberg lens, the Luneberg reflector, and the Eaton-Lippmann lens, respectively, as they should. For the general case, $n(r)$ may be computed as before. The results for several θ' are shown in Fig. 5 for a lens of Type III.

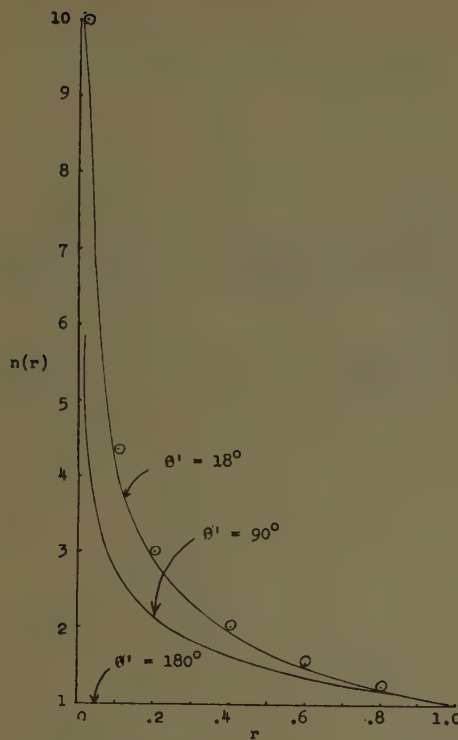


Fig. 5—Conical beam lens, Type III, beam angle $=\theta'$, Eaton-Lippmann: $\theta'=0$.

THE SINGULARITY AT THE CENTER OF TYPE III LENSES

Unless the ray at $y=0$ is not deviated at all, all lenses of Type III have a singularity in $n(r)$ at $r=0$. At the center, the bistatic lens has a singularity of the same order as the Eaton-Lippmann lens. In fact, for small r , from (26),

$$n(r) \simeq \sqrt{\frac{2}{r}} e^{-\theta_l/2\pi}, \text{ bistatic lens, } r \ll 1. \quad (35)$$

The order of the singularity at the center of the conical beam, Type III, lens depends on θ' . From (34), it is not hard to show that

$$n(r) \simeq \left(\frac{2}{r}\right)^{(\pi-\theta')/(2\pi-\theta')}, \text{ conical beam lens, } r \ll 1. \quad (36)$$

The order of the singularity at the origin decreases from $-\frac{1}{2}$ when θ' is zero to 0 when $\theta'=\pi$. Only the limiting case $\theta'=\pi$ has no singularity whatever at the origin.

The existence of the singularity for the Type III lenses implies that the theoretical index cannot be adhered to near the center. Let us consider the practical effect of this limitation. Suppose that n_m is the index of the material of maximum index suitable for construction of the lens. An inner cylinder of the lens, defined by $0 < r < r_m$, where

$$n(r_m) = n_m, \quad n(r) > n_m, \quad 0 < r < r_m, \quad (37)$$

must be omitted from the construction. As a first approximation, we may assume that all rays which would have entered this cylinder are not properly focused.

This consists of all rays in a strip of the wavefront of radius y_m , where

$$y_m = r_m n_m. \quad (38)$$

The limiting ray which enters at $y=y_m$ emerges at angle θ_L , given from (10) and (12), by

$$y_m = \int_{\theta_0}^{\theta_L} F(\Psi) d\Psi / \int_{\theta_0}^{\theta_1} F(\theta) d\theta. \quad (39)$$

Within the limitations of the validity of the geometrical optics assumption, therefore, the shaped beam pattern is unaffected in the region

$$\theta_L < \theta < \theta_1, \quad (40)$$

and seriously degraded in the region

$$\theta_0 < \theta < \theta_L. \quad (41)$$

For a pencil or conical beam Type III lens, these remarks are not applicable. The important phenomenon becomes the effect of the singularity on the scattering cross sections of these lenses. For example, σ , the back scattering cross section of a cylindrical Eaton-Lippmann lens of finite length l when a free space plane wave is incident in the azimuthal plane, is given by

$$\sigma = G \cdot A, \quad (42)$$

where G is the gain of the scattering pattern, and A is the area of that part of the incoming wavefront whose rays are actually focused. Thus

$$A = 2(a - y_m)l, \quad (43)$$

where a is the radius of the lens, and y_m is given by (38). The gain of a perfectly focused aperture of area A_0 is

$$G = 4\pi A_0 / \lambda^2. \quad (44)$$

Because of the symmetry of the ray paths about the axis, $A = A_0$. Thus (42) becomes

$$\sigma = \frac{16\pi l^2}{\lambda^2} (a - y_m)^2. \quad (45)$$

Therefore, the db loss in scattering cross section for the Eaton-Lippmann lens, due to the omission of the cylinder $0 < r < r_m$, is

$$10 \log_{10} (1 - y_m)^2 = 20 \log_{10} \left\{ \frac{(n_m - 1)^2}{n_m^2 + 1} \right\}. \quad (46)$$

This is plotted in Fig. 6 vs n_m .

From (39), for the bistatic lens

$$\theta_L = y_m \theta_1 = r_m n_m \theta_1. \quad (47)$$

For $n_m=4$, we obtain the following values:

Bistatic Lens	Minimum Focussed Angle
θ_1	θ_L
18°	7.56°
90°	27.4°
180°	31°

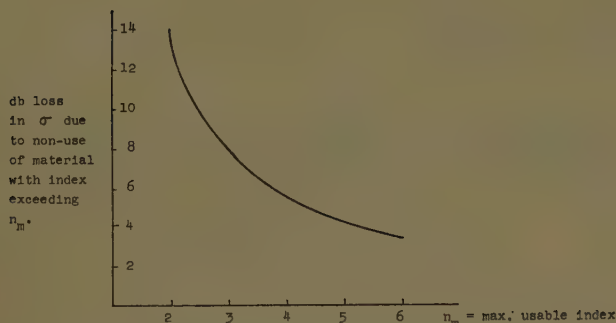


Fig. 6—Cylindrical Eaton-Lippmann lens.

SPHERICAL LENSES

The formulas which express conservation of energy flow must be appropriately modified for spherical lenses. In (8) through (12), in order to allow for the correct area elements, we must replace dy , $d\alpha$, $d\theta$, $d\beta$, and $d\psi$ by ydy , $\sin \alpha d\alpha$, $\sin \theta d\theta$, $\sin \beta d\beta$, and $\sin \psi d\psi$, respectively. These changes do not affect the index variation for the conical beam lenses. For the broad-beam lenses of all three types defined by (2), we must replace (20) by

$$P = 2(1 - \cos \theta_i), \quad (52)$$

and (21) by

$$\theta = \cos^{-1}[1 - (1 - \cos \theta_i)y^2] = 2 \sin^{-1}\left(y \sin \frac{\theta_i}{2}\right). \quad (53)$$

This implies that (23) must be written as

$$\log r = \begin{cases} 2h_3(\xi) - h_1(\xi), & \text{Type I} \\ h_3(\xi) - h_1(\xi), & \text{Type II} \\ 2h_3(\xi) - 2h_1(\xi), & \text{Type III}, \end{cases} \quad (54)$$

where¹¹

¹¹ S. P. Morgan, "General Solution of the Luneberg Lens Problem," Bell Telephone Labs., Inc., Murray Hill, N. J. (submitted for publication in *J. Appl. Phys.*). The author is indebted to Dr. Morgan for first pointing out the necessary changes in the formulas in passing from cylindrical to spherical lenses.

$$h_3(\xi) = \frac{1}{\pi} \int_{\xi}^1 \frac{\sin^{-1}\left(y \sin \frac{\theta_i}{2}\right)}{\sqrt{y^2 - \xi^2}} dy. \quad (55)$$

The function $h_3(\xi)$ was first defined by Luneberg.¹² Fletcher, Murphy, and Young¹³ developed a power series for it in powers of $\sin(\theta_i/2)$ which according to Morgan¹¹ is satisfactory for θ less than about 60° . For larger values, the function has been tabulated by Morgan.

Eq. (54), then, implicitly defines $n(r)$ as a function of r as in the cylindrical cases.

APPENDIX

Evaluation of $h_1(t)$

To evaluate the integral in (25), let $y = ut$, then

$$h_1(t) = \int_1^{1/t} \frac{\pi - \sin^{-1} ut}{\sqrt{u^2 - 1}} du. \quad (56)$$

We differentiate (56) with respect to t .

$$h_1'(t) = \frac{-\pi}{2t\sqrt{1-t^2}} - \frac{1}{t} \int_1^{1/t} \frac{udu}{\sqrt{u^2 - 1}\sqrt{(1/t)^2 - u^2}}. \quad (57)$$

By means of the Abel identity (15), (57) reduces to

$$h_1'(t) = -\frac{\pi}{2t\sqrt{1-t^2}} - \frac{\pi}{2t}. \quad (58)$$

Standard integrals yield

$$\begin{aligned} h_1(t) &= \frac{\pi}{2} \log \left\{ \frac{1 + \sqrt{1-t^2}}{t} \right\} - \frac{\pi}{2} \log t \\ &= \frac{\pi}{2} \log \left\{ \frac{1 + \sqrt{1-t^2}}{t^2} \right\}, \end{aligned} \quad (59)$$

which satisfies the initial condition $h_1(1) = 0$.

¹² R. K. Luneberg, "Mathematical Theory of Optics," Brown University, Providence, R. I., pp. 189-213; 1944.

¹³ A. Fletcher, T. Murphy and A. Young, "Solutions of two optical problems," *Proc. Roy. Soc. (London) A*, vol. 223, pp. 216-225; April 22, 1954.

On the Design of Some Rhombic Antenna Arrays*

A. A. DE CARVALHO FERNANDES†

Summary—The expression of the field radiated by a rhombic antenna, taking into consideration both the vertical and the horizontal polarization components, is used to establish the theory of the array of two stacked rhombics and of the array of four rhombics in a stacked and interlaced arrangement. The main conclusions obtained are that for convenient values of the vertical and horizontal spacings between the antennas of the array, there is a greater concentration of power radiated along the directions of the main lobe of the pattern and, as a result, these arrays show an appreciable gain over a conventional rhombic. Practical rules for the design of these arrays for point-to-point and broadcasting are given in some detail.

INTRODUCTION

HORIZONTAL ANTENNA IN PRESENCE OF GROUND

RHOMBIC antennas and rhombic antenna arrays are still a very convenient solution for many radio communications problems both in the HF and in the VHF field. The theory of the rhombic antenna has been described in several papers^{1,2} and the arrays of perhaps greatest practical interest were described by Christiansen.³⁻⁵

LIST OF SYMBOLS

ASR=array of stacked rhombic antennas.

ASIR=array of stacked and interlaced rhombic antennas.

H=average height of an horizontal antenna or array above ground.

l=side of the rhombus.

s_h=horizontal spacing of the two partial *ASR* of an *ASIR*.

s_v=vertical spacing between the two antennas of an *ASR*.

ϕ=tilt angle.

Δ=angle formed by the direction of radiation with the plane of the antenna (angle of elevation or angle of fire in horizontal antennas).

ψ=angle formed with the main diagonal of the rhombus by the projection of the direction of radiation on the plane of the antenna (azimuth angle in horizontal antennas).

λ=wavelength.

* Original manuscript received by the PGAP, March 24, 1958; revised manuscript received, October 20, 1958.

† Technical University of Lisbon, Portugal. Also, Standard Electrica, S.A.R.L., Lisbon.

¹ E. Bruce, "Developments in short-wave directive antennas," PROC. IRE, vol. 19, pp. 1406-1433; August, 1931.

² E. Bruce, A. C. Beck, and L. R. Lowry, "Horizontal rhombic antennas," PROC. IRE, vol. 23, pp. 24-46; January, 1935.

³ W. N. Christiansen, "Directional patterns of rhombic antennae," AWA Tech. Rev., vol. 7, pp. 33-51; September, 1946.

⁴ W. N. Christiansen, W. W. Jenvey, and R. D. Carman, "R.F. measurements on rhombic antennae," AWA Tech. Rev., vol. 7, pp. 131-144; December, 1946.

⁵ W. N. Christiansen, "Rhombic antenna arrays," AWA Tech. Rev., vol. 7, pp. 361-383; October, 1947.

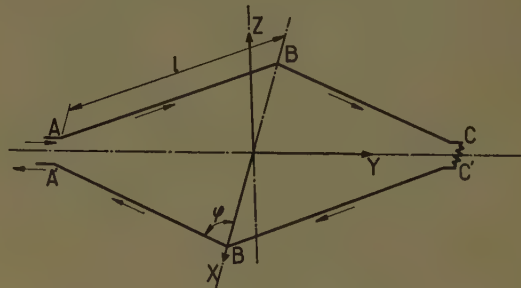


Fig. 1—Schematic representation of a rhombic antenna. *l* is the side of the rhombus and ϕ is the angle made by the side with the transverse diagonal (tilt angle).

If we use the symbols summarized in this list, in reference to Fig. 1, we may obtain the following equation,⁶

$$E = 480 \frac{I}{r} \cos \phi | F_1(\Delta, \phi - \psi) \cdot F_2(\Delta, \phi + \psi) \cdot F_H(\Delta) |, \quad (1)$$

which gives the far field (taking into consideration both the horizontal and the vertical polarization components), due to the radiation from an horizontal rhombic antenna situated at height *H* above ground. Factors *F₁*, *F₂*, and *F_H* are given respectively by (2)-(4).

$$F_1(\Delta, \phi - \psi) = \frac{\sin \left\{ \frac{\pi l}{\lambda} [1 - \cos \Delta \sin (\phi - \psi)] \right\}}{[1 - \cos \Delta \sin (\phi - \psi)]^{1/2}}. \quad (2)$$

$$F_2(\Delta, \phi + \psi) = \frac{\sin \left\{ \frac{\pi l}{\lambda} [1 - \cos \Delta \sin (\phi + \psi)] \right\}}{[1 - \cos \Delta \sin (\phi + \psi)]^{1/2}}. \quad (3)$$

$$F_H(\Delta) = \sin \frac{2\pi H \sin \Delta}{\lambda}. \quad (4)$$

To calculate *I* used in (1), one must know the power supplied to the antenna at its input terminals and the terminal impedance of the antenna. The theoretical derivation for the self and mutual impedances for rhombics is very complex and has recently been made by Channey.⁷⁻⁹ However, the formulas obtained seem

⁶ A. A. De C. Fernandes, "Teoria e Projeto de Antenas Rômbicas," Coimbra Editora, Lda., Lisbon, Portugal, 1955. [See Secs. 9.2, 9.3, and 9.4, where the basic assumptions underlying (1)-(7) are stated. For (1)-(4), it is assumed and justified that the current distribution can be considered without attenuation, and the ground can be taken as an infinite plan of a perfect conductor.]

⁷ J. G. Channey, "Free space radiation impedance of rhombic antenna," J. Appl. Phys., vol. 24, pp. 536-540; May, 1953.

⁸ J. G. Channey, "Simplifications for mutual impedance of certain antennas," J. Appl. Phys., vol. 24, pp. 747-750; June, 1953.

⁹ J. G. Channey, "Mutual impedance of stacked rhombic antennas," IRE TRANS. ON ANTENNAS AND PROPAGATION, vol. AP-2, p. 39; January, 1954.

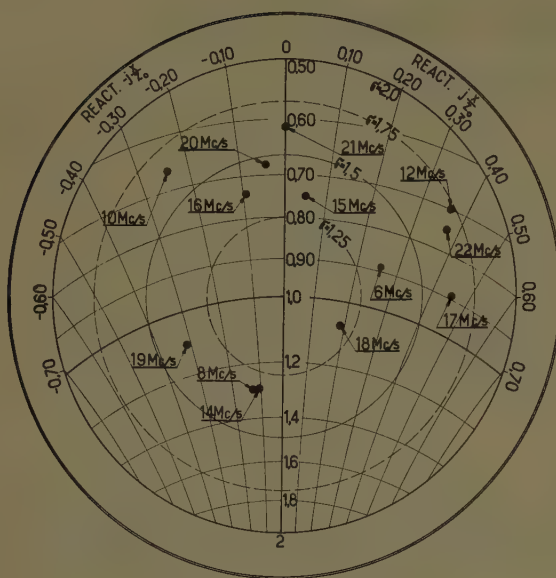


Fig. 2—Values of normalized terminal impedance (in relation to $Z_0 = 700$ ohms) in a 2-wire rhombic antenna with $l=61$ m, $\phi=60^\circ$, $H=25$ m; spacing between wires at side poles, 2 m.

to be so complicated that they are of little practical use. On the other hand, it is relatively simple to measure the terminal impedance of a rhombic antenna, and experience shows that in most practical cases the mutual impedance between the antenna and its image is small compared with its self-impedance Z_{11} . Experience also shows that the terminal impedance Z_1 has a resistance component that varies slightly with the frequency (values of 600 and 700 ohms¹⁰ are representative for 3-wire and 2-wire rhombics, respectively), and a reactance component that varies more widely with the frequency although its value is usually only a fraction of the resistance component. In Fig. 2, we represent in a partial Smith chart the values of Z_1/Z_0 (for $Z_0=700$ ohms) obtained experimentally with a 2-wire rhombic over a frequency range from 6-22 mc.

For approximate field intensity or gain calculations, one may consider the terminal impedance Z_1 reduced to its resistance component R_1 , and the value of I (rms value) could be obtained from approximate (5), where P represents the power supplied to the antenna at its terminals.

$$I = \sqrt{\frac{P}{R_1}} \approx \sqrt{\frac{P}{R_{11}}}. \quad (5)$$

ARRAY OF STACKED RHOMBICS—VERTICAL SPACING FACTOR

If two rhombics are *stacked*, as shown in Fig. 3, and if they are fed in parallel, as indicated in Fig. 4, we have a typical case of a uniform broadside array since the currents at the input terminals of both antennas can be considered approximately of the same magni-

¹⁰ A. E. Harper, "Rhombic Antenna Design," D. Van Nostrand Co., Inc., New York, N. Y., secs. 12-15; 1941. See also, Fernandes, *op. cit.*, sec. 9.4.

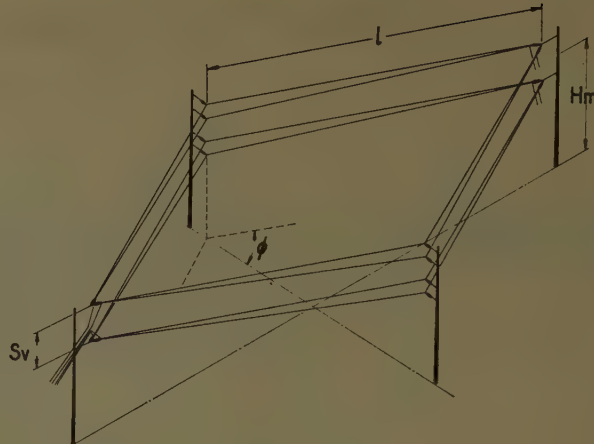


Fig. 3—Schematic representation of an ASR. s_v is the vertical spacing between the two antennas of the array; H is the average height above ground.



Fig. 4—Four-wire lead-down transmission line and feeding arrangement in an ASR.

tude and phase. The magnitude of the radiated field can therefore be obtained by multiplying (1) by the *vertical spacing factor*, which can be derived from conventional array theory and is given by (6), s_v being the vertical spacing of the two antennas.

$$2F_{vs}(\Delta) = 2 \left| \cos \left(\frac{\pi s_v}{\lambda} \sin \Delta \right) \right|. \quad (6)$$

The magnitude of the radiated field due to an array of two stacked rhombics is therefore given by (7),

$$E = 960 \frac{I}{r} \cos \phi \left| F_1(\Delta, \phi - \psi) \cdot F_2(\Delta, \phi + \psi) \cdot F_H(\Delta) \cdot F_{vs}(\Delta) \right|, \quad (7)$$

where I is the input current at each of the antennas of the array. To calculate the height factor $F_H(\Delta)$, we use (4) where H now represents the average height of the array above ground.

The calculation of current I is now more complicated than for a single rhombic because we will have to take into consideration the mutual impedances between the

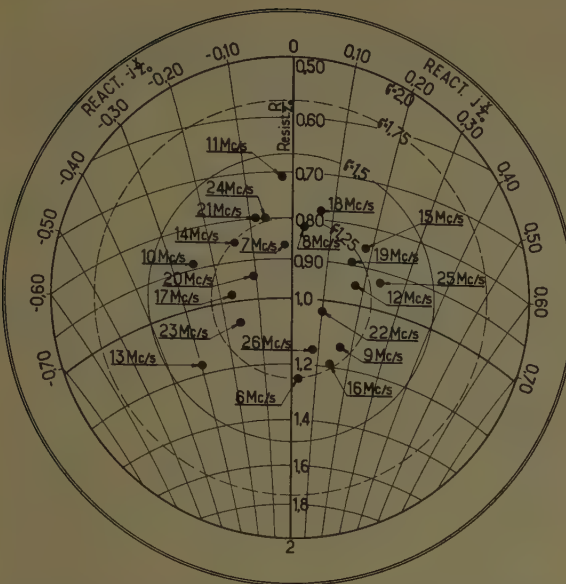


Fig. 5—Values of normalized terminal impedance (in relation to $Z_0 = 320$ ohms) of an ASR where $l = 90$ m, $\phi = 60^\circ$, $H = 42.7$ m, and $s_0 = 6$ m.

two antennas of the array and between them and their images.

It is fortunate, however, that the influence of the mutual impedance in the terminal impedance of the array seems to be small if the two antennas of the array are reasonably separated. In Fig. 5 we represent, in a partial Smith chart, the values of Z_1/Z_0 (for $Z_0 = 320$ ohms) obtained experimentally with an array of two 2-wire stacked rhombics over a frequency range from 6 to 26 mc. The measurements were made at the end of the lead-down 4-wire tapered transmission line matching the theoretical 350 ohms driving point impedance to the value of 320 ohms used as characteristic impedance of the feeding transmission line. The analysis of Fig. 5 shows that the terminal impedance of the array is remarkably constant over such a wide frequency range. On this basis we may write the approximate equation,

$$I \cong \sqrt{\frac{P}{2R_{11}}}, \quad (8)$$

where R_{11} can be taken as 600 ohms for 3-wire rhombics and 700 ohms for 2-wire rhombics. The value of I (rms) mentioned in (7), required for approximate field intensity or gain calculations, can therefore be obtained from (8).

The pattern diagram of this type of array can be obtained from (7) and, to make it easier to study the influence of the vertical spacing factor on the pattern diagram of the array, the values of $F_{vs}(\Delta)$ have been plotted in Fig. 6 for different values of s_v/λ and of Δ . From this figure we can see that for values of s_v up to 35 per cent of λ and for angles of elevation Δ less than 24° , the value of $F_{vs}(\Delta)$ is above 0.9. We also see that the smaller s_v/λ is, the closer $F_{vs}(\Delta)$ is to unity; but in fixing the value of s_v in practice, we must not make it too

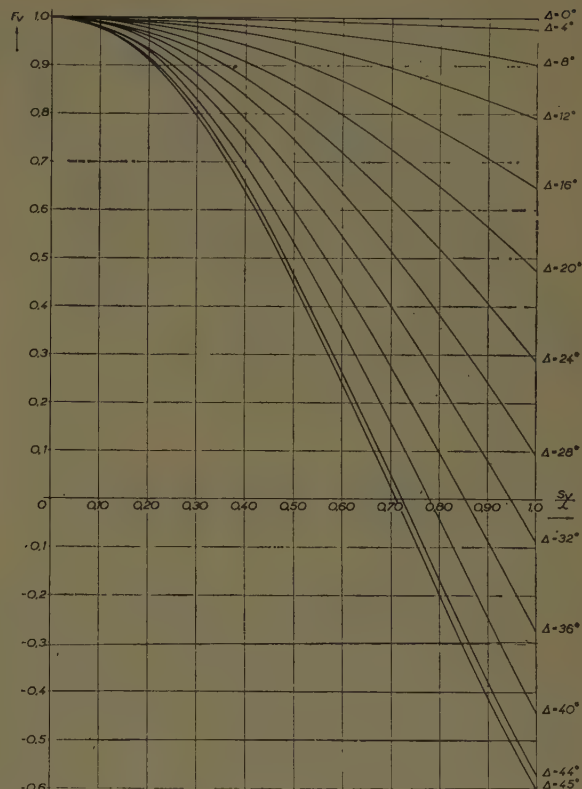


Fig. 6—Variations of $F_{vs}(\Delta)$ in function of the vertical spacing s_v for different values of the angle of elevation Δ .

small, otherwise the mutual impedance between the two antennas may become of great importance. A good practical rule is to make s_v not smaller than twice the separation between the extreme wires of each rhombic at the side poles, when 2-wire or 3-wire rhombics are used (this separation is normally of the order of 15 per cent to 20 per cent of the average height of the antenna above ground). Following this criterion, we arrive normally at values of $F_{vs}(\Delta)$ which are reasonably close to unity for the main lobe of the radiation pattern. Under these circumstances, the influence of the vertical spacing factor in the form of the main lobe of the pattern is very small and in most cases negligible.

If, however, the position of the "nulls" of the diagram or the secondary lobes are to be taken into consideration, the graphs of Fig. 6 can be of great assistance either to fix the most convenient value of s_v or, once it is already determined, to study in detail the influence of the vertical spacing factor in the complete pattern diagram of the array.

It is also to be noted that the vertical spacing factor is not a function of the azimuthal angle ψ , which means that the form of the horizontal radiation pattern of an array of stacked rhombics is the same as of a single rhombic.

Comparing (7) and (1) and taking into consideration the values of I in both equations, we conclude that when $F_{vs}(\Delta)$ is approximately equal to unity, an array of two stacked rhombics has a theoretical gain of 3 db over a single rhombic; in practice, when the ideal con-

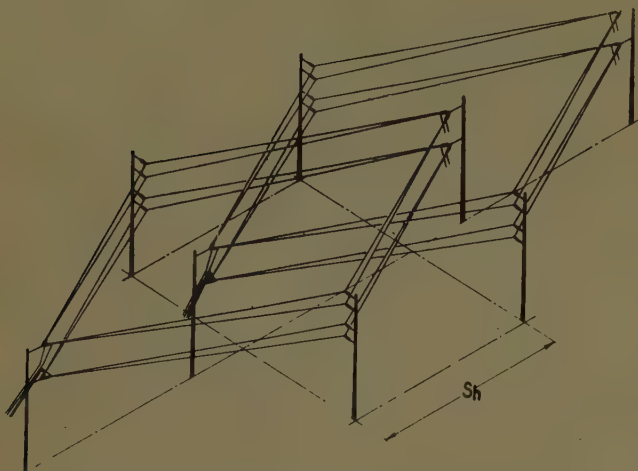


Fig. 7—Schematic representation of an ASIR. s_h is the horizontal spacing between the two partial ASR's.

ditions on which the derivation of (1) and (7) cannot be completely met, a gain slightly smaller than 3 db is to be expected. The condition of $F_{vs}(\Delta)$ being approximately equal to unity will occur, as indicated above, for the directions of radiation covered by the main lobe in the majority of cases of practical interest. This circumstance leads us to conclude that there is a greater concentration of radiated power in the main lobe, to which a reduction of the importance of the secondary lobes must necessarily correspond. In fact, by plotting the complete pattern diagrams using (7) and (1), this same conclusion can be reached.

As regards power dissipated in the termination device, published data¹¹ seem to indicate that the dissipation is less in an array of stacked rhombics than in a conventional rhombic. This fact is, however, more difficult to take theoretically into consideration.

ARRAY OF STACKED AND INTERLACED RHOMBICS (ASIR)—HORIZONTAL SPACING FACTOR

If two arrays of stacked rhombics (ASR) are *interlaced*, as shown in Fig. 7, and are fed with currents of the same magnitude but with a difference in phase equal to the phase delay in a wave traveling in the same direction along a distance equal to the horizontal spacing s_h , the two partial arrays are then associated as a typical uniform end-fire arrangement. The magnitude of the radiated field due to the complete array comprising the 4 rhombics can therefore be obtained by multiplying (7) by the *horizontal spacing factor*. This can be derived from conventional array theory and is given by (9) where Δ is the angle of elevation and ψ the azimuthal angle.

$$2F_{hs}(\Delta, \psi) = 2 \left| \cos \left[\frac{\pi s_h}{\lambda} (1 - \cos \Delta \cos \psi) \right] \right|. \quad (9)$$

The magnitude of the radiated field due to an array of four rhombics in the stacked and interlaced arrange-

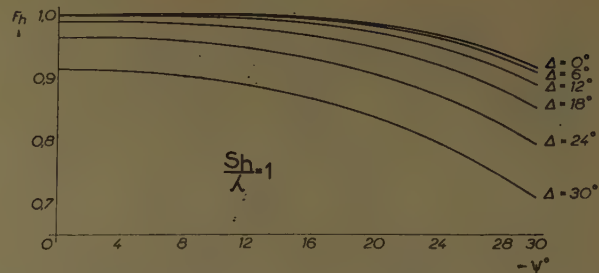


Fig. 8—Variation of $F_{hs}(\Delta, \psi)$ in function of the azimuthal angle ψ for different values of the angle of elevation Δ and for $s_h/\lambda = 1$.

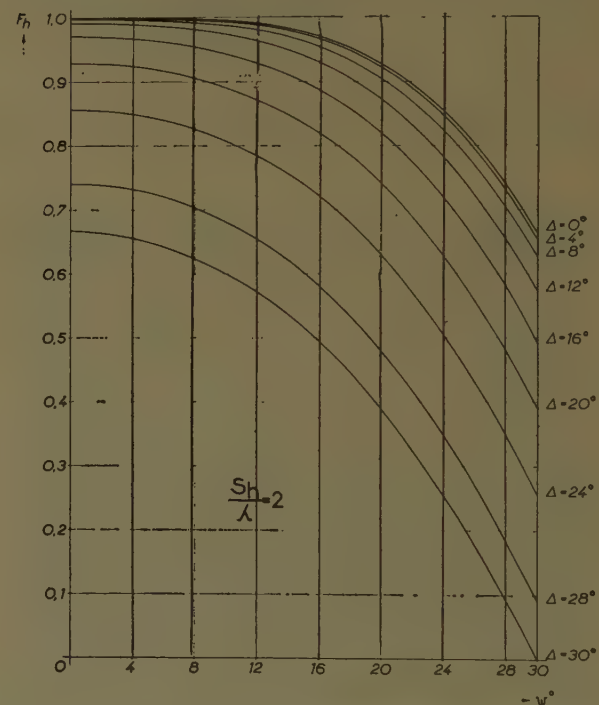


Fig. 9—Variation of $F_{hs}(\Delta, \psi)$ in function of the azimuthal angle ψ for different values of the angle of elevation Δ and for $s_h/\lambda = 2$.

ment described above is given therefore by (10),

$$E = 1920 \frac{I}{r} \cos \phi \left| F_1(\Delta, \phi - \psi) \cdot F_2(\Delta, \phi + \psi) \cdot F_H(\Delta) \cdot F_{vs}(\Delta) \cdot F_{hs}(\Delta, \psi) \right|, \quad (10)$$

where I is the input current at each of the antennas of the array.

In practice, the ASIR has a feeding point from which depart the transmission lines feeding each of the partial ASR. It is essential that the standing-wave ratio in both lines is as close to unity as possible and that the input impedances of both lines at the feeding point are the same. Also, in order to satisfy the condition of the phase difference at the input of the two, partial ASR being equal to the phase delay in a wave traveling along a distance equal to s_h , one must insure that the difference in length of the two transmission lines from the common feeding point to the input of each ASR is equal to s_h .

As regards the mutual impedances between the antennas of the array, experience shows that in most

¹¹ Christiansen, *op. cit.*, "Rhombic antenna arrays," p. 379.

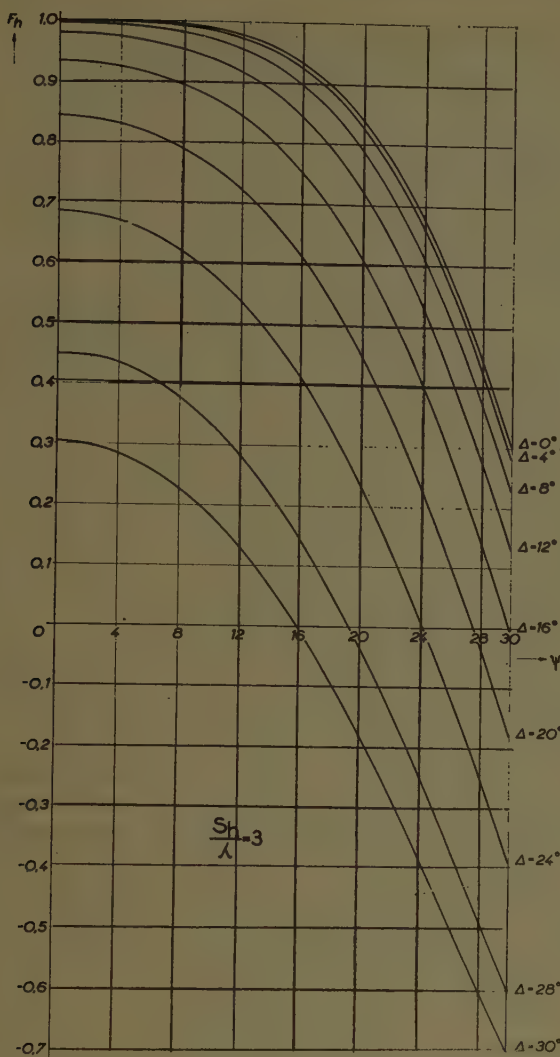


Fig. 10—Variation of $F_{ha}(\Delta, \psi)$ in function of the azimuthal angle ψ for different values of the angle of elevation Δ and for $s_h/\lambda = 3$.

practical cases their influence in the terminal impedances of both partial ASR is small. The magnitude of the current I (rms value), shown in (10), can therefore be calculated by the approximate equation (11), where R_{11} has the value mentioned

$$I \cong \sqrt{\frac{P}{4R_{11}}}, \quad (11)$$

à propos of (8). These equations can be used for approximate field intensity or gain calculations involving these types of arrays.

The influence of the horizontal spacing factor on the pattern diagram of an array can be studied by using the graphs shown in Figs. 8-11, each one having been drawn for a certain value of s_h/λ from 1-4. From these graphs we can see that for the values of Δ and ψ usually covered by the main lobe of the radiation pattern, the value of $F_{ha}(\Delta, \psi)$ is approximately equal to unity, which means that the form of that main lobe is not affected much by the interlacing if the value of s_h is within the limits covered by the above graphs. In these circum-

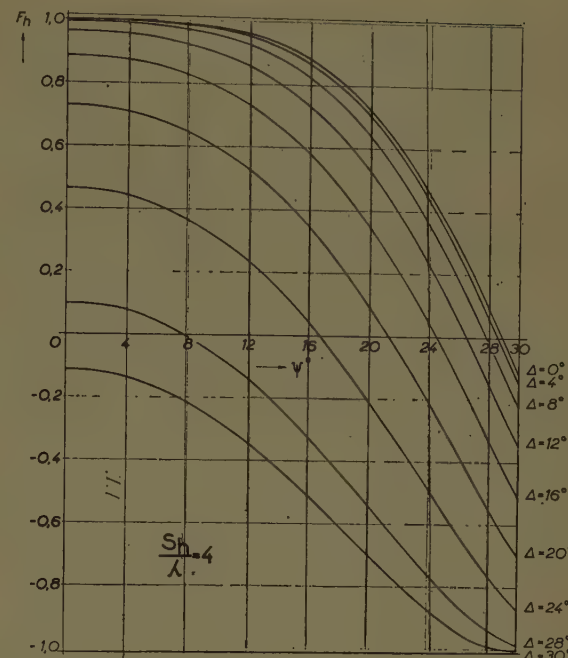


Fig. 11—Variation of $F_{ha}(\Delta, \psi)$ in function of the azimuthal angle ψ for different values of the angle of elevation Δ and for $s_h/\lambda = 4$.

stances, and by comparing (10), (7), and (1), we conclude that the ASIR described has a theoretical gain of about 6 db over a conventional rhombic and of about 3 db over an ASR with the same basic dimensions. It means that there is a greater concentration of power radiated in the directions covered by the main lobe of the pattern, with the corresponding reduction in the secondary lobes. Furthermore, experience shows¹¹ that the percentage of power dissipated in the termination devices of the rhombics is lower than in the case of a conventional rhombic.

In designing these arrays (ASR and ASIR), one should have in mind that the vertical and the horizontal spacings s_v and s_h should be large enough for the mutual impedances of the antennas of the array to have a negligible effect on the terminal impedance; but s_v and s_h should also be small enough for $F_{ve}(\Delta)$ and $F_{ha}(\Delta, \psi)$ to be as close as possible to unity for the useful directions of radiation. It is also to be noted that (6), (7), (9), and (10) assume that coupling between the antennas of the array has a negligible effect on the amplitude and phase of the current distribution in the antennas.

PRACTICAL DESIGN

Field of Application of Rhombic Antennas

Among the antennas more commonly used for VHF and HF directional radiation, the rhombics and the arrays of rhombics have an outstanding position because they offer a reasonably high directivity at low cost, with the additional advantage of being useful over a wide range (1-2 or 1-3) of frequencies.

With almost all types of antenna systems, cost increases with directivity (arrays of dipoles are a typical example). In the rhombic antenna, the directivity varies

with the geometric configuration of the antenna, the cost being only slightly affected; in consequence, the advantages of the rhombic antenna are accentuated with the increase of directivity.

One of the inconveniences of the rhombics is the dissipation of power in the terminating device, but more importance has been given to this point than it probably merits. Actually, when we have an antenna system intended to provide a certain radiation beam, we are mainly interested in concentrating in that beam as much as possible of the available transmitter power; whether the wasted power is dissipated in the antenna or radiated in wrong directions is of no consequence to the main purpose of the antenna, the former case being obviously less harmful.

For point-to-point communications or for highly directional broadcasting (with a total beamwidth up to, say, 15° – 20°), the rhombic antenna is a very convenient and, in general, the most economical solution; the array of 2 stacked rhombics (*ASR*) costs little more than a conventional rhombic (higher masts and more antenna wire, etc.), but introduces many advantages over a conventional rhombic (greater concentration of the power in the main beam and therefore less power wasted in secondary lobes and in the terminating device). The signal gain, which can be obtained with rhombic antennas, is about 10–15 db over a horizontal half-wave dipole at the same average height, while the directivity gain¹² over a hypothetical isotropic antenna in free space is about 20–25 db. The use of arrays of stacked and interlaced rhombics introduces still greater concentration of power in the desired beam, but one must take into consideration that the cost of an *ASIR* is slightly more than twice the cost of an *ASR*.

For broadcasting use and when a total beamwidth of about 20° – 30° is required, conventional rhombic antennas have seldom been used because the curtains of dipoles can insure a higher gain for such a beamwidth. Actually, if one uses *ASIR*, the same order of magnitude of gain can be obtained at appreciably lower cost, with the additional advantage of a wide frequency range.¹³

Geometric Configuration of the Antenna System

The first step in the design of a rhombic antenna or of an array of rhombics is to calculate the optimum values of H (average height above ground), l (side of the rhombus), ϕ (tilt angle), s_v (vertical spacing), and s_h (horizontal spacing), *i.e.*, to calculate the geometric configuration of the antenna system. In order to check the values obtained, the radiation pattern diagram should then be calculated; in practice, it is usually sufficient to calculate and draw the so-called vertical diagram (vary-

ing Δ for $\psi=0$) and the "horizontal" diagram (varying ψ for optimum Δ) for the different frequencies of interest. Additional steps involve the mechanical design of the antenna system and both the electrical and the mechanical design of the feeding and of the terminating arrangements (including the wide-band impedance matching sections when required).

Several methods of calculating the geometric configuration of a rhombic antenna have been described in the available literature, but almost all of them ignore the horizontal beamwidth requirement which is essential when the antenna is intended for broadcasting use. This is especially important when calculating the length l and the tilt angle ϕ . Another requirement, which is often ignored, is the necessity of the antenna having to operate in a certain frequency range. In the method described below, all these conditions are taken into consideration, enabling the most convenient compromise solution to be obtained. However, this solution will need to be analyzed further, bearing in mind the mechanical limitations of the system, availability of ground space, and other factors affecting the particular case being studied.

In order to calculate the height H above ground, a simple criterion consists in obtaining the value that makes the factor $F_H(\Delta)$, given by (4), equal to unity (its maximum value) for the desired value of Δ (conditioned by the propagation path) and for the wavelength λ_0 corresponding to the midpoint frequency of the range and which will be given by

$$\lambda_0 = \frac{2\lambda_{\min}\lambda_{\max}}{\lambda_{\min} + \lambda_{\max}}. \quad (12)$$

It can be easily seen that under these conditions, the value of $F_H(\Delta)$ will be the same at the two extreme frequencies of the range. The value of H can therefore be calculated using (13), which follows directly from (4), if we take the minimum possible value of H , which makes $F_H(\Delta)$ equal to unity.

$$H = \frac{\lambda_0}{4 \sin \Delta}. \quad (13)$$

In order to arrive at the most convenient values for l and ϕ , we must take into consideration two conflicting conditions: 1) we want the maximum possible field in the main direction of radiation; 2) we must insure that the horizontal beamwidth is greater than the minimum given by the specifications laid down for the antenna.

If we consider (1)–(3), we conclude that for $\psi=0$ (*i.e.*, in the plane of maximum radiation) and when $F_H(\Delta)=1$, the value of E is proportional to a factor which we shall call *gain factor*,¹⁴ given by

$$F_G = \frac{\cos \phi}{1 - \cos \Delta \sin \phi}, \quad (14)$$

¹² Harper, *op. cit.*, pp. 50–60.
¹³ The Portuguese Broadcasting Authority (Emissora Nacional de Radiodifusão) has in use, for the same service, curtains of 16 horizontal dipoles with reflectors (*HR4/4 arrays*) and arrays of stacked and interlaced rhombics (*ASIR*), giving a beamwidth of the order of 30° and having approximately the same gain. The tilt angle (ϕ) of the rhombics is 40° which means that they are slightly "squashed" in the direction of radiation.

¹⁴ A graph of F_G in function of Δ and ϕ can be found in H. P. Williams, "Antenna Theory and Design," Sir Isaac Pitman & Sons, Ltd., London, Eng., p. 287, Fig. 6.44; 1950.

and to the so-called *length factor*,¹⁵ given by

$$F_l = \sin^2 \left[\frac{\pi l}{\lambda} (1 - \cos \Delta \sin \phi) \right]. \quad (15)$$

The maximum value of the *length factor* is obviously unity and the maximum value of the *gain factor*, for the desired value of $\Delta = \Delta_0$, is reached when $\cos \Delta_0 = \sin \phi$, *i.e.*, for practical purposes, when $\phi = (\pi/2) - \Delta_0$. These conditions could be a basis for design, of course, if the beamwidth did not have to be considered.

However, if this is an important factor, and it normally is, even in point-to-point communications where it is sound to insure a certain beamwidth to take care of variations of direction at reflection points, another criterion will have to be followed. For the desired angle of fire Δ_0 , we must insure that the ratio

$$\frac{E(\psi = 0)}{E(\psi = \psi_0)}$$

is below a certain limit if the total beamwidth $2\psi_0$ is to be obtained. For instance, for a 6-db drop at the "edges" of the beam, that ratio should have a maximum value of 2 over the whole frequency range of the antenna.

Taking into consideration (1)–(3) and calculating the above ratio, we obtain the following approximate value

$$\frac{E(\psi=0)}{E(\psi=\psi_0)} = \frac{\sin^2 \left[\frac{\pi l}{\lambda} (1 - \cos \Delta_0 \sin \phi) \right]}{\sin \left\{ \frac{\pi l}{\lambda} [1 - \cos \Delta_0 \sin (\phi + \psi_0)] \right\} \cdot \sin \left\{ \frac{\pi l}{\lambda} [1 - \cos \Delta_0 \sin (\phi - \psi_0)] \right\}}. \quad (16)$$

in view of the fact that (17)

$$\frac{[1 - \cos \Delta \sin (\phi - \psi)]^{1/2} \cdot [1 - \cos \Delta \sin (\phi + \psi)]^{1/2}}{1 - \cos \Delta \sin \phi} \quad (17)$$

is roughly equal to unity for the directions of radiation of interest for the main lobe of the radiation pattern.

The values of l and ϕ should heretofore be calculated so that (16) is below the value previously fixed (2, in the example seen) for all the frequencies of the range and for the desired angle of fire Δ_0 . Because, for a certain antenna, the beamwidth decreases when the frequency increases, it is usually sufficient to make this calculation for the highest frequency of the range. Of the possible pairs of values for l and ϕ , we should select those that make higher the gain factor of (14) and the length factor of (15). Tables or graphs of F_G and F_l ¹⁵ will be of considerable help in making these calculations.

Actually the process outlined above is much simpler than it looks at first glance, and after a little practice it is very easy to follow. The most convenient values for l and ϕ can then be obtained after one or two attempts.

¹⁵ Graphs of F_l in function of Δ and $1/\lambda$, for different values of ϕ can be found in Williams, *ibid.*, pp. 288–289, Figs. 6.45(a)–6.45(d).

When we want to design an *ASR*, it is necessary to determine the value of the vertical spacing s_v ; the criterion outlined on page 41 can then be followed.

For an *ASIR*, the value of s_h will also have to be established. This is not critical and a sound criterion is to make it from 30–50 per cent of the main diagonal of the rhombus; the exact value to be used may depend on the mechanical conditions affecting the erection of the masts and the interlacing of the antennas.

Feeding Arrangement

It is well known that in a simple rhombic transmitting antenna it is common to have a 2-wire feeder with 600 ohms characteristic impedance, and in a receiving antenna the most common solution consists in installing a wide-band impedance matching unit at the top of the end mast, the transmission line between it and the receiver being of coaxial type.

In a transmitting array of stacked rhombics where the terminal impedance on the driving point of the array is about 300 to 350 ohms, the lead-down transmission line should be of the 4-wire type (the two wires of each side at the same potential). When high-power transmitters are used (about above 50 kw), it is convenient¹⁶ to choose a 4-wire transmission line, and a value of the characteristic impedance from 300 to 350 ohm is a convenient one. It is of great interest to note that a slight

impedance matching can be effected by varying conveniently the distance between the side conductors of the feeding line from top to "ground" level; thus, we can make sure that the terminal impedance offered to the transmission line in all working frequencies of interest is within the desired values. If, however, the line coming from the transmitter is of the 2-wire type with a characteristic impedance of about 600 to 700 ohm, the lead-down transmission line must take care of the impedance matching from the 4-wire 350-ohm (when using 2-wire rhombics) driving point at the top to the 2-wire 600-ohm one at the bottom. An exponential tapered line, where we vary gradually (from top to bottom) the separation of the side wires and the distance between the conductors, will provide the wideband impedance matching required.

In the case of an array of stacked and interlaced rhombics, exponential lines can also be used for impedance matching. In Fig. 12 we see (at the bottom of the figure) the common feeding point for both *ASR*.

¹⁶ F. C. McLean and F. D. Bolt, "The design and use of RF open-wire transmission lines and switchgear for broadcasting systems," *Proc. IEE*, vol. 93, pt. 3, sec. 2.1.2, p. 192, and sec. 6.1, p. 204; 1946.



Fig. 12—Detail of feeding arrangement in an ASIR.

Two transmission lines (2-wire 640-ohm) depart from this point to each *ASR* and the parallel connection is made to the 320-ohm 4-wire line coming from the transmitter. The exponential transmission line matching 2-wire 640-ohm to 4-wire 350-ohm can also be seen in this figure.

Terminating Arrangement

In order to insure a progressive wave current distribution in the antenna conductors, we must terminate a rhombic antenna by a resistance of the order of 700 to 800 ohms in which a certain power will be dissipated. When this power is up to about 5 to 10 kw, it is easy

to build an association of noninductive resistances in a convenient housing at ground level and connect it to the antenna terminating points by means of a dissipative transmission line. This last detail is very important since the line itself might dissipate almost as much power as the terminating resistances and an appreciable saving therefore can be made. For higher power, a greater length of dissipative line must be interposed between the terminating points of the antenna and the resistances. The most economical solution consists in using a tapered dissipative line and in reducing progressively¹⁷ the size of the wires so that a greater uniformity of power dissipated per meter of line is obtained. The line required is then much shorter than if it were of constant characteristics.

In an *ASR*, we can either terminate each rhombic separately or terminate both of them together by means of a 4-wire dissipative line; in this case the tapering arrangement mentioned above can be of particular interest. In an *ASIR* the two partial *ASR*'s will have to be terminated separately.

ACKNOWLEDGMENT

In his work on design and construction of antenna systems, the author has greatly benefited from visits made to BBC transmitting stations and from conversations, years ago, with BBC engineers. Some of the construction details illustrated in this paper have been mechanically designed with the cooperation of Standard Telephones & Cables and Coubro & Scrutton, of England. The author wishes to thank the Technical Director of the Emissora Nacional de Radiodifusão (Portuguese Broadcasting), of Lisbon, for permission to publish some of the photographs and diagrams shown in this paper.

¹⁷ *Ibid.*, sec. 2.1.5, p. 194.

Radiation Field of an Elliptical Helical Antenna*

J. Y. WONG† AND S. C. LOH†

Summary—Rigorous expressions for the radiation field of a helical antenna of elliptical shape are derived on the assumption of a traveling-wave type of current distribution along the helix conductor.

* Manuscript received by the PGAP, June 19, 1958; revised manuscript received, September 24, 1958. This contribution is from the Radio and Elec. Eng. Div., National Research Council, Ottawa, Can., and was presented at the URSI-IRE Spring Meeting, Washington, D. C.; April 24, 1958.

† National Research Labs., Ottawa, Ont., Can.

The analysis is valid for integral and nonintegral numbers of turns. These expressions for the general helix are employed to determine the fields for the limiting case of a circular helical antenna, and the results are essentially the same as those derived by both Knudsen and Kornhauser. Allowing the ellipse to degenerate to the other limiting case, a solution for the radiation field is obtained for the planar or commonly known zig-zag antenna. Therefore, it is possible to achieve a truly circularly polarized field with an elliptical helix of slight ellipticity.

INTRODUCTION

THE helical beam antenna described by Kraus¹ is characterized by two significant properties, namely, the antenna radiation pattern is single-lobed over a rather broad frequency band, and the field is very nearly circularly polarized in a direction along the axis of the helix. In order to derive the far-field expressions, Kraus first approximates the circular helix with one consisting of square turns. Assuming a traveling-wave current distribution along the conductor the two electric field components are determined for one turn. Considering the single turn as one element in an array, the antenna radiation pattern is obtained by multiplying the unit pattern by an array factor appropriate to the number of turns and the turn-spacing of the helix.

A different and somewhat more rigorous method of solving the radiation problem of a helical beam antenna has been presented by both Kornhauser² and Knudsen.³ Assuming a current distribution of the form considered by Kraus,¹ the field components are formulated in terms of a vector potential. The total vector potential, and consequently the radiation field of the antenna, are determined by integrating the appropriate integrals over the length of the helix.

In this paper, the radiation problem of a helical antenna of elliptical cross section is investigated. Expressions for the radiation field are developed using a method similar to the one employed by Knudsen.³ From the general expressions, the radiation of a circular helix can be obtained readily by allowing the ellipse to degenerate to a circle. In the other limiting case, the resulting configuration is a planar helix, or the commonly known "zig-zag" antenna. This antenna was first described by Cumming⁴ who used a method of solution similar to that used by Kraus for the helical antenna. In a recent paper, Sengupta⁵ has reported some theoretical and experimental investigations about the radiation properties of the single "zig-zag" antenna. Both of these degenerate or special cases are considered in this paper. The axial ratio of a helical antenna is a quantity of practical interest, and some calculations are included to illustrate the effect of helix shape on the polarization. It is shown that a truly circularly polarized field can result from a helix of mild ellipticity.

DERIVATION OF THE RADIATION FIELD

Consider a helical antenna of elliptical cross section located at the origin with its axis oriented along the

¹ J. D. Kraus, "The helical antenna," PROC. IRE, vol. 37, pp. 263-272; March, 1949.

² E. T. Kornhauser, "Radiation field of helical antennas with sinusoidal current," J. Appl. Phys., vol. 22, pp. 887-891; July, 1951.

³ H. L. Knudsen, "The field radiated by circular and square helical beam antennas," Trans. Danish Acad. Tech. Sciences, no. 8, pp. 3-55; 1950.

⁴ W. A. Cumming, "A non-resonant end-fire array for VHF and UHF," IRE TRANS. ON ANTENNAS AND PROPAGATION, vol. AP-3, pp. 52-58; April, 1955.

⁵ D. L. Sengupta, "The radiation characteristics of a zig-zag antenna," IRE TRANS. ON ANTENNAS AND PROPAGATION, vol. AP-6, pp. 191-194; April, 1958.

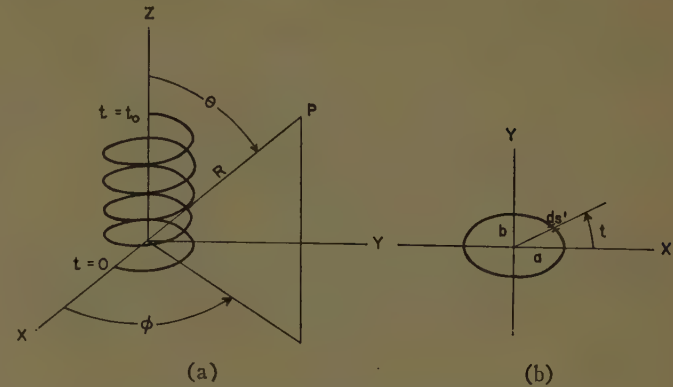


Fig. 1—(a) Helical antenna located at origin of coordinate system. (b) Cross section of helix in x - y plane.

z axis of the coordinate system extending from $t=0$ to $t=t_0$, as illustrated in Fig. 1(a). The helix is assumed to carry a traveling-wave current distribution of constant amplitude. It is required to determine the radiation field of the antenna at a distant point P .

The problem will be formulated in terms of a Hertzian vector potential. In order to facilitate the analysis, the vector potential will be determined in rectangular components and by applying the appropriate rectangular-spherical coordinate transformation equations, the field is expressed in terms of a single spherical component. In the following analysis, the rationalized mks system of units is employed, and the time variation $\exp(i\omega t)$ is understood.

We shall first develop the equations of the helical antenna. As shown in Fig. 1(b), the cross section of the helix in the x - y plane is an ellipse which can be described by the following parametric equations:

$$\begin{aligned} x &= a \cos t \\ y &= b \sin t \end{aligned} \quad 0 \leq t \leq t_0, \quad (1)$$

where a is the length of the semimajor axis and b is the length of the semiminor axis.

The element of arc length ds' along the ellipse is given by

$$\begin{aligned} ds' &= \sqrt{dx^2 + dy^2} \\ &= a\sqrt{1 - e^2 \cos^2 t} dt \end{aligned} \quad (2)$$

where $e = \sqrt{1 - (b/a)^2}$ is the eccentricity of the ellipse. Let α' be the pitch angle. The element of length dz , along the axis of the helix, is then

$$dz = a \tan \alpha' \sqrt{1 - e^2 \cos^2 t} dt. \quad (3)$$

Therefore

$$z = a \tan \alpha' K(e, t)$$

where

$$K(e, t) = \int_0^t \sqrt{1 - e^2 \cos^2 t} dt$$

is an elliptic integral of the second kind. From the

geometry, the arc length s along the helix conductor is given by

$$s = a \sec \alpha' K(e, t). \quad (4)$$

For purposes of the analysis, let us expand

$$\sqrt{1 - e^2 \cos^2 t}$$

by use of the binomial theorem, and then integrate term by term. Retaining only two terms of the development we have then an approximate expression for $K(e, t)$ given by

$$K(e, t) \approx c_1 t - c_2 \sin 2t,$$

where

$$\begin{aligned} c_1 &= 1 - \left[\frac{e^2}{4} + \frac{3}{64} e^4 + \frac{5}{256} e^6 \dots \right] \\ c_2 &= \frac{e^2}{8} + \frac{e^4}{32} + \frac{15}{1024} e^6 \dots \end{aligned} \quad (5)$$

Summarizing, the equations of the elliptical helix of pitch angle α' are

$$\begin{aligned} x &= a \cos t \\ y &= b \sin t \quad 0 \leq t \leq t_0. \\ z &= a \tan \alpha' K(e, t) \end{aligned} \quad (6)$$

In Fig. 2, the function $K(e, t)$ is plotted for various values of e from tabulated values given by Spenceley,⁶ and from the approximate expression of (5). The agreement between the approximate and tabulated values is seen to be very good.

The Hertzian vector potential $\bar{\Pi}$ of any arbitrary electric current distribution is given by

$$\bar{\Pi} = \frac{1}{4\pi\epsilon\omega} \frac{\exp(-ikR)}{R} \int \bar{I}(s) \exp(ik\bar{r} \cdot \bar{p}) ds, \quad (7)$$

where

- ϵ = the permittivity of free space,
- $k = 2\pi/\lambda$ where λ is the free-space wavelength,
- $\bar{I}(s)$ = the current in an element of length ds located at a point denoted by the vector \bar{r} ,
- \bar{p} = a unit vector in the direction of R .

In terms of the coordinate system shown in Fig. 1, (7) can be expanded as follows:

$$\begin{aligned} \bar{\Pi} &= \frac{1}{4\pi\epsilon\omega} \frac{\exp(-ikR)}{R} \int \bar{I}(s) \\ &\quad \cdot \exp[ik(x \cos \phi \sin \theta + y \sin \phi \sin \theta + z \cos \theta)] ds. \end{aligned} \quad (8)$$

We shall assume that the current distribution along the helix conductor is a traveling wave of constant amplitude given by the following form:

⁶ G. W. Spenceley and R. M. Spenceley, "Smithsonian Elliptic Functions Tables," Smithsonian Institution, Washington, D. C., 1947.

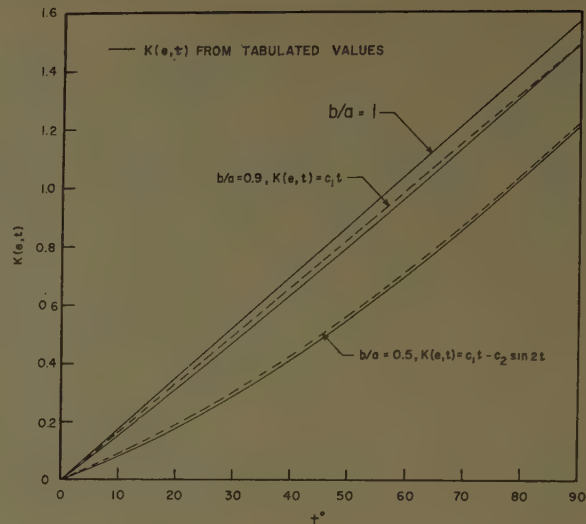


Fig. 2—Tabulated and approximate values of $K(e, t)$ for three different b/a ratios.

$$I(s) = I_0 \exp\left(-i \frac{k}{p} s\right) \quad (9)$$

where I_0 is the amplitude and p is the phase velocity of the current along the conductor relative to the velocity of light in free space.

As mentioned earlier, the first task will be to determine the three rectangular components of $\bar{\Pi}$. The expression for the Π_x component becomes

$$\begin{aligned} \Pi_x &= \frac{-aI_0}{4\pi\epsilon\omega} \frac{\exp(-ikR)}{R} \int_0^{t_0} \exp\left(-i \frac{k}{p} s\right) \\ &\quad \cdot \exp[ik(x \cos \phi \sin \theta + y \sin \phi \sin \theta + z \cos \theta)] \sin t dt. \end{aligned} \quad (10)$$

In terms of the helix described in (6), one obtains upon substitution in (10), the following result:

$$\begin{aligned} \Pi_x &= \frac{-aI_0}{4\pi\epsilon\omega} \frac{\exp(-ikR)}{R} \int_0^{t_0} \sin t \\ &\quad \cdot \left\{ \exp\left[ik\left(-\frac{a}{p} \sec \alpha' K(e, t) + a \tan \alpha' K(e, t) \cos \theta \right. \right. \right. \\ &\quad \left. \left. \left. + a \cos \phi \sin \theta \cos t + b \sin \phi \sin \theta \sin t\right)\right] \right\} dt. \end{aligned} \quad (11)$$

Simplification of (11) yields

$$\begin{aligned} \Pi_x &= \frac{-aI_0}{4\pi\epsilon\omega} \frac{\exp(-ikR)}{R} \int_0^{t_0} \sin t \\ &\quad \cdot \left\{ \exp[i(\alpha K(e, t) + \beta \cos t + \gamma \sin t)] \right\} dt \end{aligned} \quad (12)$$

where

$$\begin{aligned} \alpha &= ka \left(\tan \alpha' \cos \theta - \frac{\sec \alpha'}{p} \right), \\ \beta &= ka \sin \theta \cos \phi, \end{aligned}$$

and

$$\gamma = kb \sin \theta \sin \phi.$$

A further simplification of (12) can be obtained by employing the following trigonometric identity:

$$\xi \cos(t - \tau) = \beta \cos t + \gamma \sin t \quad (13)$$

where

$$\xi = \sqrt{\beta^2 + \gamma^2}$$

$$\tau = \tan^{-1}\left(\frac{\gamma}{\beta}\right) = \tan^{-1}\left(\frac{b}{a} \tan \phi\right).$$

Therefore, it follows that

$$\begin{aligned} \Pi_x &= \frac{-aI_0}{4\pi\epsilon i\omega} \frac{\exp(-ikR)}{R} \int_0^{t_0} \sin t \\ &\quad \cdot \{\exp[i(\alpha K(e, t) + \xi \cos(t - \tau))]\} dt \\ &= \frac{-aI_0}{4\pi\epsilon i\omega} \frac{\exp(-ikR)}{R} \int_0^{t_0} \sin t \\ &\quad \cdot \{\exp[i(\alpha c_1 t - \alpha c_2 \sin 2t + \xi \cos(t - \tau))]\} dt. \end{aligned} \quad (14)$$

We may obtain a series expansion for (14) by utilizing the well-known Fourier-Bessel expansions,

$$\begin{aligned} \exp[i\xi \cos(t - \tau)] &= \sum_{m=-\infty}^{\infty} i^m J_m(\xi) \exp[im(t - \tau)] \\ \exp[i\alpha c_2 \sin 2t] &= \sum_{n=-\infty}^{\infty} J_n(\alpha c_2) \exp(i2nt). \end{aligned} \quad (15)$$

Substituting the above identities in (14) yields the following result:

$$\begin{aligned} \Pi_x &= \frac{-aI_0}{4\pi\epsilon i\omega} \frac{\exp(-ikR)}{R} \sum_m \sum_n i^m J_m(\xi) J_n(\alpha c_2) \\ &\quad \cdot \exp(-im\tau) \int_0^{t_0} \sin t \{\exp[i(\alpha c_1 + m - 2n)t]\} dt. \end{aligned} \quad (16)$$

The integral in (16) can be evaluated by expressing $\sin t$ in terms of its exponential equivalent; therefore,

$$\begin{aligned} \Pi_x &= \frac{aI_0}{8\pi\epsilon i\omega} \frac{\exp(-ikR)}{R} \sum_m \sum_n i^m J_m(\xi) J_n(\alpha c_2) \\ &\quad \cdot \exp(-im\tau) \left\{ \frac{\exp[i(\alpha c_1 + m - 2n + 1)t_0] - 1}{\alpha c_1 + m - 2n + 1} \right. \\ &\quad \left. - \frac{\exp[i(\alpha c_1 + m - 2n - 1)t_0] - 1}{\alpha c_1 + m - 2n - 1} \right\}. \end{aligned} \quad (17)$$

The y component of $\bar{\Pi}$ can be determined in exactly the same manner. Hence, for Π_y we have

$$\begin{aligned} \Pi_y &= \frac{bI_0}{4\pi\epsilon i\omega} \frac{\exp(-ikR)}{R} \int_0^{t_0} \cos t \\ &\quad \cdot \{\exp[i(\alpha c_1 t - \alpha c_2 \sin 2t + \xi \cos(t - \tau))]\} dt \\ &= \frac{bI_0}{4\pi\epsilon i\omega} \frac{\exp(-ikR)}{R} \sum_m \sum_n i^m J_m(\xi) J_n(\alpha c_2) \\ &\quad \cdot \exp(-im\tau) \int_0^{t_0} \cos t \{\exp[i(\alpha c_1 + m - 2n)t]\} dt. \end{aligned} \quad (18)$$

Evaluation of the integral yields

$$\begin{aligned} \Pi_y &= \frac{-bI_0}{8\pi\epsilon\omega} \frac{\exp(-ikR)}{R} \sum_m \sum_n i^m J_m(\xi) J_n(\alpha c_2) \\ &\quad \cdot \exp(-im\tau) \left\{ \frac{\exp[i(\alpha c_1 + m - 2n + 1)t_0] - 1}{\alpha c_1 + m - 2n + 1} \right. \\ &\quad \left. + \frac{\exp[i(\alpha c_1 + m - 2n - 1)t_0] - 1}{\alpha c_1 + m - 2n - 1} \right\}. \end{aligned} \quad (19)$$

Similarly, the expression for Π_z becomes

$$\begin{aligned} \Pi_z &= \frac{aI_0 \tan \alpha'}{4\pi\epsilon i\omega} \frac{\exp(-ikR)}{R} \left\{ c_1 \int_0^{t_0} \exp[i(\alpha c_1 t - \alpha c_2 \sin 2t + \xi \cos(t - \tau))] dt \right. \\ &\quad - 2c_2 \int_0^{t_0} \cos 2t \exp[i(\alpha c_1 t - \alpha c_2 \sin 2t + \xi \cos(t - \tau))] dt \\ &= \frac{\alpha I_0 \tan \alpha'}{4\pi\epsilon i\omega} \frac{\exp(-ikR)}{R} \sum_m \sum_n i^m J_m(\xi) J_n(\alpha c_2) \\ &\quad \cdot \exp(-im\tau) \left\{ c_1 \int_0^{t_0} \exp[i(\alpha c_1 + m - 2n)t] dt \right. \\ &\quad \left. - 2c_2 \int_0^{t_0} \cos 2t \exp[i(\alpha c_1 + m - 2n)t] dt \right\}. \end{aligned} \quad (20)$$

Evaluation of (20) gives

$$\begin{aligned} \Pi_z &= \frac{\alpha I_0 \tan \alpha'}{4\pi\epsilon\omega} \frac{\exp(-ikR)}{R} \sum_m \sum_n i^m J_m(\xi) J_n(\alpha c_2) \\ &\quad \cdot \exp(-im\tau) \left\{ -c_1 \frac{\exp[i(\alpha c_1 + m - 2n)t_0] - 1}{\alpha c_1 + m - 2n} \right. \\ &\quad \left. + c_2 \left[\frac{\exp[i(\alpha c_1 + m - 2n + 2)t_0] - 1}{\alpha c_1 + m - 2n + 2} \right. \right. \\ &\quad \left. \left. + \frac{\exp[i(\alpha c_1 + m - 2n - 2)t_0] - 1}{\alpha c_1 + m - 2n - 2} \right] \right\}. \end{aligned} \quad (21)$$

Case I: Near-Circular $b \approx a$

The expressions developed above are valid for an elliptical helix of arbitrary shape. Where the helix is almost circular or only slightly elliptical, the expressions can be greatly simplified. For this case, we let $c_2 = 0$, and approximate $K(e, t)$ with only the first term. From inspection of the expressions for $\bar{\Pi}$, the resulting equations are as follows:

$$\begin{aligned} \Pi_x &= \frac{aI_0}{8\pi\epsilon i\omega} \frac{\exp(-ikR)}{R} \sum_m i^m J_m(\xi) \\ &\quad \cdot \exp(-im\tau) \left\{ \frac{\exp[i(\alpha c_1 + m + 1)t_0] - 1}{\alpha c_1 + m + 1} \right. \\ &\quad \left. - \frac{\exp[i(\alpha c_1 + m - 1)t_0] - 1}{\alpha c_1 + m - 1} \right\} \end{aligned} \quad (22)$$

$$\Pi_y = \frac{-bI_0}{8\pi\epsilon\omega} \frac{\exp(-ikR)}{R} \sum_m i^m J_m(\xi) \exp(-im\tau) \\ \cdot \exp(-im\tau) \left\{ \frac{\exp[i(\alpha c_1 + m + 1)t_0] - 1}{\alpha c_1 + m + 1} \right. \\ \left. + \frac{\exp[i(\alpha c_1 + m - 1)t_0] - 1}{\alpha c_1 + m - 1} \right\} \quad (23)$$

$$\Pi_z = \frac{aI_0 \tan \alpha'}{4\pi\epsilon\omega} \frac{\exp(-ikR)}{R} \sum_m i^m J_m(\xi) \\ \cdot \exp(-im\tau) \left\{ -c_1 \frac{\exp[i(\alpha c_1 + m)t_0] - 1}{\alpha c_1 + m} \right\}. \quad (24)$$

Case II: Circular Helix $b=a$

When $b=a$ the ellipse degenerates to a circle, and for this limiting case, $e=0$. Therefore, $c_1=1$, and from (13) we find that

$$\xi = ka \sin \theta, \quad \tau = \phi. \quad (25)$$

Introducing the results of (25) in the expressions for the near-circular case, one obtains directly the expressions for the circular helix, namely

$$\Pi_x = \frac{aI_0}{8\pi\epsilon i\omega} \frac{\exp(-ikR)}{R} \sum_m i^m J_m(ka \sin \theta) \\ \cdot \exp(-im\phi) \left\{ \frac{\exp[i(\alpha + m + 1)t_0] - 1}{\alpha + m + 1} \right. \\ \left. - \frac{\exp[i(\alpha + m - 1)t_0] - 1}{\alpha + m - 1} \right\} \quad (26)$$

$$|AR| = \frac{a}{b} \cdot \frac{\sum_n J_n(\alpha c_2) \left[\frac{\exp[i(\alpha c_1 - 2n + 1)t_0] - 1}{\alpha c_1 - 2n + 1} - \frac{\exp[i(\alpha c_1 - 2n - 1)t_0] - 1}{\alpha c_1 - 2n - 1} \right]}{\sum_n J_n(\alpha c_2) \left[\frac{\exp[i(\alpha c_1 - 2n + 1)t_0] - 1}{\alpha c_1 - 2n + 1} + \frac{\exp[i(\alpha c_1 - 2n - 1)t_0] - 1}{\alpha c_1 - 2n - 1} \right]}. \quad (32)$$

$$\Pi_y = \frac{-aI_0}{8\pi\epsilon\omega} \frac{\exp(-ikR)}{R} \sum_m i^m J_m(ka \sin \theta) \\ \cdot \exp(-im\phi) \left\{ \frac{\exp[i(\alpha + m + 1)t_0] - 1}{\alpha + m + 1} \right. \\ \left. + \frac{\exp[i(\alpha + m - 1)t_0] - 1}{\alpha + m - 1} \right\} \quad (27)$$

$$\Pi_z = \frac{aI_0 \tan \alpha'}{4\pi\epsilon\omega} \frac{\exp(-ikR)}{R} \sum_m i^m J_m(ka \sin \theta) \\ \cdot \exp(-im\phi) \left\{ - \frac{\exp[i(\alpha + m)t_0] - 1}{\alpha + m} \right\}. \quad (28)$$

In order to determine the components of $\bar{\Pi}$ in spherical coordinates, we employ the following coordinate transformation equations:⁷

$$\begin{aligned} \Pi_r &= \Pi_x \sin \theta \cos \phi + \Pi_y \sin \theta \sin \phi + \Pi_z \cos \theta \\ \Pi_\theta &= \Pi_x \cos \theta \cos \phi + \Pi_y \cos \theta \sin \phi - \Pi_z \sin \theta \\ \Pi_\phi &= -\Pi_x \sin \phi + \Pi_y \cos \phi. \end{aligned} \quad (29)$$

The electric field components can be derived from the Hertzian vector by applying the following vector relationship:

$$\bar{E} = \omega^2 \mu \epsilon \bar{\Pi} + \nabla(\nabla \cdot \bar{\Pi}) \quad (30)$$

where μ is the permeability of free space.

A useful quantity which is often employed to describe the polarization of the radiation field of a helical antenna is the axial ratio. The axial ratio AR is defined as the ratio of the E_θ and E_ϕ components; that is,

$$|AR| = \frac{E_\theta}{E_\phi}.$$

We shall restrict our attention to the fields along the z axis of the helix. Hence $\theta=\phi=0$ and from (29) it follows that

$$\begin{aligned} \Pi_\theta &= \Pi_x \\ \Pi_\phi &= \Pi_y. \end{aligned} \quad (31)$$

Since the electric field is directly proportional to $\bar{\Pi}$ in spherical coordinates, the axial ratio can be obtained directly from the rectangular components already determined. Consequently, for the three cases considered we have:

1) Elliptical:

2) Near-Circular:

$$|AR| = \frac{a}{b} \cdot \frac{1 - \frac{\exp[i(\alpha c_1 - 1)t_0] - 1}{\alpha c_1 - 1} \cdot \frac{\alpha c_1 + 1}{\alpha c_1 - 1}}{1 + \frac{\exp[i(\alpha c_1 - 1)t_0] - 1}{\alpha c_1 - 1} \cdot \frac{\alpha c_1 + 1}{\alpha c_1 - 1}}. \quad (33)$$

3) Circular:

$$|AR| = \frac{1 - \frac{\exp[i(\alpha - 1)t_0] - 1}{\exp[i(\alpha + 1)t_0] - 1} \cdot \frac{\alpha + 1}{\alpha - 1}}{1 + \frac{\exp[i(\alpha - 1)t_0] - 1}{\exp[i(\alpha + 1)t_0] - 1} \cdot \frac{\alpha + 1}{\alpha - 1}}. \quad (34)$$

⁷ S. A. Schelkunoff, "Electromagnetic Waves," D. Van Nostrand Co., Inc., New York, N. Y.; 1943.

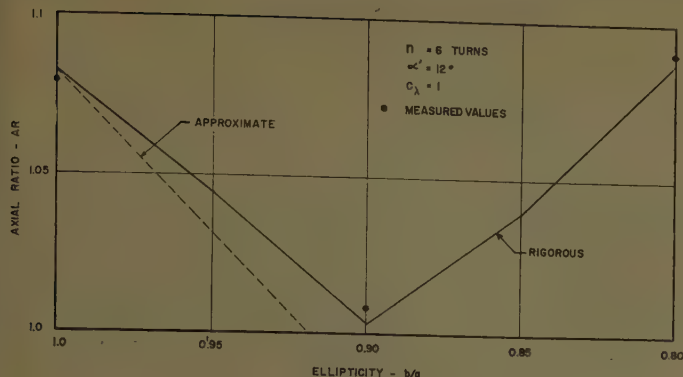


Fig. 3—Effect of helix shape on the axial ratio of the radiation field.

Note that for all three cases, the two field components are in phase quadrature.

For a helix possessing an integral number of turns, that is, $t_0 = 2n\pi$ ($n = 1, 2, \dots$), where n is the number of turns, a relatively simple relationship for AR can be derived for the near-circular case. From (33) it follows that

$$AR = \frac{a}{b} \cdot \frac{1 - \frac{\alpha c_1 + 1}{\alpha c_1 - 1}}{1 + \frac{\alpha c_1 + 1}{\alpha c_1 - 1}}. \quad (35)$$

Hence, we have

$$AR = \frac{a}{b} \cdot \frac{1}{\alpha c_1}. \quad (36)$$

If one assumes that the value for the relative phase velocity p of the current corresponds to the condition of increased directivity, as considered by Kraus,¹ we have

$$p = \frac{1}{\sin \alpha' + \left(\frac{2n+1}{2n} \right) \frac{\cos \alpha'}{C_\lambda}} \quad (37)$$

where C_λ is the circumference of the helix in wavelengths. Inserting the value of p in (12), we obtain the following result for α :

$$\alpha = ka \left(\frac{2n+1}{2n} \right) \frac{\lambda}{\pi(a+b)}. \quad (38)$$

In (38) the following approximation has been used for C_λ :

$$C_\lambda \approx \pi(a+b).$$

Inserting α in (36) yields

$$AR = \frac{a+b}{2b} \left(\frac{2n+1}{2n} \right) \frac{1}{c_1}. \quad (39)$$

Eq. (39) gives the axial ratio of a near-circular helix in terms of its shape and length. For a circular helix, the result is identical with the one given by Kraus.¹



Fig. 4—One of the helical antennas used in the axial ratio measurements.

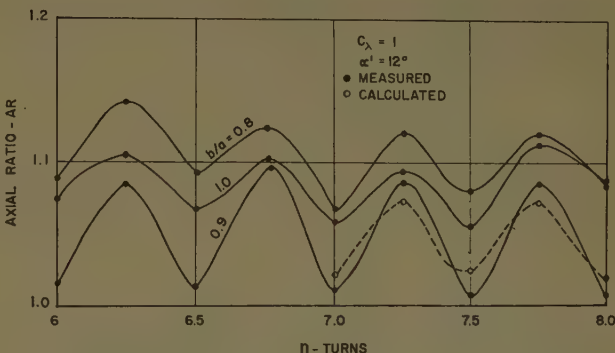


Fig. 5—Effect of number of turns on the axial ratio of the radiation field.

In order to determine the effect of helix shape on the polarization of the radiation field, the axial ratio is plotted as a function of the b/a ratio, as shown in Fig. 3. A 6-turn helix of pitch angle 12° and a circumference of one wavelength was assumed in the calculations. The relative phase velocity p was determined from (37), and the solid curve was calculated using the rigorous expression given by (32). It is observed that as the helix departs from circular, the axial ratio approaches unity. For a b/a ratio of about 0.9 the field is almost circularly polarized. The dotted curve was obtained from (39) and illustrates to what extent the approximate expression can be used to determine the axial ratio. The circled points are measured values and the agreement between calculated and measured results is quite good.

A photograph of one of the helical antennas used in the measurements is shown in Fig. 4. The helix conductor is supported by means of a polystyrene foam form of low permittivity. The ground plane is about $\frac{3}{4}$ wavelength in diameter and the helix is energized at its periphery.

Fig. 5 illustrates the effect of helix turns on the axial ratio. The axial ratio was measured for three different values of ellipticity corresponding to b/a ratios of 1.0, 0.9, and 0.8. It can be seen that the axial ratio is an oscillating function of the number of turns and the mini-

mum axial ratio occurs for a helix containing an integral or a half-integral number of turns. Calculations were carried out for a 0.9 helix, represented by the dashed curve of Fig. 5. Again, the agreement between measured and calculated values is seen to be fairly good.

Case III: Planar Helix $b=0$

For the case where $b=0$, the resulting configuration is a planar helix or the commonly known "zig-zag" antenna. This degenerate case can be described by the following parametric equations:

$$\begin{aligned} x &= a \cos t \\ y &= 0 \\ z &= 2/\pi \text{ at } \tan \alpha' \\ s &= 2/\pi \text{ at } \sec \alpha'. \end{aligned} \quad (40)$$

Since $b=0$, only Π_x and Π_z components exist. Comparing (39) with (6) we observe that

$$K(e, t) = \frac{2}{\pi} t.$$

Hence from (5) we find that

$$c_1 = \frac{2}{\pi}; \quad c_2 = 0.$$

From the general expression for Π_x given by (17), the x component of $\bar{\Pi}$ for this special case becomes

$$\begin{aligned} \Pi_x &= \frac{aI_0}{8\pi\epsilon i\omega} \frac{\exp(-ikR)}{R} \sum_m i^m J_m(\beta) \\ &\cdot \left\{ \frac{\exp[i(\alpha c_1 + m + 1)t_0] - 1}{\alpha c_1 + m + 1} \right. \\ &\quad \left. - \frac{\exp[i(\alpha c_1 + m - 1)t_0] - 1}{\alpha c_1 + m - 1} \right\}. \end{aligned} \quad (41)$$

Similarly, the Π_z component becomes

$$\begin{aligned} \Pi_z &= \frac{aI_0 \tan \alpha'}{4\pi\epsilon\omega} \frac{\exp(-ikR)}{R} \sum_m i^m J_m(\beta) \\ &\cdot \left\{ -\frac{2}{\pi} \frac{\exp[i(\alpha c_1 + m)t_0] - 1}{\alpha c_1 + m} \right\}. \end{aligned} \quad (42)$$

The spherical components of $\bar{\Pi}$ are then obtained through the following transformation equations:

$$\begin{aligned} \Pi_\theta &= \Pi_x \cos \theta \cos \phi - \Pi_z \sin \theta, \\ \Pi_\phi &= -\Pi_x \sin \phi. \end{aligned} \quad (43)$$

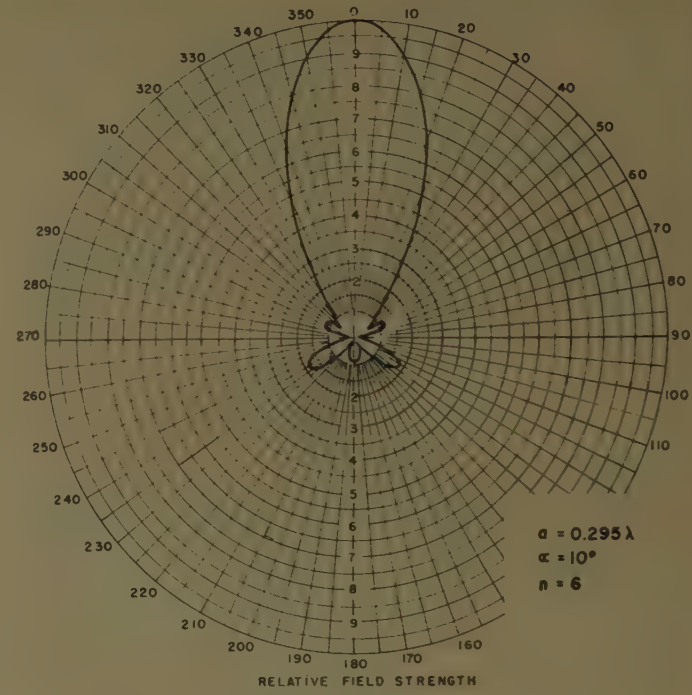


Fig. 6—Calculated radiation pattern for a 6-turn planar helix antenna.

We note that for this degenerate case, the radiation field in a plane containing the antenna is linearly polarized.

As an example to illustrate the results given by (41) and (42), the radiation pattern was calculated for a 6-turn planar helix. The values for a and the pitch angle α' were chosen to be 0.295λ and 10° to correspond with the dimensions used by Cumming,⁴ who found that a phase velocity of 91 per cent gave the best fit with the measured pattern; consequently, in our calculations a value of $p=0.91$ was used. Fig. 6 shows a pattern of the antenna in the y - z plane.

CONCLUSIONS

Expressions for the radiation field of a helical antenna of elliptical shape have been derived assuming a traveling-wave current distribution of constant amplitude. Furthermore, in the calculations we have assumed that the value for the relative phase velocity of the current is the same as that calculated from the increased directivity condition considered by Kraus¹ for the circular case. For elliptical helices of slight ellipticity this assumption seems very reasonable. However, for small values of b/a ratio, one would expect that this assumption would no longer be valid.

The Rectangular Loop Antenna as a Dipole*

RONOLD KING†

Summary—An integral equation for the current in a rectangular loop of wire is derived for a loop that is driven by two generators located at the centers of one pair of opposite sides. The EMF's are equal in magnitude and in phase in the sense that they maintain currents in the generators that are in the same direction relative to the coordinate system and, therefore, in opposite directions from the point of view of circulation around the loop. An approximate solution is obtained for the distribution of current around the loop and for the driving-point impedance. It is shown that the solution for the rectangle of wire reduces to that of the symmetrically driven folded dipole when one dimension is made electrically small and to a section of transmission line driven simultaneously at both ends when the other dimension is made small. The loop that is electrically small in both directions is also examined.

INTRODUCTION

THE circuit properties of the rectangular loop antenna have been studied in the past primarily in two special cases: the electrically small loop shown in Fig. 1(a) and the folded dipole shown in Fig. 1(b). An analysis¹ of the former usually depends upon the assumption that the current is essentially uniform in amplitude and phase in a circulatory sense around the loop when this is driven by a generator located at the center of one side. The currents at corresponding points in opposite sides are then equal in magnitude and instantaneously opposite in direction with respect to the space coordinates, so that, by analogy with the balanced open-wire line, they may be called currents in a *transmission-line mode*. Possible currents in opposite pairs of sides that are equal and instantaneously codirectional at corresponding points, currents that belong to what may be called a *transverse dipole mode*, are ignored or neglected in such an analysis. The conventional folded dipole shown in Fig. 1(b) is a rectangular loop that is electrically small in one dimension but not in the other; it is driven by a generator at the center of one of the longer sides. The folded dipole has been analyzed by the method of symmetrical components^{2,3} which, in effect, divides the current into two independent parts and permits their separate determination as currents in the antisymmetrical or transmission-line mode, and currents in the symmetrical or dipole mode. The former are excited by equal and opposite generators, the latter by

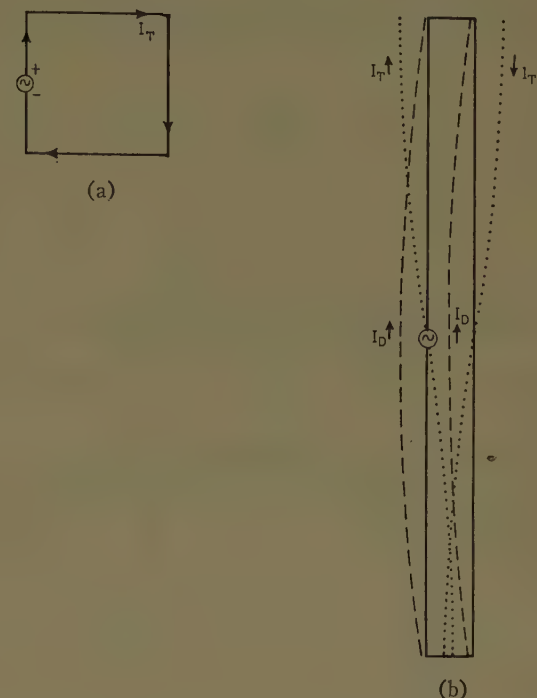


Fig. 1—Extreme types of loop antennas. (a) Conventional loop. Perimeter is small compared to wavelength; currents are equal in amplitude and opposite in direction on opposite sides. (b) Folded dipole. Perimeter is near a wavelength; dipole-mode currents I_D are equal and codirectional. Transmission-line currents I_T are equal and opposite.

equal and codirectional generators at the centers of both of the longer sides. By superposition the generator EMF's add on one side, subtract and cancel on the other.

When a rectangular loop of arbitrary dimensions is driven at the center of one side by a voltage V^e , currents in *both* the transmission-line mode and the dipole mode are excited. The former are maintained by the voltages $\frac{1}{2}V^e$ and $-\frac{1}{2}V^e$, respectively, at the centers of the two longer sides, the latter by two equal voltages $\frac{1}{2}V^e$ at the centers of these sides. As an essential step in the complete analysis of the general rectangular loop as a transmitting and receiving antenna, and in order to determine the circuit properties of the rectangular loop as a dipole antenna in its own right (Fig. 2) it is the purpose of the present study to investigate the currents in, and impedance of a rectangle of dimensions $2c$ and $2d$ constructed of a single turn of wire of radius a and driven at the centers of the sides of length $2d$ by generators with equal and codirectional EMF's. The currents maintained by these generators are in the vertical dipole mode and no others are generated. The loop to be analyzed is shown in Fig. 3. Note that the method used

* Manuscript received by the PGAP, October 14, 1957. The research reported in this document was made possible through support extended to Harvard University by the Armed Forces Special Weapons Project, under ONR Contract Nonr-1866(26).

† Crift Lab., Harvard Univ., Cambridge, Mass.

¹ See, e.g., R. W. P. King, "Electromagnetic Engineering," McGraw-Hill Book Co., Inc., New York, N. Y., pp. 421-431; 1945.

² R. W. P. King, H. R. Minno, and A. H. Wing, Jr., "Transmission Lines, Antennas, and Wave Guides," McGraw-Hill Book Co., Inc., New York, N. Y., pp. 224-226; 1945.

³ R. W. P. King, "Theory of Linear Antennas," Harvard University Press, Cambridge, Mass., pp. 334-361; 1956.

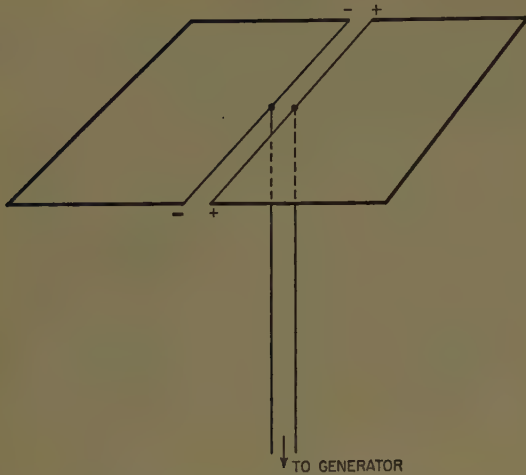


Fig. 2—Horizontal loop as a dipole antenna maintaining a horizontally polarized electric field.

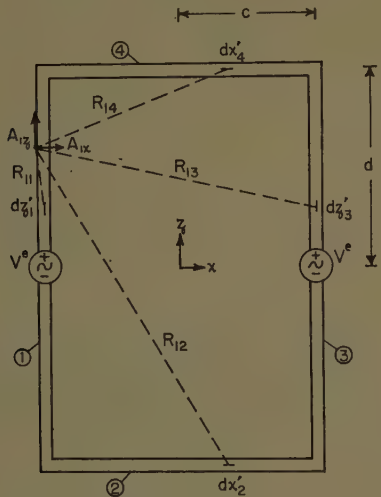


Fig. 3—Rectangular loop excited in the vertical dipole mode.

in the previous analysis^{2,3} of the symmetrical or dipole mode specifically in the folded dipole cannot be applied in general, since it assumes that the pair of sides of length $2c$ is so short that it contributes negligibly to the problem. In the proposed analysis the sides of length $2c$ are not so restricted. They may be electrically long or short, and longer or shorter than the other pair of sides that contain the generators.

THE INTEGRAL EQUATIONS

The integral equations for the currents in the four sides of the loop may be obtained from the boundary conditions obeyed by the tangential component of the electric field at the highly conducting surfaces of the rectangle of wire. For sides 1 and 2 they may be expressed in terms of the scalar and vector potentials ϕ and \mathbf{A} as follows:

$$E_{1z} = \frac{-\partial \phi_{1z}}{\partial z} - \frac{j\omega}{\beta_0^2} \left(\frac{\partial^2 A_{1z}}{\partial z^2} + \beta_0^2 A_{1z} \right) \doteq 0 \quad (1a)$$

$$E_{2z} = \frac{-\partial \phi_{2z}}{\partial x} - \frac{j\omega}{\beta_0^2} \left(\frac{\partial^2 A_{2z}}{\partial x^2} + \beta_0^2 A_{2z} \right) \doteq 0 \quad (1b)$$

where $\beta_0 = \omega/v_0 = 2\pi/\lambda_0$ and $v_0 = 1/\sqrt{\epsilon_0 \mu_0} = 3 \times 10^8$ meters/sec. The vector and scalar potentials at arbitrary points on the surface of conductors 1 and 2 have the following forms. Note that the symmetry relations,

$$A_3 = A_1, \quad A_4 = -A_2, \quad (2)$$

have been invoked.

$$A_1 = \hat{x} A_{1z} + \hat{z} A_{1x}, \quad \phi_1 = \phi_{1z} + \phi_{1x};$$

$$\phi_{1z} = \frac{j\omega}{\beta_0^2} \frac{\partial A_{1z}}{\partial x}, \quad \phi_{1x} = \frac{j\omega}{\beta_0^2} \frac{\partial A_{1x}}{\partial z}; \quad (3a)$$

$$A_2 = \hat{x} A_{2z} + \hat{z} A_{2x}, \quad \phi_2 = \phi_{2z} + \phi_{2x};$$

$$\phi_{2z} = \frac{j\omega}{\beta_0^2} \frac{\partial A_{2z}}{\partial x}, \quad \phi_{2x} = \frac{j\omega}{\beta_0^2} \frac{\partial A_{2x}}{\partial z}; \quad (3b)$$

where

$$A_{1z} = \frac{1}{4\pi\nu_0} \int_{-d}^d I_{1z}(z') \mathcal{K}_{1A}(z, z') dz',$$

$$\phi_{1z} = \frac{1}{4\pi\epsilon_0} \int_{-c}^c q_2(x') \mathcal{K}_{1B}(z, x') dx' \quad (4a)$$

$$A_{2z} = \frac{1}{4\pi\nu_0} \int_{-c}^c I_{2z}(x) \mathcal{K}_{2A}(x, z') dx',$$

$$\phi_{2z} = \frac{1}{4\pi\epsilon_0} \int_{-d}^d q_1(z') \mathcal{K}_{2B}(x, z') dz'. \quad (4b)$$

The notation $\nu_0 = 1/\mu_0$ is used, where $\mu_0 = 4\pi \times 10^{-7}$ farad/m. The kernels are defined as follows:

$$\mathcal{K}_{1A}(z, z') = \mathcal{K}_{11}(z, z') + \mathcal{K}_{13}(z, z'),$$

$$\mathcal{K}_{1B}(z, x') = \mathcal{K}_{12}(z, x') - \mathcal{K}_{14}(z, x'), \quad (5a)$$

$$\mathcal{K}_{2A}(x, z') = \mathcal{K}_{22}(x, z') - \mathcal{K}_{24}(x, z'),$$

$$\mathcal{K}_{2B}(x, z') = \mathcal{K}_{21}(x, z') + \mathcal{K}_{23}(x, z'), \quad (5b)$$

where

$$\mathcal{K}_{ij}(u, v') = \frac{e^{-i\beta_0 R_{ij}}}{R_{ij}}. \quad (5c)$$

The several distances are defined as follows:

$$R_{11} = \sqrt{(z' - z)^2 + a^2} \quad R_{13} = \sqrt{(z' - z)^2 + 4d^2}, \quad (6a)$$

$$R_{12} = \sqrt{(d + z)^2 + (c + x')^2}, \quad R_{14} = \sqrt{(d - z)^2 + (c + x')^2}, \quad (6b)$$

$$R_{22} = \sqrt{(x' - x)^2 + a^2}, \quad R_{24} = \sqrt{(x' - x)^2 + 4c^2}, \quad (6c)$$

$$R_{21} = \sqrt{(c + x)^2 + (d + z')^2}, \quad R_{23} = \sqrt{(c - x)^2 + (d + z')^2}. \quad (6d)$$

The solutions of (1a) and (1b) for A_{1z} and A_{2z} , respectively, may be expressed as sums of trigonometric functions and a particular integral. They may then be combined with (4a) and (4b) to obtain the following integral equations in which $\xi_0 = \sqrt{\mu_0 \epsilon_0}$:

$$4\pi\nu_0 A_{1z}(z) = \int_{-d}^d I_{1z}(z') \mathcal{K}_{1A}(z, z') dz' \\ = \frac{-j4\pi}{\xi_0} [C_{1z} \cos \beta_0 z + C_{2z} \sin \beta_0 z - \theta_{1A}(z)], \quad (7a)$$

$$4\pi\nu_0 A_{2x}(x) = \int_{-c}^c I_{2x}(x') \mathcal{K}_{2A}(x, x') dx' \\ = \frac{-j4\pi}{\xi_0} [C_{1x} \cos \beta_0 x + C_{2x} \sin \beta_0 x - \theta_{2A}(x)]. \quad (7b)$$

The particular integrals in (7a) and (7b) are

$$\theta_{1A}(z) = \beta_0 \int_0^z \phi_{1(z)}(w) \cos \beta_0(z-w) dw \\ - \phi_{1(z)}(0) \sin \beta_0 z, \quad (8a)$$

$$\theta_{2A}(x) = \beta_0 \int_0^x \phi_{2(x)}(w) \cos \beta_0(x-w) dw \\ - \phi_{2(x)}(0) \sin \beta_0 x. \quad (8b)$$

As a consequence of geometrical and electrical symmetry and the assumed driving conditions, the following relations obtain:

$$A_{1z}(-z) = A_{1z}(z), \quad A_{1z}(-z) = -A_{1z}(z) \quad (9a)$$

$$\phi_1(-z) = -\phi_1(z), \quad \phi_{1(z)}(0) = 0, \quad (9b)$$

$$\lim_{z \rightarrow 0} [\phi_1(z) - \phi_1(-z)] = 2\phi_{1(z)}(0) = V^e \quad (9b)$$

$$I_1(-z) = I_1(z), \quad q_1(-z) = -q_1(z) \quad (9c)$$

$$A_{2x}(-x) = -A_{2x}(x), \quad A_{2x}(-x) = A_{2x}(x), \quad A_{2x}(0) = 0 \quad (9d)$$

$$\phi_2(-x) = \phi_2(x) \quad (9e)$$

$$I_{2x}(-x) = -I_{2x}(x), \quad q_2(-x) = q_2(x). \quad (9f)$$

The continuity of both current and scalar potential at the corners demands that

$$I_{1z}(-d) = -I_{2x}(-c), \quad \phi_1(-d) = \phi_2(-c). \quad (10)$$

It follows directly from (7b) with (9d) that

$$C_{1z} = 0. \quad (11)$$

Expressions for the scalar potentials corresponding to (7a) and (7b) for the vector potentials but specialized to satisfy (9a)–(9f) and (11) are readily obtained. Thus,

$$\phi_1(z) = -C_{1z} \sin \beta_0 z + C_{2z} \cos \beta_0 z + \theta_{1V}(z), \quad z \geq 0, \quad (12)$$

$$\phi_1(z) = -C_{1z} \sin \beta_0 z - C_{2z} \cos \beta_0 z + \theta_{1V}(z), \quad z \leq 0, \quad (13)$$

where

$$\theta_{1V}(z) = \beta_0 \int_0^z \phi_{1(z)}(w) \sin \beta_0(z-w) dw. \quad (14)$$

Similarly, and for positive and negative values of x ,

$$\phi_2(x) = C_{2x} \cos \beta_0 x - \frac{1}{\beta_0} \frac{\partial \theta_{2A}(x)}{\partial x} + \phi_{2(x)}(x) \\ = C_{2x} \cos \beta_0 x + \theta_{2V}(x), \quad (15)$$

where

$$\theta_{2V}(x) = \beta_0 \int_0^x \phi_{2(x)}(w) \sin \beta_0(x-w) dw \\ + \phi_{2(x)}(0) \cos \beta_0 x. \quad (16)$$

The driving voltage as defined in (9b) now may be introduced. With (12) and (13) it follows that

$$C_{2z} = \frac{1}{2} V^e. \quad (17)$$

The simultaneous integral equations for the currents I_{1z} and I_{2x} are:

$$\int_{-d}^d I_{1z}(z') \mathcal{K}_{1A}(z, z') dz' \\ = \frac{-j4\pi}{\xi_0} \left[C_{1z} \cos \beta_0 z + \frac{1}{2} V^e \sin \beta_0 |z| - \theta_{1A}(z) \right] \quad (18a)$$

$$\int_{-c}^c I_{2x}(x) \mathcal{K}_{2A}(x, x') dx' = \frac{-j4\pi}{\xi_0} [C_{2x} \sin \beta_0 x - \theta_{2A}(x)] \quad (18b)$$

where C_{1z} and C_{2x} may be evaluated by requiring continuity of current and scalar potential at the corners, as specified in (10). Note that with the equations of continuity,

$$\frac{\partial I_{1z}}{\partial z} + j\omega q_1 = 0, \quad \frac{\partial I_{2x}}{\partial x} + j\omega q_2 = 0, \quad (19)$$

$\theta_{1A}(z)$ is a function of $I_{2A}(x)$, and $\theta_{2A}(x)$ is a function of I_{1z} .

APPROXIMATE SOLUTIONS OF THE INTEGRAL EQUATIONS

The simultaneous integral equations (18a) and (18b) may be solved approximately for the currents $I_1(z) = I_3(z)$ and $I_2(x) = -I_4(x)$ by a method of iteration resembling that used in the analysis of coupled parallel antennas.⁴ The present problem is complicated by the presence of two equations rather than one. In devising a suitable iteration procedure two points are noteworthy. First, the mutual terms interrelating the two equations are limited to the particular integrals which take account of capacitive coupling between adjacent, mutually perpendicular sides. Since this effect is significant primarily near the corners, it may be assumed that it is not of primary significance in determining the distributions of current and may be included in the first correction term. The second point to be noted is that the oscillation of charges and currents in the rectangle when excited in the dipole mode as shown in Fig. 3 must correspond roughly to that in two parallel center-driven antennas each of length $2(c+d)$. This follows from the fact that the currents are continuous at the corners and vanish at the centers $x=0, z=\pm d$, of the two sides without generators. This suggests that (18a) and (18b) may be expressed as follows:

⁴ *Ibid.*, p. 264 ff.

$$\begin{aligned}
 & \int_{-(d+c)}^{d+c} I_{1z}(z') \mathcal{K}_{11}(z, z') dz' + \int_{-d}^d I_{1z}(z') \mathcal{K}_{13}(z, z') dz' \\
 & - \left(\int_{-(d+c)}^{-d} \int_d^{d+c} \right) I_{1z}(z') \mathcal{K}_{24}(z, z) dz' \\
 & = \frac{-j4\pi}{\xi_0} \left[C_{1z} \cos \beta_0 z + \frac{1}{2} V^e \sin \beta_0 |z| - \theta_{1A}(z) \right] + g_1(z) \quad (20a)
 \end{aligned}$$

$$\begin{aligned}
 & \int_{-(d+c)}^{d+c} I_{2x}(x) \mathcal{K}_{22}(x, x') dx' - \int_{-c}^c I_{2x}(x') \mathcal{K}_{24}(x, x') dx' \\
 & - \left(\int_{-(d+c)}^{-c} + \int_c^{d+c} \right) I_{2x}(x') \mathcal{K}_{13}(x, x') dx' \\
 & = \frac{-j4\pi}{\xi_0} [C_{2x} \sin \beta_0 x - \theta_{2A}(x)] + g_2(x) \quad (20b)
 \end{aligned}$$

where

$$g_1(z) = \left(\int_{-(d+c)}^{-d} + \int_d^{d+c} \right) I_{1z}(z') \mathcal{K}_{2A}(z, z') dz' \quad (21a)$$

$$g_2(x) = \left(\int_{-(d+c)}^{-c} + \int_c^{d+c} \right) I_{2x}(x') \mathcal{K}_{1A}(x, x') dx'. \quad (21b)$$

Note that $\mathcal{K}_{2A}(z, z')$, $\mathcal{K}_{1A}(x, x')$, R_{24} in (20a), and R_{13} in (20b) are obtained from (5) and (6) with x substituted for z and vice versa.

In the integral on the left in (20a), $I_{1z}(z')$ is the actual current in side 1 of the rectangle in the range $-d \leq z' \leq d$. In the ranges $-(c+d) \leq z \leq -d$ and $d \leq z \leq (c+d)$, the current is the fictitious extension in the z direction of currents actually existing in the top and bottom of the loop as $I_{2x}(x')$ and $I_{4x}(x')$. Similarly, in the integral on the left in (20b), $I_{2x}(x')$ actually exists only in the range $-c \leq x \leq c$. Outside this range the currents are the fictitious extension in the x direction of actual currents in the vertical sides in the z direction. This is shown schematically in Fig. 4 for sides 1 and 2. The addition of the integrals $g_1(z)$ and $g_2(x)$, respectively, to both sides of (21a) and (21b) modifies the left sides (which are proportional to the tangential components of the vector potential) in a manner to improve the constancy of the ratio of vector potential to current especially near the corners where large deviations occur. Note that whereas the change in the direction of the current at a corner, for example at $z = -d$, $x = -c$, can involve no great modification in its amplitude or distribution as compared with the current at the corresponding point $z = -d$ in two parallel antennas of length $2(c+d)$ when driven by equal generators in phase, this is not true of the component of the vector potential tangent to the conductor. The currents in the conductor on the two sides of the right-angle bend do not contribute to the same component of the vector potential as they do when there is no bend and the conductor is straight.

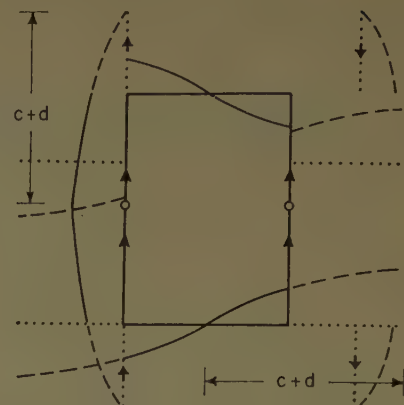


Fig. 4—Actual and fictitious conductors and currents used in establishing the integral equation in a form suitable for iteration.

The solutions of (21) by iteration may be carried out much as in the case of two parallel antennas.⁴ For this purpose let

$$g_1(z, z') \doteq \frac{I_{1z}(z')}{I_{1z}(z)}; \quad g_2(x, x') \doteq \frac{I_{2x}(x')}{I_{2x}(x)} \quad (22)$$

be approximate relative distributions of current. Also let the following functions be defined:

$$\begin{aligned}
 \Psi_1(z) &= \Psi_s + \gamma_1(z) = \int_{-(d+c)}^{d+c} g_1(z, z') \mathcal{K}_{11}(z, z') dz' \\
 &+ \int_{-d}^d g_1(z, z') \mathcal{K}_{13}(z, z') dz' \\
 &- \left(\int_{-(d+c)}^{-d} + \int_d^{d+c} \right) g_1(z, z') \mathcal{K}_{24}(z, z') dz' \quad (23a)
 \end{aligned}$$

$$\begin{aligned}
 \Psi_2(x) &= \Psi_s + \gamma_2(x) = \int_{-(d+c)}^{d+c} g_2(x, x') \mathcal{K}_{22}(x, x') dx' \\
 &- \int_{-c}^c g_2(x, x') \mathcal{K}_{24}(x, x') dx' \\
 &+ \left(\int_{-(d+c)}^{-c} + \int_c^{d+c} \right) g_2(x, x') \mathcal{K}_{13}(x, x') dx' \quad (23b)
 \end{aligned}$$

where Ψ_s is an appropriately defined magnitude and $\gamma_1(z)$ and $\gamma_2(x)$ are the necessary and presumably small functions required to make (23) exact. If $g_1(z, z')$ and $g_2(x, x')$ can be so chosen that they are good approximations of the actual current distributions, the following integrals are small:

$$\begin{aligned}
 \mathfrak{D}_1(z) &= \int_{-(d+c)}^{d+c} [I_{1z}(z') - I_{1z}(z)g_1(z, z')] \mathcal{K}_{11}(z, z') dz' \\
 &- \int_{-d}^d [I_{1z}(z') - I_{1z}(z)g_1(z, z')] \mathcal{K}_{13}(z, z') dz' \\
 &- \left(\int_{-(d+c)}^{-d} + \int_d^{d+c} \right) [I_{1z}(z') \\
 &- I_{1z}(z)g_1(z, z')] \mathcal{K}_{24}(z, z') dz' \quad (24a)
 \end{aligned}$$

$$\begin{aligned} \mathfrak{D}_2(x) = & \int_{-(d+c)}^{d+c} [I_{2x}(x') - I_{2x}(x)g_2(x, x')] \mathcal{K}_{22}(x, x') dx' \\ & - \int_{-c}^c [I_{2x}(x') - I_{2x}(x)g_2(x, x')] \mathcal{K}_{24}(x, x') dx' \\ & - \left(\int_{-(d+c)}^{-c} + \int_c^{d+c} \right) [I_{2x}(x') \\ & - I_{2x}(x)g_2(x, x')] \mathcal{K}_{13}(x, x') dx'. \quad (24b) \end{aligned}$$

With (23) and (24), the integral equations of (20) may be rearranged as follows:

$$\begin{aligned} I_{1z} = & \frac{-j4\pi}{\xi_0 \Psi_s} \left[C_{1z} \cos \beta_0 z + \frac{1}{2} V^e \sin \beta_0 |z| \right] \\ & + \frac{L_1(z)}{\Psi_s} \quad (25a) \end{aligned}$$

$$I_{2x}(x) = \frac{-j4\pi}{\xi_0 \Psi_s} C_{2x} \sin \beta_0 x + \frac{L_2(x)}{\Psi_s} \quad (25b)$$

where

$$L_1(z) = \frac{j4\pi}{\xi_0} \theta_{1A}(z) + P_1(z), \quad (26a)$$

$$L_2(x) = \frac{j4\pi}{\xi_0} \theta_{2A}(x) + P_2(x), \quad (26b)$$

and

$$\begin{aligned} P_1(z) = & g_1(z) - \mathfrak{D}_1(z) - I_{1z}(z) \gamma_1(z) \\ = & I_{1z}(z) \Psi_s - \int_{-d}^d I_{1z}(z') \mathcal{K}_{1A}(z, z') dz'. \quad (26c) \end{aligned}$$

The functions $\theta_{1A}(z)$ and $\theta_{2A}(x)$ are defined in (8). In order to assure *exact* continuity of current at the corners in the form $I_{1z}(-d) = -I_{2x}(-c)$ even in approximate expressions, it is advantageous to subtract the quantity $0 = I_{1z}(-d) + I_{2x}(-c)$ from (25a). The result is

$$\begin{aligned} I_{1z}(z) = & \frac{-j4\pi}{\xi_0 \Psi_s} \left[C_{1z} (\cos \beta_0 z - \cos \beta_0 d) \right. \\ & + \frac{1}{2} V^e (\sin \beta_0 |z| - \sin \beta_0 d) + C_{2x} \sin \beta_0 c \\ & \left. + \frac{1}{\Psi_s} [L_1(z) - L_1(-d) - L_2(-c)] \right]. \quad (27) \end{aligned}$$

Note that (25) or (27) and (25b) are still integral equations for the currents since these occur on the right in $L_1(z)$ and $L_2(x)$ under the signs of integration. However, the expressions are now so arranged that if a proper choice is made of the distribution functions $g_1(z, z')$ and $g_2(x, x')$ and of the parameter Ψ_s , the sum of the terms on the right in which the currents occur is small compared with the zeroth-order terms. Accordingly, (27) and (25b) are in forms appropriate for iteration. Suggested zeroth-order currents and charges are:

$$\begin{aligned} [I_{1z}(z)]_0 = & \frac{-j4\pi}{\xi_0 \Psi_s} \left[C_{1z} (\cos \beta_0 z - \cos \beta_0 d) \right. \\ & \left. + \frac{1}{2} V^e (\sin \beta_0 |z| - \sin \beta_0 d) + C_{2x} \sin \beta_0 c \right], \quad (28a) \end{aligned}$$

$$\begin{aligned} [q^1(z)]_0 = & \frac{4\pi \epsilon_0}{\Psi_s} \left[-C_{1z} \sin \beta_0 z + \frac{1}{2} V^e \cos \beta_0 z \right], \\ 0 \leq z \leq d, \quad (28b) \end{aligned}$$

$$\begin{aligned} [q_1(z)]_0 = & \frac{-4\pi \epsilon_0}{\Psi_s} \left[C_{1z} \sin \beta_0 z + \frac{1}{2} V^e \cos \beta_0 z \right], \\ -d \leq z \leq 0, \quad (28c) \end{aligned}$$

$$[I_{2x}(x)]_0 = \frac{-j4\pi}{\xi_0 \Psi_s} C_{2x} \sin \beta_0 x, \quad (29a)$$

$$[q_2(x)]_0 = \frac{4\pi \epsilon_0}{\Psi_s} C_{2x} \cos \beta_0 x. \quad (29b)$$

The substitution of these zeroth-order currents and charges in the several parts of $L_1(z)$ and $L_2(x)$ as defined in (26), and the use of (23) leads to the following first-order integrals:

$$\begin{aligned} F_{11}(z) = & \Psi_s (\cos \beta_0 z - \cos \beta_0 d) - [C_a(d, z) + C_{2c}(d, z)] \\ & + [E_a(d, z) + E_{2c}(d, z)] \cos \beta_0 d \quad (30a) \end{aligned}$$

$$\begin{aligned} G_{11}(z) = & \Psi_s (\sin \beta_0 |z| - \sin \beta_0 d) - [S_a(d, z) + S_{2c}(d, z)] \\ & + [E_a(d, z) + E_{2c}(d, z)] \sin \beta_0 d \quad (30b) \end{aligned}$$

$$H_{11}(z) = [\Psi_s - E_a(d, z) - E_{2c}(d, z)] \sin \beta_0 c \quad (30d)$$

$$G_{21}(x) = \Psi_s \sin \beta_0 x - S_a(c, x) + S_{2d}(c, x) \quad (30c)$$

where the following functions are involved:

$$C_i(h, z) = \int_0^h \cos \beta_0 z' \left[\frac{e^{-j\beta_0 R_{1i}}}{R_{1i}} + \frac{e^{-j\beta_0 R_{2i}}}{R_{2i}} \right] dz', \quad (31a)$$

$$S_i(h, z) = \int_0^h \sin \beta_0 z' \left[\frac{e^{-j\beta_0 R_{1i}}}{R_{1i}} + \frac{e^{-j\beta_0 R_{2i}}}{R_{2i}} \right] dz', \quad (31b)$$

$$E_i(h, z) = \int_0^h \left[\frac{e^{-j\beta_0 R_{1i}}}{R_{1i}} + \frac{e^{-j\beta_0 R_{2i}}}{R_{2i}} \right] dz', \quad (31c)$$

$$S_i(h, z) = \int_0^h \sin \beta_0 z' \left[\frac{e^{-j\beta_0 R_{1i}}}{R_{1i}} - \frac{e^{-j\beta_0 R_{2i}}}{R_{2i}} \right] dz'. \quad (31d)$$

In these expressions

$$R_{1i} = \sqrt{(z' - z)^2 + i^2}; \quad R_{2i} = \sqrt{(z' + z)^2 + i^2}. \quad (32)$$

The integral functions in (31) may be expressed in terms of the tabulated generalized sine and cosine integral functions.^{5,6} Other integrals involved in $L_1(z)$ and

⁵ *Ibid.*, pp. 97, 274.

⁶ "Tables of Generalized Sine- and Cosine-Integral Functions," Harvard University Press, Cambridge, Mass.; 1948.

$L_2(x)$ are

$$f_{11}(z) = \int_0^z \rho_{11}(w) \cos \beta_0(z-w) \beta_0 dw, \quad (33a)$$

$$f_{21}(x) = \int_0^x \rho_{21}(w) \cos \beta_0(x-w) \beta_0 dw - \rho_{21}(0) \sin \beta_0 x, \quad (33b)$$

$$p_{21}(x) = \int_0^x \sigma_{21}(w) \cos \beta_0(x-w) \beta_0 dw - \sigma_{21}(0) \sin \beta_0 x. \quad (33c)$$

The quantities ρ_{11} , ρ_{21} , and σ_{21} introduced in (33) are defined as follows. Note that $\mathcal{K}_{1B}(z, x')$ and $\mathcal{K}_{2B}(x, z')$ are defined in (5).

$$\rho_{11}(z) = \int_{-c}^c \cos \beta_0 x' \mathcal{K}_{1B}(z, x') \quad (34a)$$

$$\rho_{21}(x) = \int_{-d}^d \cos \beta_0 z' [\mathcal{K}_{2B}(x, z') - \mathcal{K}_{2B}(x, -z')] dz' \quad (34b)$$

$$\sigma_{21}(x) = \int_{-d}^d \sin \beta_0 z' \mathcal{K}_{2B}(x, z') dz'. \quad (34c)$$

These integrals can also be expressed in terms of the tabulated generalized sine and cosine integrals. In terms of the integrals (31a)–(31c) and (33) the first-order expressions for $L_1(z)$ and $L_2(x)$ are

$$[L_1(z)]_1 = \frac{-j4\pi}{\xi_0 \Psi_s} \left\{ C_{1z} F_{11}(z) + \frac{1}{2} V^e G_{11}(z) + C_{2x} [H_{11}(z) - f_{11}(z)] \right\} \quad (35a)$$

$$[L_2(x)]_1 = \frac{-j4\pi}{\xi_0 \Psi_s} \left\{ C_{2x} G_{21}(x) + C_{1z} p_{21}(x) - \frac{1}{2} V^e f_{21}(x) \right\}. \quad (35b)$$

If these values are substituted in (27) and (25b), the following first-order solutions for the currents are obtained:

$$[I_{1z}(z)]_1 = \frac{-j4\pi}{\xi_0 \Psi_s} \left[C_{1z} \left\{ F_{0z} + \frac{1}{\Psi_s} [F_{11z} - p_{21}(-c)] \right\} + \frac{1}{2} V^e \left\{ G_{0z} + \frac{1}{\Psi_s} [G_{11z} + f_{21}(-c)] \right\} + C_{2x} \left\{ \sin \beta_0 c + \frac{1}{\Psi_s} [H_{11z} - f_{11z} - G_{21}(-c)] \right\} \right] \quad (36a)$$

$$[I_{2x}(x)]_1 = \frac{-j4\pi}{\xi_0 \Psi_s} \left[C_{2x} \left\{ \sin \beta_0 x + \frac{G_{21}(x)}{\Psi_s} \right\} + C_{1z} \frac{p_{21}(x)}{\Psi_s} - \frac{1}{2} V^e \frac{f_{21}(x)}{\Psi_s} \right] \quad (36b)$$

where

$$F_{0z} = \cos \beta_0 z - \cos \beta_0 d, \quad (36c)$$

$$G_{0z} = \sin \beta_0 |z| - \sin \beta_0 d, \quad (36c)$$

$$F_{11z} = F_{11}(z) - F_{11}(-d), \quad (36d)$$

$$G_{11z} = G_{11}(z) - G_{11}(-d), \quad (36d)$$

$$H_{11z} = H_{11}(z) - H_{11}(-d), \quad (36e)$$

$$f_{11z} = f_{11}(z) - f_{11}(-d). \quad (36e)$$

In order to evaluate the constants C_{1z} and C_{2x} in terms of V^e the conditions (10) requiring continuity of scalar potential and current at the corners must be introduced. The first-order expressions for the scalar potential are obtained from (13) and (15) by substituting zeroth-order values of the charges in (14) and (16). The following integrals are involved:

$$h_{11}(z) = \beta_0 \int_0^z \rho_{11}(w) \sin \beta_0(z-w) dw, \quad (37a)$$

$$h_{21}(x) = \beta_0 \int_{-d}^x \rho_{21}(w) \sin \beta_0(x-w) dw + \rho_{21}(0) \cos \beta_0 x, \quad (37b)$$

$$k_{21}(x) = \beta_0 \int_0^x \sigma_{21}(w) \sin \beta_0(x-w) dw + \sigma_{21}(0) \cos \beta_0 x. \quad (37c)$$

In terms of these integrals the first-order potentials are:

$$[\phi_1(z)]_1 = -C_{1z} \sin \beta_0 z - \frac{1}{2} V^e \cos \beta_0 z + \frac{C_{2x} h_{11}(z)}{\Psi_s}, \quad z \leq 0, \quad (38a)$$

$$[\phi_2(x)]_1 = C_{2x} \cos \beta_0 x - \frac{1}{\Psi_s} \left[C_{1z} k_{21}(x) + \frac{1}{2} V^e h_{21}(x) \right]. \quad (38b)$$

With (10), (25), (35), and (38) the following pair of equations is obtained for the two constants C_{1z} and C_{2x} :

$$C_{1z} a_{11} + C_{2x} a_{12} = \frac{1}{2} V^e b_1 \quad (39a)$$

$$C_{1z} a_{21} + C_{2x} a_{22} = \frac{1}{2} V^e b_2 \quad (39b)$$

where, for first-order values,

$$a_{11} = \cos \beta_0 d + \frac{1}{\Psi_s} [F_{11}(-d) + p_{21}(-c)], \quad (40a)$$

$$a_{12} = -\beta_0 c + \frac{1}{\Psi_s} [G_{21}(-c) + H_{11}(-d) - f_{11}(-d)], \quad (40b)$$

$$b_1 = -\sin \beta_0 d - \frac{1}{\Psi_s} [G_{11}(-d) - f_{21}(-c)], \quad (40c)$$

$$a_{21} = \sin \beta_0 d + \frac{k_{21}(-c)}{\Psi_s}, \quad (41a)$$

$$a_{22} = -\cos \beta_0 c + \frac{h_{11}(-d)}{\Psi_s}, \quad (41b)$$

$$b_2 = \cos \beta_0 d - \frac{h_{21}(-c)}{\Psi_s}. \quad (41c)$$

It follows directly that

$$C_{1s} = \frac{V^e N_1}{2D}, \quad C_{2s} = \frac{V^e N_2}{2D}, \quad (42)$$

where

$$N_1 = b_1 a_{22} - b_2 a_{12} = \sin \beta_0 (c + d) + N_{11}/\Psi_s + N_{12}/\Psi_s^2, \quad (43a)$$

$$N_2 = b_2 a_{11} b_1 a_{21} = 1 + N_{21}/\Psi_s + N_{22}/\Psi_s^2, \quad (43b)$$

$$D = a_{11} a_{22} - a_{12} a_{21} = [\cos \beta_0 (c + d) + D_1/\Psi_s + D_2/\Psi_s^2]. \quad (43c)$$

The following quantities occur in (43):

$$N_{11} = -h_{11}(-d) \sin \beta_0 d + [G_{11}(-d) - f_{21}(-c)] \cos \beta_0 c - h_{21}(-c) \sin \beta_0 c - [G_{21}(-c) + H_{11}(-d) - f_{11}(-d)] \cos \beta_0 d \quad (44a)$$

$$N_{12} = h_{11}(-d) [-G_{11}(-d) + f_{21}(-c)] + h_{21}(-c) [G_{21}(-c) + H_{11}(-d) - f_{11}(-d)] \quad (44b)$$

$$N_{21} = [F_{11}(-d) + p_{21}(-c)] \cos \beta_0 d + [G_{11}(-d) - f_{21}(-c) + k_{21}(-c)] \sin \beta_0 d \quad (44c)$$

$$N_{22} = k_{21}(-c) [G_{11}(-d) - f_{21}(-c)] - h_{21}(-c) [F_{11}(-d) + p_{21}(-c)] \quad (44d)$$

$$D_1 = [F_{11}(-d) + p_{21}(-c)] \cos \beta_0 c - h_{11}(-d) \cos \beta_0 d + [G_{21}(-c) + H_{11}(-d) - f_{11}(-d)] \sin \beta_0 d - k_{21}(-c) \sin \beta_0 c \quad (44e)$$

$$D_2 = -[F_{11}(-d) + p_{21}(-c)] h_{11}(-d) + [G_{21}(-c) + H_{11}(-d) - f_{11}(-d)] k_{21}(-c). \quad (44f)$$

If the equations of (43) are substituted for (42) and (36a) and (36b), the following expressions are obtained for the currents if only terms of order $1/\Psi_s$ are retained in both numerator and denominator:

$$[I_{1s}(z)]_1 = \frac{j2\pi V^e}{\xi_0 \Psi_s} \left[\frac{\sin \beta_0 (c + d - |z|) + B_1(z)/\Psi_s}{\cos \beta_0 (c + d) + D_1/\Psi_s} \right], \quad (45a)$$

$$[I_{2s}(x)]_1 = \frac{j2\pi V^e}{\xi_0 \Psi_s} \left[\frac{\sin \beta_0 x + M_{21}(x)/\Psi_s}{\cos \beta_0 (c + d) + D_1/\Psi_s} \right], \quad (45b)$$

where

$$B_1(z) = M_{11}(z) - M_{11}(-d) - M_{21}(-c) \quad (46a)$$

and

$$M_{11}(z) = N_{11} \cos \beta_0 z - D_1 \sin \beta_0 |z| + F_{11}(z) \sin \beta_0 (c + d) - G_{11}(z) \cos \beta_0 (c + d) + H_{11}(z) - f_{11}(z),$$

$$M_{21}(x) = N_{21} \sin \beta_0 x + G_{21}(x) + p_{21}(x) \sin \beta_0 (c + d) + f_{21}(x) \cos \beta_0 (c + d). \quad (46b)$$

Higher-order terms may be obtained by continuing the iteration.

The first-order driving-point impedance is given by

$$[Z_{1\text{in}}]_1 = \frac{-j\xi_0 \Psi_s}{2\pi} \left[\frac{\cos \beta_0 (c + d) + D_1/\Psi_s}{\sin \beta_0 (c + d) + B_1(0)/\Psi_s} \right]. \quad (47)$$

The corresponding admittance is $[Y_{1\text{in}}]_1 = 1/[Z_{1\text{in}}]_1$. The coefficient D_1 in (47) is given by (44e). The corresponding value of $B_1(0)$ is obtained from (46a) with $z=0$. It is:

$$B_1(0) = F_{11}(0) \sin \beta_0 (c + d) - G_{11}(0) \cos \beta_0 (c + d) + G_{11}(-d) \cos \beta_0 c - G_{21}(-c) \cos \beta_0 d + H_{11}(0) - H_{11}(-d) \cos \beta_0 d - f_{11}(0) + f_{11}(-d) \cos \beta_0 d - h_{11}(-d) \sin \beta_0 d - f_{21}(-c) \cos \beta_0 c - h_{21}(-c) \sin \beta_0 c. \quad (48a)$$

If use is made of (30) in (48a) and (44e) the following formulas are obtained:

$$B_1(0) = [\Psi_s - C_a(d, 0) - C_{2a}(d, 0) + E_a(d, -d) + E_{2a}(d, -d)] \sin \beta_0 (c + d) + [S_a(d, 0) + S_{2a}(d, 0)] \cos \beta_0 (c + d) - [S_a(d, -d) + S_{2a}(d, -d)] \cos \beta_0 c + [S_a(c, -c) - S_{2a}(c, -c)] \cos \beta_0 d - f_{11}(0) + f_{11}(-d) \cos \beta_0 d - h_{11}(-d) \sin \beta_0 d - f_{21}(-c) \cos \beta_0 c - h_{21}(-c) \sin \beta_0 c, \quad (48b)$$

$$D_1 = [E_a(d, -d) + E_{2a}(d, -d)] \cos \beta_0 (c + d) - [C_a(d, -d) + C_{2a}(d, -d)] \cos \beta_0 c - [S_a(c, -c) - S_{2a}(c, -c)] \sin \beta_0 d - f_{11}(-d) \sin \beta_0 d - h_{11}(-d) \cos \beta_0 d + p_{21}(-c) \cos \beta_0 c - k_{21}(-c) \sin \beta_0 c. \quad (48c)$$

If the real and imaginary parts of D_1 and $B_1(0)$ are separated and the notation $D_1 = D_1^I + jD_1^{\text{II}}$, $B_1(0) = B_1^I + jB_1^{\text{II}}$, is introduced, the impedance $[Z_{1\text{in}}]_1 = [R_{1\text{in}}]_1 + j[X_{1\text{in}}]_1$ may be separated into its resistive and reactive parts as follows:

$$[R_{1\text{in}}]_1 = \frac{\xi_0}{2\pi} \left\{ \frac{D_1^{\text{II}} \sin \beta_0 (c + d) - B_1^{\text{II}} \cos \beta_0 (c + d) + [D_1^{\text{II}} B_1^I - D_1^I B_1^{\text{II}}]/\Psi_s}{[\sin \beta_0 (c + d) + B_1^I/\Psi_s]^2 + [B_1^{\text{II}}/\Psi_s]^2} \right\} \quad (49a)$$

$$[X_{1\text{in}}]_1 = \frac{-\xi_0}{2\pi} \left\{ \frac{[\sin \beta_0 (c + d) + B_1^I/\Psi_s][\cos \beta_0 (c + d) + D_1^I/\Psi_s] + B_1^{\text{II}} D_1^{\text{II}}/\Psi_s^2}{[\sin \beta_0 (c + d) + B_1^I/\Psi_s]^2 [B_1^{\text{II}}/\Psi_s]^2} \right\}. \quad (49b)$$

These are the final first-order formulas.

THE EXPANSION PARAMETER

The selection of an appropriate expansion parameter Ψ_s depends upon the evaluation of $\Psi_1(z)$ and $\Psi_2(x)$ as defined in (23). As shown for the comparable problem in the analysis of the linear antenna⁸ very satisfactory results are obtained with zeroth-order distribution functions. In the case at hand this means that the distribution functions,

$$g_1(z, z') = \frac{\sin \beta_0(c + d - |z|)}{\sin \beta_0(c + d - |z'|)},$$

$$g_2(x, x') = \frac{\sin \beta_0 x'}{\sin \beta_0 x}, \quad (50)$$

are to be substituted in (23a) and (23b). The result for $\Psi_1(z)$ with $z \geq 0$ and the definitions (31) is:

$$\Psi_1(z) = \csc \beta_0(c + d - z) \{ \sin \beta_0(c + d) [C_a(c + d, z) + C_{2c}(d, z) - C_{2d}(c + d, z) + C_{2d}(d, z)] - \cos \beta_0(c + d) [S_a(c + d, z) + S_{2c}(d, z) - S_{2d}(c + d, z) + C_{2d}(d, z)] \}. \quad (51)$$

Correspondingly with (31d) the result for $\Psi_2(x)$ is:

$$\Psi_2(x) = \csc \beta_0 x [S_a(c + d, x) - S_{2d}(c, x) + S_{2c}(c + d, x) - S_{2c}(c, x)]. \quad (52)$$

Since both $\Psi_1(z)$ and $\Psi_2(x)$ are proportional to the ratio of zeroth-order vector potential to zeroth-order current at points along conductors that have the same radii and similar distributions of current, the magnitude of $\Psi_1(z)$ and $\Psi_2(x)$ should be essentially constant and equal except as modified by asymmetries. In general, a good choice of Ψ is the magnitude of $\Psi(z)$ at a point z where the vector potential and the current both have maxima. In the presently considered case of the loop excited in the dipole mode, an even better choice owing to more complete symmetry is at the centers of the sides without generators (with fictitious extensions) where both the vector potential and the current vanish, but where their ratio has a definite and constant value. Thus, let $\Psi_s = |\lim_{z \rightarrow 0} \Psi_2(0)|$. This function is readily evaluated directly from the integrals by differentiating the indeterminate form when expressed as 0/0. An integration by parts in the numerator leads to the following formula for the expansion parameter Ψ_s of the symmetrical or dipole mode in the rectangle:

$$\Psi_s = \Psi_2 = \left| C_a(c + d, 0) + C_b(c + d, 0) - C_{2d}(c, 0) - C_b(c, 0) - \frac{2}{\beta_0} \left\{ \sin \beta_0(c + d) \left[\frac{e^{-i\beta_0 R_1}}{R_1} + \frac{e^{-i\beta_0 R_3}}{R_3} \right] - \sin \beta_0 c \left[\frac{e^{-i\beta_0 R_2}}{R_2} + \frac{e^{-i\beta_0 R_4}}{R_4} \right] \right\} \right| \quad (53)$$

where

$$b = \sqrt{4c^2 + a^2} \quad (54a)$$

$$R_1 = \sqrt{(c + d)^2 + a^2}, \quad R_2 = \sqrt{c^2 + 4d^2 + a^2}$$

$$R_3 = \sqrt{(c + d)^2 + 4c^2 + a^2}, \quad R_4 = \sqrt{5c^2 + a^2}. \quad (54b)$$

Note that in (54) a^2 usually is negligible except when c or d becomes very small. The difference functions $\gamma_1(z)$ and $\gamma_2(x)$ are given by

$$\gamma_1(z) = \Psi_1(z) - \Psi_s, \quad \gamma_2(x) = \Psi_2(x) - \Psi_s. \quad (55)$$

With the expansion parameter Ψ_s as defined in (53), substituted in (45) for the distributions of current, and in (47) or (49a) and (49b) for the impedance, the first-order circuit properties of the rectangular loop of arbitrary size are determined when it is driven so that only the vertical dipole mode is excited. Important special cases must still be considered.

FOLDED DIPOLE AND TRANSMISSION LINE

When the dimension $2d$ or $2c$ of the rectangle of wire is kept electrically small ($\beta_0 d \ll 1$ or $\beta_0 c \ll 1$) while the other dimension is unrestricted, the loop becomes on the one hand a symmetrically driven folded dipole, on the other hand a section of transmission line driven simultaneously at both ends by codirectional generators. Both of these special cases have been analyzed: the former (see King^{5,7}) by neglecting corner effects and treating the two sides of the long and narrow rectangle as two closely spaced symmetrically driven dipoles; the latter in terms of transmission-line theory for the reactance and the Poynting vector theorem for the radiation resistance.^{8,9}

It is readily verified that when c is small (53) becomes

$$\Psi_s = 2 \left| C_a(d, 0) - \ln \frac{2c}{a} - \frac{\sin \beta_0 d}{\beta_0 d} e^{-i\beta_0 d} \right|. \quad (56)$$

This is essentially equivalent to the expansion parameter Ψ_s for two closely spaced symmetrically driven antennas or for the folded dipole.^{5,7} Moreover, if the capacitive coupling at the corners is neglected when c is sufficiently small by setting the functions $f_{11}(z)$, $f_{21}(x)$, and $p_{21}(x)$ as defined in (33) equal to zero, (46b) and (48c) for $M_{11}(z)$ and D_1 reduce essentially to the corresponding functions characteristic of the symmetrically driven pair of parallel antennas. Small differences are a consequence of the definition of Ψ_s in (53) in terms of $\Psi_2(x)$ instead of $\Psi_1(z)$. It follows that (47) reduces to the formula for the folded dipole.

⁵ King, "Theory of Linear Antennas," *op. cit.*, pp. 267-270, 335-337.

⁶ J. E. Storer and R. W. P. King, "Radiation resistance of two-wire line," *PROC. IRE*, vol. 39, pp. 1408-1412; November, 1951.

⁷ R. W. P. King, "Transmission-Line Theory," McGraw-Hill Book Co., Inc., New York, N. Y.; 1955.

When the dimension $2d$ is small compared with the wavelength and c so that $\beta_0 d \ll 1$, $c^2 \gg d^2$, the expansion parameter ψ_s reduces to

$$\psi_s = 2 \ln \frac{2d}{a}. \quad (57)$$

The leading term in the reactance is

$$X_{in} = -R_s \cot \beta_0 c \quad (58a)$$

where

$$R_s = \frac{\xi_0 \Psi_s}{2\pi} = \frac{\xi_0}{\pi} \ln \frac{2d}{a}, \quad (58b)$$

is the familiar expression for the characteristic impedance of a lossless two-wire line with wire spacing $2d$.

The leading term in the resistance has not been evaluated in general when $\beta_0 d \ll 1$ and $\beta_0 c$ is unrestricted. However, the special case when both $\beta_0 d$ and $\beta_0 c$ are small is considered below.

THE ELECTRICALLY SMALL LOOP AS A DIPOLE

An important special case is the electrically small rectangular loop defined by the inequality

$$\beta_0^2(c + d)^2 \ll 1. \quad (59)$$

The general formula for the expansion parameter reduces to the following approximate form:

$$\begin{aligned} \Psi_s \doteq 2 & \left[\sinh^{-1} \frac{c+d}{a} + \sinh^{-1} \frac{c+d}{\sqrt{4c^2 + a^2}} \right. \\ & - \left. \sinh^{-1} \frac{c}{2d} - \sinh^{-1} \frac{c}{\sqrt{4c^2 + a^2}} \right] \\ & - (c+d) \left(\frac{1}{R_1} + \frac{1}{R_3} \right) + c \left(\frac{1}{R_2} + \frac{1}{R_4} \right) \quad (60) \end{aligned}$$

where the R 's are defined in (54). It is readily verified that when d is small compared with c , (60) reduces to (57). Alternatively, when d is large compared with c but small enough to satisfy the inequality $\beta_0^2 d^2 \ll 1$, (60) and (56) both give

$$\Psi_s = 2 \left[2 \ln \frac{2d}{a} - \ln \frac{2c}{a} - 2 \right] \quad (61)$$

in agreement with the value found in the literature¹⁰ for an electrically short two-element cage antenna.

Approximate expressions for the resistance and reactance may be obtained by simplifying (49a) and (49b). With (59) it is clear that the small integrals (33) are predominately real, so that the leading terms in B_1^{II} and D_1^{II} are:

$$B_1^{\text{II}} \doteq 2\beta_0^4 d^3 \left(\frac{d}{3} + c \right) + \frac{4}{3} \beta_0^4 d^2 c^2;$$

$$D_1^{\text{II}} \doteq 4\beta_0^8 d^3 \left(\frac{d}{3} + c \right). \quad (62)$$

With these values the leading terms in the resistance and reactance are:

$$R_{1in} \doteq \frac{\xi_0}{3\pi} \beta_0^2 d^2 \left[\frac{(d+3c)(d+2c) - 4c^2}{(d+c)^2} \right] \quad (63)$$

$$X_{in} \doteq \frac{\xi_0 \Psi_s}{2\pi \beta_0 (c+d)} \quad (64)$$

where Ψ_s is given by (60) in general, and by (57) or (61) in special cases.

Note that with $c \ll d$,

$$R_{1in} \doteq \frac{\xi_0}{3\pi} \beta_0^2 d^2 = 40\beta_0^2 d^2 \text{ ohms} \quad (65)$$

in agreement with the approximate formula

$$R_{1in} \doteq \frac{\xi_0}{6\pi} \beta_0^2 d^2 = 20\beta_0^2 d^2 \text{ ohms}$$

for the isolated dipole of half-length d . The factor 2 is explained by the fact that the symmetrical impedances of two parallel dipoles driven in phase by two generators are in zeroth order, double the value for a single isolated antenna. Alternatively, when $d \ll c$ the rectangle becomes a transmission line of length $2c$ and with spacing $b = 2d$. The line is driven at each end so that the currents vanish at the centers of the long sides. In this case

$$R_{1in} = \frac{2\xi_0}{3\pi} \beta_0^2 d^2 = 80\beta_0^2 d^2 \text{ ohms} = 20\beta_0^2 b^2 \text{ ohms}. \quad (66)$$

This is the resistance seen by each generator. It is equal to the resistance of a short end-loaded dipole of half-length d with an essentially uniform current. Contributions to the radiation from the equal and opposite currents in the electrically short sections of line is of higher order than contributions from the short ends.

CONCLUSION

The circuit properties of the rectangular loop antenna have been determined when the loop is driven in a transverse mode by equal and codirectional generators at the centers of one pair of parallel sides. First-order expressions for the currents and the identical input impedances at the two driving points are given in a form that involves only tabulated functions. It is shown that the new formula for the impedance is consistent with previously available formulas for the symmetrically driven folded dipole and for the transmission line.

¹⁰ King, "Theory of Linear Antennas," *op. cit.*, p. 274.

Properties of Slotted Dielectric Interfaces*

ROBERT E. COLLIN†

Summary—A theoretical analysis of slotted dielectric interfaces based on an application of the Rayleigh-Ritz method is presented. Formulas for calculating the equivalent circuit parameters are derived for arbitrary polarization and angles of incidence. Numerical results are given which show that the slotted dielectric interface behaves essentially as a homogeneous anisotropic dielectric interface. Formulas and numerical values of the equivalent dielectric constants are also given.

INTRODUCTION

THE increasing use of millimeter wavelength radiation has made the use of solid dielectric lenses more attractive since size and weight are no longer serious limiting factors, while at the same time construction of artificial dielectric lenses is more difficult. This same trend towards shorter wavelengths has brought about the introduction of optical techniques and components such as dielectric prisms and plates. The above components require quarter-wave matching layers at all air-dielectric and dielectric-dielectric interfaces if their performance is not to be seriously degraded by reflections at the interfaces. Homogeneous dielectric matching layers are usually not feasible because of the lack of homogeneous dielectric material having the required variation in dielectric constant. This has brought about the technique of slotting the dielectric interface so as to obtain a simulated quarter-wave transformer.

The idea of using a slotted dielectric interface for a matching section is not new. It apparently was applied by Fox, prior to 1943, to the problem of matching an empty and dielectric filled waveguide.¹ A brief study of slotted dielectric interfaces was made by Garnham in 1951.² However, the interface effect was not studied in detail and the results were limited to normal incidence. Further results were presented by Collin and Brown,³ but again, only the case of normal incidence with the electric vector parallel to the slots was analyzed in detail. These results were subsequently extended to the case of oblique incidence.⁴ The results obtained show that the dominant effect of the slotted interface is just a change in wave impedance. Experimental work by

Jones, Morita, and Cohn⁵⁻⁷ have substantiated these results to some extent. To date no systematic study of the slotted dielectric interface parameters as a function of angle of incidence and polarization has been made. The desire for a more detailed knowledge of the interface parameters resulted in the following analysis being undertaken.

In principle, there is no great difficulty in determining the proper modes of propagation for the slotted dielectric and solid dielectric regions, and matching the tangential field components at the interface. In practice, the numerical work is very tedious because of the complexity of the eigenfunctions in the slotted section. A reduction in numerical work is obtained by approximating the eigenfunctions in the slotted section by a finite series of the eigenfunctions for the solid dielectric region by means of the Rayleigh-Ritz method.⁸ If the slotted section is assumed semi-infinite in length (or terminated in a matched load) the mode amplitudes, reflection, and transmission coefficients are complex. This complication in the subsequent numerical calculations can be avoided by terminating the slotted section in a short-circuit. All the mode amplitudes in this case may be taken as either pure real or imaginary. Using this technique, one obtains an expression for the bilinear transformation relating the electric field null on the input side to the short-circuit position on the output side. From the four coefficients involved in this transformation, the equivalent circuit parameters are readily determined.⁹

The analysis to be presented here shows that the slotted dielectric medium behaves essentially as a homogeneous anisotropic dielectric with equivalent dielectric constants determined, so as to yield the same phase velocities in the equivalent homogeneous medium as actually exist in the slotted medium. In particular, the Brewster angle phenomenon is still preserved.

FIRST-ORDER ANALYSIS OF INTERFACE PARAMETERS

The basic slotted dielectric interface to be considered is illustrated in Fig. 1. It consists of dielectric slabs of

* Manuscript received by the PGAP, October 23, 1957; revised manuscript received September 9, 1958.

† Elec. Eng. Dept., Case Inst. of Tech., Cleveland 6, Ohio. Formerly at Canadian Armament Res. and Dev. Estab., Valcartier, P.Q., Can.

¹ A. G. Fox, U. S. Patent No. 2,411,534; filed March 30, 1943.

² R. H. Garnham, "Some Methods of Preventing the Reflection of Electromagnetic Waves at the Boundary Between Two Dielectrics," T.R.E. Tech. Note 131; August, 1951.

³ R. E. Collin and J. Brown, "The design of quarter-wave matching layers for dielectric surfaces," *Proc. IEE (London)*, vol. 103, pt. C, pp. 153-158; March, 1956.

⁴ R. E. Collin, "Reflection and transmission at a slotted dielectric interface," *Can. J. Phys.*, vol. 34, pp. 398-411; April, 1956.

⁵ E. M. T. Jones and S. B. Cohn, "Surface matching of dielectric lenses," *J. Appl. Phys.*, vol. 26, pp. 452-457; April, 1955.

⁶ E. M. T. Jones, T. Morita, and S. B. Cohn, "Measured performance of matched dielectric lenses," *IRE TRANS. ON ANTENNAS AND PROPAGATION*, vol. AP-4, pp. 31-33, January, 1956.

⁷ T. Morita and S. B. Cohn, "Microwave lens matching by simulated quarter-wave transformers," *IRE TRANS. ON ANTENNAS AND PROPAGATION*, vol. AP-4, pp. 33-39; January, 1956.

⁸ R. E. Collin and R. Vaillancourt, "Application of Rayleigh-Ritz method to dielectric steps in waveguides," *IRE TRANS. ON MICROWAVE THEORY AND TECHNIQUES*, vol. MTT-5, pp. 177-184; July, 1957.

⁹ R. E. Collin, "Determination of equivalent circuit parameters," *IRE TRANS. ON MICROWAVE THEORY AND TECHNIQUES*, vol. MTT-5, pp. 266-267; October, 1957.

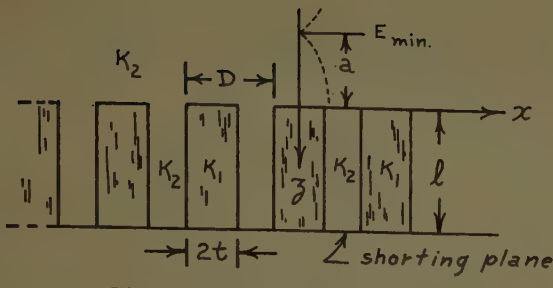


Fig. 1—Slotted dielectric interface.

thickness $2t$ and dielectric constant κ_2 separated by slabs of thickness $2d$ and dielectric constant κ_1 . The homogeneous medium in $z < 0$ is assumed to have a dielectric constant κ_2 also. For convenience, all the dielectric constants will be normalized with respect to that of the medium in $z < 0$ and the dielectric constant of the slabs denoted by κ where $\kappa = \kappa_1/\kappa_2$. The spacing of the slabs is D and is chosen small enough so no higher order modes propagate; *i.e.*,

$$D < \frac{\lambda_0}{\kappa_i^{1/2}(1 + \cos \theta_x)},$$

where κ_i is the largest of κ_1 or κ_2 , λ_0 is the free space wavelength, and $\cos \theta_x$ is the direction cosine between the wave normal and the x axis in the medium with dielectric constant κ_i .

Four separate cases of importance in practice will be considered.

- 1) Plane of incidence in xz plane and with incident electric vector parallel to slabs (perpendicular polarization).
- 2) Plane of incidence in yz plane and with incident electric vector parallel to slabs (parallel polarization).
- 3) Plane of incidence as in case 2 but with incident electric vector perpendicular to slabs (perpendicular polarization).
- 4) Plane of incidence as in case 1 but with incident electric vector perpendicular to slabs (parallel polarization).

In addition, first-order results will be given for a general angle of incidence and arbitrary polarization for the case when D is small as compared with the wavelength.

The two basic sets of modes which may exist in the slotted dielectric region are the longitudinal section electric and magnetic (LSE and LSM) modes. These modes may be derived from a magnetic and an electric Hertzian potential function, respectively, by means of the following equations⁸ for the LSE modes;

$$\mathbf{E} = -j\omega\mu_0\nabla \times \boldsymbol{\pi}_M \quad (1a)$$

$$\mathbf{H} = \nabla \times \nabla \times \boldsymbol{\pi}_M \quad (1b)$$

$$\nabla^2 \boldsymbol{\pi}_M + \kappa k^2 \boldsymbol{\pi}_M = 0, \quad (1c)$$

while for the LSM modes,

$$\mathbf{H} = j\omega\epsilon_0\kappa_2\nabla \times \boldsymbol{\pi}_E \quad (2a)$$

$$\kappa(x)\mathbf{E} = \nabla \times \nabla \times \boldsymbol{\pi}_E \quad (2b)$$

$$\nabla^2 \boldsymbol{\pi}_E + \kappa k^2 \boldsymbol{\pi}_E - \kappa^{-1}(\nabla \kappa)\nabla \cdot \boldsymbol{\pi}_E = 0, \quad (2c)$$

where $\boldsymbol{\pi}_M$ and $\boldsymbol{\pi}_E$ have components along the x axis only, $k^2 = \omega^2\mu_0\kappa_2\epsilon_0$, and κ is given by

$$\kappa = \begin{cases} \kappa_1/\kappa_2, & -t + nD \leq x \leq t + nD, \quad z \geq 0, \\ 1, & \text{otherwise,} \end{cases}$$

with n an arbitrary integer.

Instead of solving (1) and (2) rigorously, the solutions for the modes in the slotted section are approximated by a series of the corresponding modes in the homogeneous region $z < 0$ as determined by the Rayleigh-Ritz method. The basic theory has already been covered⁸ so the derivation of the required solutions will only be outlined briefly here. Initially, a first-order approximate solution, utilizing only the dominant modes, will be given. This solution gives results for the equivalent dielectric constants, accurate to within a few per cent, but does not give any information on the relative phase shifts of the reflected and transmitted waves which arise from the higher order mode contributions at the interface. This additional information and the corrections to the equivalent dielectric constants, as obtained by taking the first two higher order modes into account, are considered in a later section.

For the four special cases listed above, the interface can be characterized by a lossless four-terminal network. A convenient equivalent circuit representation is an ideal transformer of turns ratio $n:1$ and two lengths of transmission line of electrical lengths θ_1 and θ_2 , as illustrated in Fig. 2. Let ϕ_2 be the electrical position of a short-circuit in the slotted section and ϕ_1 be the electrical distance of an electric field null from the interface on the input side. The relationship between ϕ_1 and ϕ_2 which will be derived below is of the form

$$\tan \phi_1 = \frac{A + B \tan \phi_2}{C + D \tan \phi_2}; \quad (3)$$

and the equivalent circuit parameters are given by,⁹

$$\theta_2 = -\frac{1}{2} \tan^{-1} \frac{2(AB + CD)}{A^2 + C^2 - B^2 - D^2}, \quad (4a)$$

$$\theta_1 = -\tan^{-1} \frac{A - B \tan \theta_2}{C - D \tan \theta_2}, \quad (4b)$$

$$n^2 Z_1 = \frac{(AD - BC)(1 + \tan^2 \theta_2)}{(C - D \tan \theta_2)^2(1 + \tan^2 \theta_1)}, \quad (4c)$$

where for parallel polarization

$$Z_1 = \frac{\sqrt{\kappa_e - \sin^2 \theta_1}}{\kappa_e \cos \theta_1}, \quad (4d)$$

and for perpendicular polarization

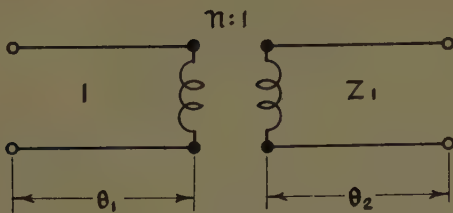


Fig. 2—Equivalent circuit of interface for one mode.

$$Z_1 = \frac{\cos \theta_i}{\sqrt{\kappa_e - \sin^2 \theta_i}}. \quad (4e)$$

In the expressions for Z_1 , θ_i is the angle of incidence measured from the interface normal, and κ_e is the equivalent dielectric constant of the slotted medium normalized with respect to κ_2 . Eqs. (4d) and (4e) are the usual normalized wave impedances of an isotropic, homogeneous, dielectric medium. When only the dominant modes are taken into account, the constants A and D in (3) are zero, and the only circuit parameter required is $n^2 Z_1$.

For case 4, as well as for general angles of incidence, the slotted dielectric medium has anisotropic properties and (4d) is not the appropriate expression to use for the normalized wave impedance.¹⁰ Also, for general angles of incidence both LSE and LSM propagating modes are excited when either an LSM or LSE mode is incident. The interface must, therefore, be characterized by an equivalent circuit with ten parameters connecting together four transmission lines. For a dominant mode approximation, this equivalent circuit simplifies to one with three parameters only. The coupling of the two modes is brought about by the polarization current in the dielectric slabs.

Case 1

The incident field is an H mode, and only higher order H modes are excited (with no variation with y , the LSE and LSM modes are identical with the E and H modes). The fields may be derived from the one scalar component $E_y(x, z)$. The boundary conditions are continuity of E_y and its normal derivative at all interfaces. For a wave incident at an angle θ_i , E_y has the following form for the incident wave,

$$E_y = A_0 e^{-j\Gamma_0 z}, \quad (5)$$

where

$$h = k \sin \theta_i$$

$$\Gamma_0^2 = h^2 - k^2.$$

Since the structure is periodic along the x axis with a period D , the electric field in the slotted section is of the form

$$\psi(x) e^{\pm \beta z} = F(x) e^{-j\Gamma_0 z \pm \beta z},$$

¹⁰ R. E. Collin, "A simple artificial anisotropic dielectric medium," IRE TRANS. ON MICROWAVE THEORY AND TECHNIQUES, vol. MTT-6, pp. 206-209; April, 1958.

where $F(x)$ is a periodic function of x with period D . For the approximation of the K th mode in the slotted section the following form is chosen:

$$\psi_K(x) e^{\pm \beta_K z} = e^{\pm \beta_K z} \sum_{n=-N}^N b_{nK} \sqrt{\frac{1}{D}} e^{-i(h+2n\pi/D)x}. \quad (6)$$

The wave equation satisfied by ψ_k in the slotted section is

$$\frac{d^2 \psi_K}{dx^2} + (\kappa(x)k^2 + \beta_K^2)\psi_K = 0. \quad (7)$$

Multiplying by ψ_k^* (the asterisk denotes conjugate value) and integrating the second derivative by parts once over the range

$$-\frac{D}{2} \leq x \leq \frac{D}{2}$$

gives

$$\int_{-D/2}^{D/2} \left[\frac{d\psi_K}{dx} \frac{d\psi_K^*}{dx} - (\kappa(x)k^2 + \beta_K^2)\psi_K \psi_K^* \right] dx = 0, \quad (8)$$

since both ψ_k and $d\psi_k/dx$ are continuous, and $\psi_k(d\psi_k^*/dx)$ is periodic. Eq. (8) is a variational expression for β_K^2 . Substituting the expression for ψ_k from (6) into (8) and equating all the partial derivatives $\partial/\partial b_{nk}^*$ to zero yields the following matrix eigenvalue system for determining the eigenvalues β_K^2 and eigenvector components b_{nk} :

$$\sum_{n=-N}^N b_{nk} [\Gamma_n^2 \delta_{sn} - k^2 T_{sn} - \beta_K^2 \delta_{sn}] = 0, \quad s = -N, \dots, N, \quad (9)$$

where

$$\Gamma_n^2 = \left(h + \frac{2n\pi}{D} \right)^2 - k^2$$

$$T_{sn} = \chi_e \frac{\sin(n-s)\pi \frac{2\ell}{D}}{(n-s)\pi}$$

$$\chi_e = \kappa - 1$$

$$\delta_{sn} = \begin{cases} 1, & n = s, \\ 0, & n \neq s, \end{cases}$$

and the b_{nk} are subjected to the normalization condition

$$\sum_{n=-N}^N b_{nK} b_{nL} = \delta_{KL}.$$

The matrix elements in (9) are real and, hence, the b_{nk} may be chosen as real also.

For a one-mode approximation (9) gives the following result for β_0^2 ,

$$\beta_0^2 = h^2 - \left(1 + \chi_e \frac{2\ell}{D} \right) k^2. \quad (10)$$

The equivalent dielectric constant of a homogeneous dielectric, which would give the same value of β_0 , is readily seen to be given by

$$\kappa_e = 1 + \chi_e \frac{2t}{D}, \quad (11)$$

where κ_e is normalized with respect to κ_2 . The value for κ_e given by (11) is just the average value of κ and is equal to the low-frequency value given by Morita and Cohn.⁷ For a one-mode approximation the electric field on the input side is taken as

$$A_0 e^{-i\hbar x} \sin |\Gamma_0| (z + a),$$

and on the output side as

$$B_0 e^{-i\hbar x} \sin |\beta_0| (z - l),$$

where a is the location of a field minimum in the region $z < 0$ and l is the short-circuit position in the region $z > 0$. From the continuity condition on E_y and $\partial E_y / \partial z$ at $z = 0$, one obtains the relation

$$\tan |\Gamma_0| a = \tan \phi_1 = - \frac{\Gamma_0}{\beta_0} \tan |\beta_0| l = - \frac{\Gamma_0}{\beta_0} \tan \phi_2. \quad (12)$$

Using (3) and (4c) shows that $n^2 Z_1$ is equal to Γ_0 / β_0 . From (9) and (10) one finds that

$$Z_1 = \frac{\Gamma_0}{\beta_0} = \frac{\cos \theta_i}{\sqrt{\kappa_e - \sin^2 \theta_i}}, \quad (13)$$

hence, the turns ratio n of the ideal transformer is equal to unity, and the slotted section is equivalent to a homogeneous medium with a normalized wave impedance given by (4e), and an equivalent dielectric constant given by (11).

Case 2

The incident mode is an LSE mode, and both higher order LSE and LSM modes are excited by the interface. For the first-order approximation only the dominant LSE mode is considered. The analysis is similar to that for case 1 with the exception that the factor $e^{-i\hbar x}$ is replaced by $e^{-i\hbar y}$. In the region $z < 0$, the Hertzian potential for the incident and reflected fields is

$$\pi_M = A_0 e^{-i\hbar y} \cos |\Gamma_0| (z + a),$$

while for the fields in the slotted section

$$\pi_M = B_0 e^{-i\hbar y} \cos |\beta_0| (z - l),$$

where

$$\begin{aligned} \Gamma_0^2 &= h^2 - k^2 \\ \beta_0^2 &= h^2 - \kappa_e k^2 \\ h &= k \sin \theta_i \\ \kappa_e &= 1 + \chi_e \frac{2t}{D}. \end{aligned}$$

The transverse field components E_y and H_z are given by (1a) and (1b) as follows:

$$E_y = \frac{\partial \pi_M}{\partial z}$$

$$H_z = \kappa k^2 \pi_M.$$

The continuity of these fields at $z = 0$ gives

$$\tan \phi_1 = - \frac{\beta_0}{\kappa_e \Gamma_0} \tan \phi_2. \quad (14)$$

From the definition of β_0 and Γ_0 , one obtains the relation

$$n^2 Z_1 = \frac{\beta_0}{\kappa_e \Gamma_0} = \frac{\sqrt{\kappa_e - \sin^2 \theta_i}}{\kappa_e \cos \theta_i}, \quad (15)$$

which is identical with (4d). Thus the slotted section behaves as a homogeneous medium with an equivalent dielectric constant κ_e given by (11) again. Since the incident wave is parallel polarized, an angle of incidence θ_b (the Brewster angle) exists so that Z_1 equals unity and no reflection occurs. From (15) one obtains

$$\sin \theta_b = \sqrt{\frac{\kappa_e}{\kappa_e + 1}} \quad (16)$$

in direct analogy with homogeneous dielectric material. For $\theta_i < \theta_b$, Z_1 is less than unity while for $\theta_i > \theta_b$, Z_1 is greater than unity. Thus as θ_i increases from zero to a value greater than θ_b , the phase angle of the reflection coefficient changes discontinuously from π to 0 as the angle θ_b is passed through. The equivalent transmission line circuit for the interface may be chosen as the junction of two lines with characteristic impedances of unity and Z_1 , or alternatively, as two transmission lines of characteristic impedance unity and Z_1 connected together through two sections of line and an ideal transformer as in Fig. 2 with

$$\begin{aligned} n &= 1, & \theta_1 = \theta_2 = 0, & \theta_i < \theta_b \\ n &= Z_1^{-1}, & \theta_1 = -\theta_2 = -\pi/2, & \theta_i > \theta_b. \end{aligned}$$

This latter representation corresponds to the type of equivalent circuit given by (4), when $n^2 Z_1$ is always chosen less than unity and higher order modes are taken into account. Fig. 3 illustrates the discontinuous change in θ_1 and θ_2 as the Brewster angle is passed through, as well as the continuous but rapid change in these angles when higher order modes are included.

Case 3

The incident mode is an LSM mode, and both LSM and LSE higher order modes are excited at the interface. An appropriate form for the Hertzian potential π_E in the region $z < 0$ is

$$\begin{aligned} \pi_E &= A_0 e^{-i\hbar y} \sin |\Gamma_0| (z + a) \\ &+ \sum_{n=-N}^N A_n e^{-i\hbar y - j(2n\pi/D)x + \Gamma_n z}, \end{aligned} \quad (17)$$

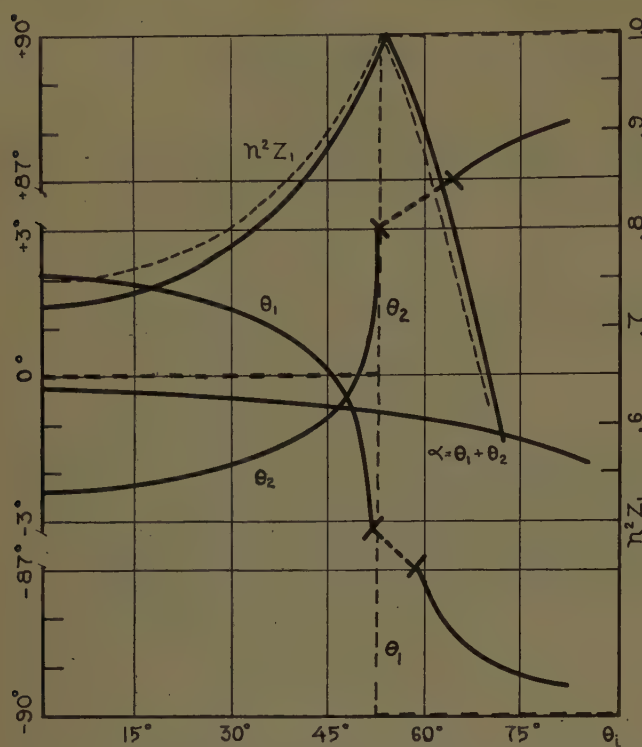


Fig. 3—Equivalent circuit parameters for $2t/D = \frac{1}{2}$, $D = 0.75 \lambda/\kappa^{1/2}$, $\kappa = 2.56$ (parallel polarization, plane of incidence parallel to slabs). Broken curves = first-order solution.

where

$$\Gamma_n^2 = \left(\frac{2n\pi}{D} \right)^2 + h^2 - k^2,$$

and the prime means omission of the term $n=0$. The variational expression for the propagation constants ψ_K for the K th LSM mode in the slotted section is

$$\int_{-D/2}^{D/2} \frac{1}{\kappa} \left[\frac{d\psi_K}{dx} \frac{d\psi_K^*}{dx} + (h^2 - \kappa k^2 - \gamma_K^2) \psi_K \psi_K^* \right] dx = 0, \quad (18)$$

where ψ_K is the approximation to the K th eigenfunction; i.e.,

$$\psi_K = \sum_{n=0}^N a_{nK} \cos \frac{2n\pi x}{D} e^{-i\gamma_K x - \gamma_K z}. \quad (19)$$

The coefficients A_{nk} are determined by a minimization of (18). For a single mode approximation it is found that

$$\left. \begin{aligned} \gamma_0^2 &= h^2 - \kappa_e k^2 \\ \kappa_e &= \left[1 - \frac{\chi_e}{\kappa} \frac{2t}{D} \right]^{-1} \\ \tan \phi_1 &= -\frac{\Gamma_0}{\gamma_0} \tan \phi_2 \\ n^2 Z_1 &= \frac{\Gamma_0}{\gamma_0} = \frac{\cos \theta_i}{\sqrt{\kappa_e - \sin^2 \theta_i}} \end{aligned} \right\}. \quad (20)$$

Again the slotted section behaves as a homogeneous dielectric with a dielectric constant κ_e which may be shown to be equal to the low-frequency value obtained from the rigorous eigenvalue equation as D/λ approaches zero.⁷

Case 4

From the analysis of the previous cases, it is seen that the equivalent dielectric constant is different for the two polarizations, the electric vector parallel to the slabs, and the electric vector perpendicular to the slabs. For this reason, the dielectric slab medium behaves essentially like a uniaxial anisotropic dielectric medium. With incidence in the xz plane and parallel polarization, the electric vector has components both parallel and perpendicular to the slabs. The incident mode is an E mode and only higher order E modes are excited. These modes may be derived from a suitable Hertzian potential π_E . The approximate eigenfunctions and propagation constants in the slotted region are obtained from a variational integral of the form given in (18). In the region $z < 0$, the Hertzian potential for the incident and reflected waves is

$$\pi_E = A_0 e^{-ihz} \sin |\Gamma_0| (z + a).$$

If the approximation $\psi_0 = e^{-ihz - \gamma_0 z}$ is substituted into (18), the resulting value of γ_0^2 is $h^2 - \kappa_e k^2$ where κ_e is given in (20). This approximation does not even bring out the anisotropic effects and is a poor one to use. A better first-order solution for this case is given in the next section as a special case of the first-order solution for a general angle of incidence.

GENERAL ANGLE OF INCIDENCE

A plane wave incident at a general angle can be represented as a superposition of an LSE and an LSM mode. Both LSE and LSM modes are excited in the slotted section when either an LSE or LSM mode is incident at a general angle. The fundamental LSE and LSM modes in the slotted dielectric section propagate with different phase velocities and, hence, such a medium has anisotropic properties. The anisotropic properties of such a medium are discussed in detail elsewhere.¹⁰ A first-order solution for the reflection and transmission coefficients of the interface for general angles of incidence, will be given here; i.e., no higher order modes are taken into account. A further assumption, that $D \ll \lambda$, will be made so that the slotted dielectric section may be treated as a homogeneous anisotropic dielectric.

For the slotted dielectric medium, the equivalent normalized dielectric constants are κ_a along the x axis and κ_b along the y and z axes where

$$\kappa_a = \left[1 - \frac{\chi_e}{\kappa} \frac{2t}{D} \right]^{-1} \quad (21a)$$

$$\kappa_b = 1 + \chi_e \frac{2t}{D}. \quad (21b)$$

From Collin,¹⁰ the two fundamental modes of propagation are derivable from π_M and π_E as follows:

for the ordinary wave

$$\mathbf{E} = -j\omega\mu_0\nabla \times \pi_M \quad (22a)$$

$$\mathbf{H} = \nabla \times \nabla \times \pi_M \quad (22b)$$

$$\pi_M = \mathbf{a}_x \exp -jk_b \mathbf{L} \cdot \mathbf{r}, \quad (22c)$$

for the extraordinary wave

$$\mathbf{E} = k^2 \pi_E + \kappa_b^{-1} \nabla \nabla \cdot \pi_E \quad (23a)$$

$$\mathbf{H} = j\omega\epsilon_0\kappa_2 \nabla \times \pi_E \quad (23b)$$

$$\pi_E = \mathbf{a}_x \exp -j\beta \mathbf{L} \cdot \mathbf{r}, \quad (23c)$$

where \mathbf{L} is a unit vector in the direction of the wave normal, and \mathbf{r} is the position vector $\mathbf{a}_x x + \mathbf{a}_y y + \mathbf{a}_z z$. The propagation constants are given below;

$$k_b = \kappa_b^{1/2} k \quad (24a)$$

$$\beta = \frac{k_a k_b}{[L_x^2 k_a^2 + (1 - L_x^2) k_b^2]^{1/2}}, \quad (24b)$$

where $k_a = \kappa_a^{1/2} k$. When these two modes are excited by a plane wave incident from $z < 0$, they do not have the same wave normals. Let the Hertzian potentials for the waves in the region $z < 0$ be

$$\pi_M = \mathbf{a}_x [\omega\mu_0 k^3 N_z (1 - N_x^2)]^{-1/2}$$

$$\cdot [A_0 \exp -jk \mathbf{N} \cdot \mathbf{r} + A_1 \exp -jk \mathbf{N}' \cdot \mathbf{r}] \quad (25a)$$

$$\pi_E = \mathbf{a}_x [\omega\epsilon_0\kappa_2 k^3 N_z (1 - N_x^2)]^{-1/2}$$

$$\cdot [B_0 \exp -jk \mathbf{N} \cdot \mathbf{r} + B_1 \exp -jk \mathbf{N}' \cdot \mathbf{r}], \quad (25b)$$

where the wave unit normals are given by

$$\mathbf{N} = \mathbf{a}_x N_z + \mathbf{a}_y N_y + \mathbf{a}_z N_z$$

$$\mathbf{N}' = \mathbf{a}_x N_z + \mathbf{a}_y N_y - \mathbf{a}_z N_z.$$

On the output side, suitable forms for the Hertzian potentials are

$$\pi_M = \mathbf{a}_x [\omega\mu_0 k^3 L_{1z} (1 - L_{1x}^2)]^{-1/2}$$

$$\cdot [C_1 \exp -jk_b L_{1z} \cdot \mathbf{r} + C_0 \exp -jk_b L_{1z}' \cdot \mathbf{r}] \quad (26a)$$

$$\pi_E = \mathbf{a}_x [\omega\epsilon_0\kappa_2 \beta k^3 L_{2z} (1 - L_{1x}^2)]^{-1/2}$$

$$\cdot [D_1 \exp -j\beta L_{2z} \cdot \mathbf{r} + D_0 \exp -j\beta L_{2z}' \cdot \mathbf{r}] \quad (26b)$$

where L_{1z}' and L_{2z}' have the same relation to L_{1z} and L_{2z} as \mathbf{N}' does to \mathbf{N} . The potentials have been normalized so that $\frac{1}{2} A_0 A_0^*$, etc., corresponds to the power per unit area flowing across the xy plane. All the field components must have the same variation with x and y and, hence,

$$kN_x = k_b L_{1x} = \beta L_{2x} \quad (27a)$$

$$kN_y = k_b L_{1y} = \beta L_{2y}. \quad (27b)$$

Solving (24b) and (27a) for β and L_{2z} gives

$$\beta = [\kappa_a + N_x^2 (1 - \kappa_a/\kappa_b)]^{1/2} k, \quad (28a)$$

$$L_{2z} = \kappa_b^{1/2} N_x [\kappa_a \kappa_b + N_x^2 (\kappa_b - \kappa_a)]^{-1/2}. \quad (28b)$$

The tangential field components follow from the given Hertzian potentials by means of (22) and (23) with appropriate modifications for the region $z < 0$. When the tangential field components are equated at the interface plane $z = 0$, we obtain

$$\begin{aligned} & \left(\frac{1 - N_x^2}{N_x} \right)^{1/2} (A_0 + A_1) \\ & = \left(\frac{\kappa_b^{1/2} (1 - L_{1x}^2)}{L_{1z}} \right)^{1/2} (C_1 + C_0) \quad (29a) \end{aligned}$$

$$\begin{aligned} & \left(\frac{1 - N_x^2}{N_x} \right)^{1/2} (B_0 + B_1) \\ & = \left(\frac{k (1 - L_{1x}^2)}{\beta L_{2z}} \right)^{1/2} (D_1 + D_0) \quad (29b) \end{aligned}$$

$$\begin{aligned} & \frac{-N_x N_y}{[N_z (1 - N_x^2)]^{1/2}} (A_0 + A_1) + \left(\frac{N_z}{1 - N_x^2} \right)^{1/2} (B_0 - B_1) \\ & = \frac{-L_{1x} L_{1y} \kappa_b^{1/4}}{[L_{1z} (1 - L_{1x}^2)]^{1/2}} (C_1 + C_0) \\ & + \left(\frac{\beta L_{2z}}{k (1 - L_{1x}^2)} \right)^{1/2} (D_1 - D_0), \quad (29c) \end{aligned}$$

$$\begin{aligned} & \frac{N_x N_y}{[N_z (1 - N_x^2)]^{1/2}} (B_0 + B_1) + \left(\frac{N_z}{1 - N_x^2} \right)^{1/2} (A_0 - A_1) \\ & = \frac{L_{1x} L_{1y} k^{1/2}}{[\beta L_{2z} (1 - L_{1x}^2)]^{1/2}} (D_1 + D_0) \\ & + \left(\frac{L_{1z}}{\kappa_b^{1/2} (1 - L_{1x}^2)} \right)^{1/2} (C_1 - C_0). \quad (29d) \end{aligned}$$

If transmission lines are introduced to represent the propagation of the two modes on the input and output sides and numbered according to the following scheme,

Mode	Input Side	Output Side
π_M	1	3
π_E	2	4

then the interface may be characterized by a four-by-four scattering matrix $[S]$ where S_{ij} represents the transmission coefficient from line i to line j , and S_{ii} is the reflection coefficient for line i . The scattering matrix is symmetrical and unitary. By introducing the following amplitude matrices which are proportional to the transverse electric field,

$$[a] = \begin{bmatrix} a_1 \\ a_2 \\ a_3 \\ a_4 \end{bmatrix}, \quad [b] = \begin{bmatrix} -A_0 \\ B_0 \\ C_0 \\ D_0 \end{bmatrix}, \quad [b] = \begin{bmatrix} b_1 \\ b_2 \\ b_3 \\ b_4 \end{bmatrix} = \begin{bmatrix} A_1 \\ B_1 \\ -C_1 \\ D_1 \end{bmatrix},$$

one may write

$$[b] = [S][a]. \quad (30)$$

Alternatively, one may introduce transmission line voltages $V_i = a_i + b_i$ and currents $I_i = a_i - b_i$ and the interface may be characterized by an equivalent circuit as illustrated in Fig. 4. The turns ratios of the ideal transformers are given by

$$n_1 = \frac{N_x N_y}{N_s} - \frac{L_{1x} L_{1y}}{N_s} \frac{1 - N_x^2}{1 - L_{1x}^2}, \quad (31a)$$

$$n_2 = 1, \quad (31b)$$

$$n_3 = \frac{\kappa_b^{1/4} [N_x N_y (1 - L_{1x}^2) - L_{1x} L_{1y} (1 - N_x^2)]}{[L_{1x} N_s (1 - N_x^2) (1 - L_{1x}^2)]^{1/2}} \quad (31c)$$

$$n_4 = \left[\frac{(1 - N_x^2) \beta L_{2x}}{(1 - L_{1x}^2) N_s k} \right]^{1/2}, \quad (31d)$$

where n_2 has been placed equal to unity since one of the turns ratios may be chosen arbitrarily. As a typical example, the scattering matrix elements were computed for the following parameters:

$$\frac{2t}{D} = \frac{1}{2}, \quad \kappa_2 = 1, \quad \kappa_1 = 2.56, \quad N_x = N_y = 0.5,$$

and are given as

$$\begin{bmatrix} -0.11 & 0.086 & 0.986 & 0.096 \\ 0.086 & -0.11 & -0.077 & 0.988 \\ 0.986 & -0.077 & 0.13 & -0.085 \\ 0.096 & 0.988 & -0.085 & 0.095 \end{bmatrix}.$$

Essentially all of the power is transmitted as a mode corresponding to the incident mode. When a parallel or perpendicular polarized wave is incident, the reflected wave is of mixed polarization because of the coupling of the modes at the interface.

The scattering matrix parameters are readily evaluated from the equivalent circuit given in Fig. 4. This equivalent circuit contains three parameters only because all higher order modes have been neglected. When these higher order modes are included, the equivalent circuit will contain reactive elements also.

The solutions for the case when the incident wave is a parallel or perpendicular polarized wave, may be obtained by a superposition of the π_M and π_E modes. For a parallel polarized wave, H_s equals zero and the appropriate relation between A_0 and B_0 is

$$A_0 = -\frac{N_y}{N_x N_z} B_0, \quad (32a)$$

while for a perpendicular polarized wave E_s equals zero and

$$A_0 = \frac{N_x N_z}{N_y} B_0. \quad (32b)$$

When N_x or N_y equals zero, (27) and (29) show that there is no coupling between the π_E and π_M modes. When $N_y = 0$, (29a) and (29d) give the first-order solu-

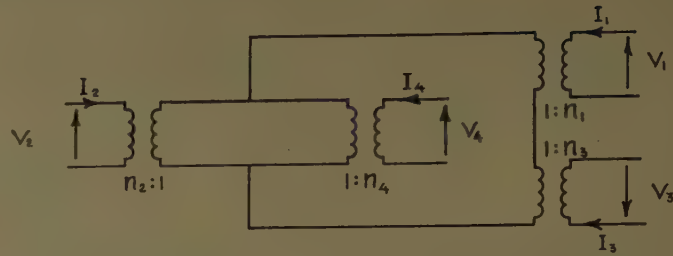


Fig. 4—Equivalent circuit of an anisotropic dielectric interface.

tion for case 1, while for $N_x = 0$, they give the same solution for case 2 as presented earlier. Eqs. (29b) and (29c) give the first-order solution for case 3 when $N_x = 0$, and for case 4 when $N_y = 0$. The solution for case 4 is of interest since it differs from that for ordinary dielectric material because of the anisotropic properties of the slotted section. The input impedance to the slotted section is

$$n^2 Z_1 = \left(\frac{n_2}{n_4} \right)^2 = \frac{[\kappa_b - \sin^2 \theta_i]^{1/2}}{(\kappa_a \kappa_b)^{1/2} \cos \theta_i}, \quad (33a)$$

and the propagation constant γ_0^2 is given by

$$\gamma_0^2 = -\beta^2 L_{2z}^2 = \frac{\kappa_a}{\kappa_b} h^2 - \kappa_a k^2, \quad (33b)$$

where $h = k \sin \theta_i = k N_x$. An examination of (33a) shows that a Brewster angle exists. This angle is given by

$$\sin \theta_b = \left[\frac{\kappa_b (\kappa_a - 1)}{\kappa_a \kappa_b - 1} \right]^{1/2} \quad (34)$$

and differs from that for an isotropic dielectric. In particular, a value of θ_b less than $\pi/4$ may exist, in contrast to isotropic dielectrics for which θ_b is always greater than $\pi/4$ for a direction of incidence from the less dense medium into the denser medium.

SECOND-ORDER SOLUTIONS FOR EQUIVALENT CIRCUIT PARAMETERS

When higher order modes are taken into account in the Rayleigh-Ritz method, more accurate expressions for the propagation constants β_0 and γ_0 are obtained. This leads directly to more accurate values for the equivalent dielectric constants. In addition, approximate values for the equivalent circuit parameters θ_1 and θ_2 are obtained. These latter two parameters determine the phase shifts in the reflected and transmitted waves. For many practical cases, these additional lengths of transmission lines are small. In the design of quarter wave matching sections, there is considerable compensation from the two ends of the transformer section so that the parameters θ_1 and θ_2 need not be taken into account in the design except perhaps for critical applications.³

In the following sections, the formulas for calculating the equivalent circuit parameters for the first four cases

treated earlier will be given. In all cases only three modes are taken into account. Typical numerical results are also given. All numerical calculations were done with a slide rule and hence, are limited in accuracy; nevertheless they indicate the type of behavior to be expected.

Case 1

For a three-mode approximation, the electric field on input side is taken as

$$A_0 e^{-i\beta_0 z} \sin |\Gamma_0| (z + a) + A_1 e^{-i(\beta_1 + 2n\pi/D)z + \Gamma_1 z} + A_{-1} e^{-i(\beta_{-1} - 2n\pi/D)z + \Gamma_{-1} z}$$

and on the output side as

$$B_0 \sin |\beta_0| (z + l) \sum_{n=-1}^1 b_{n0} e^{-i(\beta_0 + (2n\pi/D))z} + B_1 e^{-\beta_1 z} \sum_{n=-1}^1 b_{n1} e^{-i(\beta_1 + (2n\pi/D))z} + B_{-1} e^{-\beta_{-1} z} \sum_{n=-1}^1 b_{n-1} e^{-i(\beta_{-1} + (2n\pi/D))z}.$$

The propagation constants and eigenvector components b_{nk} are determined from (9) given earlier. When the coefficients of $e^{-i(2n\pi/D)z}$ are equated in the expressions for E_y and $\partial E_y / \partial z$ at $z=0$, a homogeneous set of equations is obtained for the amplitude coefficients A_i and B_i . A solution for these coefficients exists provided their determinant vanishes. The vanishing of the determinant gives the desired relation between $\phi_1 = |\Gamma_0|a$ and $\phi_2 = |\beta_0|l$. The determinant of the coefficients is given below:

$$\Delta = \begin{vmatrix} b_{00}(|\Gamma_0| \cot \phi_1 + |\beta_0| \cot \phi_2) & b_{01}(|\Gamma_0| \cot \phi_1 + \beta_1) & b_{0-1}(|\Gamma_0| \cot \phi_1 + \beta_{-1}) \\ b_{10}(\Gamma_1 + |\beta_0| \cot \phi_2) & b_{11}(\Gamma_1 + \beta_1) & b_{1-1}(\Gamma_1 + \beta_{-1}) \\ b_{-10}(\Gamma_{-1} + |\beta_0| \cot \phi_2) & b_{-11}(\Gamma_{-1} + \beta_1) & b_{-1-1}(\Gamma_{-1} + \beta_{-1}) \end{vmatrix}. \quad (35)$$

From (9) for $N=1$ the expression for the equivalent dielectric constant κ_e may be obtained by substituting $h^2 - \kappa_e k^2$ for β_0^2 . The resultant is a cubic equation in κ_e , the correct root being the largest positive root. An approximate solution which is a lower bound is the static value

$$\kappa_b = 1 + \chi_e \frac{2t}{D},$$

normalized with respect to κ_2 . Actually $\kappa_e - \kappa_b$ appears explicitly in this cubic equation and the solution for $\kappa_e - \kappa_b$ is readily obtained by successive approximations since it is a small quantity. For this case, κ_e is a function of θ_i although not a very sensitive function of θ_i .

For normal incidence the three-mode approximation reduces to a two-mode approximation. The matrix eigenvalue system (9) becomes

$$\sum_{n=0}^1 b_{nk} [(\Gamma_n^2 - \beta_k^2) \delta_{kn} - k^2 R_{sn}] = 0, \quad s = 0, 1, \quad (36)$$

where

$$R_{sn} = \chi_e \frac{\sqrt{\epsilon_{0n}\epsilon_{0s}}}{2\pi} \left[\frac{\sin(n-s)\pi \frac{2t}{D}}{n-s} + \frac{\sin(n+s)\pi \frac{2t}{D}}{n+s} \right]$$

and $\epsilon_{0n}=1$ for $n=0$ and 2 for $n>0$. The equivalent normalized dielectric constant for normal incidence as determined from (36) is given by

$$\kappa_e = \frac{R_{00} + R_{11}}{2} + 1 - \frac{\lambda^2}{2D^2} + \left[\left(\frac{R_{00} + R_{11}}{2} + 1 - \frac{\lambda^2}{2D^2} \right)^2 + (1 + R_{00}) \left(\frac{\lambda^2}{D^2} - R_{11} - 1 \right) + R_{10}^2 \right]^{1/2} \quad (37)$$

where $\lambda = \lambda_0/\kappa_2^{1/2}$. As λ/D approaches zero $\kappa_e \rightarrow \kappa_b$. Fig. 5 is a plot of $\kappa_e - \kappa_b$ as a function of $2t/D$ for $\kappa=2.56$, and four values of D/λ . Curves of $\kappa_e - \kappa_b$ are plotted instead of curves of κ_e to give greater accuracy, although admittedly there is some inconvenience in their use. The maximum correction to κ_e is around 2 per cent for $(2t/D) \approx \frac{1}{2}$ and $D=0.5 \lambda/\sqrt{\kappa}$.

For normal incidence the values of the coefficients A , B , C , and D , for determining the equivalent circuit parameters from (4), are given by

$$A = -b_{10}^2 \frac{k}{\beta_1} \quad (38a)$$

$$B = -\frac{\Gamma_0}{\beta_0} \left(b_{00}^2 + \frac{\Gamma_1}{\beta_1} \right) \quad (38b)$$

$$C = 1 + b_{00}^2 \Gamma_1 / \beta_1 \quad (38c)$$

$$D = b_{01}^2 \Gamma_1 / |\beta_0|, \quad (38d)$$

and $b_{00}=b_{11}$, $b_{01}=-b_{10}$, $Z_1=\Gamma_0/\beta_0$. Figs. 6 and 7 give plots of the equivalent circuit parameters θ_1 , θ_2 , and $n^2 Z_1$ as a function of κ_1 and κ_2 , respectively, for the two

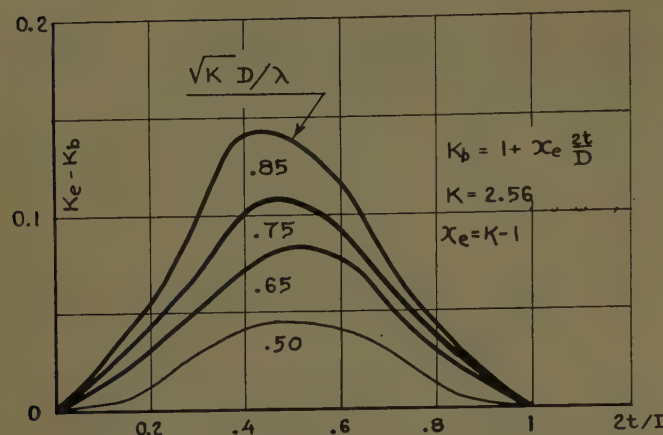


Fig. 5—Correction to first-order values of equivalent dielectric constant for parallel polarization and plane of incidence parallel to slabs.

following typical cases: $2t/D = 0.5$, $\kappa_1 = 1$, $\theta_i = 0$, $D\kappa_1^{1/2} = 0.75\lambda_0$; and $2t/D = 0.5$, $\kappa_1 = 1$, $\theta_i = 0$, $D\kappa_2^{1/2} = 0.75\lambda_0$. The turns ratio $n:1$ of the ideal transformer was found to be equal to unity to within an accuracy of three significant figures for the total range of variables considered above. The phase shift through the interface is $\alpha = \theta_1 + \theta_2$ and was only one or two degrees. Apart from the phase shifts represented by θ_1 and θ_2 , this slotted dielectric interface is equivalent to a homogeneous dielectric interface with an equivalent normalized dielectric constant κ_e given by (37). Fig. 6 corresponds to the case of a plane wave incident from free space into the slotted dielectric section, while Fig. 7 corresponds to a wave incident from the solid dielectric region onto the slotted section. It should be noted that θ_1 and θ_2 are of opposite sign for the two cases. It is this property which results in the correction to the length of a quarter wave section to be negligible for most practical purposes. The dashed curves in Fig. 6 are the upper and lower bounds for θ_1 and θ_2 obtained by a variational method employing a single mode approximation to the aperture field.⁴ These results indicate that the Rayleigh-Ritz method gives acceptable accuracy.

Case 2

For this case the incident mode is an LSE mode, and both higher order LSE and LSM modes are excited by the interface. Two LSE modes and one LSM mode will be taken into account. In the slotted section, the LSE modes are determined by a solution of the following matrix eigenvalue system:

$$\sum_{n=0}^1 b_{nK} [(\Gamma_n^2 - \beta_K^2) \delta_{sn} - k^2 R_{sn}] = 0, \quad s = 0, 1, \quad (39)$$

together with the normalization condition

$$\sum_{n=0}^1 b_{nK} b_{nL} = \delta_{KL},$$

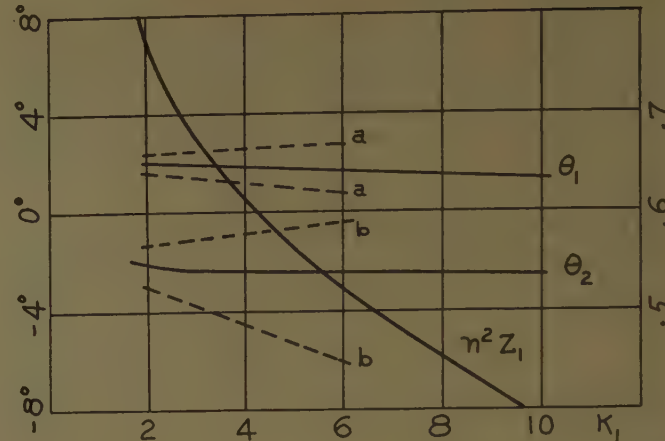


Fig. 6—Equivalent circuit parameters for $2t/D = \frac{1}{2}$, $D = 0.75 \lambda/\kappa_1^{1/2}$, $\kappa_2 = 1$, $\theta_i = 0^\circ$. (Electric vector parallel to slabs.) (a) Upper and lower bounds for θ_1 , (b) upper and lower bounds for θ_2 .

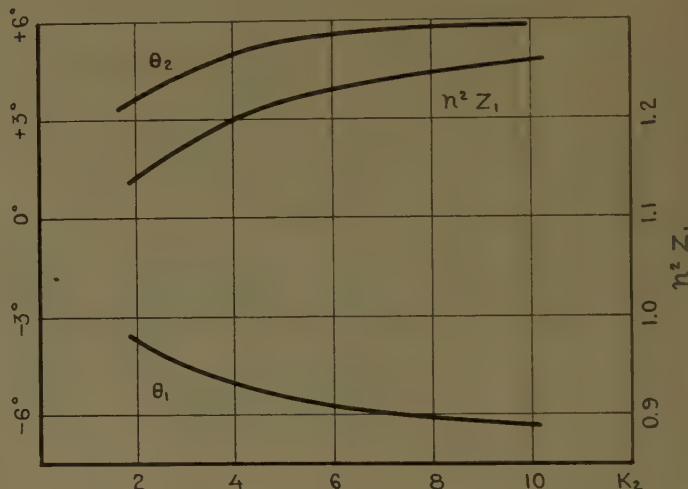


Fig. 7—Equivalent circuit parameters for $2t/D = \frac{1}{2}$, $D = 0.75 \lambda/\kappa_2^{1/2}$, $\kappa_1 = 1$, $\theta_i = 0^\circ$. (Electric vector parallel to slabs.)

where

$$\Gamma_n^2 = h^2 + 4 \left(\frac{n\pi}{D} \right)^2 - k^2,$$

and R_{sn} is the expression given after (36). The propagation constant for the first approximate LSM mode is given by

$$\Gamma_1^2 = h^2 - \frac{R_{11}}{\kappa} \frac{4\pi^2}{D^2} + \frac{P_{11}}{P_{11}} \quad (40)$$

where

$$P_{11} = 1 - \frac{\chi_e}{\kappa} \left[\frac{2t}{D} - \frac{1}{2\pi} \sin 4\pi \frac{t}{D} \right].$$

The required relation between $\phi_1 = |\Gamma_0| a$ and $\phi_2 = |\beta_0| l$ is given by the vanishing of the following determinant:

$$\Delta = \begin{vmatrix} b_{10} \left(\frac{1}{h^2 - \beta_0^2} - \frac{1}{h^2 - \Gamma_1^2} \right) & b_{11} \left(\frac{1}{h^2 - \beta_1^2} - \frac{1}{h^2 - \Gamma_1^2} \right) & \left(\frac{Dk}{2\pi h} \right)^2 \left[\frac{\gamma_1 P_{11}}{h^2 - \gamma_1^2} + \frac{\Gamma_1}{h^2 - \Gamma_1^2} \right] \\ b_{00} \left[\frac{|\beta_0| \tan \phi_2}{h^2 - \beta_0^2} + \frac{|\Gamma_0| \tan \phi_1}{h^2 - \Gamma_0^2} \right] & b_{01} \left[\frac{|\Gamma_0| \tan \phi_1}{h^2 - \Gamma_0^2} - \frac{\beta_1}{h^2 - \beta_1^2} \right] & \frac{R_{10}}{\kappa P_{11} (h^2 - \gamma_1^2)} \\ b_{10} \left[\frac{|\beta_0| \tan \phi_2}{h^2 - \beta_0^2} - \frac{\Gamma_1}{h^2 - \Gamma_1^2} \right] & -b_{11} \left[\frac{\Gamma_1}{h^2 - \Gamma_1^2} + \frac{\beta_1}{h^2 - \beta_1^2} \right] & \frac{1}{h^2 - \Gamma_1^2} - \frac{\kappa - R_{11}}{\kappa P_{11} (h^2 - \gamma_1^2)} \end{vmatrix}. \quad (41)$$

For this case the equivalent dielectric constant is independent of the angle of incidence θ_i and is given by (37). The normalized wave impedance of the slotted section is $\beta_0/\kappa_e \Gamma_0$. Numerical results for the equivalent circuit parameters are plotted in Fig. 3 as a function of θ_i for the following parameters:

$$2t = 0.5D, \quad \kappa = 2.56, \quad Dk^{1/2} = 0.75\lambda.$$

Again the turns ratio $n:1$ was equal to unity to within an accuracy of three significant figures for all values of θ_i . In the vicinity of the Brewster angle, θ_1 and θ_2 change very rapidly to account for the 180° change in the phase angle of the reflection coefficient. The Brewster angle is given by

$$\sin \theta_b = \sqrt{\frac{\kappa_e}{\kappa_e + 1}}$$

to a high degree of accuracy.

Case 3

The incident mode is an LSM mode and both LSM and LSE modes are excited by the slotted interface. The LSM modes in the slotted section are determined by a solution of the following matrix eigenvalue system,

$$\sum_{n=0}^1 a_{nK} \left[(\Gamma_n^2 - h^2) \delta_{sn} - \frac{4ns\pi^2}{D^2} T_{sn} - (\gamma_K^2 - h^2) P_{sn} \right] = 0, \quad (42)$$

where

$$s = 0, 1,$$

$$P_{sn} = \delta_{sn} - \frac{\chi_e}{\kappa} \frac{\sqrt{\epsilon_{0n}\epsilon_{0s}}}{2\pi} \left[\frac{\sin(n-s)\pi \frac{2t}{D}}{n-s} + \frac{\sin(n+s)\pi \frac{2t}{D}}{n+s} \right],$$

$$T_{sn} = \delta_{sn} - P_{sn}$$

$$- \frac{\chi_e}{\kappa} \frac{\sqrt{\epsilon_{0n}\epsilon_{0s}}}{\pi} \frac{\sin(n+s)\pi \frac{2t}{D}}{n+s},$$

$$\Gamma_n^2 = h^2 + 4 \left(\frac{\pi n}{D} \right)^2 - k^2,$$

and the coefficients a_{nK} are normalized so that

$$\sum_{n=0}^1 \sum_{s=0}^1 a_{nK} a_{sL} P_{sn} = \delta_{KL}.$$

(This normalization is not necessary for the evaluation of ϕ_1 vs ϕ_2 .) The propagation constant for the first approximate LSE mode is given by

$$\beta_1^2 = \Gamma_1^2 - \kappa k^2 T_{11}. \quad (43)$$

The vanishing of the following determinant gives the desired relation between ϕ_1 and ϕ_2 ,

$$\Delta = \begin{vmatrix} \frac{|\Gamma_0| (a_{00}P_{00} + a_{10}P_{10}) \cot \phi_1}{h^2 - \Gamma_0^2} + \frac{|\gamma_0| a_{00} \cot \phi_2}{h^2 - \gamma_0^2} & \frac{|\Gamma_0| (a_{10}P_{00} + a_{11}P_{10}) \cot \phi_1}{h^2 - \Gamma_0^2} + \frac{\gamma_1 a_{01}}{h^2 - \gamma_1^2} & 0 \\ \frac{\Gamma_1 (a_{00}P_{01} + a_{10}P_{11})}{h^2 - \Gamma_1^2} + \frac{|\gamma_0| a_{10} \cot \phi_2}{h^2 - \gamma_0^2} & \frac{\Gamma_1 (a_{01}P_{01} + a_{11}P_{11})}{h^2 - \Gamma_1^2} + \frac{\gamma_1 a_{11}}{h^2 - \gamma_1^2} & \left(\frac{h\lambda}{D} \right)^2 \\ \frac{a_{10}(1 - T_{11})}{h^2 - \gamma_0^2} - \frac{(a_{00}P_{01} + a_{10}P_{11})}{h^2 - \Gamma_1^2} & \frac{a_{11}(1 - T_{11})}{h^2 - \gamma_1^2} - \frac{(a_{01}P_{01} + a_{11}P_{11})}{h^2 - \Gamma_1^2} & \frac{\Gamma_1(\beta_1^2 - h^2)}{\Gamma_1^2 - \beta_1^2} + \frac{\beta_1(\Gamma_1^2 - h^2)}{\Gamma_1^2 - \beta_1^2} \end{vmatrix}. \quad (44)$$

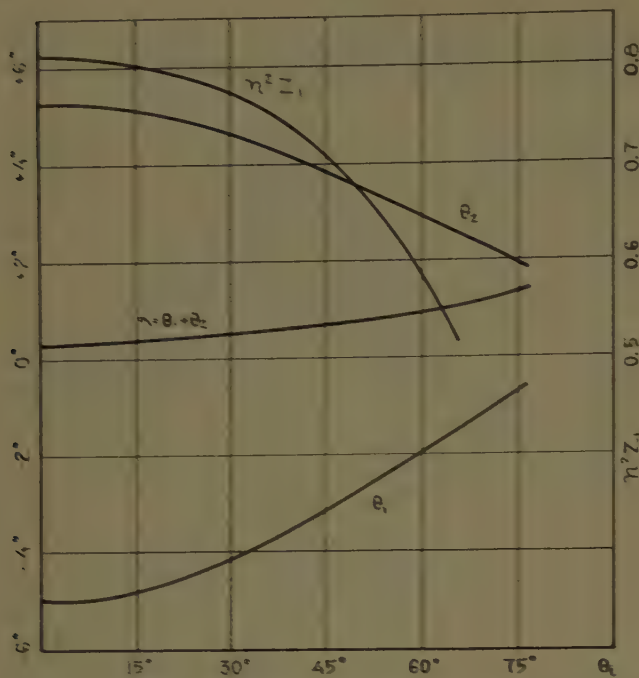


Fig. 8—Equivalent circuit parameters for $2t/D = 1/2$, $D = 0.75 \lambda$, $\kappa = 2.56$. (Perpendicular polarization, plane of incidence parallel to slabs.)

Numerical values of the interface parameters for $2t=0.5D$, $\kappa=2.56$, $D\kappa^2=0.75\lambda$ are given in Fig. 8. The turns ratio $n:1$ is equal to unity to within an accuracy of three significant figures. The normalized wave impedance of the slotted section is Γ_0/γ_0 , and the normalized equivalent dielectric constant is given by

$$\kappa_e = \frac{k^2 - \gamma_0^2}{\kappa^2} = \frac{P_{11} + P_{00}(1-Q)}{2W} + \left[\left(\frac{P_{11} + P_{00}(1-Q)}{2W} \right)^2 + \frac{Q-1}{W} \right]^{1/2} \quad (45)$$

where

$$Q = \frac{\lambda^2}{D^2}(1 - T_{11}), \quad W = P_{11}P_{00} - P_{11}^2.$$

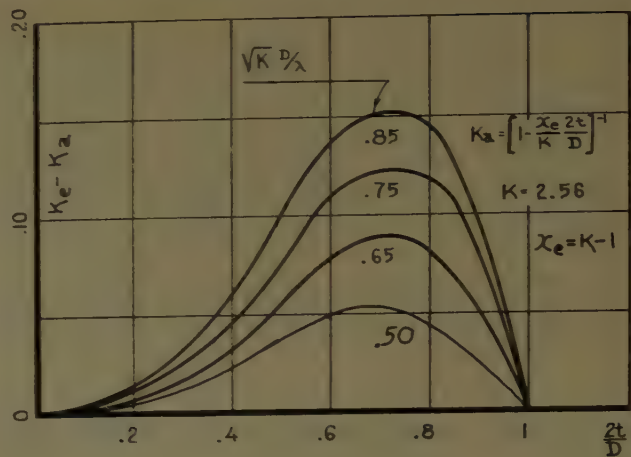


Fig. 9—Correction to equivalent dielectric constant for perpendicular polarization and plane of incidence parallel to slabs.

Case 4

This case is similar to the first one considered, except that E modes are involved instead of H modes. The eigenvector components a_{nK} and eigenvalues γ_K^2 for the modes in the slotted section are found from a solution of the following equations:

$$\sum_{s=-N}^N a_{nK} [T_{sn} - k^2 \delta_{sn} - \gamma_K^2 P_{sn}] = 0, \quad s = -N, \dots, N, \quad (46)$$

where

$$P_{sn} = \delta_{sn} - \frac{\chi_e}{\kappa} \frac{\sin(n-s)\pi \frac{2t}{D}}{(n-s)\pi},$$

$$T_{sn} = \left(h + \frac{2s\pi}{D} \right) \left(h + \frac{2n\pi}{D} \right) P_{sn},$$

and $N=1$ for a three-mode approximation. The coefficients a_{nK} satisfy the normalization conditions given after (42) although for the purpose of evaluating the relation between ϕ_1 and ϕ_2 , this normalization is not necessary. The required solution for ϕ_1 vs ϕ_2 is found from the vanishing of the following determinant:

$$\Delta = \begin{vmatrix} \gamma_1 \tan \phi_1 \sum a_{n1} P_{n1} - \Gamma_{11} a_{01} \tan \phi_1 & \gamma_1 \sum a_{n1} P_{n0} - \Gamma_{01} a_{01} \tan \phi_1 & \gamma_{-1} \sum a_{n-1} P_{n0} - |\Gamma_0| a_{0-1} \tan \phi_1 \\ \gamma_1 \tan \phi_1 \sum a_{n1} P_{n1} - \Gamma_{11} a_{01} & \gamma_1 \sum a_{n1} P_{n0} + \Gamma_{11} a_{01} & \gamma_{-1} \sum a_{n-1} P_{n0} + \Gamma_{11} a_{0-1} \\ \gamma_1 \tan \phi_1 \sum a_{n1} P_{n-1} - \Gamma_{-11} a_{0-1} & \gamma_1 \sum a_{n1} P_{n-1} + \Gamma_{-11} a_{0-1} & \gamma_{-1} \sum a_{n-1} P_{n-1} + \Gamma_{-11} a_{0-1-1} \end{vmatrix}. \quad (47)$$

As

In (47)

$$D\lambda \rightarrow 0, \quad \kappa \rightarrow \kappa_2 = \left[1 - \frac{\chi_e}{\kappa} \frac{2t}{D} \right]^{-1}$$

which is the static value. Fig. 9 is a plot of $\kappa_e - \kappa_a$ as a function of $2t/D$ for four values of $D\lambda$.

$$\Gamma_n^2 = \left(h + \frac{2n\pi}{D} \right)^2 - k^2$$

and the summations are over $-1 \leq n \leq 1$. Since the propagation factor γ_0^2 and the wave impedance for this case is a function of the two principal dielectric con-



Fig. 10—Equivalent circuit parameters for $2t/D = \frac{1}{2}$, $D = 0.75 \lambda/\kappa^{1/2}$, $\kappa = 2.56$. (Parallel polarization, plane of incidence perpendicular to slabs.) Broken curves = first-order solution.

stants because of the anisotropic properties of the medium, it becomes difficult to define the equivalent dielectric constants from the solution obtained here. However, the equivalent circuit parameters θ_1 , θ_2 , and n^2Z_1 are readily evaluated. These parameters are plotted as a function of θ_i in Fig. 10 for the following parameters:

$$2t = 0.5D, \quad \kappa = 2.56, \quad D\kappa^{1/2} = 0.75\lambda.$$

In the same figure, the first-order solution for n^2Z_1 (33a) is also given. For $\theta_i > 52^\circ$ the second mode propagates in the slotted dielectric section. Even though a relatively large spacing to wavelength ratio was used, the first-order solution still gives a good approximation for n^2Z_1 . If the second-order solutions for the principal dielectric constants are used in (33a), even closer

agreement is obtained for n^2Z_1 . For normal incidence this case is identical with the third one considered, and the curves of Fig. 9 for $\kappa_e - \kappa_a$ apply.

CONCLUSIONS

Theoretical formulas for computing the equivalent circuit parameters and equivalent dielectric constants of slotted dielectric interfaces have been presented. When the period of the slotted dielectric medium is small compared with the wavelength, it behaves like a homogeneous anisotropic dielectric medium. Even for larger spacings the anisotropic properties are retained because of the existence of two distinct modes of propagation. The numerical results presented have provided a theoretical justification for neglecting the effect of the higher order modes in the design of practical lens matching surfaces. When angles of incidence greater than 20° in the zz plane are used, the spacing, D , must be chosen less than $0.75 \kappa^{-1/2}\lambda$ to prevent higher order modes propagating in the solid dielectric region. For smaller spacing to wavelength ratios, the equivalent circuit parameters θ_1 and θ_2 are even smaller than for the numerical examples given above.

The accuracy of the formulas presented is difficult to establish on a theoretical basis. The upper and lower bounds on θ_1 and θ_2 given for a particular case in Fig. 6 indicate satisfactory accuracy. For case 1 with $\theta_i = 30^\circ$, $\kappa = 2.56$, $2t = 0.35 D$, and $D = 0.318 \lambda$, the following results were obtained by a variational method:⁴ $n = 1.00 \pm 0.005$, $\theta_1 = 0.85^\circ \pm 0.4^\circ$, $\theta_2 = -1.15 \pm 0.4^\circ$. Using the formulas given here one obtains¹¹ $n = 1.000$, $\theta_1 = 0.74^\circ$, $\theta_2 = -0.91^\circ$. It would be expected that the rigorous values of θ_1 and θ_2 would be somewhat greater than those given by the second-order solution presented here since a first-order solution gives zero for θ_1 and θ_2 , a second-order solution gives finite values, and higher order solutions would be unlikely to give results in between the first and second-order solutions.

¹¹ The author is indebted to one of the reviewers for this computation.

Traveling-Wave Cylindrical Antenna Design— A Graphical Synthesis Method*

PETER FOLDES†

Summary—A simple graphical method is given for the synthesis of a special line source system. The elements of the line source system are excited with equal amplitudes and continuously increasing phases. The sources lie on a cylindrical surface. The shape of this surface depends on the given pattern functions.

INTRODUCTION

IN THIS PAPER the space radiation is given, and from this the locations in space of the radiation sources and their complex excitation functions are determined.

With certain assumptions the theory of space antennas can be reduced to that of plane antennas, and again the theory of plane antennas to that of linear radiators.¹ In the above cases, one can express the source distribution along the antenna aperture as a product. This product contains factors which depend on only one of the space coordinates and so, in the realization of the antenna, the complex source distribution along each coordinate can be adjusted independently, *i.e.*, separability can be assumed. If the antenna size is large compared to the wavelength, the necessary amplitude and phase functions on the basis of geometrical optics can be realized (*i.e.*, with a double surface lens, or double reflectors), but unfortunately we cannot use the theory of geometrical optics if the antenna is small.²⁻⁴ Another approach would be to build up the antenna from discrete sources. However, it is rather difficult to adjust the excitations of the sources, and therefore, this otherwise elegant method is impractical.

A synthesis method is shown here which leads to a traveling-wave antenna design with a simple feed system and enables a wide range of directional characteristics to be realized. The calculations are done in one plane only, giving the source distribution along a line. The discrete sources of this antenna are distributed along a curved, cylindrical surface instead of the usual plane aperture. It is assumed that the traveling wave propagates transversely along the circumference of the cylindrical (actually polygon) surface with constant amplitude and linearly increasing phase. The basic calculations are done only in the plane transverse to the

axis of the cylinder, but a short discussion is given of the space factor for such a curve distribution of discrete sources outside the plane containing the curve.

ARRANGEMENT OF THE SOURCES

As mentioned before, the elementary sources are on a cylindrical (polygon) surface. The break points of this polygon can be determined by the angle α_k and by the polygon side length, l_k (see Fig. 1). Let us assume that the lengths of all sides are equal. This simplifies the procedure considerably but does not limit generality because the angle α_k is arbitrary, and so it is always possible to obtain any arbitrary cylindrical surface if the side length l is small enough. Furthermore, we assume that the exciting amplitudes of the elements are the same, while their phases increase linearly from element to element. Thus the complex amplitudes are $e^{i\beta_0 l_0}$, $e^{i2\beta_0 l_0}$, \dots , $e^{in\beta_0 l_0}$ where $\beta_0 = 2\pi/\lambda_0$ is the phase constant of the transmission line, and l_0 is the physical length of this line between two sources.

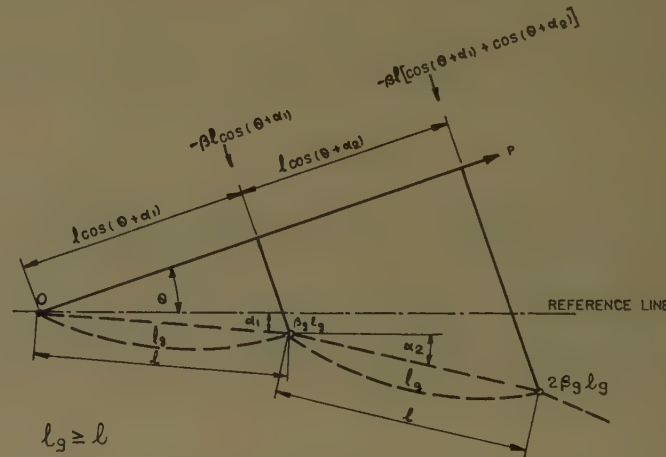


Fig. 1.

At first we assume isotropic elementary sources. Later we will take into account the effect of the non-uniform directional pattern of the actual sources.

CALCULATION OF THE DIRECTIONAL PATTERN

The directional pattern of the given source arrangement can be determined easily (see Fig. 1). The resulting directional pattern is the complex sum of the elementary patterns; *i.e.*,

$$f_0 = \sum_1^n e^{i\phi_k}, \quad (1)$$

where n is the number of elements and ϕ_k is the phase

* Manuscript received by the PGAP, May 6, 1958; revised manuscript received, August 8, 1958.

† RCA Victor Co., Ltd., Montreal, P.Q., Can.

¹ S. A. Schelkunoff, "A mathematical theory of linear arrays," *Bell Syst. Tech. J.*, vol. 22, pp. 80-107; January, 1943.

² S. Silver, "Microwave Antenna Theory and Design," McGraw-Hill Book Co., Inc., New York, N. Y., p. 497; 1946.

³ A. S. Dunbar, "Metal Plate Lens for csc² Antenna," Rad. Lab., M.I.T., Cambridge, Mass., Rep. No. 1070; February 15, 1946.

⁴ P. M. Woodward, "A method of calculating the field over a plane aperture required to produce a given polar diagram," *J. IEE*, vol. 93, pt. IIIA, pp. 1554-1558; April, 1946.

of the fields of the k th element at a distant space point; i.e.,

$$\begin{aligned}\phi_k &= k\beta_0 l_0 - \beta l \sum_1^k \cos(\theta + \alpha_i) \\ &= [k\beta_0 l_0 - k\beta l \cos \theta] \\ &\quad + \left[k\beta l \cos \theta - \beta l \sum_1^k \cos(\theta + \alpha_i) \right] \\ &= ku + s_k\end{aligned}\quad (2)$$

where θ is the angle between the reference direction and the direction of the distant point, $\beta = 2\pi/\lambda$ is the phase constant of the free space, and

$$u = \frac{2\pi l}{\lambda} [\Delta - \cos \theta], \quad (3)$$

$$\Delta = \frac{\beta_0 l_0}{\beta l} = \frac{\lambda l_0}{\lambda_0 l} \quad (4)$$

$$s_k = \frac{2\pi}{\lambda} \left[k \cos \theta - \sum_1^k \cos(\theta + \alpha_i) \right] \quad (5)$$

$$\approx \frac{2\pi}{\lambda} \sin \theta \cdot \sum_1^k \alpha_i \text{ if } \alpha_i \ll 1. \quad (5a)$$

Let us define y_k by

$$y_k = \frac{s_k}{\frac{l}{2\pi} \frac{\sin \theta}{\lambda}} \quad (6)$$

and, therefore,

$$y_k = \frac{1}{\sin \theta} \left[k \cos \theta - \sum_1^k \cos(\theta + \alpha_i) \right] \quad (7)$$

$$= \sum_1^k \alpha_i \quad \text{if } \alpha_i \ll 1. \quad (7a)$$

Introducing

$$v = 2\pi \frac{l}{\lambda} \sin \theta, \quad (8)$$

then substituting (6) and (8) into (1)

$$f_0 = \sum_1^n e^{jku} e^{jvv_k}, \quad (9)$$

If the elementary sources are not isotropic, but have some f^* directional patterns, and these patterns have the same position in the space, (in other words they are not rotated relative to each other) then the resulting pattern is:

$$f_1 = f^* f_0. \quad (10)$$

Let us suppose that f_1' is the specified directional pattern. If we divide f_1' by the elementary pattern f^* then we get f , a "predistorted" pattern, which we may attempt to realize using isotropic source system. In this case we would require the $f = f_1'/f^*$ directional pattern.

In general it is impossible to make f identical to f_0 over the whole specified θ range but it can be assumed to be equal at a certain number of θ_m points; i.e.,

$$f(\theta_m) = f_0(\theta_m), \quad m = 0, 1, 2, \dots, h-1. \quad (11)$$

GRAPHICAL SOLUTION OF (11)

Once we have determined from (11) y_k , n , l/λ , and Δ , our synthesis problem is solved. This will give the pattern function f_0 , which is equal to the predistorted pattern at a minimum of h points. The first step is to determine the over-all length of the antenna. If we want to exclude the tolerance sensitive, "supergain" antennas, then the over-all length of the line source determines the maximum possible value of $df/d\theta$, i.e., the rate of change of the directional pattern as function of θ .⁵ (From the maximum value of $df/d\theta$ in the cases of pencil beam antennas, the angle between the 3-db points of the main lobe can be calculated approximately.)

For any given directional pattern, the place and value of this maximum can be calculated. From this the size of a uniformly excited linear antenna can be determined which has a main lobe with the same value of maximum slope as the analyzed antenna. (See Fig. 2.) After this it is possible to choose this size for the first approximation of the antenna length.

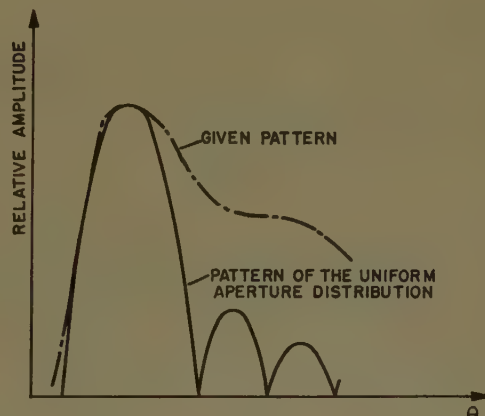


Fig. 2.

Let us assume that $f_H = \sin U/U$ is the pattern of the uniformly excited antenna, where $U = (\beta L/2) \sin \theta$ and to L is the length of this antenna. Then

$$\left| \frac{df(\theta)}{d\theta} \right|_{\theta=\theta_M} = \left| \frac{df_H(U)}{dU} \right|_{U=U_M=(\beta L/2) \sin \theta_M} \quad (12)$$

where θ_M is the angle for the given pattern and U_M is the angle where the pattern of the uniform aperture distribution has the maximum rate. The exact value of U_M can be determined, but one gets a good approximation for df_H/dU assuming $U_M = \pi/2$.

⁵ H. A. Wheeler, "Fundamental limitations of small antennas," Proc. IRE, vol. 35, pp. 1479-1484; December, 1947.

Thus

$$\left| \frac{df_H}{d\theta} \right| = \left| \frac{df_H}{dU} \right| \left| \frac{dU}{d\theta} \right|$$

$$\left| \frac{df_H}{dU} \right|_{U=\pi/2} = \left| \frac{\cos U}{U} - \frac{\sin U}{U^2} \right|_{U=\pi/2} = \frac{4}{\pi^2}, \quad (13)$$

$$\left| \frac{dU}{d\theta} \right|_{\theta=\theta_M} = \pi \frac{L}{\lambda} \cos \theta_M \quad (14)$$

and

$$\left| \frac{df}{d\theta} \right|_{\theta=\theta_M} = \frac{4}{\pi} \frac{L}{\lambda} \cos \theta_M. \quad (15)$$

Then

$$(n-1) \frac{l}{\lambda} = \frac{L}{\lambda} = \frac{\pi}{4 \cos \theta_M} \left| \frac{df}{d\theta} \right|_{\theta=\theta_M}. \quad (16)$$

The above formula gives n , or l/λ . As seen from (9), $n \geq n$ means the maximum possible number of points where the specified and the actual patterns could be equal. This approximation can be improved by increasing n , but at the same time this increases the difficulty of calculation and our system becomes a "supergain" antenna. Therefore in practice it is preferable to choose the value of n such that

$$\frac{\lambda}{2} \leq l \leq \lambda.$$

The next problem is to obtain the value of

$$\Delta = \frac{\beta_g l_g}{\beta l}. \quad (4)$$

In the case of the most simple feeding $l=l_g$ and so $\Delta=\lambda/\lambda_g$; i.e., Δ is larger or smaller than unity in dielectric cables and waveguides, respectively, and it is equal to one in air-insulated transmission lines. Increasing Δ the phase of the pattern function changes more rapidly; this may cause considerable variation in the absolute value of the pattern function, particularly at large θ angle. Therefore, Δ can be larger than unity when the directional pattern is given only in a relatively narrow region (e.g., $10^\circ < \theta < 50^\circ$). If the pattern is specified over a wider range, it is preferable to choose Δ equal to unity, or less.

After determining n , l/λ , and Δ we can start solving the main problem—the calculation of the values of y_k . It is preferable that the points of approximation θ_M be chosen so that the values v defined in (8) are

$$v_m = 2\pi \frac{l}{\lambda} \sin \theta_m = Am, \quad m = 0, 1, \dots, h-1. \quad (17)$$

$$h \leq \frac{2\pi}{A} \frac{l}{\lambda},$$

where m is a positive integer and A is a constant. In (17) m must not exhaust all the integers between 0 and $h-1$. The number A determines how many points of approximation are used from the possible n . If m assumes all integers between 0 and $h-1$ then

$$A = \frac{2\pi}{\lambda} \frac{l}{n}.$$

From (17)

$$\theta_m = \sin^{-1} \left[\frac{Am\lambda}{2\pi l} \right]. \quad (18)$$

The values of the pattern function at the points θ_m are, according to (11) and (17)

$$f(\theta_m) = \sum_{k=1}^n e^{ikum} e^{iAymk}, \quad m = 0, 1, \dots, h-1. \quad (19)$$

The values of $Aym_k = s_k$ can be determined from the transcendental equations, (19). Then with the help of the basic equation, (7), we can get α_k . Introducing $\varphi_i = \theta_m + \alpha_i$

$$s_k = \frac{2\pi l}{\lambda} \left[k \cos \theta_m - \sum_i^k \cos \varphi_i \right]. \quad (20)$$

From this

$$\varphi_k = \cos^{-1} \left[k \cos \theta_m - \frac{\lambda}{2\pi l} s_k - \sum_{i=1}^{k-1} \cos \varphi_i \right], \quad k > 1 \quad (21)$$

$$\varphi_1 = \cos^{-1} \left[\cos \theta_m - \frac{\lambda}{2\pi l} s_1 \right]$$

and

$$\alpha_k = \varphi_k - \theta_m. \quad (22)$$

Eq. (19) has no simple analytic solution for y_k . But with successive geometrical approximation we can get a solution. For any value of m , (19) represents a set of complex vectors. Their end points are on a circle of unity radius. Fig. 3 represents (19) assuming $A=1$ and $n=3$, for $m=1, 2, 3$. The values of m determine u_1, u_2, u_3 . Marking these values on the circles, we have to choose the y_k values on the circles to satisfy the given specification f_1, f_2, f_3 .

In general f_m is complex, but in practice only its magnitude is given; in our case $|f_2/f_1|$ and $|f_3/f_1|$ are given, so only these must be adjusted. Our starting points can be $y_{10} = y_{20} = y_{30} = 0$. (Here the 0 index refers to the zeroth order of approximation.) On this basis the vectors f_{10}, f_{20} , and f_{30} , can be drawn. Then one of the y 's, say y_{20} , may be shifted, so that

$$\left| \frac{f_{21}}{f_{10}} \right| = \left| \frac{f_2}{f_1} \right|.$$

This gives the first approximation for y_2 (represented by y_{21}). The shifting of y_2 of course changes the value

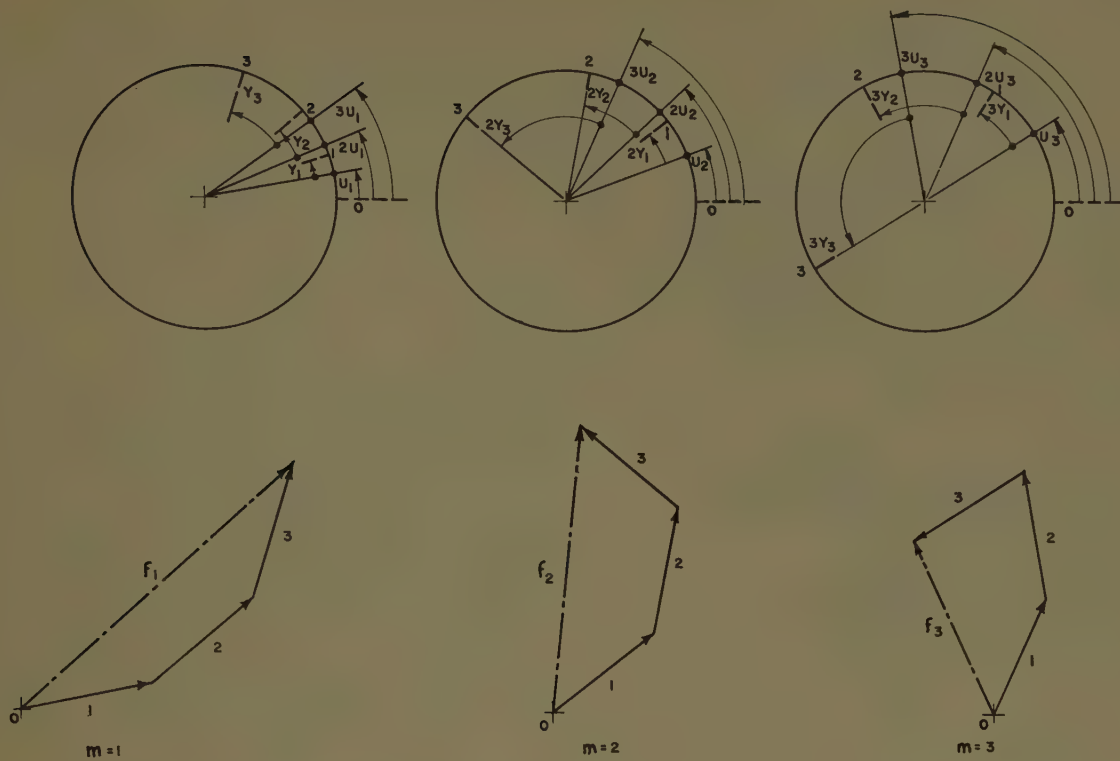


Fig. 3.

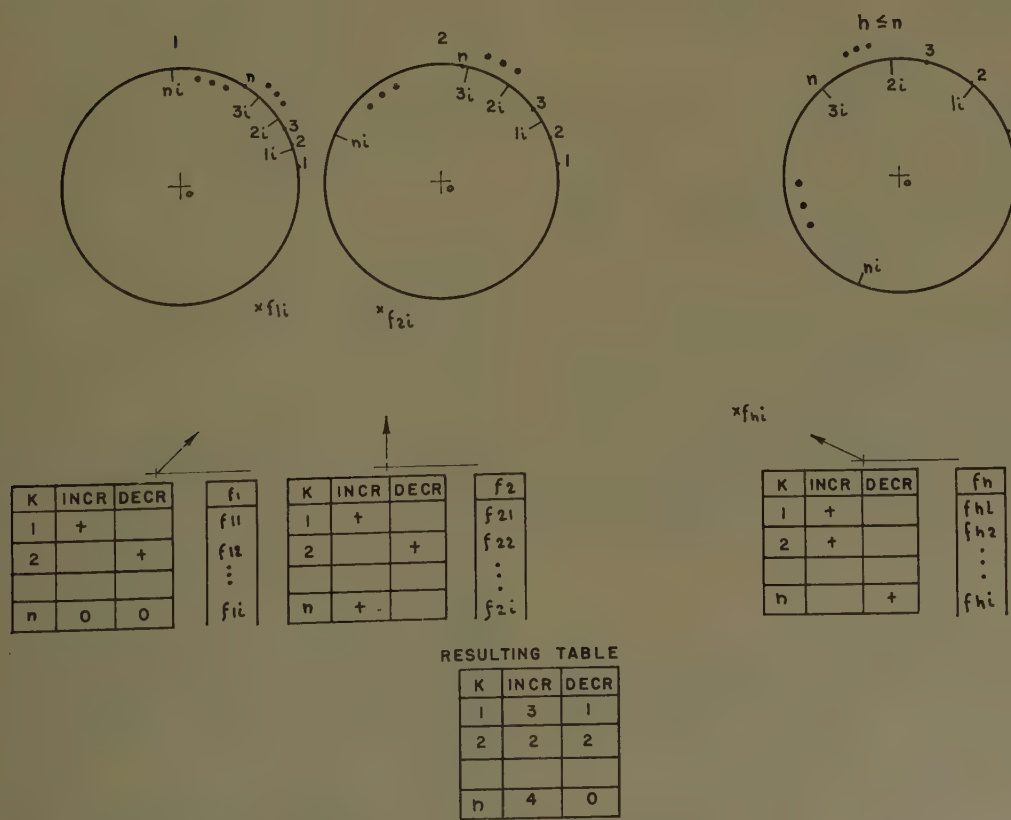


Fig. 4.

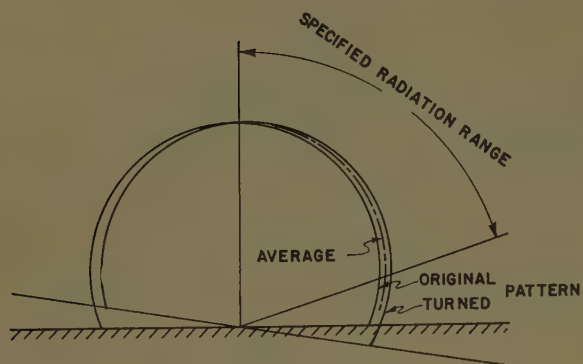


Fig. 5.

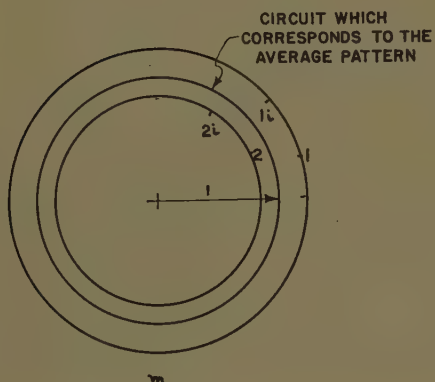


Fig. 6.

of f_{10} to f_{11} . This changes the relative value of the pattern too, and so now

$$\left| \frac{f_{21}}{f_{11}} \right| \neq \left| \frac{f_2}{f_1} \right|.$$

But

$$\left| \left| \frac{f_{21}}{f_{11}} \right| - \left| \frac{f_2}{f_1} \right| \right| < \left| \left| \frac{f_{20}}{f_{10}} \right| - \left| \frac{f_2}{f_1} \right| \right|,$$

because the point y_k moves with half velocity on the first circle as on the second. The procedure is convergent if the approximating process is started at the maximum values of f_m and continued towards the lower level part of the pattern function. After adjusting y_2 we can go on to y_3 so that we get the specified value for $|f_3/f_1|$. This is possible, because on the third circle all y move faster than on the first, or second, and we assumed that $|f_3| < |f_1|$, or $|f_2|$.

DESIGN ADVICE

In practice, when n is large, it is preferable to refine our method for increasing the rate of convergence. For this purpose it is better to tabulate the effect of shifting y_k . The practical procedure is shown on Fig. 4.

First draw the h circles with unity radius and make the tables for y_k . Then mark the values of $u_1, 2u_1, |h-1|u_1$ on the circumference of the first circle, the values $u_2, 2u_2, |h-1|u_2$ on the second, and so on. We

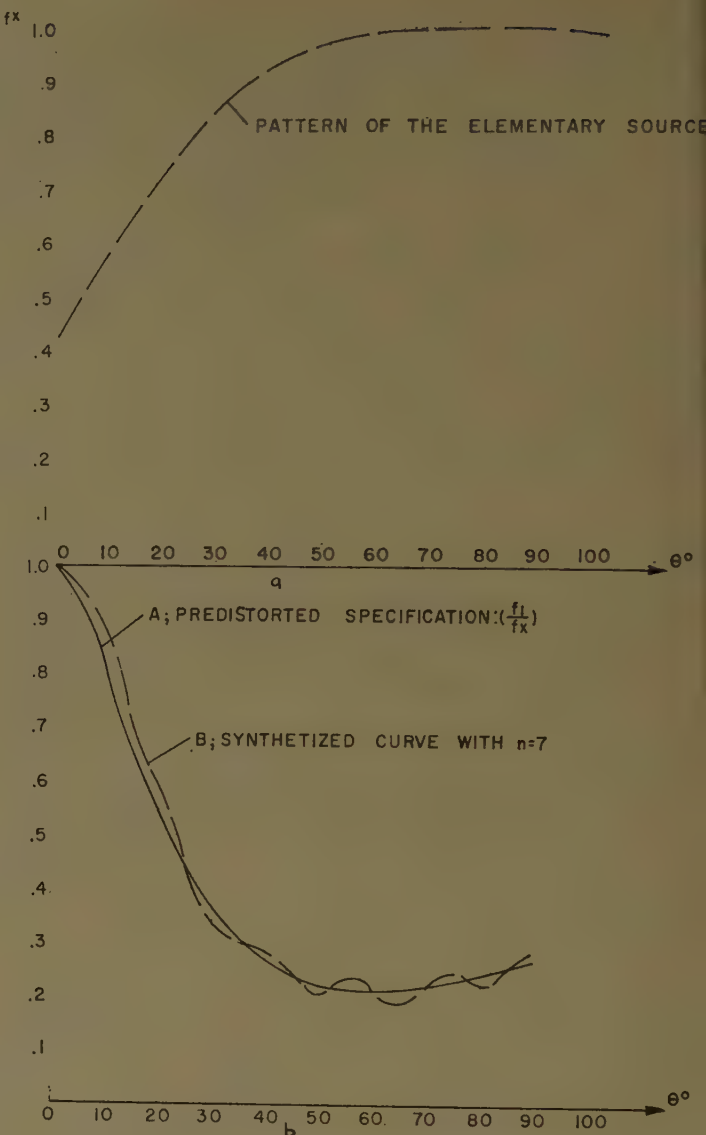


Fig. 7.

can write on the inner side of the circumference the first approximations of y_k 's. Let us call this k_i . After this, mark the polar coordinate systems for the specified f_m values. If $Δ=1$ and $α_k$'s are small, these values do not change much during the approximation process because the maximum value of f_m occurs at $m=0$, and this is $f_0=h$. Next we tabulate the values f_{mi} of the i th approximation.

In our tables we have increasing and decreasing columns. Put a + sign in the k th row of the increasing column of the m th table if a small increasing of y_k brings the value of f_m nearer to the specified f_m . In the opposite case put a - sign in the decreasing column. It is preferable to put a 0 sign in both columns if a small change gives only a "second order" effect. (That means the vector f_{mi} and the $δf_{mi}=f_{mi}-f_{m,i+1}$ "correction" vector are in quadrature.)

Complete the h tables in a similar manner and compute in a resulting table the changing effect of any y_k . From this table choose those changes of the values of

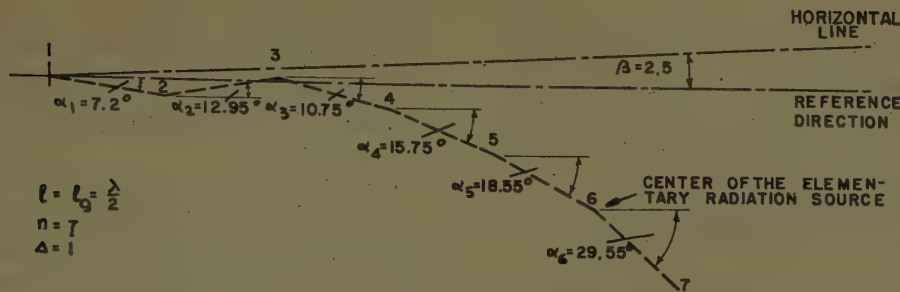


Fig. 8.

y_k which give improvement in maximum cases. It is preferable to change two y values simultaneously because we can seldom find single y_k values which improve all f_m values. Now we must follow successive approximations until all the $+$ signs disappear from the tables. After this has been obtained (19) is solved, and with this the antenna geometry is determined. After this treatment let us analyze the difference between the actual and specified patterns at those points where m differs from the ones given in (17). The maximum of the differences are in the neighborhood of the points

$$m = \frac{1}{2}, \frac{3}{2}, \dots, \frac{2h-3}{2},$$

so let us calculate these values of the pattern function from (19) or from graphical interpolation based on the drawn figures. If the actual pattern function is within the limit of the tolerance range, the problem is solved. If the function has values outside the tolerance range, repeat the whole treatment using a larger n ; if the function occupies too small a part of the tolerance range, choose a smaller n thus getting a smaller antenna.

In the case of the most frequently used shaped beam ($\text{cosec } \theta$), the angles α_k are small and the deviation of the antenna surface from the reference plane is relatively small. In such cases the above theory is approximately true not only for discrete sources, but for continuous surface antennas as well. There the assumptions of the point source theory, *i.e.*, the directional patterns of the elementary sources being directed toward the same direction in the space, are approximately satisfied. From Fig. 5 it can be seen that the pattern of a short elementary section of the antenna surface changes very slowly in the usual specified radiation range.

If it is necessary, we can get a closer approximation. Using the first approximation, take the pattern values of the slightly turned elementary antennas at the directions θ_m . Then draw circles with different radii. These different radii must be proportional to the pattern function values of the turned elementary sources. Such modified circuits are shown in Fig. 6. Fortunately the closer approximation deviates little from the first, except at small θ angle.

Finally let us see the result of a typical synthesis problem. The curve on Fig. 7(a) shows the pattern of an elementary source; curve *A* on Fig. 7(b) shows the

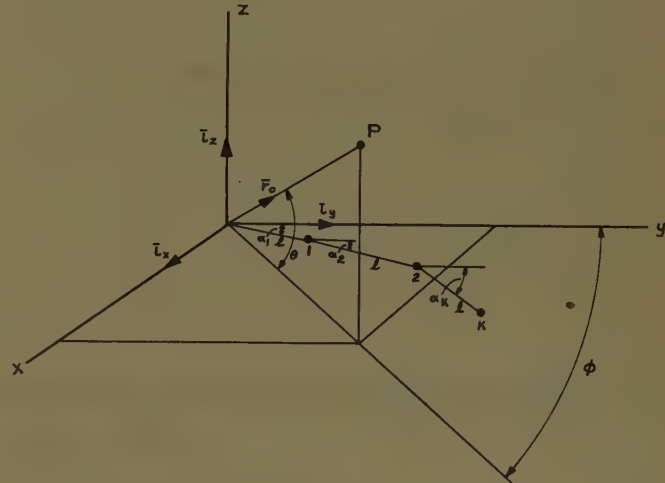


Fig. 9.

predistorted specification, and curve *B* represents the synthesized pattern, with

$$n = 7, \quad l/\lambda = \frac{1}{2}, \quad \Delta = 1.$$

The α_k values are shown on Fig. 8. We assumed a dipole and passive reflector as an elementary point source of the complete system. It may be seen that the resulting point source system lies along a curve which deviates only slightly from a straight line.

GENERAL FORM OF THE SPACE FACTOR

The radiation of the determined traveling-wave system arrives at the pattern requirement in the analyzed plane. However, in practice it is necessary to know the radiation in arbitrary directions. Eq. (1) describes the space factor but the form of the ϕ_k phase factor is now more general. On the basis of Fig. 9,

$$\phi_k = \beta_\theta lk - \beta \bar{r}_0 \bar{r}_k \quad (23)$$

where

$$\bar{r}_0 = \bar{r}_x \cos \theta \sin \phi + \bar{r}_y \cos \theta \cos \phi + \bar{r}_z \sin \theta \quad (24)$$

is the unit vector directed to the distant point, and

$$\bar{r}_k = \bar{r}_y l \sum_1^k \cos \alpha_i - \bar{r}_z l \sum_1^k \sin \alpha_i \quad (25)$$

is the position vector of a typical array element. From (24) and (25)

$$\phi_k = \beta_g l_g k$$

$$- \beta l \left[\cos \theta \cos \phi \sum_1^k \cos \alpha_i - \sin \theta \sum_1^k \sin \alpha_i \right]. \quad (26)$$

Using (1) and (26) the general form of the space factor

$$f_0(\theta, \phi) = \sum_{k=1}^n \exp \left\{ \beta_g l_g k - \beta l \left[\cos \theta \cos \phi \sum_1^k \cos \alpha_i - \sin \theta \sum_1^k \sin \alpha_i \right] \right\}. \quad (27)$$

If $\alpha_i \ll 1$, then $\sin \alpha_i \approx \alpha_i$, $\cos \alpha_i \approx 1$ and

$$f_0(\theta, \phi) \approx \sum_{k=1}^n \exp \left\{ k(\beta_g l_g - \beta l \cos \theta \cos \phi) + \sin \theta \sum_1^k \alpha_i \right\}. \quad (28)$$

From (28) it follows that

- 1) near to the $\phi=0$ plane the field is approximately the same vs θ as in the $\phi=0$ plane,
- 2) in the $\theta=0$ plane the pattern is similar to the end fire array.

CONCLUSIONS

Several types of surface antennas can be designed relatively easily with the help of this method. The new type of antenna discussed has special advantages as a shaped beam antenna. It differs from the classical type, which uses amplitude and phase variation along a straight line-antenna, by using constant amplitude and linearly increasing phase. However, the elements do not lay on a straight line. With this new method it is also possible to synthesize wide angular range cosec θ antennas.

Theoretical Research on Tropospheric Scatter Propagation in the United States, 1954-1957*

H. STARAS† AND A. D. WHEELON‡

Summary—This paper outlines recent progress in the theory of tropospheric scatter propagation in the United States. In the past three years, the emphasis of theoretical research has shifted from the analysis of the average signal level to the analysis of the signal statistics and to the underlying hydrodynamics of atmospheric turbulence. As might be expected in such a new and complex field, there is far from unanimity of opinion as to the "best" model to explain the myriad experimental results.

I. INTRODUCTION

CONSIDERABLE theoretical progress in understanding tropospheric scatter propagation beyond the optical horizon was made in the past three years. The problem may be broadly divided into: 1) characterization of the random medium, 2) electromagnetic calculations of the average signal strength as a function of distance and frequency, and 3) estimations of the signal's statistical properties. An important shifting of emphasis from the space correlation function to the spectrum of turbulent irregularities has taken place and has provided a unique representation of time variations of the medium and signal. Physical theories of turbulent irregularities have been developed on the mixing-in-gradient hypothesis and are quite suc-

cessful in explaining the radio frequency and distance dependence of the transmissions, as well as observed meteorological correlations.

Statistical descriptions of the received signal's fading envelope have been considerably improved. The distribution of amplitudes and variable frequency dependence of fading rates have been successfully predicted. Computations of space correlation for the field and height gain indicate that the scattering blobs may well be anisotropic. Antenna gain-degradation and beam-swinging experiments with very narrow beams seem to agree with theoretical estimations. Considerable attention has been directed to the bandwidth limitations of this propagation mode and to optimum modulation schemes.

A new approach to the problem based on reflection by one or more refractive layers has been proposed. Satisfactory agreement with average signal levels is provided by these theories, although the statistical properties remain to be studied. Normal mode theory based on partial internal reflections by a bilinear atmospheric profile model continues to play an offstage role for lack of specific results.

II. CHARACTERIZATION OF A TURBULENT MEDIUM

* Manuscript received by the PGAP, March 14, 1958; revised manuscript received, July 9, 1958.

† RCA Labs., Princeton, N. J.

‡ Space Technology Labs., Inc., Los Angeles, Calif.

The tropospheric index of refraction varies from point-to-point in a random manner. To describe this

effect, one decomposes the dielectric constant ($\epsilon = n^2$) into its mean value and a small stochastic component. Thus,

$$\epsilon(\mathbf{r}, t) = \epsilon_0 + \Delta\epsilon(\mathbf{r}, t). \quad (1)$$

ϵ_0 is considered to be a function of altitude (h) only and its gradient appears in several physical theories of turbulent irregularities. The function $\Delta\epsilon(\mathbf{r}, t)$ is usually treated as a stationary random process, which is spatially homogeneous and isotropic,

$$\langle \Delta\epsilon(\mathbf{r}, t) \rangle = 0$$

$$\langle \Delta\epsilon(\mathbf{r}, t) \Delta\epsilon(\mathbf{r} + \mathbf{R}, t) \rangle = \langle \Delta\epsilon^2 \rangle C(|\mathbf{R}|). \quad (2)$$

Little attention has been paid to higher moments, except to note that they are completely specified in terms of $C(r)$ if the $\Delta\epsilon$ form a Gaussian random process. The intensity of dielectric fluctuations $\langle \Delta\epsilon^2 \rangle$ is measured experimentally as several parts in 10^{-12} , while the correlation function falls to $1/\epsilon$ in a distance of several hundred feet. It is often assumed that $\langle \Delta\epsilon^2 \rangle$ decreases with altitude as h^{-m} .

The space correlation function $C(R)$ is the fundamental characterization of the turbulence, and its choice sets the radio frequency and distance dependence of scatter propagation theories. The exponential model $C(R) = \exp(-R/l_0)$ has been used extensively in the past, although the Bessel model $C(R) = (R/l_0)K_1(R/l_0)$ currently seems to give better agreement with experiment. Anisotropic irregularities can be discussed by introducing different scale lengths in orthogonal directions,^{1,2} *viz.*,

$$C(R) = \exp - \left[\frac{x^2}{l_1^2} + \frac{y^2}{l_2^2} + \frac{z^2}{l_3^2} \right]^{1/2}. \quad (3)$$

An equivalent characterization of a turbulent medium is the spectrum of irregularities,³ which is the Fourier decomposition of the space correlations functions,

$$\langle \Delta\epsilon^2 \rangle C(R) = \frac{1}{8\pi^3} \int_V d^3k S(k) \exp(-ik \cdot \mathbf{R}). \quad (4)$$

If the medium is isotropic, $S(k)$ depends only on $|\mathbf{k}|$. The mean square fluctuation at a point,

$$\langle \Delta\epsilon^2 \rangle = \frac{1}{2\pi^2} \int_0^\infty dk k^2 S(k) \quad (5)$$

indicates that the spectrum represents the ability of each blob size group to produce irregularities.

Eq. (4) may be inverted to compute the spectrum corresponding to a given correlation function. Table I indicates the spectra for the Gaussian, exponential, and Bessel models.

TABLE I

$C(R)$	e^{-R^2/l_0^2}	e^{-R/l_0}	$\frac{R}{l_0} K_1 \left(\frac{R}{l_0} \right)$
$S(k)$	$\pi^{3/2} \langle \Delta\epsilon^2 \rangle l_0^3 e^{-k^2 l_0^2/4}$	$8\pi \frac{\langle \Delta\epsilon^2 \rangle l_0^3}{[1+k^2 l_0^2]^2}$	$6\pi^2 \frac{\langle \Delta\epsilon^2 \rangle l_0^3}{[1+k^2 l_0^2]^{5/2}}$

To describe the temporal behavior of electromagnetic instabilities, one must consider the generalization of (2) displaced in both time and space. Time variations of $\Delta\epsilon$ are associated with two types of motion:

- 1) Drifting convection: The entire (frozen) structure is borne along on prevailing winds, and is equivalent to an additional space correlation distance $U\tau$.
- 2) Random motion: If one rides along with the net flow, there is still motion associated with continuous eddy breakup.

The combination of these two effects is expressed most conveniently by the spectrum method,^{3,4}

$$\langle \Delta\epsilon(\mathbf{r}, t) \Delta\epsilon(\mathbf{r} + \mathbf{R}, t + \tau) \rangle$$

$$= \frac{1}{8\pi^3} \int d^3k S(k) \exp[i\mathbf{k} \cdot (\mathbf{R} + \mathbf{U}\tau)] C(k, \tau). \quad (6)$$

$C(k, \tau)$ describes the time autocorrelation of fluctuations within a fixed wave number interval k . In the inertial subrange, dimensional arguments show the $C(k, \tau)$ should depend only on $v_0 k_0^{1/3} k^{2/3} \tau$, although no functional dependence has yet been established.

The spectrum method makes direct contact with physical theories of turbulent irregularities. Such theories identify three distinct ranges of the spectrum shown in Fig. 1: 1) input range $0 < k < k_0$, 2) inertial range $k_0 < k < k_s$, and 3) dissipation range $k > k_s$. In the troposphere, $k_s = k_s^{-1}$ is of the order of millimeters and $k_0 = k_0^{-1}$ is a hundred meters or more. Only the inertial range is of interest to tropospheric scatter, since aperture smoothing eliminates the contributions of small blobs in the dissipation range and the larger blobs are relatively inefficient scatterers. This is very important, since dimensional analysis can be used with some confidence in this range.

Variations in the tropospheric dielectric constant are governed principally by water vapor content. One is dealing therefore with the irregularities established in a passive scalar by turbulent movements of the atmosphere's (vector) velocity field. There are two popular theories⁵ which predict $S(k)$.

Obukhov's Mixing Theory

In this theory, an external source is imagined to feed fluctuations into the spectrum at the largest blob size

¹ H. Staras, "Forward scattering of radio-waves by anisotropic turbulence," *Proc. IRE*, vol. 43, pp. 1374-1380; October, 1955.

² H. G. Booker, "A theory of scattering by nonisotropic irregularities with application to radar reflections from the aurora," *J. Atmos. and Terrest. Phys.*, vol. 8, pp. 204-221; May, 1956.

³ A. D. Wheelon, "Relation of radio measurements to the spectrum of tropospheric dielectric fluctuations," *J. Appl. Phys.*, vol. 28, pp. 684-693; June, 1957.

⁴ R. A. Silverman, "Fading of radio-waves scattered by dielectric turbulence," *J. Appl. Phys.*, vol. 28, pp. 506-511; April, 1957.

⁵ Most writers now agree that the pressure fluctuation mechanism is unimportant for the troposphere.

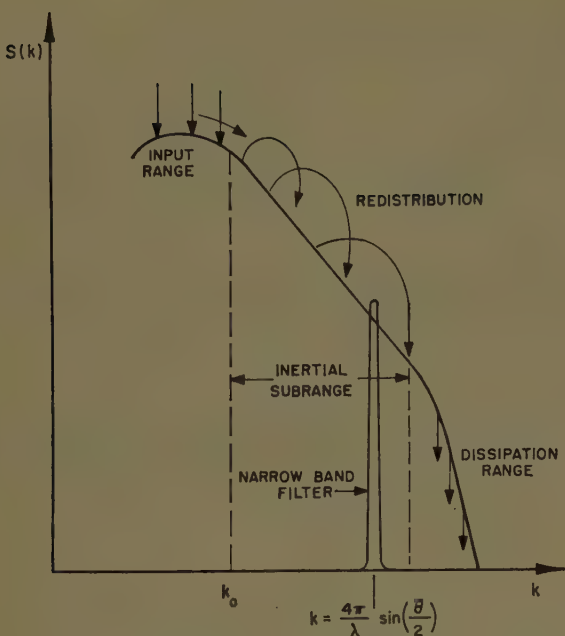


Fig. 1—Typical spectrum of dielectric irregularities, showing ranges and narrow band filter, which characterizes tropospheric scattering.

(k_0). Subsequent redistribution down the inertial range is attributed to turbulent convection, for which dimensional arguments give,⁶⁻⁸

$$S(k) = \langle \Delta \epsilon^2 \rangle \frac{k_0^{2/3}}{k^{11/3}}, \quad (k > k_0). \quad (7)$$

If the external source is identified only with the mixing of a gradient by the largest blobs,

$$\langle \Delta \epsilon^2 \rangle \cong k_0^{-2} \left(\frac{d \epsilon_0}{dh} \right)^2. \quad (8)$$

Mixing-in-Gradient Theory

In this approach, one considers an initial refractive index gradient and how it is changed by turbulent convection. As the turbulent eddies rotate, they transfer parcels of water vapor from low to high points on the profile, and vice versa. The mechanism for turbulent fluctuations appears explicitly in this theory, and no external source is required. The inertial range is again amenable to dimensional arguments,^{9,10}

$$S(k) \cong \left(\frac{d \epsilon_0}{dh} \right)^2 \frac{1}{k^5}, \quad (k > k_0). \quad (9)$$

⁶ A. M. Obukhov, "Structure of the temperature field in turbulent flow," *Izv. Akad. Nauk, SSSR, Ser. Geograf. Geofiz.*, vol. 13, pp. 58-69; 1949.

⁷ R. A. Silverman, "Turbulent mixing theory applied to radio scattering," *J. Appl. Phys.*, vol. 27, pp. 699-705; July, 1956.

⁸ R. Bolgiano, Jr., "Turbulent Mixing and Its Role in Radio Scattering," Cornell University, Ithaca, N. Y., E.E. Rep. No. 334; April, 1957.

⁹ F. Villars and V. F. Weisskopf, "On the scattering of radiowaves by turbulent fluctuations of the atmosphere," *PROC. IRE*, vol. 43, pp. 1232-1239; October, 1955.

¹⁰ A. D. Wheelon, "Spectrum of turbulent fluctuations produced by convective mixing of gradients," *Phys. Rev.*, vol. 105, pp. 1706-1710; March 15, 1957.

Both of these theories predict that the intensity of turbulent fluctuations is proportional to the gradient of the inhomogeneous mean profile. A very good correlation between the strength of scatter signals and refractive gradient has been observed experimentally on many paths.¹¹ Since strong scattered signals are associated with large dielectric fluctuations, this must be considered an important success for both mixing theories. They are compared in the next section as to their frequency and distance dependence predictions.

III. ELECTROMAGNETIC SCATTERING BY TURBULENCE

In deriving the wave equation from Maxwell's equations for an inhomogeneous medium, the electric vector is found to satisfy¹²

$$\nabla^2 \mathbf{E} - \frac{1}{c^2} \frac{\partial^2}{\partial t^2} (\epsilon \mathbf{E}) = -\nabla \left[\frac{1}{\epsilon} \mathbf{E} \cdot \nabla \epsilon \right]. \quad (10)$$

For radio propagation through the atmosphere several approximations are possible. Time derivatives operate principally on \mathbf{E} , since the field oscillates much more rapidly than the medium. The right-hand side of (10) is neglected because its contribution to the first-order scattered field is strictly zero.¹³ Thus with a harmonic time dependence ($k = \omega/c = 2\pi/\lambda$), (10) reduces to

$$[\nabla^2 + k^2(\epsilon_0 + \Delta\epsilon)] \mathbf{E} = 0. \quad (11)$$

The Born approximation is widely used as a solution of (11) and gives the total field in terms of the unperturbed wave $\mathbf{E}_0(r)$ as

$$\mathbf{E}(R) = \mathbf{E}_0(R) - \frac{k^2}{4\pi} \int_V d^3r \frac{\exp -ik \cdot |\mathbf{R} - \mathbf{r}|}{|\mathbf{R} - \mathbf{r}|} \Delta\epsilon(r, t) \mathbf{E}_0(r), \quad (12)$$

where V is the common volume of irregularities, which are both illuminated by $\mathbf{E}_0(r)$ and visible to the receiver (R). The geometry for propagation beyond the horizon, shown in Fig. 2, indicates that the radiated wave $\mathbf{E}_0(r) = \mathbf{E}_0 \exp ik_1 \cdot \mathbf{r}$ cannot reach the receiver because of earth-screening, so that the first term is dropped. Since the receiver is always many wavelengths from the scattering blobs, the far-field approximation is used,

$$\frac{\mathbf{E}_s(R)}{\mathbf{E}_0} \cong \frac{e^{-ikR}}{4\pi R} k^2 \int_V d^3r \Delta\epsilon(r, t) \exp (i\mathbf{K} \cdot \mathbf{r}) \quad (13)$$

where $\mathbf{K} = \mathbf{k}_1 - \mathbf{k}_2$ is the scattering difference vector. The magnitude,

$$|\mathbf{K}| = \frac{4\pi}{\lambda} \sin \frac{\theta}{2}, \quad (14)$$

¹¹ B. R. Bean and F. M. Meaney, "Some applications of the monthly median refractivity gradient in tropospheric propagations," *Proc. IRE*, vol. 43, pp. 1419-1431; October, 1955.

¹² A. D. Wheelon, "Near-field corrections to line-of-sight propagation," *Proc. IRE*, vol. 43, pp. 1459-1466; October, 1955.

¹³ M. Balser, "Some observations on scattering by turbulent inhomogeneities," *IRE TRANS. ON ANTENNAS AND PROPAGATION*, vol. AP-5, pp. 383-390; October, 1957.

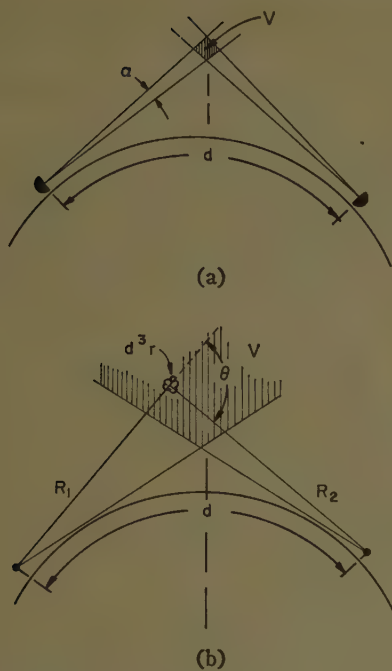


Fig. 2—Geometry for scatter-propagation calculations.
(a) Narrow beams, (b) broad beams.

depends jointly on the wavelength of the radiation and the angle θ through which the scattering proceeds (see Fig. 2).

The scattering cross section $\sigma(\theta, \lambda)$ per unit volume, per unit solid angle, and per unit incident power characterizes the scattering process for each blob,

$$\sigma = \frac{R^2}{V} \left\langle \left| \frac{E_s(R)}{E_0} \right|^2 \right\rangle. \quad (15)$$

When this is combined with (13) and (4), one is able to express the cross section directly in terms of the spectrum,¹⁴

$$\sigma(\theta, \lambda) = \frac{\pi^2}{\lambda^4} S \left[\frac{4\pi}{\lambda} \sin \frac{\theta}{2} \right]. \quad (16)$$

The scattering process acts like a narrow-band filter on the spectrum shown in Fig. 1, emphasizing the wave number $k = |\mathbf{K}|$ [see (14)]. Experimental combinations of λ and θ focus attention on the inertial range of $S(k)$. The angular dependence of σ is often interpreted as the scattering polar diagram of an average blob. Reference to Table I shows that almost all of the scattered radiation is projected into a cone of angular opening λ/l_0 about the forward direction.

It has been suggested by Feshbach¹⁵ that multiple-scattering is more efficient than one large-angle scattering. Such effects are certainly more important at higher frequencies, since the convergence of the Born series

¹⁴ Also

$$\sigma = \frac{\pi^2}{\lambda^4} \int_V d^3r \langle \Delta \epsilon^2 \rangle C(R) \exp i\mathbf{K} \cdot \mathbf{R}.$$

¹⁵ H. Feshbach, private communication.

is related to the smallness of the equivalent line-of-sight mean square phase shift

$$\langle a^2 \rangle = \pi^2 \langle \Delta \epsilon^2 \rangle Ll_0 / \lambda^2,$$

computed along the ray path. It is hoped that further research will be directed to this interesting point.

IV. FREQUENCY AND DISTANCE DEPENDENCE

The ratio of received-to-transmitted power depends upon the integral of the scattering cross section over the common volume V defined by the aerial patterns and/or earth-screening. If G_1 and G_2 are antenna gains appropriate to beams which meet at the scattering point d^3r ,

$$\frac{P_R}{P_T} = \frac{\lambda^2}{16\pi^2} \int_V d^3r \frac{2G_1 G_2 \sigma(\theta, \lambda)}{R_1^2 R_2^2}, \quad (17)$$

where R_1 and R_2 are identified in Fig. 2. The factors of two represent the ideal smooth earth ground reflection factors and are only approximately correct. If the beams are so narrow that the scattering angle (and hence the cross section) is substantially constant over the common volume, the integration can be collapsed,

$$\frac{P_R}{P_T} = \frac{2G_1}{4\pi[d/2]^2} \sigma V \frac{\lambda^2 G_2}{4\pi[d/2]^2}. \quad (18)$$

The scattering volume is set by the antenna beam-widths (α) and transmission distance (d): $V \approx 2(\alpha d/4)^3/\theta$ where $\theta \approx d/a$. The mixing-in-gradient model (9) can be combined with this expression to predict

$$\frac{P_R}{P_T} \approx \left(\frac{d\epsilon_0}{dh} \right)^2 \alpha^3 \lambda^3 \frac{a^6}{d^4}. \quad (19)$$

Such results are quickly established for other spectral models, and it would be well to compare their predictions with the considerable body of narrow beam data obtained by the M.I.T. Lincoln Laboratory.

The majority of broad-beam data is expressed with respect to the free space power which would be received over a line-of-sight path of the same length,¹⁶

$$\frac{P_R}{P_{FS}} = \frac{4\pi^2 d^2}{\lambda^4} \int_V d^3r \frac{S \left[\frac{4\pi}{\lambda} \sin \theta/2 \right]}{R_1^2 R_2^2}. \quad (20)$$

The average patterns of the broad antennas are removed here to cancel the total gains. It is this integral which has occupied the time and efforts of so many workers. The problem is partially one of finding a judicious coordinate system in which to do the integrations over the common volume, as limited by earth-screening. The NBS group¹⁷ found such a system and made numerous calculations with the exponential correlation model.

$$\text{Note: } \frac{P_{FS}}{P_T} = \frac{G_1}{4\pi d^2} \frac{\lambda^2 G_2}{4\pi}.$$

¹⁶ J. W. Herbstreit, K. A. Norton, P. L. Rice, and G. E. Schafer, "Radio scattering in tropospheric propagation," 1953 IRE CONVENTION RECORD, pt. 2, pp. 85-93.

Waterman¹⁸ has recently shown that (almost) any spectral model can be integrated exactly in this same coordinate system. Staras¹ developed a rectangular system to perform the same integrations in an approximate manner; his system has the advantage of recognizing the height-dependence of $\langle \Delta\epsilon^2 \rangle$ in a simple way and in being able to evaluate the space correlation and height gain functions.

In performing the volume integrations, one must eventually recognize a sizeable number of refinements to the spherical earth model. The influence of irregular terrain in modifying the takeoff angles led Norton, *et al.*,¹⁹ to the concept of (effective) angular distance. Refraction of the upgoing and scattered beams by tropospheric refraction has been described¹⁹ so far by the usual 4/3 earth modifications of the spherical earth results. Bean²⁰ considered the influence of atmospheric absorption on the same beams and predicted the radio frequency and distance dependence, as well as the expected correlation with meteorological conditions. The question of scattering by diffracted waves in the shadow region (below the common volume) has been studied by Arons²¹ who finds that the contributions are very small indeed. The inclusion of ground reflection factors and the inefficiency of ordinary height-gain relations is only partially complete. Anisotropic corrections to the scattering also may need to be included.^{1,2}

Insofar as the inertial range alone is of importance to the integrations in (20), one may expect the frequency and distance dependence to split apart. The mixing-in-gradient model (9) predicts a linear wavelength dependence,^{9,10} which has been deduced experimentally by careful analysis of numerous broad-beam experiments.^{20,22} It would appear that the $\lambda^{-1/3}$ dependence predicted by the Obukhov model (8) is not consistent with present radio data. The distance dependence of (20) depends upon careful integration of the spectrum's angular dependence over the common volume. The NBS group¹⁷ first pointed out the need for assuming the intensity decreases with height in order to supply the additional inverse powers of distance required to reach agreement with experiment. The mixing-in-gradient model has no adjustable turbulence constants to influence this distance dependence, but does depend on the mean profile $\epsilon_0(h)$. Estimations of this integral up to stratospheric heights using an exponential variation of

¹⁸ A. T. Waterman, "Radio Power Received via Tropospheric Scattering," Standard University, Stanford, Calif., Tech. Rep. No. 461-1; July, 1955.

¹⁹ K. A. Norton, P. L. Rice, and L. E. Vogler, "The use of angular distance in estimating transmission loss and fading range for propagation through a turbulent atmosphere over irregular terrain," Proc. IRE, vol. 43, pp. 1488-1526; October, 1955.

²⁰ B. R. Bean, "Some meteorological effects on scattered radio-waves," IRE TRANS. ON COMMUNICATIONS SYSTEMS, vol. CS-4, pp. 32-38; March, 1956.

²¹ L. D. Arons, "An Analysis of Radio-Wave Scattering in the Diffraction Region," Cornell University, Ithaca, N. Y., E.E. Rep. No. 312; October, 1956.

²² K. A. Norton, "Point-to-point radio relaying via the scatter mode of tropospheric propagation," IRE TRANS. ON COMMUNICATIONS SYSTEMS, vol. CS-4, pp. 39-49; March, 1956.

$d\epsilon_0/dh$ predict the range dependence of scattered fields quite well out to 700 miles.²³

V. STATISTICAL PROPERTIES OF THE FADING ENVELOPE

The envelope of radio-frequency signals received beyond the horizon is found experimentally to be a random function of time and is Rayleigh-distributed. This is successfully explained by noting that both the real and imaginary parts of the scattered wave in (10) are Gaussian-distributed, if $\Delta\epsilon$ is itself a Gaussian normal random process. The magnitude of the vector sum of two such components with equal variances is known to be Rayleigh-distributed.^{24,25} A more general proof which does not rely on the Born approximation applies the Central Limit Theorem to the independent scattering contributions by many blobs in the scattering volume.²⁶

Time variations of the signal envelope are physically related to the random addition of Doppler-shifted waves received from different elements of the scattering volume. The drift (U) and random (V_0) velocities of the eddies impose these frequency shifts on the scattered waves. The basic problem is to predict the radio-frequency and scattering-angle dependence of this fading, and the average rate of fading is taken as a convenient measure of the time-varying envelope. Early studies of this problem^{27,28} considered only the rms sum of these velocities as the effective speed.

$$N \cong \frac{f}{c} \left\{ \left[2U \sin\left(\frac{\bar{\theta}}{2}\right) \right]^2 + \frac{1}{3} V_0^2 \right\}^{1/2}, \quad (21)$$

$\bar{\theta}$ is the average scattering angle in the common volume.

A considerable advance was made recently in analyzing this fading phenomenon by using the spectral representation of the turbulent dielectric fluctuations.²⁶ An explicit separation of drift and random velocity contribution to the space-time correlation of $\Delta\epsilon$ is given by (6). Narrow-beam transmission is simplest to analyze, for the scattering angle is then substantially constant over the scattering volume. Since the scattered field is proportional to the Fourier transform of $\Delta\epsilon(r, t)$, the time correlation of the field²⁹ becomes

²³ H. G. Booker and W. E. Gordon, "The role of stratospheric scattering in radio communication," Proc. IRE, vol. 45, pp. 1223-1227; September, 1957.

²⁴ J. L. Lawson and G. E. Uhlenbeck, "Threshold Signals," M.I.T. Rad. Lab. Ser., McGraw-Hill Book Co., Inc., New York, N. Y., vol. 24, p. 62; 1950.

²⁵ R. A. Silverman and M. Balser, "Statistics of electromagnetic radiation scattered by a turbulent medium," Phys. Rev., vol. 96, pp. 560-563; November 1, 1954.

²⁶ R. A. Silverman, "Some remarks on scattering from eddies," Proc. IRE, vol. 43, pp. 1253-1254; October, 1955.

²⁷ W. E. Gordon, "Radio scattering in the troposphere," Proc. IRE, vol. 43, pp. 23-38; January, 1955.

²⁸ S. O. Rice, "Statistical fluctuations of radio field strength far beyond the horizon," Proc. IRE, vol. 41, pp. 274-281; February, 1953.

²⁹ The envelope (linearly detected) correlation is related to the amplitude correlation by the standard result (see Lawson and Uhlenbeck, *op. cit.*)

$$A(t) = \frac{\langle |E_s(t)| \cdot |E_s(t+\tau)| \rangle}{\langle |E_s|^2 \rangle} \cong \frac{\pi}{2} \left(1 + \frac{1}{4} \rho^2(\tau) + \frac{1}{64} \rho^4(\tau) \dots \right).$$

$$\rho(\tau) = \frac{\langle E_s(t) E_s^*(t + \tau) \rangle}{\langle E_s(t) E_s^*(t) \rangle} \\ = \exp(i\mathbf{K} \cdot \mathbf{U}\tau) C[V_0 k_0^{1/3} \mathbf{K}^{2/3} \tau], \quad (22)$$

where \mathbf{K} is the scattering difference vector defined earlier. For symmetrical scattering, \mathbf{K} points upward and only the vertical component of the mean wind contributes to Doppler fading. The self-motion influences the fading rate most strongly if U_s is small,

$$\therefore N \cong \frac{1}{\pi} \sqrt{-\frac{d^2 \rho}{d\tau^2}} \Big|_{\tau=0} \\ = \frac{V_0 k_0^{1/3}}{\pi} \ddot{C}(0) \cdot \left\{ 2 \frac{f}{c} \sin \frac{\bar{\theta}}{2} \right\}^{2/3}, \quad (23)$$

where N is the average rate of mean crossings. The fading rate due to self-motion is proportional to $f^{2/3}$, while drift motion gives the usual Doppler linear dependence on frequency. Available data indicate a variable frequency exponent less than one,³⁰ so that some mixture of the two effects is indicated. The problem should be reconsidered by integrating the above result (22) over the large scattering volumes appropriate to the present broad-beam data.

In addition to the fast fading described above, there is a long term variability of the mean signal level which is sometimes called "slow fading." This variability is presumably caused by gross changes in meteorological conditions. There is a reasonable correlation between monthly mean signal levels and averaged meteorological measurements;¹¹ but day-by-day or (especially) hour-by-hour correlations have not been established. The prominent characteristics of this slow fading are: 1) average signal levels are 10 db higher in summer than in winter, and 2) longer scatter paths exhibit less variability over a given year than short paths, since the corresponding scatter heights are greater and there is less meteorological variability at the higher altitudes.

VI. SPACE CORRELATION OF THE FIELD

A combination of two or more spaced receivers is frequently exploited to overcome signal loss during deep fades. This diversity reception depends upon spacing the antennas sufficiently far apart to insure independent fading of the two signals. Staras³¹ has solved the statistical problem of estimating the percentage of time that the greater of the two signals is below a specified level as a function of the correlation between the two fields.

The propagation problem is to estimate this space correlation. Gordon²⁷ and Rice²⁸ presented qualitative analyses which showed that correlation distances normal to the propagation path (horizontal and vertical)

ought to be of the order $\lambda a/d$, where d is the transmission distance and a the radius of the earth. The correlation distance $\lambda a^2/d^2$ along the path was also deduced. Precise calculations of all three correlations as functions of the separation were presented by Staras,¹ using the exponential correlation model and an h^{-2} dependence for the intensity of turbulence. The integrations were carried out for the entire common volume, so as to make contact with the broad-beam data. To reach agreement with this data, he found it necessary to recognize the anisotropic nature of the scattering blobs (3) and deduced a vertical-to-horizontal scale length ratio of approximately one third. Such experiments are important in that they bear directly on the question of anisotropy and more data are needed. It would be valuable to repeat such calculations for the two mixing models, to see what effect the spectrum has on the predictions.

The realization of plane-earth height-gain advantage is limited by space coherence between the actual receiver and its image. The usual height-gain curve is measured at heights less than one-half the vertical correlation distance ($\lambda a/2d$). Above this height, one gains only slight improvement by the gradual decrease of the scattering angle. Detailed calculations of this effect (with differing approximations) have been presented by Staras¹ and the NBS group.^{19,22,32} Agreement between theory and experiment on this point is probably acceptable.

VII. GAIN LOSS AND BEAM SWINGING

When very narrow beams are used on scatter circuits, it is found that free-space antenna gains are not realized. This has come to be known as gain loss or antenna-to-medium coupling loss. The coupling loss phenomenon arises from the fact that signals arrive at the receiver from an extended scattering volume V . Narrowing the antenna beam (α) eventually reduces this common volume faster than the antenna gain is increased (18) so that a relative gain loss is incurred.

This problem was first qualitatively analyzed by Booker and de Bettencourt,³³ and later generalized by Norton, Rice, and Vogler¹² and by Staras³⁴ to include nonsymmetrical antenna patterns and dissimilar antenna sizes. Staras evaluated the effect of anisotropic irregularities on the coupling loss. It would appear that the refined estimates of Norton, *et al.*¹⁹ and Staras³⁴ are in somewhat better agreement with the experimental data.

Booker and de Bettencourt³³ also considered the effect of swinging the transmitting and receiving antennas

³⁰ K. A. Norton, P. L. Rice, H. B. Janes, and A. P. Barsis, "The rate of fading in propagation through a turbulent atmosphere," *PROC. IRE*, vol. 43, pp. 1341-1353; October, 1955.

³¹ H. Staras, "Diversity reception with correlated signals," *J. Appl. Phys.*, vol. 27, pp. 93-94; January, 1956.

³² A. P. Barsis, J. W. Herbstreit, and K. O. Hornberg, "Cheyenne Mountain Tropospheric Propagation Experiments," *Natl. Bur. of Standards, Boulder, Colo., NBS Circ. No. 554*; January, 1955.

³³ H. G. Booker and J. T. de Bettencourt, "Theory of radio transmission by tropospheric scattering using very narrow beams," *PROC. IRE*, vol. 43, pp. 281-290; March, 1955.

³⁴ H. Staras, "Antenna-to-medium coupling loss," *IRE TRANS. ON ANTENNAS AND PROPAGATION*, vol. AP-5, pp. 228-231; April, 1957.

simultaneously in azimuth and elevation. In either case, the net effect is to increase the scattering angle and therefore to decrease the received power. They used the exponential correlation model to make estimates of this reduction which are apparently in good agreement with available data.

VIII. BANDWIDTH LIMITATIONS

The signal frequency bandwidth which the scatter medium can support without serious distortion is intimately related to the multipath delays which are experienced. These depend on the size of the effective scatter volume, which is determined by the antenna beamwidths and/or the scattering pattern of the blobs. When the antenna patterns are broad, the multipath is controlled by the scattering blobs and the approximate result

$$\Delta f = \frac{5ca^2}{d^3} \quad \alpha \gg \bar{\theta} \quad (24)$$

given by Gordon²⁷ shows that the bandwidth decreases rapidly with distance. Staras¹ computed the actual frequency correlation of signals at different frequencies for the anisotropic exponential correlation function. His results for the effective bandwidth are only one-eighth that predicted by Gordon; and this problem needs further resolution with experiment.

A real improvement in bandwidth capabilities is obtained with very narrow beams. Even though some antenna gain degradation is experienced with narrow beams, the angular distribution of multipath signals which are admitted to the receiver is reduced and the bandwidth thereby increased. Booker and de Betten-court²⁸ examined this problem for beams narrower than the average scattering angle $\theta = d/a$ and found

$$\Delta f = \frac{4ca}{ad^3} \quad \alpha \ll \bar{\theta}, \quad (25)$$

which increases steadily with antenna size and decreases with distance. When aircraft fly through the path, the solid bistatic reflections from them supply a multipath signal of unusual magnitude and the above estimates for broad antenna beams are meaningless.

The influence of medium bandwidth on transmission quality depends upon the instantaneous signal level in the band, and this in turn has given rise to the concept of an instantaneous bandwidth. It is not clear now whether the bandwidth limitation refers to the base band or RF band of an FM system, for instance, and considerably more work on modulation schemes is required. It is probable, however, that a double sideband modulation scheme is preferable to SSB because it automatically provides frequency diversity when synchronous detection is used.

IX. REFLECTION BY ELEVATED LAYERS

Layers are frequently observed in the troposphere as discontinuities in the vertical profile of refractive index measurements. It was suggested long ago that partial reflections from these layers might explain scatter propagation.²⁵ Friis, Crawford, and Hogg²⁶ have developed this idea in some detail using uncorrelated reflections from many layer patches in the common volume. These results depend on the size and number of layers, as well as the average refractive discontinuity across the sheets. The ratio P_E/P_{FS} (see Section IV) computed from this theory is proportional to the wavelength, in good agreement with experiment. Their predictions of beam swinging experiments and gain loss are also consistent with experiment. No explanation of fading phenomenon or bandwidth limitations has been given thus far, although it is probable that such effects can be accommodated by modulating the orientation of layers. The distinction between such layers and elongated blobs (*i.e.*, anisotropic irregularities) is not sufficiently clear.

Bauer²⁷ has studied the partial reflections from a single spherical layer above the earth. There is some question about his use of the Born approximation to represent coherent reflections by the layer. His experimental correlation of scatter signal strengths with the refractive change across elevated layers in the path is certainly interesting.

It is likely that such layers are the seat of intense irregularities, if one believes the mixing models (7) or (8). The presence of such irregularities at the point of partial reflection would provide the layer theories with an additional random component to explain fading. The problem may be looked at differently, however, by saying that turbulent blobs are probably created most strongly at layer discontinuities, so that the important scattering volume is near the layer. Gordon²⁷ has studied briefly the scattering by elevated turbulent layers.

X. NORMAL MODE THEORY

The explanation of radio propagation beyond line-of-sight in terms of coherent partial reflections from a bilinear refractive index profile has been pursued by Carroll and Ring.²⁸ Unfortunately, recent work on this theory is characterized more by strategems than new results. Two important predictions of normal mode

²⁵ K. A. Norton, "Advances in Electronics," Academic Press, New York, N. Y., vol. 1, pp. 381-423; 1948.

²⁶ H. T. Friis, A. B. Crawford, and D. C. Hogg, "A reflection theory for propagation beyond the horizon," *Bell Sys. Tech. J.*, vol. 36, pp. 627-644; May, 1957.

²⁷ J. R. Bauer, "The Suggested Role of Stratified Elevated Layers in Trans-horizon Shortwave Radio Propagation," Lincoln Lab., M.I.T., Lexington, Mass., Tech. Rep. No. 124; September 24, 1956.

²⁸ T. J. Carroll and R. M. Ring, "Propagation of short radio-waves in a normally stratified troposphere," *PROC. IRE*, vol. 43, pp. 1384-1390; October, 1955.

theory emerged from a symposium on this subject.³⁹ The received field strength: 1) varies exponentially with distance, and 2) is independent of radio frequency. The first prediction agrees best with experiments, since it is difficult to distinguish between an exponential variation and a large inverse power of the distance.

The discontinuity in the bilinear profile model of re-

³⁹ "Summary of normal mode theory symposium," IRE TRANS. ON ANTENNAS AND PROPAGATION, vol. AP-4, pp. 90-94; January, 1956.

fractive index is of continuing concern to Friedman and others.³⁹ Although coherent reflections from stable layers may contribute to the mean signal, normal mode theory offers no explanation of the following important features of scatter propagation: 1) fading envelope, 2) bandwidth limitations, 3) space correlations, and 4) antenna gain degradation effects. Unless these results can emerge from the series representation of the field employed, one must superimpose a statistical variation of the dielectric constant upon the Carroll model.

U.S.A. National Committee Report URSI Subcommission 6.3

Antennas and Waveguides, and Annotated Bibliography*

H. V. COTTONY†, R. S. ELLIOTT†, E. C. JORDAN§, V. H. RUMSEY||, K. M. SIEGEL¶, J. R. WAIT†, AND O. C. WOODYARD#

Summary—Recent developments in some of the more active areas of antenna and diffraction theory are summarized. Although concerned primarily with U.S.A. activity, some reference is made to the literature of other countries where closely allied work is in progress. Fields included in this survey are broad-band antennas, wide-angle microwave optics, antennas for ionospheric scatter propagation, traveling-wave antennas, slot radiators, diffraction, and scatter theory.

Recent work in broad-band antennas has been concerned mainly with trying to hold *both* radiation pattern and impedance independent of frequency. The problem has been approached successfully through development of that class of antenna shapes which depends on angles only. The equiangular spiral is a simple example.

In microwave optics the requirements for wide-angle scanning of antenna beams have been met largely by using new light-weight, low-loss dielectrics to construct suitable lenses such as a spherical Luneberg lens. Using the geodesic analog of the Luneberg lens in one plane a scan of 40 beamwidths without aberrations has been obtained.

The very high gain required for antennas suitable for VHF ionospheric scatter propagation has been obtained through use of long horizontal rhombics and, more recently, by corner reflector antennas driven by collinear arrays of dipoles. The latter antennas have the important advantage for this application of much lower sidelobe level.

Traveling-wave antennas have received much attention in recent years because of their inherent adaptability to flush-mounted ap-

plications. Among the forms considered are corrugated surfaces and single or double dielectric-clad surfaces. The launching problem has been studied rather intensively and recent interest has been shown in the synthesis and scanning aspects for slow-wave structures. Progress has continued in the exploitation of fast-wave systems, with major advances centering on the launching problem and the polarization problem. Strip lines are taking an important place as feeding systems for traveling-wave antennas.

Recent years have been marked by considerable research activity on flush-mounted microwave antennas. Such antennas often take the form of slots or apertures in the metallic surfaces of aircraft. The radiation pattern of the slot radiator depends upon the shape of the metallic surface in which it is cut, and for complicated shapes resort is made to experiment. However, certain simple geometric shapes have been treated mathematically. These shapes include the circular cylinder, half plane, wedge, sphere, elliptic cylinder, oblate and prolate spheroid, and cones. Various combinations of these shapes on which work also has been done are the semicircular boss on a flat ground plane, the cylindrically tipped wedge, and the spherically tipped cone.

The problem of radiation from apertures in a metallic surface is closely related to the reciprocal problem of calculating the currents excited on the surface by an incoming wave. As a direct consequence of the reciprocity theorem there is an intimate connection between slot radiators, diffraction, and scattering. The result is that the extensive body of knowledge classed as diffraction and scattering must be considered as an integral part of antenna theory. During the past three years there has been a very considerable effort in obtaining new exact solutions, several new approximate solutions, and a better physical understanding of the mechanisms involved in scattering. All of the geometric shapes mentioned above have received attention, and much experimental work has also been done. For the future it can be expected that this intensive effort will continue with emphasis on the asymptotic approaches of Kline and Keller, the method proposed by Logan, and Fock's method of obtaining asymptotic results based on local analysis.

* This material was prepared as an URSI Subcommission 6.3 contribution to the Twelfth General Assembly which was convened in Boulder, Colo., from August 22 to September 5, 1957.

† National Bureau of Standards, Boulder, Colo.

‡ Rantec Corp., Calabasas, Calif.

§ University of Illinois, Urbana, Ill.

|| University of California, Berkeley, Calif.

¶ University of Michigan, Ann Arbor, Mich.

U. S. Army Signal Engineering Lab., Fort Monmouth, N. J.

I. BROAD-BAND ANTENNAS

THE recent work on broad-band antennas has been mainly concerned with trying to hold the radiation pattern independent of frequency as well as the input impedance. The pattern problem is much more complex and more difficult than the impedance problem and consequently most of the effort has been put on the pattern problem. A successful approach has been developed by considering antenna shapes which depend on angles only [1]. The infinite biconical antenna is a familiar example. There is, however, a wide variety of these shapes which is represented by the formula $r = F(\theta)e^{a\phi}$ where r , θ , and ϕ are the usual spherical coordinates, a is a constant, and $F(\theta)$ an arbitrary function of θ . Thus the cross section of one of these surfaces on a cone $\theta = \text{constant}$ is given by $r = Ae^{a\theta}$ which is the polar equation for an equiangular spiral.

All such antennas extend to infinity. The key problem is therefore to determine whether the pattern of a finite portion of such an antenna converges to the pattern of the infinite structure as the frequency is increased. For the biconical antenna, which is represented by $a = \infty$, it is common experience that measured patterns show no sign of this convergence. Measurements have recently been made using shapes characterized by finite values of a and the remarkable result is that most of them show this convergence with practically no doubt. In effect, the current distribution remains constant with respect to wavelength and roughly concentrated in an aperture of the order of a wavelength in diameter (the effective aperture can be controlled to a useful degree by choice of the shape). Thus the pattern (and also the impedance) of such antennas is practically independent of frequency for all frequencies greater than a certain value.

Equally remarkable results have been obtained [2] with plane structures whose shape is defined by $\phi = \text{periodic function of } \ln \gamma$. Thus, if p is the period of $\ln \gamma$ the infinite antenna is essentially the same to any two wavelengths whose ratio is $\exp p$. Here there is the additional problem of choosing p small enough so that the variation over one period is insignificant. It turns out that this can be done quite easily in practice. For a wide range of such antenna shapes it has been found that the performance of the finite structure is practically independent of frequency above a certain point.

References

- [1] V. H. Rumsey, "Frequency independent antennas," 1957 IRE NATIONAL CONVENTION RECORD, pt. 1, pp. 114-118.
- [2] R. H. DuHamel and D. E. Isbell, "Broadband logarithmically periodic antenna structures," 1957 IRE NATIONAL CONVENTION RECORD, pt. 1, pp. 119-128.

WIDE ANGLE MICROWAVE OPTICS

Since the last session of URSI, requirements for wide angle scanning of antenna beams have given further impetus to the investigation of wide angle microwave optics.

Although most of the recent work has been with

lenses, some attention has also been given to improvement of the toroidal reflector. Along this line, it has been shown that the elliptical torus produces a more nearly plane phase front than does the parabolic torus and for very large apertures will produce a narrower beam.

In the field of microwave lenses, attention has been directed anew toward dielectric lenses. This has come about largely because of new developments in methods of producing light-weight, low-loss dielectric materials. Lenses have been designed for wide angle applications by designing an exact two-point corrected cylindrical lens and then rotating a section of the cylindrical lens about the axis of symmetry of the section. Although lenses designed in this way will, of course, exhibit astigmatism, experimental results have been quite good for scan angles of from 7 to 14 beamwidths (depending upon f/d ratios).

Improved techniques in dielectrics, mentioned above, have also made it possible to fabricate spherical Luneberg lenses applicable to most microwave frequencies. This has given new impetus to both experimental and theoretical study of this lens. In addition to consideration of the spherical dielectric lens, some activity has continued with the geodesic analog of the Luneberg lens in one plane. Using the geodesic analog, a completely operating radar scanner, scanning over almost 40 beamwidths without aberrations, was developed and described.

References

- [1] G. D. M. Peeler and D. H. Archer, "A toroidal microwave reflector," 1956 IRE CONVENTION RECORD, pt. 1, pp. 242-247.
- [2] F. S. Holt and A. Mayer, "A design procedure for dielectric microwave lenses of large aperture ratio and large scanning angle," IRE TRANS. ON ANTENNAS AND PROPAGATION, vol. AP-5, pp. 25-30; January, 1957.
- [3] R. L. Sternberg, "Elementary methods in the numerical design of microwave dielectric lenses," *J. Math. Phys.*, vol. 34, pp. 209-235; January, 1956.
- [4] R. M. Brown, "Dielectric bifocal lenses," 1956 IRE CONVENTION RECORD, pt. 1, pp. 180-187.
- [5] E. H. Braun, "Radiation characteristics of the spherical Luneberg lens," IRE TRANS. ON ANTENNAS AND PROPAGATION, vol. AP-4, pp. 132-138; April, 1956.
- [6] J. S. Hollis and M. W. Long, "A Luneberg lens scanning system," IRE TRANS. ON ANTENNAS AND PROPAGATION, vol. 5, pp. 21-25; January, 1957.

ANTENNAS FOR VHF IONOSPHERIC SCATTER COMMUNICATION

An important characteristic of propagation via ionospheric scatter is the relatively high loss sustained upon reflection from the ionospheric layers. Depending on the frequency and the length of the path, it may range from 70 to over 100 decibels above the free space loss. For this reason it is necessary to employ high transmitter powers and high-gain antennas for both the transmission and reception. The first antennas employed for this application were horizontal rhombic antennas employing very long, 25 to 50-wavelength, leg lengths. These are still useful, particularly for experimental purposes. They are likewise employed in some operational communication paths. Because of certain drawbacks, such as the large area occupied by the antenna, the relatively high level

of side and back radiation, and other disadvantages, there has been a trend to replace the rhombic antennas by more compact structures having a much lower level of secondary lobe radiation. Corner-reflector antennas driven by collinear arrays of dipoles have been installed at many terminals. The majority of existing corner-reflector antennas have the dimensions of five wavelengths in width, three wavelength vertical aperture, and employ a sixty-degree aperture angle. The driven element consists of eight or more half-wave dipoles.

Because of the current high sun-spot phase of the solar cycle, the most troublesome problem of the present operation is that caused by multipath propagation. The current emphasis in the design of the antennas for VHF scatter communication continues, therefore, to be in the design of low secondary radiation antennas.

A requirement which is likely to be incorporated in future VHF ionospheric scatter antennas is that it be possible to slew the main beam of the antenna to either side of the great circle path by an angle of ten to twenty degrees. This is made desirable because evidence exists that the meteoric contribution to scattered signal may be of considerable significance. The direction of arrival of the meteors varies with time of day and the optimum orientation of antenna varies accordingly.

SLOT RADIATORS¹

Research on flush-mounted microwave antennas has been extremely active in the last three or four years. In most cases, the forms of these radiators are slots or narrow rectangular shaped apertures cut in metal surfaces of aircraft fuselages, wings, or stabilizers. The radiation pattern of the antenna is very much dependent on the particular shape of the surface on which it is mounted. For this reason, recourse is often made to experiment on actual aircraft or by means of models. For a more recondite approach, the body is represented by some simple geometric shape which is amenable to rigorous mathematical treatment. The usual geometric forms, listed more or less in order of increasing complexity, are: the circular cylinder, half-plane, wedge, sphere, elliptic cylinder, oblate and prolate spheroid, and cones. Various combinations of these are also possible, such as the semicircular boss on a flat ground plane, the cylindrically-tipped wedge and the spherically-tipped cone. While none of these shapes duplicate the form of modern aircraft or missiles, they do provide a model for studying the influence of such factors as the extent and curvature of the surfaces on which the slots are cut. Furthermore, the effect of sharp edges of the surfaces can be estimated from a study of the field configurations in the vicinity of the edge of the wedge or the tip of the cone.

It is the purpose of this review to summarize some of the recent basic work in this field. It should be empha-

sized at the outset that the radiation from slots and apertures on a metallic surface is closely related to the reciprocal problem of calculating currents excited on the body by an incoming plane wave [1]. There is an intimate connection between diffraction and scattering which, of course, is a consequence of the reciprocity theorem [2]. Therefore, any literature survey of slot antennas should include papers on the aspects of diffraction theory which have a significance in the reciprocal sense.

Due to its simplicity, the circular cylinder has been the favored model. The first approach is to represent the field in terms of a Fourier series of the form

$$\sum_{m=0}^{\infty} A_m \cos m\phi$$

where ϕ is the azimuthal angle, A_m is a coefficient, and m takes all integral values. A_m is a function of the circumference of the cylinder in wavelengths (i.e., $ka = 2\pi a/\lambda$) and is determined in a straightforward manner when the field distribution over the slot is prescribed. This was the approach used by Silver and Saunders [3] to obtain an exact expression for the fields exterior to a circular cylinder of infinite length for a specified distribution of tangential voltage on the cylinder. By using a saddle point technique, the infinite integral in the solution could be reduced when the observer is in the far field. Extensive numerical results and patterns for circumferential half-wave slots for $ka = 2, 3$, and 5 and various elevation angles have been presented by Wait and Kahana [4]. In this case the field is, in general, plane polarized in the principal planes but elliptically polarized for other directions. Similar numerical results for both axial and circumferential slots on large cylinders have been given by Bailin [5] for $ka = 8$ and 12, and Wait and others for a range of ka up to 21 [6], [7].

The patterns of single and pairs of circumferential slots on circular cylinders have been measured at S band by Keys [8] in a parallel plate region and they compare favorably to the calculated data [7]. Patterns of stub antennas on slots on cylinders have been measured directly by Bain [9] using an antenna range and they compare very favorably with calculated patterns for ka ranging from about 3 to 21 [10].

In most of the above-mentioned work the harmonic series representation of the field is employed. This series, which involves integral order Bessel functions, becomes very poorly convergent when ka is large compared to one. Usually, something of the order of 2 ka terms is required to secure 2 per cent accuracy. Extending the classical method of G. N. Watson, this slowly converging harmonic series is converted into a contour integral which can, in turn, after a deformation of the path of integration, be expressed as a new series. Individual terms are the residues of the poles encircled by the deformed contour. For this reason, such a representation is called the "residue series." This technique has

¹ Much of the material in this section is included in a forthcoming book where it has been brought up to date. J. R. Wait, "Electromagnetic Radiation from Cylindrical Structures," Pergamon Press, London, Eng.; 1959.

been applied to the slotted cylinder problem by Sensiper [11], and others [7], [12]. A very similar approach to the reciprocal problem of diffraction by a cylinder has been outlined by Franz [13], [14] and Imai [15]. Sometimes these residue terms are called creeping waves [16] as they have the characteristics of waves that creep around the cylinder with an exponential attenuation.

The residue series representation for the pattern of a slotted cylinder antenna is highly convergent in the direction away from the slot (*i.e.*, deep in the shadow). On the other hand, the field in the forward direction (*i.e.*, the illuminated region) can be obtained by geometrical optics [17]. Difficulty occurs in the transition region near the classical light-shadow boundary. Some slight improvement can be made by considering higher order geometrical-optics terms [12]. It can be shown from the harmonic series representation, however, that the field along this boundary is almost independent of ka , and hence a calculated point on the "light-shadow" boundary is always available [6]. It is then possible to interpolate between the geometrical-optics and the residue series representation. The nature of the field in this transition region has been studied experimentally at Harvard [18] by an examination of the currents excited on a circular cylinder by an incident plane wave. They obtained surprisingly good agreement with the approximate theory of Fock [19].

The mutual impedance of the slots on circular cylinders is fundamentally more difficult to compute than the patterns, because the saddle point technique of integration cannot be utilized. However, if the slots are axial and infinite in length, it is possible to compute the coupling between these by either a harmonic series [20] or a residue series representation [21]. Also, it is possible to obtain the radiation conductance of finite slots on a cylinder by a Poynting vector integration of the far field [22]–[34]. A mathematical justification for this procedure has been presented by Northover [25]. The general mutual impedance between slots of finite length on a circular cylinder, however, has yet to be expressed in a form suitable for computation.

A general analysis has been carried out for an arbitrary slot on an elliptic cylinder [26]. Extensive numerical results were carried out for the limiting case [27] when the minor axis is zero (*i.e.*, a ribbon). The current distribution on the ribbon has been evaluated for a range of widths [28]. Patterns and conductances for infinitesimal slots on elliptic cylinders with a finite minor axis have been published by Wong [24], [29].

The methods for treating slots on spheres are very similar to the corresponding cylinder problems. Using a harmonic series representation, the patterns of zonal slots with uniform excitation have been calculated by Karr [30] for various polar locations of the annular slot. When the slot has a nonuniform excitation, the formalism becomes more complicated since there is no longer azimuthal symmetry [31]. Numerical results for this case are also available for a moderate range of ka values

[32], [33]. The application of the residue series technique to the calculation of the principal plane patterns of finite slots on a sphere for large values of ka has been reported [34] and fairly good agreement was obtained with the experimental results of Cohn [35] and Bain [9]. Very recently a general analysis has been presented by Mushiake and Webster [32] for the fields produced by arbitrary slots on a sphere in terms of the harmonic series representation. They presented radiation patterns for half-wave slots in the principal planes and numerical data for the power gain.

The mutual impedance between slots on a sphere has been recently calculated by using a residue-series representation which is usable if the angular separation between the slots is not small. A new series representation [36] was developed for the case of small angular separations (*i.e.*, small curvature). The first term of this series corresponded to the mutual impedance of the slots on a flat surface and succeeding terms contain inverse powers of ka .

The radiation from slots on wedges has received considerable attention. A general analysis was presented for an arbitrary slot on a cylindrically-tipped wedge of any angle [37]. Using this as a basis, numerical results have been presented for the patterns of slots parallel to the edge of a half-plane (*i.e.*, a wedge angle of 2π), and a right-angled wedge [38], [27]. A similar treatment for radiating apertures on half-planes has been given by Tai [39] in an elegant analysis. Particular attention has been given to the case when the slot is perpendicular to and at the edge of the half-plane [27]. This has been called a "notch" and it has some interesting radiation properties. The conductances of half-wave slots on circular cylinders, elliptic cylinders, wedges, and half-planes have been compared to illustrate the influence of edges and curvature [40]. The more recent work on slots on wedges is concerned with developing asymptotic representations which are more suitable for calculations when the distance of the slot to the edge of the wedge is large compared to a wavelength. Schensted and Maffett [41] have shown that the geometric-optics terms can be separated out of the general solution and this step provides a new insight to the wedge problem. The difficulties associated with the asymptotic series in the transition between the illuminated and the shadow region have been overcome by Felsen [42] who applied the recent work of Oberhettinger [43], [44].

A very promising model for the treatment of radiation from slots on finite bodies of nonspherical shape is the prolate or oblate spheroid. The limiting case of the oblate spheroid of vanishing thickness (*i.e.*, a disk) has been treated in detail by Flammer [45] for an arbitrary dipolar source. His formulas, when specialized to the case of a magnetic dipole tangential to and on the surface of the disk, are directly applicable to the radiation from a slot on a circular disk. Unfortunately, numerical results for slots on spheroids are only available for the somewhat simpler cases of azimuthal symmetry [46].

with uniform excitation of annular slots on oblate spheroids and prolate spheroids [47]. With the recent publication of comprehensive tables of coefficients relating to spheroidal functions [48], [49], it is expected that the formal results of Flammer for the nonsymmetrical case of an arbitrary slot on a thin oblate spheroid could be used to obtain patterns. A solution for an arbitrary slot on the general spheroid (*i.e.*, other than a disk or a sphere) does not seem to be available. It would appear that the results of Schultz [50] for the plane wave scattering of spheroid could be extended without too much trouble. Certainly, numerical results based on such a solution would be most valuable.

The very complicated problem of slots on cones has been approached in a formal way by Bailin and Silver [51]. The solution involves Legendre functions and Bessel functions of fractional order. Numerical work based on their solution is very difficult although it is justified if information concerning the effect of the cone tip on the radiation characteristics of the slot is needed. An interesting comparison of Bailin's and Silver's results using a geometrical-optics approach has been made by Siegel, *et al.* [17]. The various, but equivalent, representations for the field of slots on cones have been discussed in detail by Felsen [52]. This latter work should pave the way for any future numerical work on the cone problem.

Most of the above-mentioned investigations can be classified as exterior boundary value problems. That is, the distribution of the field over the slot is assumed without regard to the nature of the feed system. For electrically small slots or apertures, the actual distribution does not influence the exterior fields. Furthermore, even for half-wave slots the assumed sinusoidal distribution is very good if the slot width is small compared to the slot length. However, in general, the interior region cannot be considered separately from the exterior region since both of these determine the distribution of field over the slot. The work of Stevenson [53] in this connection is now classical. He treated the problem of matching the modes inside a rectangular waveguide through narrow resonant slots in the side walls to the region external to the guide. Recently, Oliner [54] has made some very significant extensions and he has developed formulas for the equivalent circuit of both resonant and nonresonant slots in the broad face of a rectangular guide of finite wall thickness. His experimental results show exceptionally good agreement with the theory. Some further experimental data for inclined and transverse slots in the narrow and broad walls of a waveguide have been reported recently [55], [56].

In the theoretical work of both Stevenson and Oliner, the external region was assumed to be a half space corresponding to an infinite baffle flush with the broad wall of the slotted guide. The modification of Stevenson's formulas for resonant slots due to the finite extent and curvature of the baffle has been discussed by Wait [6], [40]. Extensive work concerning the analysis of slots

in multimode waveguides has been carried out at Berkeley [57]–[59].

The effects associated with covering the slots with a dielectric coating such as fabric has been given some attention [6], [38], [60]. A general solution is now available for the field of an arbitrary slot on a circular metallic cylinder with a concentric dielectric coating [61]. Some numerical results have been obtained for ka values up to 8 for various dielectric constants and thicknesses of the coating [61].

The pattern calculation for arrays of slots is usually a straightforward manner. The technique is based on the principle of superposition [6], [62] wherein the total field of N slots is obtained by a complex addition. For this reason, the relative phase, as well as the amplitude of the radiated field of a single slot, is of interest. In certain beacon applications the voltage induced on pairs of slots on cylinders may be rectified before addition to obtain omnidirectional coverage [63]. Some special problems associated with long arrays of slots have been discussed [64], [66]. The radiation from large slots [67] and U shaped slots [68] and crossed slots [69] has also been considered.

The field of slots on convex cylindrical surfaces whose curvature is slowly changing could be investigated by adapting Keller's geometrical theory of diffraction [70]. In his recent work on the diffraction by a convex cylinder [71], a method is proposed for evaluating the surface currents excited by an incoming plane or cylindrical wave. The reciprocity theorem, properly applied, should yield the pattern of a slot on such a convex surface. The generalization of Keller's [71] treatment of the convex cylinder and Fock's [19] solution for the parabolic cylinder in the penumbral region has been carried out by Logan [72]. He indicates that with a table of two auxiliary functions, the patterns of slots on circular and elliptic cylinders, oblate and prolate spheroids, and other smooth curved surfaces can be readily computed to sufficient accuracy for engineering purposes. This work of Logan constitutes a major contribution to the field.

The foregoing survey is intended to provide an overall, though brief, view of the recent work on slot antennas. It is hoped that the bibliography will be a guide for others working in this field and prevent duplication in effort.

References

- [1] G. Sinclair, "The pattern of slotted-cylinder antennas," *PROC. IRE*, vol. 36, pp. 1487–1492; December, 1948.
- [2] K. M. Siegel and A. L. Maffett, "Relation of scattering problems to radiation from simple shapes," presented at WESCON, Los Angeles, Calif.; August, 1956.
- [3] S. Silver and W. K. Saunders, "The external field produced by a slot on an infinite circular cylinder," *J. Appl. Phys.*, vol. 21, pp. 153–158; February, 1950.
- [4] J. R. Wait and S. H. Kahana, "Calculated patterns of circumferential slots on a circular conducting cylinder," *Can. J. Tech.*, vol. 33, pp. 77–97; January, 1955.
- [5] L. L. Bailin, "Field produced by a slot on a large circular cylinder," *IRE TRANS. ON ANTENNAS AND PROPAGATION*, vol. AP-3, pp. 128–137; July, 1955.
- [6] J. R. Wait, "Radiation characteristics of axial slots on a conducting cylinder," *Wireless Engr.*, vol. 32, pp. 316–323; De-

ember, 1955. (See also Addendum to Radio Physics Lab. Rep. No. 19-0-11, Ottawa, Can., November, 1954.) (A paper entitled "Pattern of a flush mounted microwave antenna" dealing with this subject is to be published in *J. Res. NBS*.)

[7] J. R. Wait and J. Kates, "Radiation patterns of circumferential slots on moderately large conducting cylinders," Monograph No. 167 R, IEE (London), republished in *Proc. IEE*, vol. 103, pt. C; September, 1956.

[8] J. E. Keys, "The Radiation Pattern of Slotted Cylinders Measured in the Parallel Plate Region," Radio Physics Lab., Ottawa, Can., Project Rep. No. 5-0-2; October, 1955.

[9] J. Bain, "Radiation Pattern Measurements of Stub and Slot Antennas on Spheres and Cylinders," Stanford Res. Inst., Stanford, Calif., Tech. Rep. No. 42; April, 1953.

[10] J. R. Wait and K. Okashimo, "Patterns of stub antennas on cylindrical (and semi-cylindrical) surfaces," *Can. J. Phys.*, vol. 34, pp. 190-202; February, 1956.

[11] S. Sensiper, "Cylindrical radio waves," *IRE TRANS. ON ANTENNAS AND PROPAGATION*, vol. AP-5, pp. 56-70; January, 1957.

[12] L. L. Bailin and R. J. Spellmire, "Convergent Representations for the Radiation Fields from Slots in Large Circular Cylinders," Microwave Lab., Hughes Aircraft Co., Tech. Memo. No. 386; July, 1955.

[13] W. Franz, "The Green's functions of cylinders and spheres," *Z. Naturforsch.*, vol. 9a, pp. 705-716; September, 1954.

[14] W. Franz and R. Galle, "Semiasymptotic series for the diffraction of a plane wave by a cylinder," *Z. Naturforsch.*, vol. 10a, pp. 374-378; May, 1955.

[15] I. Imai, "The diffraction of electromagnetic waves by a circular cylinder," *Z. Phys.*, vol. 137, pp. 31-48; 1954.

[16] W. Franz and P. Beckman, "Creeping waves for objects of finite conductivity," *IRE TRANS. ON ANTENNAS AND PROPAGATION*, vol. AP-4, pp. 203-208; July, 1956.

[17] R. F. Goodrich, A. L. Maffett, N. Reitlinger, C. E. Schensted, and K. M. Siegel, "Studies in Radar Cross Sections XXII, Elementary Slot Radiators," Eng. Res. Inst., Univ. of Michigan, Ann Arbor, Mich.; November, 1956.

[18] L. Wetzel and D. B. Brick, "An Experimental Investigation of High-Frequency Current Distributions on Conducting Cylinders," Crut Lab., Harvard Univ., Cambridge, Mass., Sci. Rep. No. 4; December, 1955.

[19] V. Fock, "Distribution of currents induced by a plane wave on the surface of a conductor," *J. Phys. (U.S.S.R.)*, vol. 10, pp. 130-140; 1946.

[20] C. H. Papas and R. W. P. King, "Currents on the surface of an infinite cylinder excited by an axial slot," *Quart. Appl. Math.*, vol. 16, pp. 175-182; 1948.

[21] W. S. Lucke, "Mutual Admittance of Slots in Cylinders," Stanford Res. Inst., Menlo Park, Calif., Tech. Rep. No. 36; February, 1953.

[22] J. R. Wait and J. Y. Wong, "Radiation Conductance of Slots in Plane and Curved Conducting Surfaces," paper presented at Symp. on Electromagnetic Theory, Ann Arbor, Mich.; June, 1955.

[23] D. G. H. Frood and K. W. Armstrong, "The (Measured) Admittance of Axial Slots Cut in Metal Cylinders," Radio Physics Lab., Ottawa, Can., Proj. Rep. No. 19-0-17; August, 1955.

[24] J. Y. Wong, "Radiation conductance of axial and transverse slots in cylinders of elliptical cross section," *Proc. IRE*, vol. 41, pp. 1172-1177; September, 1953.

[25] F. H. Northover, "On the Electromagnetic Field Produced by a Thin Transverse Slot in a Cylindrical Antenna," pts. 1 and 2, Rad. Phys. Lab., Ottawa, Can., Proj. Rep. No. 19-0-16; August, 1955.

[26] J. R. Wait, "Field produced by an arbitrary slot on an elliptic cylinder," *J. Appl. Phys.*, vol. 26, pp. 458-463; April, 1955.

[27] J. R. Wait and R. E. Walpole, "Calculated radiation characteristics of slots cut in metal sheets," *Can. J. Tech.*, pt. 1, vol. 33, pp. 211-227, May, 1955; pt. 2, vol. 34, pp. 60-70, January, 1956.

[28] J. R. Wait and M. O'Grady, "Surface currents excited by an infinite slot on half-planes and ribbons," *IRE TRANS. ON ANTENNAS AND PROPAGATION*, vol. AP-4, pp. 47-50; January, 1956.

[29] J. Y. Wong, "Radiation patterns of slotted elliptic cylinder antennas," *IRE TRANS. ON ANTENNAS AND PROPAGATION*, vol. AP-3, pp. 200-203; October, 1955.

[30] P. R. Karr, "Radiation properties of spherical antennas as a function of location of the driving force," *J. Res. NBS*, vol. 46, pp. 422-436; May, 1951.

[31] C. T. Tai, "Some Electromagnetic Problems Involving a Sphere," Stanford Res. Inst., Menlo Park, Calif., Tech. Rep. No. 41; April, 1953.

[32] Y. Mushiake and R. E. Webster, "Radiation characteristics with power gain for slots on a sphere," *IRE TRANS. ON ANTENNAS AND PROPAGATION*, vol. AP-5, pp. 47-55; January, 1957.

[33] D. McCoy, "Numerical Calculations of Admittances of Narrow Zonal Slots in a Sphere," Antenna Lab., U. S. Army Signal Corps., Fort Monmouth, N. J., Tech. Rep. No. 522-8; April, 1954. See also R. C. Hansen, unpublished work dealing with the non-symmetrical excitation of the spherical antenna, Univ. of Illinois.

[34] J. R. Wait, "Radiation pattern of an antenna mounted on a surface of large radius of curvature," *PROC. IRE*, vol. 44, p. 694; May, 1956.

[35] S. B. Cohn and T. Morita, "Microwave Radiation from Large Finite Bodies," Stanford Res. Inst., Menlo Park, Calif., Tech. Rep.; No. 48; January, 1955.

[36] J. R. Wait, "Currents excited on a conducting surface of large radius of curvature," *IRE TRANS. ON MICROWAVE THEORY AND TECHNIQUES*, vol. MTT-4, pp. 143-145; July, 1956. (For a more general treatment see "Radiation from a vertical antenna over a curved stratified ground," *J. Res. NBS*, vol. 56, pp. 230-240; July, 1956.)

[37] J. R. Wait and S. Kahana, "Radiation from a slot on a cylindrically tipped wedge," *Can. J. Phys.*, vol. 32, pp. 714-722; November, 1954.

[38] D. G. Frood and J. R. Wait, "An investigation of slot radiators in metal plates," *Proc. IEE*, vol. 103, pt. B, pp. 103-110; January, 1956.

[39] C. T. Tai, "Radiation from Current Elements and Apertures in the Presence of a Perfectly Conducting Half Plane," Stanford Res. Inst., Menlo Park, Calif., Tech. Rep. No. 45; July, 1954.

[40] J. R. Wait, "On the conductance of slots," *IRE TRANS. ON ANTENNAS AND PROPAGATION*, vol. AP-4, pp. 124-127; April, 1956.

[41] C. E. Schensted and A. L. Maffett, "Evaluation of the Field Produced by Slots on a Wedge," presented at URSI Spring Meeting, Washington, D. C.; May, 1956.

[42] L. B. Felsen, "Radiation from slots on a perfectly conducting wedge," presented at WESCON, Los Angeles; August, 1956. (See also Memo No. 13 from Electrophysics Group, Polytechnic Inst. of Brooklyn, Brooklyn, N. Y.; May, 1956.)

[43] F. Oberhettinger, "Diffraction of waves by a wedge," *Commun. Pure Appl. Math.*, vol. 4, pp. 75-94; June, 1951.

[44] F. Oberhettinger, "On asymptotic series for functions occurring in the theory of diffraction of waves by wedges," *J. Math. Phys.*, vol. 34, pp. 245-255; January, 1956.

[45] C. Flammer, "Radiation from Electric and Magnetic Dipoles in the Presence of a Conducting Circular Disk," Stanford Res. Inst., Menlo Park, Calif., Tech. Rep. No. 49; February, 1955.

[46] J. Meixner, "The radiation pattern and induced current in a circular antenna with a circular slit," *IRE TRANS. ON ANTENNAS AND PROPAGATION*, vol. AP-4, pp. 408-411; July, 1956.

[47] H. A. Myers, "Radiation patterns of unsymmetrically fed prolate spheroidal antennas," *IRE TRANS. ON ANTENNAS AND PROPAGATION*, vol. AP-4, pp. 58-64; January, 1956.

[48] Stratton, Morse, Chu, Little, and Corbato, "Spheroidal Wave Functions," Tech. Press of M.I.T., John Wiley and Sons, New York, N. Y.; 1956.

[49] W. Andrejewski, "Die Beugung elektromagnetischer Wellen an der leitenden Kreisscheibe und an der kreisförmigen Öffnung im leitenden ebenen Schirm," dissertation, Technical University, Aachen, Ger.; February, 1952.

[50] F. V. Schultz, "Studies in Radar Cross Sections. I. Scattering by a Probate Spheroid," Engineering Res. Inst., Univ. of Michigan, Ann Arbor, Mich., Rep. No. UMM-126; December, 1953.

[51] L. L. Bailin and S. Silver, "Exterior electromagnetic boundary value problems for spheres and cones," *IRE TRANS. ON ANTENNAS AND PROPAGATION*, vol. AP-4, pp. 5-10; January, 1956.

[52] L. B. Felsen, "Alternative field representations in regions bounded by spheres, cones and planes," *IRE TRANS. ON ANTENNAS AND PROPAGATION*, vol. AP-5, pp. 109-120; January, 1957.

[53] A. F. Stevenson, "Theory of slots in rectangular wave guides," *J. Appl. Phys.*, vol. 19, pp. 24-34; January, 1948.

[54] A. A. Oliner, "The impedance properties of narrow radiating slots in the broad face of a rectangular waveguide," *IRE TRANS. ON ANTENNAS AND PROPAGATION*, vol. AP-5, pp. 4-20; January, 1957.

[55] M. G. Chernin, "Slot admittance at K band," *IRE TRANS. ON ANTENNAS AND PROPAGATION*, vol. AP-4, pp. 632-636; October, 1956.

[56] R. F. Hyneman, "Closely Spaced Traverse Slots in Rectangular Waveguides," Dept. of Elec. Eng., Univ. of Illinois, Urbana, Ill., Tech. Rep. No. 14; December 20, 1956.

[57] G. Held, "Scattering by a Slot in a Multimode Waveguide," Univ. of California, Berkeley, Calif., Inst. of Eng. Res. Ser. No. 60, Issue No. 114; June 15, 1954.

[58] D. J. Angelakos and G. Held, "Scattering by a Slot of Arbitrary Length in a Multimode Waveguide," Univ. of California, Berkeley, Calif., Inst. of Eng. Res. Ser. No. 60, Issue No. 115; June 30, 1954.

- [59] W. H. Kummer, "Measurement Techniques for Multimode Systems and the Properties of Half-Wave Slots in Two-Mode Rectangular Wave Guides," Univ. of California, Berkeley, Calif., Inst. of Eng. Res. Ser. No. 60, Issue No. 135; April 20, 1955.
- [60] R. A. Hurd, "Radiation patterns of a dielectric coated axially-slotted cylinder," *Can. J. Phys.*, vol. 34, p. 638; July, 1956.
- [61] J. R. Wait and W. E. Mientka, "Slotted cylinder antennas with a dielectric coating," *J. Res. NBS*, vol. 58; June, 1957. Also see J. R. Wait and A. M. Conda, "Radiation from dielectric clad and corrugated cylinders," *J. Res. NBS* (in preparation).
- [62] R. A. Hurd, "End-fire arrays of magnetic line sources mounted on a conducting half-plane," *Can. J. Phys.*, vol. 34, pp. 370-376; April, 1956. See also J. R. Wait, "Radiation from a line source adjacent to a conducting half plane," *J. Appl. Phys.*, vol. 24, pp. 1528-1529; December, 1953.
- [63] R. F. Harrington and J. D. Reale, "A Study of Aperture Antennas," Dept. of Elec. Eng., Univ. of Syracuse, Syracuse, N. Y. Final Rep. to Signal Corps, Fort Monmouth, N. J. for period September, 1953 to September, 1955.
- [64] H. Gruenberg, "A waveguide array for solar noise studies," *IRE TRANS. ON ANTENNAS AND PROPAGATION*, vol. AP-2, pp. 147-151; October, 1954.
- [65] B. T. Stephenson and C. H. Walter, "Endfire slot antennas," *IRE TRANS. ON ANTENNAS AND PROPAGATION*, vol. AP-3, pp. 81-86; April, 1955.
- [66] H. Gruenberg, "Second order beams of slotted wave guide arrays," *Can. J. Phys.*, vol. 31, pp. 55-69; January, 1953.
- [67] S. Silver and A. Otle, "Large Slots in Rectangular Waveguides," Univ. of California, Berkeley, Calif., Inst. of Eng. Res. Ser. No. 60, Issue No. 12; April 15, 1956.
- [68] R. C. Becker, "Directional Characteristics of a U-shaped Slot Antenna," Dept. of Elec. Eng., Univ. of Illinois, Urbana, Ill., Tech. Rep. No. 12; September 30, 1956.
- [69] A. J. Simmons, "Circularly polarized slot radiators," *IRE TRANS. ON ANTENNAS AND PROPAGATION*, vol. AP-5, pp. 31-35; January, 1957.
- [70] J. B. Keller, "The Geometrical Theory of Diffraction," Proc. Symp. on Microwave Optics, McGill Univ., Montreal, P. Q., Can.; June, 1953.
- [71] J. B. Keller, "Diffraction by a convex cylinder," *IRE TRANS. ON ANTENNAS AND PROPAGATION*, vol. AP-4, pp. 312-321; July, 1956.
- [72] Private communications from Nelson A. Logan of the Air Force Cambridge Research Center, Bedford, Mass. This work is to be published in a series of AFCRC reports.

TRAVELING-WAVE ANTENNAS

Definition

A traveling-wave antenna will be identified by a continuous or quasi-continuous nonmetallic connection between the feeding structure and the antenna aperture. Thus, a resonantly-spaced waveguide slot array is not considered to be a traveling-wave antenna, whereas a closely-spaced waveguide slot array is so considered. Similarly, an array of dipoles fed by a coaxial harness is not defined as a traveling-wave antenna, although an array of dipoles parasitically excited by a corrugated surface is so defined.

Survey

There has been an increased activity in this area of antenna research in the last three years, due to the inherent adaptability of such antennas to flush mounted applications. Papers have appeared which deal with corrugated and dielectric-clad surfaces, both single layer and double layer. Much attention has been given to the launching problem and recent interest has been shown in the synthesis and scanning aspects for slow-wave structures. Progress has continued in the exploitation of fast-wave systems, with major advances centering on the launching problem and on the polarization

problem. Equiangular antennas are emerging as important broad-band elements and new feeding systems, notably strip lines, are taking an important place as features of practical traveling-wave antennas.

One of the early types of traveling-wave antennas received some attention in this three-year period. Panakel and Mueller [1] performed an experimental study designed to optimize the directivity of single polystyrene rod antennas. They achieved some success, but found the dimensions extremely critical. The earlier work of Attwood was extended by Hatkin [2] in a theoretical study of higher order modes in dielectric sheets. In addition to formulas connecting the modal wavelengths to dielectric properties, Hatkin presents curves of these wavelengths for the first four modes of each type. Elliott [3] unified the theory of corrugated plane surfaces, by treating the corrugated waveguide and considering corrugated parallel plates and a single corrugated surface as limiting special cases of the corrugated waveguide. He also considered the launching problem and the effect of the finiteness of a ground plane. Angulo [4] solved a difficult portion of the theoretical radiation problem for plane trapping surfaces, by considering diffraction by a semi-infinite slab. He thus provided a rigorous solution for the case of no ground plane. A paper delivered by Ehrenspeck, Gerbes, and Zucker [5] provided an interesting point of view to the explanation of why trapping surfaces radiate. The properties of two-layer dielectric surfaces were also reported. Elliott [6], [7] offered a theoretical treatment of surface waves on cylinders and spheres. He demonstrated that such waves must leak, and his theory yielded complex propagation constants. Experimental verification also showed the practical effects of this leakage through beam placement and null-filling in the radiation pattern. The properties of surface waves over an infinite ferrite ground slab were studied by Pease [8]. He was able to show that for the practical case of a small ferrite layer, the fields and propagation constant could be expressed as simple closed forms and could be controlled by the magnitude of a steady magnetic field applied to the ferrite.

The launching problem for surface waves received considerable attention. Papers by Lo [9], Brick [10], and Friedman and Williams [11] dealt with the classical problem of surface waves excited by a dipole placed over a trapping surface. Lo and Brick gave a general theoretical treatment, with Brick's paper supported by experimental data. Friedman and Williams were concerned with the specific problem of properly locating the dipole to produce either as pure a surface wave as possible, or to maximize the amount of energy carried by the surface wave. Kay and Zucker [12] studied the launching problem for a general source through the use of Fourier transforms. They drew an important distinction between the problems of launching a surface wave onto a transmission line and onto an antenna, reaching the conclusion that the amplitude of excitation of the surface wave is proportional to the gain of the source

in free space in the complex direction that corresponds to the propagation constant of the surface wave.

The Illinois group has been studying the launching of traveling waves by means of a distributed source. Papers by Royal [13], Hodges [14], and Weeks [15] bear on this problem. Theory and experiment are in good accord. Practical significance is attached to these studies, because the distributed source is capable of producing tapered aperture distributions and thus improved radiation patterns. Royal reports excellent side-lobe levels in his experimental corroboration. Barone [16] has considered the line source equivalent of the problem treated by Lo and Brick.

The synthesis problem for surface waves has been severely hampered in a theoretical sense. This is because the method of stationary phase is not applicable to a constant velocity slow wave. An iteration technique was attempted for slow waves by Stephenson and Walter [17], with only limited success. An experimental investigation by Elliott [18] concluded that two practical methods for controlling a radiation pattern of a surface-wave antenna were to use a curved geometry and to taper the degree of trapping. Application of these techniques to practical antennas were reported by Plummer [19] and Butterfield [20]. An experimental study of parasitic excitation of radiating elements was also undertaken by Elliott and Rodda [21]. The geometric parameters were so critical that the conclusion was reached that a rigid connection between the parasites and surface wave would be necessary in any practical application. An interesting experiment was described by Ehrlich and Williams [22]. They treated a radiating discontinuity in a surface-wave transmission line as a four-terminal network, and attempted to measure the circuit properties through the use of efficient launching and receiving horns. The high degree of accuracy required to obtain the circuit data resulted in an extremely delicate experiment, only limited success being achieved.

A significant advance in the synthesis of radiation patterns from surface waves has been made recently. The limitations of the method of stationary phase to fast waves have been overcome by a study of *modulated* slow waves. This problem has been studied by Zucker and Thomas [23] and by Pease [24]. They were able to show that a modulated slow wave could result in a very high endfire gain or in a beam tilted at an arbitrary angle with the surface.

Scanning of surface-wave antennas is a difficult problem. (Except, of course, the case in which the entire antenna is mechanically rotated.) Two attempts at scanning have been reported. In the first of these, Ehrlich and Williams [25] described an investigation wherein they attempted to pass a constant frequency surface wave over a corrugated surface at an arbitrary angle to the corrugations. They found that the pattern deteriorated rapidly as the scan angle departed from the normal longitudinal direction. Hougaard and Hansen [26] performed the same experiment using a frequency-

scanned source. The frequency change compensated for the scan angle by making the corrugations appear electrically deeper. This resulted in an acceptable pattern over an appreciable scan angle.

The considerable body of work done by the Ohio State group on the subject of fast-wave antennas was summarized in a paper by Hines, Rumsey, and Walter [29]. A theoretical method for computing complex propagation constants was presented separately by Rumsey. This paper contains an important theorem on reciprocity for traveling waves. Recently, a simplified method for computing leaky propagation constants has been provided by Goldstone and Oliner [31]. Their procedure employs a perturbation method which is based on the transverse resonance condition for the existence of the pertinent leaky wave. An application of Rumsey's method to the specific problem of an axially slotted cylinder was reported by Harrington [32]. Stephenson and Walter [33], in a separate paper, gave further details of the Ohio State program. They reported several practical antenna designs and disclosed the development of successful discontinuity minimizers which greatly aided the launching problem. Walter [34] reported the extension of many of these ideas to a curved traveling-wave slot aperture. Hines, Rumsey, and Tice [35] pointed out the need to define properly the element pattern in the design of an array. The usual method of pattern multiplication can lead to errors when scattering from the elements is appreciable.

The continuous slots reported by Ohio State were successful for transverse polarization, but contained practical difficulties in the case of longitudinal polarization. By going to a quasi-continuous aperture, the Hughes group was able to achieve comparable success with longitudinal polarization. Stegen and Reed [36] initiated this program by using closely spaced nonresonant slots at the outer conductor of a loaded coaxial transmission line. The loading was used to speed up the wave and the size of the slots were used to control the leakage. Satisfactory patterns with longitudinal polarization resulted. Elliott [37] applied this technique to rectangular waveguide and recognized that this structure was a corrugated waveguide opened to outer space. He then applied corrugated waveguide theory to this problem and was able to determine theoretically the leaky propagation constants. In a separate paper, Kelly and Elliott [38] reported the experimental verification of the theory and several practical antenna forms. Recently the Illinois group has become interested in this problem, and Hyneman [39] has treated the complementary problem with excellent agreement between theory and experiment. Kelly [40] has applied these techniques to closely spaced annular slots on cones.

Hines and Upson [41] report success with a variable polarization traveling-wave antenna. Their technique uses edge slots cut in a rectangular waveguide as a line source radiating into a parallel plate transmission line. By mechanically changing the geometry, they continu-

ously varied the polarization from linear to circular. Another application of traveling-wave antennas was reported by Bergman and Schultz [42]. They used a circular conductor feed at one point and so terminated at the diametrically opposite point, that only a traveling wave existed on the antenna. Their experimental results were hampered by high sidelobe levels.

A unifying paper was presented by Reynolds [43] in which he pointed up the basic identity of such diverse antenna systems as the helical antenna, the dielectric antenna, the corrugated surface, and the long Yagi antenna. Also speaking in general terms, Marcuvitz [44] pointed out that leaky modes cannot comprise an orthonormal set nor can they satisfy the field requirements at infinity. However, in a restricted space region, they provide highly convergent approximations to problems in which the fundamental operation of the electromagnetic system results in a leaky wave.

The published literature on spiral antennas and their equivalents is still fragmentary. However, in 1954 Barnett and Crowley [45] pointed out the wide-band possibilities of equiangular antennas whose geometries were thereby frequency-independent. In a general paper, Rumsey [46] discussed the need to investigate those antennas of this class which could be properly terminated and pointed out several practical examples. An investigation of one of these practical examples was undertaken by DuHamel and Isbell [47].

Major progress has been made in the fabrication of strip lines. This has opened up the possibility of using transmission lines of this type to feed antennas, and has even resulted in the integration of the strip line and antenna aperture. Keen [48] and Frost [49] report the progress in component development, and McDonough and Malech [50] and Rotman and Karas [51], [52] propose many interesting applications to traveling-wave antenna systems.

Assessment and Projection

In a review of the progress represented by the papers discussed above, several conclusions seem reasonable. Electromagnetic field solutions for fast and slow waves are now well understood for all structures of the simpler geometric shapes. Some progress will undoubtedly still be made in simplifications and refinements of the present theories. An excellent start has been made on the theoretical synthesis of patterns from slow-wave structures by use of the modulation concept. The exploitation of wide-band antennas through the use of geometries in which angles are preserved is a new subject which will probably receive considerable emphasis in the years to come. A major breakthrough in the fabrication problem is needed and the increased use of strip line techniques may offer a solution. It would seem from this vantage point that the activity in traveling-wave antennas in the next three years will be principally characterized by experimental programs designed to improve development techniques and provide practical antennas.

References

- [1] J. J. Panakel and G. Mueller, "An Investigation of Polystyrene Rod Antennas," *Antenna Res. Lab., Ohio State Univ., Columbus, Ohio, Rep. No. 510-11*; June, 1954.
- [2] L. Hatkin, "Analysis of propagating modes in dielectric sheets," *PROC. IRE*, vol. 42, pp. 1565-1568; October, 1954.
- [3] R. S. Elliott, "On the theory of corrugated plane surfaces," *IRE TRANS. ON ANTENNAS AND PROPAGATION*, vol. AP-2, pp. 71-81; April, 1954.
- [4] C. M. Angulo, "Diffraction of surface waves by a semi-infinite slab," *IRE Trans. ON ANTENNAS AND PROPAGATION*, vol. AP-5, pp. 100-108; January, 1957.
- [5] H. Ehrenspeck, W. Gerbes, and F. J. Zucker, "Trapped wave antennas," *1954 IRE CONVENTION RECORD*, pt. 1, pp. 25-30.
- [6] R. S. Elliott, "Azimuthal surface waves on circular cylinders," *J. Appl. Phys.*, vol. 26, pp. 368-376; April, 1955.
- [7] R. S. Elliott, "Spherical surface wave antennas," *IRE TRANS. ON ANTENNAS AND PROPAGATION*, vol. AP-4, pp. 422-428; July, 1956.
- [8] R. L. Pease, "On the Propagation of Surface Waves over an Infinite Grounded Ferrite Slab," *Res. Labs., Hughes Aircraft Co., Culver City, Calif., Sci. Rep. No. 12*; June, 1956.
- [9] Y. T. Lo, "Electromagnetic field of a dipole source above a grounded dielectric slab," *J. Appl. Phys.*, vol. 25, pp. 733-740; June, 1954.
- [10] D. B. Brick, "The excitation of surface waves by a vertical antenna," *PROC. IRE*, vol. 43, pp. 721-727; June, 1955.
- [11] B. Friedman and W. E. Williams, "Excitation of Surface Waves," *Inst. of Mathematical Sciences, Div. of Electromagnetic Research, New York Univ., New York, N. Y., Res. Rep. No. EM-99*; October, 1956.
- [12] A. F. Kay and F. J. Zucker, "Efficiency of surface wave excitation," *1955 IRE CONVENTION RECORD*, pt. 1, pp. 1-5.
- [13] D. E. Royal, "Axially Excited Surface Wave Antennas," *Antenna Lab., Univ. of Illinois, Urbana, Ill., Tech. Rep. No. 7*; October, 1955.
- [14] R. R. Hodges, "Distributed Coupling to Surface Wave Antennas," *Antenna Lab., Univ. of Illinois, Urbana, Ill., Tech. Rep. No. 15*; January, 1957.
- [15] W. L. Weeks, "Coupled Waveguide Excitation of Traveling Wave Slot Antennas," *Antenna Lab., Univ. of Illinois, Urbana, Ill., Tech. Rep. No. 27*; December, 1957.
- [16] S. Barone, "Leaky Wave Contributions to the Field of a Line Source above a Dielectric Slab," *Microwave Res. Inst., Polytechnic Inst. of Brooklyn, Brooklyn, N. Y., Rep. No. R-532-56*; 1956.
- [17] B. T. Stephenson and C. H. Walter, "Approximate Pattern Synthesis Techniques for Continuous Line Sources," *Antenna Research Lab., Ohio State Univ., Columbus Ohio*; June, 1955.
- [18] R. S. Elliott, "Pattern Shaping with Surface Wave Antennas," *Res. Labs., Hughes Aircraft Co., Culver City, Calif., Sci. Rep. No. 3*; March, 1955.
- [19] R. E. Plummer, "Surface Wave Beacon Antennas," *Res. Labs., Hughes Aircraft Co., Culver City, Calif., Tech. Memo. No. 422*; April, 1956.
- [20] F. E. Butterfield, "Dielectric sheet radiators," *IRE TRANS. ON ANTENNAS AND PROPAGATION*, vol. AP-3, pp. 152-158; October, 1954.
- [21] R. S. Elliott and E. N. Rodda, "Parasitic arrays excited by surface waves," *IRE TRANS. ON ANTENNAS AND PROPAGATION*, vol. AP-3, pp. 140-142; July, 1955.
- [22] M. J. Ehrlich and I. K. Williams, "Radiating Discontinuity on a Corrugated Surface Transmission Line," *Microwave Radiation Co., Rep. No. 205*; March, 1955.
- [23] F. J. Zucker and A. S. Thomas, "Radiation from modulated surface wave structures—I," *1957 IRE NATIONAL CONVENTION RECORD*, pt. 1, pp. 153-160.
- [24] R. L. Pease, "Radiation from modulated surface wave structures—II" *1957 IRE NATIONAL CONVENTION RECORD*, pt. 1, pp. 161-165.
- [25] M. J. Ehrlich and I. K. Williams, "Scanning of a Two-Dimensional Corrugated Surface Antenna," *Microwave Radiation Co., Rep. No. 219*; 1956.
- [26] R. W. Hougardy and R. C. Hansen, "Scanning Surface Wave Antennas," *Res. Labs., Hughes Aircraft Co., Culver City, Calif., Sci. Rep. No. 13*; August, 1956.
- [27] R. C. Hansen, "Single Slab Circular Polarization Surface Wave Structure," *Res. Labs., Hughes Aircraft Co., Culver City, Calif., Sci. Rep. No. 9*; February, 1956.
- [28] R. E. Plummer and R. C. Hansen, "Double Slab Arbitrary Polarization Surface Wave Structure," *Res. Labs., Hughes Aircraft Co., Culver City, Calif., Sci. Rep. No. 10*; June, 1956.
- [29] J. N. Hines, V. H. Rumsey, and C. H. Walter, "Traveling-wave slot antennas," *PROC. IRE*, vol. 41, pp. 1624-1631; November, 1953.

- [30] V. H. Rumsey, "Traveling-wave slot antennas," *J. Appl. Phys.*, vol. 24, pp. 1358-1365; November, 1953.
- [31] L. O. Goldstone and A. A. Oliner, "A Perturbation Method for the Analysis of Leaky Wave Antennas," presented at URSI Spring Meeting, Washington, D. C.; May, 1956.
- [32] R. F. Harrington, "Propagation along a slotted cylinder," *J. Appl. Phys.*, vol. 24, pp. 1366-1371; November, 1953.
- [33] B. T. Stephenson and C. H. Walter, "Endfire slot antennas," *IRE TRANS. ON ANTENNAS AND PROPAGATION*, vol. AP-3, pp. 81-86; April, 1955.
- [34] C. H. Walter, "Curved Slot Antennas," *Antenna Res. Lab., Ohio State Univ.*, Columbus, Ohio; April, 1956.
- [35] J. N. Hines, V. H. Rumsey, and T. E. Tice, "On the design of arrays," *PROC. IRE*, vol. 43, pp. 1262-1267; August, 1954.
- [36] R. J. Stegen and R. H. Reed, "Arrays of closely spaced non-resonant slots," *IRE TRANS. ON ANTENNAS AND PROPAGATION*, vol. AP-2, pp. 109-112; July, 1954.
- [37] R. S. Elliott, "Serrated Waveguide, Part 1—Theory," *Res. Labs., Hughes Aircraft Co.*, Culver City, Calif., Sci. Rep. No. 2; March, 1955.
- [38] K. C. Kelly and R. S. Elliott, "Serrated Waveguide, Part II—Experiment," *Res. Labs., Hughes Aircraft Co.*, Culver City, Calif., Sci. Rep. No. 7; October, 1955.
- [39] R. F. Hyneman, "Closely Spaced Traverse Slots in Rectangular Waveguide," *Antenna Lab., Univ. of Illinois*, Urbana, Ill., Tech. Rep. No. 14; December, 1956.
- [40] K. C. Kelly, "Recent annular slot array experiments," 1957 *IRE NATIONAL CONVENTION RECORD*, pt. 1, pp. 144-152.
- [41] J. N. Hines and J. Upson, "A Line Source with Variable Polarization," *Antenna Res. Lab., Ohio State Univ.*, Columbus, Ohio; November, 1956.
- [42] W. J. Bergman and F. V. Schultz, "The circular traveling wave antenna," 1955 *CONVENTION RECORD*, pt. 1, pp. 40-50.
- [43] D. K. Reynolds, "Broadband traveling wave antennas," 1957 *IRE NATIONAL CONVENTION RECORD*, pt. 1, pp. 99-107.
- [44] N. Marcuvitz, "On field representations in terms of leaky modes or eigenmodes," *IRE TRANS. ON ANTENNAS AND PROPAGATION*, vol. AP-4, pp. 192-194; July, 1956.
- [45] R. Barnett and T. H. Crowley, "A wide band directional antenna," *Antenna Res. Lab., Ohio State Univ.*, Columbus, Ohio, Tech. Rep. No. 510-12; June, 1954.
- [46] V. H. Rumsey, "Frequency independent antennas," 1957 *IRE NATIONAL CONVENTION RECORD*, pt. 1, pp. 114-118.
- [47] R. H. DuHamel and D. E. Isbell, "Broadband logarithmically periodic antenna structures," 1957 *IRE NATIONAL CONVENTION RECORD*, pt. 1, pp. 119-128.
- [48] H. S. Keen, "Final Report on Theoretical and Experimental Investigation of Microwave Printed Circuits," *Airborne Instruments Lab.*, Mineola, N. Y.; November, 1956.
- [49] A. D. Frost, "Final Report on Experimental and Theoretical Aspects of the Design of Microwave Strip Transmission Lines," *Dept. of Phys., Tufts Univ.*, Medford, Mass.; December, 1956.
- [50] J. A. McDonough and R. G. Malech, "Recent developments in the study of printed antennas," 1957 *IRE NATIONAL CONVENTION RECORD*, pt. 1, pp. 173-181.
- [51] W. Rotman and N. V. Karas, "The sandwich wire antenna: a new microwave line source radiator," 1957 *IRE NATIONAL CONVENTION RECORD*, pt. 1, pp. 166-172.
- [52] W. Rotman and N. V. Karas, "Some new antenna designs based on the trough waveguide," 1956 *IRE NATIONAL CONVENTION RECORD*, pt. 1, pp. 230-235.

DIFFRACTION AND SCATTERING

The period from July 1, 1954, through May 1, 1957, in the United States was marked by a considerable effort in the diffraction and scattering field. This effort consisted primarily in obtaining new exact solutions, several new approximate solutions, and a better physical understanding of the mechanisms involved in scattering. Since this survey was limited to United States contributions, it is rather difficult to isolate particular efforts because many of them were inspired by the work of individuals of other countries; for example, by Bremmer, Fock, Franz, and Friedlander. Methods not used during the previous three years were applied to solving boundary value problems during this period. There was also considerably heightened interest in the experimental

determination of diffraction and scattering answers.

Considerable work has been done on reformulating and obtaining new solutions. Emphasis here has been on the wedge, cylinder, sphere, dielectric coated sphere, cone, paraboloid, special angled corners, parabolic cylinder, prolate spheroid, and many apertures and wedges with cylindrically tipped edges.

Asymptotic results have been obtained for the cylinder, sphere, paraboloid, and for apertures, wedges, and cones. These asymptotic evaluations have in many cases resulted from methods outlined during the last period. Keller conceived the geometric diffracted ray technique. He applied this technique to cylinders of arbitrary cross section, including the parabolic cylinder and the circular cylinder as special cases [1]. By the same method he solved the arbitrary aperture problem [2], and compared his results with other asymptotic aperture methods [3]. Rice [4] obtained the exact parabolic cylinder results, which he shows approach the correct limit when the cylinder approaches the half-plane of Sommerfeld, or the thick half-plane of Armann. Rice's results can be predicted using Fock's approximation where the latter is valid. Schensted [5] used the Luneberg Kline asymptotic series to solve the paraboloid boundary value problem with the transmitter on the axis. He showed that for the perfectly conducting paraboloid the leading term of the Luneberg Kline series was, in fact, the exact far zone field. Schensted also solved the general body of revolution problem for a plane wave incident along the axis of symmetry by Luneberg Kline expansion. Felsen [6] and Siegel, Crispin, and Schensted [7] solved the exact back scattering cone problem and compared the results with the asymptotic results obtained from the Kirchhoff theory. They found, for large and small cone angles, that the leading term in the cross section, when the plane wave was on the axis, was in agreement with the exact solution. Felsen showed further that for the case in which the transmitter is on the axis of symmetry and the receiver is not, Kirchhoff theory was in good agreement with the exact solution. Kirchhoff results for these shapes and many others are presented by Siegel, Alperin, Bonkowski, Crispin, Maffett, Schensted, and Schensted [8]. Felsen has extended the cone answer to obtain the results in a transition region and the region close to the boundary.

Oberhettinger [9], [10] has found many neat asymptotic formulations for wedge problems. Keller, Seckler, and Lewis [11] have given additional terms in the asymptotic series for many simple shapes. Kline [12] has extended his asymptotic development obtaining an expansion in fractional powers of the wavelength. Schensted [13] obtained an asymptotic solution for a plane obstacle by neglecting higher variations in the geometrical optics approximation to the phase.

Cohen [14] applied Rumsey's reaction concept to obtain a scattering result for the dielectric cylinder. Wu [15] used a creeping wave concept and applied Riemann

surface techniques to the cylinder problem. This had been suggested in a paper by Friedlander [16]. Rubinow and Wu [17] succeeded in finding several terms of an asymptotic expansion for the total scattering from cylinders and spheres. Schiff [18] generalized the Born approximation to include scattering governed by Maxwell's equations. This method is particularly useful for scattering in nonspherical regions where the index of refraction is a slowly varying function of value nearly unity. Kay and Keller [19] have obtained the Luneberg expansion of the field of a caustic. Many asymptotic solutions for the scattering of waves by gratings have been given by Twersky [20]. Karp and Russek obtained asymptotic results for the diffraction of a wide slit [21]. Huang, Kodis and Levine [22] have made many important numerical computations comparing theoretical and experimental aperture diffraction results. Hirshfield and Zieman [23] made measurements of microwave diffraction from long slits in a thin conducting plane.

Other Important Results

Marcuvitz [24] has extended his field representation to be applicable to leaky modes or eigenmodes. Significant results by variational theory, in addition to those of Huang, Kodis, and Levine mentioned above, were obtained by Kouyoumjian [25] in his treatment of a circular loop. These results are in agreement with the exact solution of Weston [26]. Erdelyi and Papas [27] used a variational method to obtain solutions for an infinite strip. They used a trial function that ignored edge effects and obtained good numerical results for the entire range in wavelength. Heins [28] obtained the scattering due to a dipole field incident on a perfectly conducting half-plane. He and Silver [29] gave results which led to new insight concerning edge conditions and field representation theorems in the general theory of diffraction. However their emphasis was primarily on aperture problems. Row [30] has obtained theoretical and experimental results for two identical conducting cylinders in the resonance region.

Basic Foundations

The tensor scattering matrix for the electromagnetic scattering field has been derived by Saxon [31]. An expansion theorem for electromagnetic fields was given by Wilcox [32]. Wilcox also has shown that in any finite region the electromagnetic field can be represented by Debye potentials [33]. Peters and Stoker [34], [35] gave a unique decomposition of the radiation condition for application of uniqueness theorems to semi-infinite bodies. A new method for obtaining scattering solutions for bodies that can be mapped conformally on a circle has been given by Garabedian [36]. Siegel, Schultz, Gere, and Sleator [37] obtained numerical results for nose-on back scattering by a 10:1 prolate spheroid. A digital computer was used to sum the exact series solution.

Experimental Work

A great deal of experimental work has been done which has not yet appeared in journal articles. Among the important unpublished results is the experimental work of Brick and Wetzel at Harvard on circular and elliptic cylinders. Measurements on spheroids and finite cones have been made by Honda at the University of California at Berkeley. Broadside measurements of spheroids and cylinders were undertaken by Rabino-witz at The Johns Hopkins University. The University of Texas has performed many experiments on wedges and corners.

The United States has a large body of theoretical and experimental data collected but not journalized in the past three years. These data can usually be obtained by writing or visiting the Air Force Cambridge Research Center, Cornell Aeronautical Laboratory, Inc., Stanford Research Institute, Harvard University, The Johns Hopkins University, The Ohio State University, Radiation Inc., the University of California at Berkeley, the Universities of Illinois, Texas, and Michigan.

Epilogue

The fact that so much information exists in report form but not yet in journal form makes it quite easy to predict what the next three years should bring to journal literature in the diffraction and scattering field in the United States. A good deal of emphasis is being placed on the results of Fock. His method of obtaining asymptotic results, based on local analysis, will probably be used to derive new results. Further emphasis will be placed on geometric diffracted rays by the Keller approach. A method proposed by Logan which replaces the divergence condition by a condition on the field at infinity, applying an idea due to Müller, will undoubtedly lead to new representations for exact solutions. The effect of creeping waves which are focused towards an effective point singularity, then reflected and defocused, will also be the subject of analysis during the next three years. Weston's method of obtaining exact solutions for Maxwell's equations for bodies which are not contour surfaces of separable coordinate systems will undoubtedly be the subject of considerable analysis. It is expected that scattering in the Rayleigh region will receive more attention than it has in the past three years. The work of Stevenson, Mushiaki, and Tai probably will lead to new theories and new methods of solving Rayleigh problems.

The asymptotic approaches used by Kline and Keller will undoubtedly receive considerable attention and will be used to solve many more problems than previously.

The work of Fock will undoubtedly receive additional attention from people in the antenna field. It is expected that radiation theorists will place more emphasis on scattering results than they have in the past. The reaction concept will undoubtedly be analyzed and used more as it becomes better understood.

The large variety of publications in the diffraction and scattering field has required that a certain number of these be left out. Rough surface work and scattering from colloidal particles and collections of spheres have been deliberately omitted as being more properly the subject of other commissions.

References

- [1] J. B. Keller, "Diffraction by a convex cylinder," *IRE TRANS. ON ANTENNAS AND PROPAGATION*, vol. AP-4, pp. 312-321; July, 1956.
- [2] J. B. Keller, "Diffraction by an aperture," *J. Appl. Phys.*, vol. 28, pp. 426-444; April, 1957.
- [3] J. B. Keller, R. M. Lewis, and B. D. Seckler, "Diffraction by an aperture—II," *J. Appl. Phys.*, vol. 28, pp. 570-579; May, 1957.
- [4] S. O. Rice, "Diffraction of plane radio waves by a parabolic cylinder—calculation of shadows, behind hills," *Bell Sys. Tech. J.*, vol. 33, pp. 417-504; March, 1954.
- [5] C. E. Schensted, "Electromagnetic and acoustic scattering by a semi-infinite body of revolution," *J. Appl. Phys.*, vol. 26; pp. 306-308; March, 1955.
- [6] L. B. Felsen, "Back scattering from wide-angle and narrow-angle cones," *J. Appl. Phys.*, vol. 26, pp. 138-151; February, 1955.
- [7] K. M. Siegel, J. W. Crispin, and C. E. Schensted, "Electromagnetic and acoustical scattering from a semi-infinite cone," *J. Appl. Phys.*, vol. 26, pp. 309-313; March, 1955.
- [8] K. M. Siegel, H. A. Alperin, R. R. Bonkowski, J. W. Crispin, A. L. Maffett, C. E. Schensted, and I. V. Schensted, "Bistatic radar cross sections of surfaces of revolution," *J. Appl. Phys.*, vol. 26, pp. 297-305; March, 1955.
- [9] F. Oberhettinger, "Diffraction of waves by a wedge," *Commun. Pure Appl. Math.*, vol. 7, pp. 551-563; August, 1954.
- [10] F. Oberhettinger, "On asymptotic series for functions occurring in the theory of diffraction of waves by wedges," *J. Math. Phys.*, vol. 34, pp. 245-255; January, 1956.
- [11] J. B. Keller, R. M. Lewis, and B. D. Seckler, "Asymptotic solution of some diffraction problem," *Commun. Pure Appl. Math.*, vol. 9, pp. 207-265; May, 1956.
- [12] M. Kline, "Asymptotic solutions of Maxwell's equations involving fractional powers of the frequency," *Commun. Pure Appl. Math.*, vol. 7, pp. 595-614; November, 1955.
- [13] C. E. Schensted, "Approximate method for scattering problems," *IRE TRANS. ON ANTENNAS AND PROPAGATION*, vol. AP-4, pp. 240-242; July, 1956.
- [14] M. H. Cohen, "Application of the reaction concept to scattering problems," *IRE TRANS. ON ANTENNAS AND PROPAGATION*, vol. AP-3, pp. 193-199; October, 1955.
- [15] T. T. Wu, "High frequency scattering," *Phys. Rev.*, vol. 104, pp. 1201-1212; December, 1956.
- [16] F. G. Friedlander, "Diffraction of pulses by a circular cylinder," *Commun. Pure Appl. Math.*, vol. 7, pp. 705-732; November, 1954.
- [17] S. I. Rubinow, and T. T. Wu, "First corrections to the geometric optics cross section from cylinders and spheres," *J. Appl. Phys.*, vol. 27, pp. 1032-1039; September, 1956.
- [18] L. I. Schiff, "Approximation method for short wavelength or high energy scattering," *Phys. Rev.*, vol. 104, pp. 1481-1485; December, 1956.
- [19] I. Kay and J. B. Keller, "Asymptotic evaluation of the field at a caustic," *J. Appl. Phys.*, vol. 25, pp. 876-883; July, 1954.
- [20] V. Twersky, "On the scattering of waves by an infinite grating," *IRE TRANS. ON ANTENNAS AND PROPAGATION*, vol. AP-4, pp. 330-345; July, 1956.
- [21] S. N. Karp, and A. Russek, "Diffraction by a wide slit," *J. Appl. Phys.*, vol. 27, pp. 886-894; August, 1956.
- [22] C. Huang, R. D. Kodis, and H. Levine, "Diffraction by apertures," *J. Appl. Phys.*, vol. 26, pp. 151-165; February, 1955.
- [23] J. L. Hirschfield and C. M. Zieman, "Measurement of microwave diffraction from a long slit in a thin conducting plane," *J. Appl. Phys.*, vol. 26, pp. 135-137; February, 1955.
- [24] N. Marcuvitz, "On field representations in terms of leaky modes or eigenmodes," *IRE TRANS. ON ANTENNAS AND PROPAGATION*, vol. AP-4, pp. 192-194; July, 1956.
- [25] R. G. Kouyoumjian, "The back scattering from a circular loop," *Appl. Sci. Res.*, vol. B6, No. 3, pp. 165-179; 1956.
- [26] V. H. Weston, "Solutions of the toroidal wave equation and their applications," thesis, Univ. of Toronto, Can.; 1956.
- [27] A. Erdelyi and C. A. Papas, "On diffraction by a strip," *Proc. Natl. Acad. Sciences*, vol. 40, p. 128; 1954.
- [28] A. E. Heins, "The excitation of a perfectly conducting half-plane by a dipole field," *IRE TRANS. ON ANTENNAS AND PROPAGATION*, vol. AP-4, pp. 294-296; July, 1956.
- [29] A. E. Heins and S. Silver, "The edge condition and field representation theorems in the theory of electromagnetic diffraction," *Proc. Cambridge Phil. Soc.*, vol. 51, pp. 149-161; January, 1955.
- [30] R. V. Row, "Theoretical and experimental study of electromagnetic scattering by two identical conducting cylinders," *J. Appl. Phys.*, vol. 26, pp. 666-675; June, 1955.
- [31] D. Saxon, "Tensor scattering matrix for the electromagnetic field," *Phys. Rev.*, vol. 100, pp. 1771-1775; December, 1955.
- [32] C. H. Wilcox, "An expansion theorem for electromagnetic fields," *Commun. Pure Appl. Math.*, vol. 9, pp. 115-134; May, 1956.
- [33] C. H. Wilcox, "Debye potentials," *J. Math. Mech.*, vol. 6, pp. 167-201; March, 1957.
- [34] A. S. Peters and J. J. Stoker, "A uniqueness theorem and a new solution for Sommerfeld's and other diffraction problems," *Commun. Pure Appl. Math.*, vol. 7, pp. 565-585; August, 1954.
- [35] J. J. Stoker, "On radiation conditions," *Commun. Pure Appl. Math.*, vol. 9, pp. 577-595; August, 1956.
- [36] P. R. Garabedian, "An integral equation governing electromagnetic waves," *Quart. Appl. Math.*, vol. 12, pp. 428-433; January, 1955.
- [37] K. M. Siegel, F. V. Schultz, B. H. Gere, and F. B. Sleator, "The theoretical and numerical determination of the radar cross section of a prolate spheroid," *IRE TRANS. ON ANTENNAS AND PROPAGATION*, vol. AP-4, pp. 266-275; July, 1956.

communications

Preliminary Results of Measurements on Doppler Shift of Satellite Emissions*

P. R. ARENDT†

MANY observations have indicated a distinct difference in the behavior of ionospheric transmission on the frequencies of 40 and 20 mc emitted from the Russian satellites. Therefore, it was considered necessary to investigate the influence of the propagation path on the observed data. Since many experiments include the assumption of straight line or quasi-optical propagation (at least during times of close approach of the vehicle) it is of some value to know what differences or discrepancies should be expected if the thesis of quasi-optical propagation is used without limitation.

A very simple method for comparing the two frequencies involved is offered by the well-known measurement of the Doppler shift of the received signal. Fig. 1 shows a simultaneous Doppler observation on both frequencies. In spite of the fact that both curves look rather regular and symmetrical, a closer inspection indicates a remarkable difference. For this purpose, the difference of the observed frequencies (two times f_{20} minus f_{40}) is shown in the lower part of the figure. If the propagation paths were identical on both frequencies, one could expect a straight horizontal line for this difference. The observed saddle point in the neighborhood of the time for closest approach indicates that neither the relative slopes nor the times for closest approach are identical. By this means we can obtain confirmation of other well-known observations that the

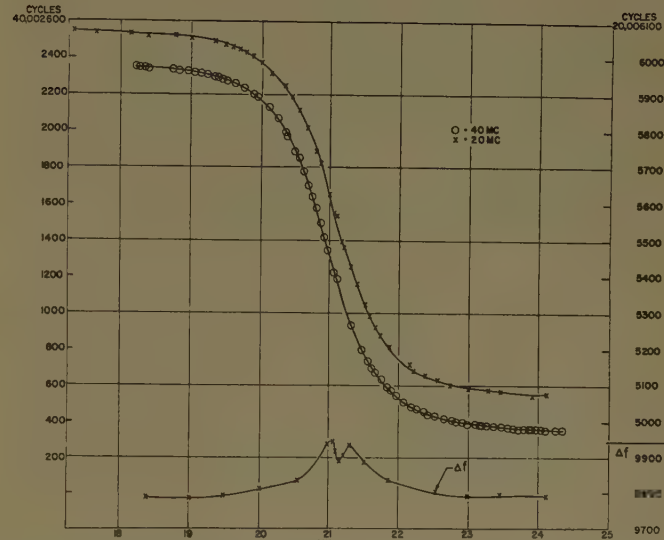


Fig. 1—Satellite 8 1957. Orbit 74, November 8, 1957, 10 18 00 GCT (05 18 00 EST). Measurement from Frequency Control Division

satellite signals on 20 and 40 mc are strongly influenced by bending and by reflections in the ionosphere. The same effect can also be demonstrated by azimuth measurements from direction finding equipment. Fig. 2 shows the results of a typical observation, again simultaneously for both frequencies.

The data of Fig. 1 were used for a numerical evaluation. For this purpose those parts of the curves where the observations can be made with highest precision in frequency were selected, *i.e.*, the curved parts before

* Manuscript received by the PGAP, August 5, 1958.

† U. S. Army Signal Res. and Dev. Lab., Ft. Monmouth, N. J.

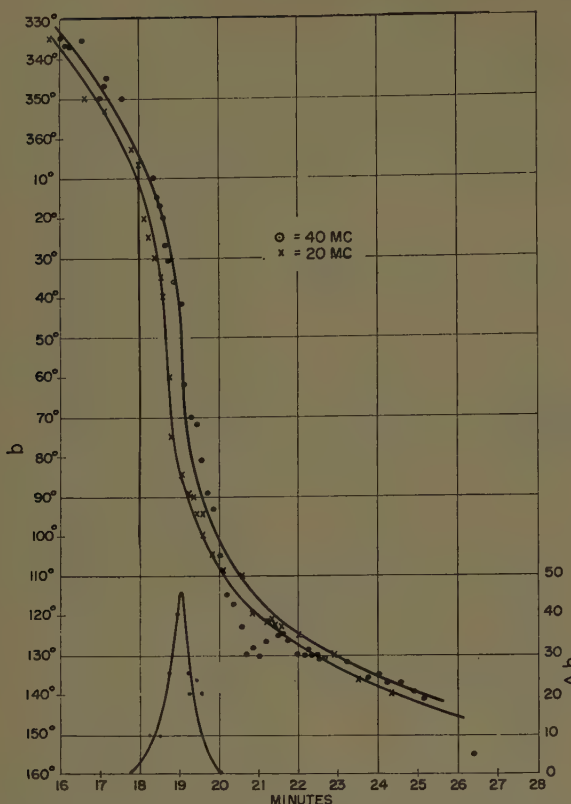


Fig. 2—Satellite α 1957. Orbit 136, October 14, 1957, 06 16 00 EDST. Measurements at Collingswood from Countermeasures Division.

and after closest approach. The close approach data were excluded as well as a few other observations which show clear deviations from the symmetrical curve which indicated that other disturbances occurred (fadings, reflections, etc.).

The numerical evaluation was based on the known relation for the Doppler measurement:

$$\left(\frac{f}{f - f_0} \frac{V_s}{V_p} \right)^2 = \frac{a^2}{V_s^2(t - t_0)^2} + 1$$

where V_s is the velocity of the satellite; a , its closest distance to the observer; and V_p , the phase velocity of the emitted waves. The index 0 at frequency f and times t refers to the moment of closest approach. Taking two observations at times t_1 and t_2 of frequencies f_1 and f_2 we have

$$\left(f_0 \frac{V_s}{V_p} \right)^2 = \frac{(t_1 - t_0)^2 - (t_2 - t_0)^2}{\left(\frac{t_1 - t_0}{f_1 - f_0} \right)^2 - \left(\frac{t_2 - t_0}{f_2 - f_0} \right)^2}.$$

The time and frequency of closest approach are not known as precisely as the single observations. The lack of perfect symmetry of the curves in Fig. 1 leads to uncertainties in t_0 of ± 1 second and in f_0 of ± 5 cycles per second from individual pairs of observations. More precise values are obtained by a comparison of the differences in the above formula for several pairs of possible t_0 and f_0 . The best average value is reached if equal values of Δt in the upper and in the lower part of

the curves are related to the same value of Δf . By this method the following values were found for the passage of Fig. 1.

$$\begin{aligned} \text{on 20 mc:} \\ t_0 &= 10 21 05 \text{ GCT;} & f_0 &= 20 00 55 65 \text{ cycles} \\ \text{on 40 mc:} \\ t_0 &= 10 20 57.5 \text{ GCT;} & f_0 &= 40 00 13 50 \text{ cycles.} \end{aligned}$$

The values for $(f_0(V_s/V_p))^2$ obtained on this basis are given in Table I. Each value corresponds to an average of 12 to 15 pairs of observations.

TABLE I

	Before Closest Approach	After Closest Approach	Average
On 20 mc	$0.274 \cdot 10^6$	$0.254 \cdot 10^6$	$0.2647 \cdot 10^6$
On 40 mc	$1.103 \cdot 10^6$	$1.106 \cdot 10^6$	$1.1049 \cdot 10^6$

The average on 40 mc should be equal to 4 times the average on 20 mc; however, 4 times 0.2647 equals 1.0588. This discrepancy indicates a different phase propagation velocity for the two frequencies. We obtain the relationship of these two velocities by division to

$$\frac{V_p(40)}{V_p(20)} = 0.9789$$

which means that the 40-mc wave travels about 2 per cent slower than the 20-mc. This is a fairly large difference for frequencies in this order of magnitude. It raises the question whether similar effects might be expected for even higher frequencies, *i.e.*, for frequencies in the neighborhood of 100 mc for which one generally assumes a strictly optical behavior. (However, measurements on moon reflection seem to indicate a nonoptical propagation even for frequencies higher than 100 mc.)

Further, the remarkable time difference of 7.5 sec for the apparent moments of closest approach indicates that strong bending occurs at least for the 20-mc signal. This is in coincidence with other observations.

The above relation between the propagation velocities can be used to make an approximate calculation of the critical frequency for that path of propagation in using the known relation

$$\frac{V_p}{C} = \left(1 - \frac{f_c^2}{f^2} \right)^{-1/2}$$

where C is the velocity of light in free space, and f_c the critical frequency. Using the above equation for 20 and 40 mc we have

$$\left[\frac{V_p(40)}{V_p(20)} \right]^2 = \frac{1 - \frac{f_c^2}{(20)^2}}{1 - \frac{f_c^2}{(40)^2}}.$$

With the above value we arrive at a critical frequency of 4.7 mc which is of the right order of magnitude. The vertical incidence critical frequency at 10 00 00 GCT

was measured to be 5 mc on that day in Fort Monmouth.

The observations referred to here were made under the direction of H. K. Ziegler of the U. S. Army Signal Engineering Laboratory, Fort Monmouth, N. J. The satellite recording was done by the Deal Receiving

Center. The frequency measurements were made under the supervision of H. D. Tanzman in the Frequency Control Division, and the azimuth bearings were taken under the supervision of H. M. Jaffee of the Countermeasures Division.

Suppressed Sidelobe Antenna of 32 Elements*

G. REBER†

EARLY in 1953, consideration was given to conducting some radio astronomy experiments upon cosmic static at medium waves. Part of the study involved the design of a 32-element array with suppressed sidelobes.¹ This antenna was never constructed because events took a different course.² However the

TABLE I

Number of Elements	32	32	32	32	32	33
R	11.107	19.557	39.908	106.68	243.85	17.783
db	20.92	25.80	32.02	40.56	47.74	25.00
Z	1.005	1.007	1.010	1.015	1.020	1.0062
Element Number	Values of Element Currents					
0	—	—	—	—	—	1.4730
1	0.8615	1.7411	4.1215	11.689	28.245	1.4666
2	0.8552	1.7045	3.9913	11.498	27.719	1.4477
3	0.8425	1.6558	3.8036	11.125	26.738	1.4164
4	0.8238	1.6040	3.6143	10.586	25.339	1.3736
5	0.7993	1.5422	3.4227	9.901	23.526	1.3200
6	0.7695	1.4678	3.2098	9.099	21.342	1.2568
7	0.7348	1.3823	2.9697	8.208	18.894	1.1850
8	0.6957	1.2876	2.7075	7.260	16.312	1.1061
9	0.6531	1.1854	2.4302	6.287	13.714	1.0215
10	0.6074	1.0779	2.1451	5.321	11.204	0.9329
11	0.5594	0.9672	1.8594	4.391	8.866	0.8417
12	0.5099	0.8554	1.5796	3.521	6.767	0.7496
13	0.4595	0.7446	1.3117	2.731	4.948	0.6580
14	0.4090	0.6366	1.0609	2.036	3.433	0.5684
15	0.3591	0.5332	0.8315	1.443	2.224	0.4821
16	0.1672	1.2414	1.3613	1.587	1.848	1.2200

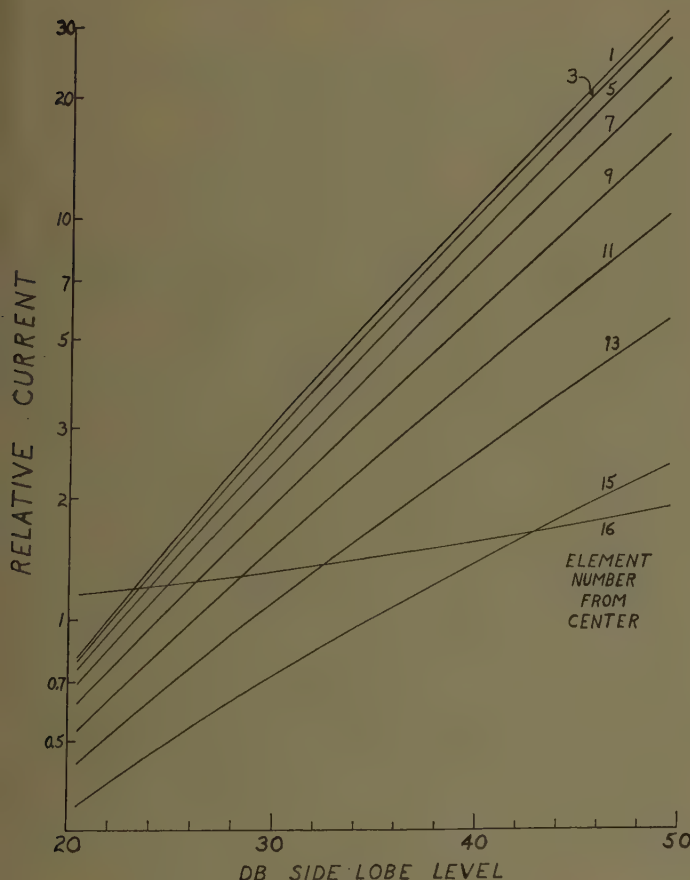


Fig. 1.

* Manuscript received by the PGAP, September 2, 1958.

† Green Bank, W. Va.

¹ C. L. Dolph, "Current distribution for broadside arrays," Proc. IRE, vol. 34, pp. 335-348; June, 1946.

² G. Reber, "Between the atmospherics," J. Geophys. Res., vol. 63, pp. 109-123; March, 1958.

results given in Fig. 1 and Table I may be of use to others. Only the currents in the odd-numbered elements plus the outside element are shown in the figure to prevent crowding the curves. It may be observed that the currents in the outside element and inside element are equal at 23.2-db suppression; and that the currents in outside and next to outside elements are equal at 42.8-db suppression. Since this study, a bulletin³ has appeared giving an analysis of quite a variety of configurations. The closest is a 33-element array with 25-db suppression. These values are included in the table for comparison.

The calculations were largely made by P. T. Miller. They were carried to fifteen places using a cross-multiplying scheme on a nine-place machine. The smoothness of curves and regularity of tables indicates the results are probably free from significant errors.

³ L. L. Bailin, et al., "Empirical Approximations to the Current Values for Large Dolph-Tchebyscheff Arrays," Tech. Mem. No. 328, Hughes Aircraft Co., Culver City, Calif.; 1953.

Measuring the Capacitance Per Unit Length of Two Infinite Cones of Arbitrary Cross Section*

J. D. DYSON†

Summary—The capacitance per unit length, and hence the characteristic impedance of two infinite cones, may be accurately measured by employing an extension of conventional guard techniques.

An appropriate gap is cut in one of the cones, converting the structure into a three-terminal capacitor. If the arm beyond the gap is long enough, the desired field distribution will be maintained past the gap and the capacitance per unit length of the isolated or guarded section may be measured by a conventional low-frequency capacitance bridge.

INTRODUCTION

IN A RECENT PAPER, Carrel¹ has considered a theoretical solution to the characteristic impedance of coaxial and noncoaxial biconical structures of arbitrary cross section, including the fin of zero thickness. These structures have been shown to be, basically, lossless transmission lines which have a constant capacitance per unit length. Carrel has shown that for the TEM spherical wave the boundary value problem involved is reducible to a two-dimensional potential problem and he has then employed conjugate function theory to obtain the capacitance per unit length.

The simple relationship between the characteristic impedance and the capacitance per unit length of a lossless uniform transmission line, immersed in a lossless medium, is well known and has been used to obtain the characteristic impedance of coaxial and strip lines by relatively simple low-frequency bridge measurements. For these transmission lines one need only make the line of sufficient length to insure that the fringing capacitance at the end of the line is negligible compared to the total capacitance of the sample.

If an attempt is made to measure the capacitance between the arms of the biconical line using the same procedure, it immediately becomes obvious that the end effect is a constant. The size of the arm end increases in proportion to the length of the arm. The fringing capacitance at the end of the finite length biconical line can be controlled, however, by resorting to an extension of the guard technique as used for the precise measurement of parallel plate capacitors, and converting the biconical line into a three-terminal capacitance.

* Manuscript received by the PGAP, January 6, 1958. This work was supported by the Wright Air Development Center under contract no. AF 33(616)-3220 and is treated in more detail in Tech. Rep. no. 29, January 10, 1958, Antenna Lab., University of Illinois, Urbana.

† Antenna Lab., Dept. of Elect. Eng., University of Illinois, Urbana, Ill.

¹ R. L. Carrel, "The characteristic impedance of two infinite cones of arbitrary cross section," TRANS. ON ANTENNAS AND PROPAGATION, vol. AP-6, pp. 197-201; April, 1958.

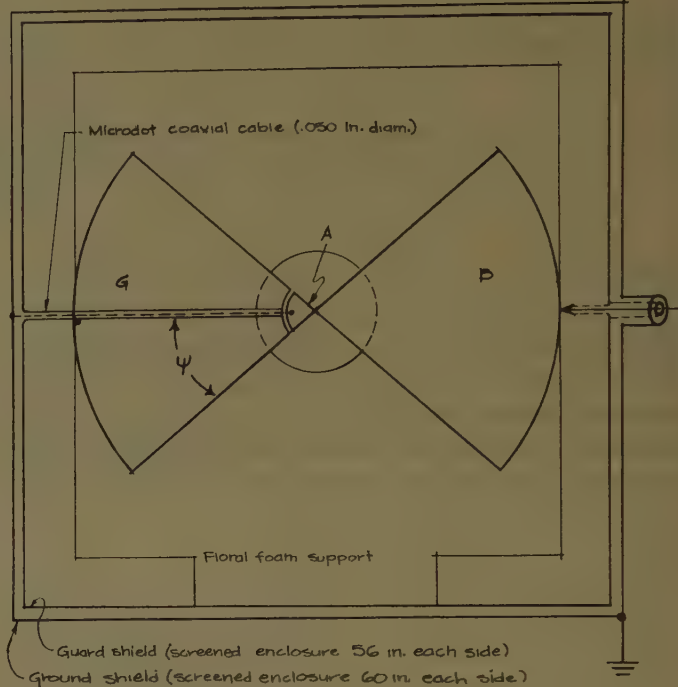


Fig. 1—Biconical line mounted in double shielded enclosure.

The electric field lines lie along a spherical surface, hence if a gap is cut in one arm sufficiently far from the end, as in Fig. 1, and if at the moment of balancing the bridge the two arm segments *A* and *G* are brought to the same potential, the field lines will be undistorted beyond the gap. By the same bridge techniques employed with the normal parallel plate capacitor it is possible to isolate the capacitance between the guarded segment of the arm, segment *A*, and an equivalent area of arm *B* from the capacitances C_{BG} and C_{AG} . Thus it is possible to measure the capacitance of this guarded length without fringing effects, and from this to calculate capacitance per unit length and the characteristic impedance of the structure.

This method of measuring the capacitance is applicable to all of the structures previously mentioned which are characterized by a constant capacitance per unit length. Measurements were confined, however, to structures with fin shaped arms.

EXPERIMENTAL RESULTS

A coplanar fin shaped transmission line was constructed of 0.015-inch cold rolled copper and supported by a two-inch thick sheet of "Floralfoam." The foam material was cut away from the guarded portion of the

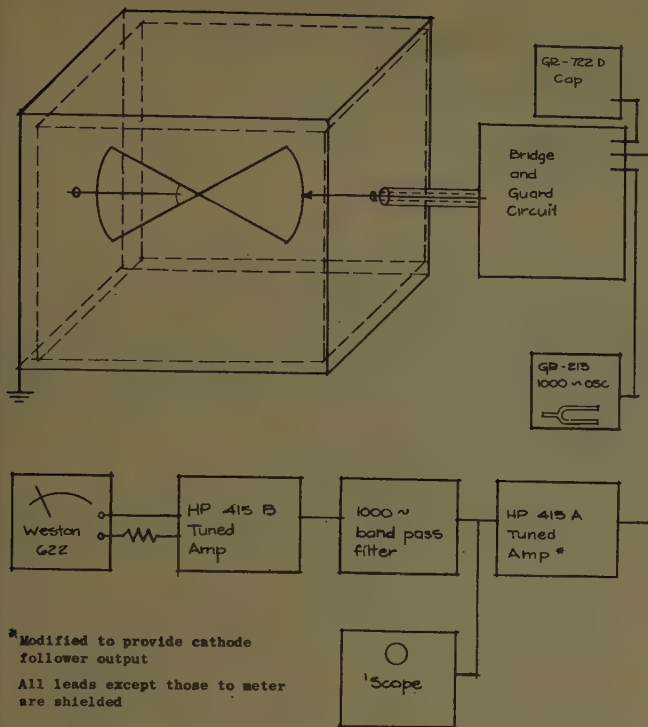


Fig. 2—Block diagram of equipment.

arms, and the structure shielded as in Fig. 1. The capacitance of the guarded line was measured with a bridge and guard circuit (equivalent to a General Radio Type 716-C capacitance bridge and Type 716-P4 guard) as indicated in Fig. 2.

The total arm length was constructed to be 21 inches and the guarded portion was varied in length to determine the effect of the guard. It was determined that as long as the guarded portion was approximately 9 per cent or less of the total arm length the capacitance per unit length appeared constant, indicating a normal distribution of the electric field in this area. A guarded arm length of one and one-half inches was chosen as providing sufficient capacity to be accurately measured and still be adequately guarded. The capacitance of this guarded line was measured for lines of half-angular width from 15° to 85° .

The impedance based upon the measured capacitance per unit length of the balanced coplanar fin line is shown in Fig. 3. The measured values agree within 1 per cent with Carrel's work for arms with γ ranging from 30° to 75° , and within 2 per cent for a half-angle of

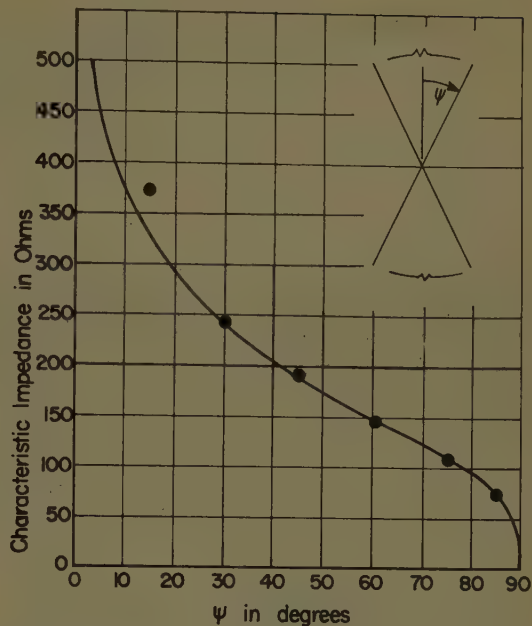


Fig. 3—Characteristic impedance of the infinite fin as a function of angular arm width.

0 = Values based on measured capacitance per unit length.
— = Theoretical values.

85° . However, the measured value has diverged from the theoretical value by approximately 9 per cent for a half-angle of 15° . This was traceable to a loss in the effectiveness of the guard as the arm became narrow. A longer guard arm and consequently a larger shielded enclosure should increase the accuracy of measurement in this region.

CONCLUSIONS

An extension of conventional guard techniques to structures such as the biconical transmission line of arbitrary cross section should provide an accurate method of measuring their capacitance per unit length. An application of the technique to the balanced fin transmission line provided measured results which were in good agreement with theoretical values.

ACKNOWLEDGMENT

The author is pleased to acknowledge several very helpful discussions with W. L. Weeks, and the assistance of R. L. Jones, of the Antenna Laboratory of the University of Illinois, who performed most of the measurements.

The Exact Solution of the Field Intensities from a Linear Radiating Source*

SHELDON S. SANDLER†

THE publication of a communication by Ghose¹ emphasizes the need for an adequate understanding of the historical background of this phase of the linear radiator problem, if only to avoid the needless repetition and republication of past work.

The exact relations for the electric field of a sinusoidal distribution of current were derived in closed form by Carter² in 1932 for antennas an integral number of half wavelengths long. The corresponding formulas for an-

tennas of any length were given by Brown³ in 1937. Thus the series approximations of Ghose were invalidated a quarter of a century ago! In 1937 Riazin⁴ expressed the complete field distribution for the linear radiator with sinusoidal current in elliptical coordinates, again in closed form. In passing, Ghose looks forward to the application of his approximate solution of the vector potential to the derivation of the self impedance of a single antenna and the mutual impedance of parallel arrays. However, calculated values of the self and mutual impedance for antennas with sinusoidal currents were displayed by Carter in 1932 and by Brown in 1937.

* Manuscript received by the PGAP, October 13, 1958.

† Croft Lab., Harvard University, Cambridge, Mass.

¹ R. N. Ghose, "The exact solution of the field intensities from a linear radiation source," IRE TRANS. ON ANTENNAS AND PROPAGATION, vol. AP-5, pp. 237-238; April, 1957.

² P. S. Carter, "Circuit relations in radiating systems and applications to antenna problems," PROC. IRE, vol. 20, pp. 1004-1041; June, 1932.

³ G. H. Brown, "Directional antennas," PROC. IRE, vol. 25, pp. 78-145; January, 1937.

⁴ P. Riazin, "Sur le calcul du rayonnement d'une antenne rectiligne à petite distance," Tech. Phys. U.S.S.R., vol. 4; 1937.

CORRECTION

H. Unz,† author of "Determination of a Current Distribution over a Cone Surface Which Will Produce a Prescribed Radiation Pattern," which appeared on pages 182-186 of the April, 1958 issue of these TRANSACTIONS, has informed the editors that a slight error was introduced in his paper due to a mistake in one of the references. The Gegenbauer integral in (20) should be

$$\int_0^\pi e^{ikR \cos \alpha \cos \theta} J_m(kR \sin \alpha \sin \theta) P_n^m(\cos \theta) \sin \theta d\theta \\ = 2i^{n-m} j_n(kR) P_n^m(\cos \alpha). \quad (20)$$

It may be found in this form in Morse and Feshbach.¹

† Rad. Lab., University of Michigan, Ann Arbor, Mich. On leave from University of Kansas, Lawrence, Kan.

¹ P. M. Morse and H. Feshbach, "Methods of Theoretical Physics," McGraw-Hill Book Co., Inc., New York, N. Y., pp. 1467 (11.3.49) and 1575; 1953.

it may be transformed into this form in Magnus and Oberhettinger,² or in Watson,³ and Whittaker and Watson.⁴ In Stratton,⁵ which was used as a reference in the original paper, the factor i^{n-m} is missing in (20). It is considered worthwhile to mention it since the Gegenbauer integral is quite useful. Due to this correction to (20), i^{n-m} should be omitted in (21), (24), and (30) in the original paper.

² W. Magnus and F. Oberhettinger, "Special Functions of Mathematical Physics," Chelsea Publishing Co., New York, N. Y., p. 77; 1954.

³ G. N. Watson, "Bessel Functions," Cambridge University Press, Cambridge, Eng., 2nd ed., p. 379 (1); 1952.

⁴ E. T. Whittaker and G. N. Watson, "Modern Analysis," Cambridge University Press, Cambridge, Eng., 4th ed., p. 329; 1952.

⁵ J. A. Stratton, "Electromagnetic Theory," McGraw-Hill Book Co., Inc., New York, N. Y., p. 411 (69); 1941.

Fall Meeting of International Scientific Radio Union

October 20-22, 1958

Pennsylvania State University

Statistical Methods in Radio Wave Propagation—W. C. Hoffman, *The RAND Corporation*—The role of statistical methodology in radio wave propagation is delineated. Statistical considerations arise in radio propagation in two ways. The first involves a combination of physical and statistical structure, as, *e.g.*, in turbulent scattering, meteor burst signals, and scattering from a rough earth. The second context occurs when there are uncontrolled factors in radio propagation research, *e.g.*, meteorological parameters in tropospheric radio propagation and fading on an ionospheric signal path.

Applications of statistical techniques to ionospheric and tropospheric radio propagation, radio noise, radio astronomy, and communication theory are outlined. Among the more significant of these applications are the determination of ionospheric drifts, the estimation of power spectra of auroral flutter and transhorizon scattered signals, the phenomenon of deep fading in tropospheric propagation, antenna tolerance errors, and information theory. Special statistical distributions, such as the Rayleigh and lognormal, are described and the problems these distributions present in practice are considered. Certain other probabilities and statistical techniques of particular merit, such as distribution-free methods, the theory of random processes, and the statistical design of experiments, are described in detail. The paper closes with a brief survey of instrumentation designed for the rapid statistical processing of radio data.

On Scattering of Waves by Random Distributions of Tenuous Objects—V. Twersky, *Sylvania Electronic Defense Laboratory*—We consider a plane wave exciting a uniformly random distribution of objects with dielectric constant near unity. Coherent multiple scattering is taken into account to obtain the resultant average field (the coherent scattering) and the corresponding differential scattering cross section per unit volume (the incoherent scattering). For the coherent part of the problem, we use a self-consistent procedure such that each scatterer within the distribution is excited by the coherent field; for the incoherent, the field which excites a scatterer is attenuated in traveling to its location, and the contribution of the scatterer is further attenuated in getting out of the "average medium." The essential features of the predicted coherent field, and of the forward incoherent scattering, are in accord with experiment* down to average spacings between scatterer centers less than one and one-half diameters.

Aeronomic Conditions in the Thermosphere†—M. Nicolet, *Ionosphere Research Laboratory, The Pennsylvania State University*—Above the mesopause (85 ± 5 km), there is a change in the composition and the structure of the atmosphere concurrent with a rapid increase of temperature with altitude. This variation is due, first, to the partial dissociation of oxygen and, secondly, to the diffusion of the constituents.

As the dissociation of molecular oxygen begins to occur, for increasing height levels, in the lower thermosphere, one is no longer free to assume a constant molecular mass. Furthermore, comparing possible concentrations of atomic oxygen between 100 km and 110 km, two extreme values may be found. The downward transport leads to $n(O) = n/2(N_2)$ and the photochemical equilibrium conditions to $n(O) = 2n(N_2)$. Instead of the constant ratio generally adopted $n(O) = n/2(N_2) - 2n(O_2)$, it is necessary to consider $n(O) \approx n(N_2)$.

Absolute times of diffusion are derived for the redistribution of a constituent due to mixing. Characteristic times describe clearly how concentration changes occur in the thermosphere under the continuous effect of diffusion. In the light of the results, it is safe to consider that, in the thermosphere above 110 km, all sufficiently inert and neutral constituents are subject to a diffusion equilibrium. Thus, the density in the thermosphere depends on a varying molecular mass decreasing rapidly according to the increasing ratio of atomic oxygen and molecular nitrogen concentrations.

Ionospheric data, rocket and satellite observations have shown that the temperature gradient must be very large in the thermosphere up to the highest altitudes. It appears that sufficient energy may be supplied to the thermosphere from two sources: at the lowest levels up to the F_2 peak by solar radiation and in the whole thermosphere by conduction from the coronal gas to the terrestrial gas.

A general picture of the behavior of the thermosphere is obtained. The thermosphere above 150 km may be described now as an atomic oxygen atmosphere subject to a conduction equilibrium. Hydrogen atoms, because of the small decrease of their density with height, must play a role at sufficiently high altitudes, *i.e.*, 900 km. Densities are not less than 10^{-15} gm/cm³ at 500 km and the atomic oxygen concentration is more than 10^9 atoms/cm³ at 300 km.

Developments in Radio Astronomy as Shown by the Paris-Moscow Meetings—

K. M. Siegel, *Department of Electrical Engineering, University of Michigan*, and F. T. Haddock, *The Observatory, University of Michigan*—The Paris Meeting concerned the lunar atmosphere, and radar reflections from the moon, structure of the solar corona, observations of the quiet and disturbed sun, solar flares and sunspots, radio emission from the planets, extra galactic radio sources, the 21-cm line, and the radio source surveys and then attempted to associate radio sources with optical objects.

The author's visit to the USSR is discussed in detail.

Propagation Characteristics of 2.15 MM Radio Waves—C. W. Tolbert, C. O. Britt, and A. W. Straiton, *Electrical Engineering Research Laboratory, The University of Texas*—This paper describes radio propagation measurements made at a wavelength of 2.15 millimeters over paths from 0.69 to 1.5 kilometers in length. Data on absorption by atmospheric gases and on fluctuations of signal level due to atmospheric anomalies are presented.

At an elevation of approximately one-fourth kilometer, the atmospheric attenuation is primarily due to water vapor. The range of the water vapor content of the atmosphere during the measurement period was not sufficient to accurately determine the y intercept of the absorption curve plotted as a function of water vapor pressure.

The slope of this curve was, however, obtainable with fairly high precision and found to be 0.25 db per kilometer per gram per cubic meter. This value is approximately ten times that predicted by Rogers from the commonly accepted line breadth constant.

A comparison of the water vapor loss with previous measurements made by this Laboratory at other millimeter wavelengths shows that the deviation from Rogers' calculations increases progressively as the frequency increases.

Mean-Squared-Error of a Band-Limited Long Line-of-Sight Radio Link Affected by Atmospheric Turbulence†—D. S. Bugnolo, *Columbia University*—One possible measure of system reliability in the presence of atmospheric turbulence is the notion of fidelity in a mean-squared sense. Given an arbitrary input $x(t)$ and the output $y(t)$, the fidelity is defined as

$$v = [x(t) - y(t)]^2.$$

This paper is concerned with the prediction of system fidelity as an application of the general theory of scattering for arbitrary in-

* C. I. Beard and V. Twersky, "Propagation through random distributions of spheres," 1958 WESCON CONVENTION RECORD, pt. 1, pp. 87-100; a large-scale dynamical model of a "gas" of 1.36³ styrofoam spheres ($\epsilon = 1.032$) was measured at 60 km.

† This research was supported in whole or in part by the United States Air Force under Contract No. AF(638)-350, monitored by the Air Force Office of Scientific Research of the Air Research and Development Command.

puts.* The results will be applied to the special case of a long line-of-sight radio link.

It will be shown that the fidelity in a mean-squared sense of a band-limited long line-of-sight radio link is directly proportional to the bandwidth.

The Phase Instability in a Microwave Ground Link—R. N. Ghose, *Ramo-Woolridge Corporation*—Tropospheric inhomogeneities and the presence of the ground plane cause multipaths for wave propagation in a microwave ground link. Since the path conditions change with time due to tropospheric turbulences, the resultant signal at the receiving station changes in amplitude and phase with respect to time. For certain communication systems, it is desirable to reduce the phase variation of the received signal only, since the system performance depends only on the phase difference between the transmitted and received signals and not on its amplitude variation.

The problem of the phase fluctuation or the phase instability of a signal in a microwave ground link has been studied in this paper. Attempts have been made to determine the maximum and expected phase fluctuation due to various tropospheric conditions.

The most commonly occurring multipaths in a ground wave link are 1) the direct path between the transmitting and receiving antennas, and 2) the ground reflected path, both lying within the turbulent troposphere. It appears that, for such links, the maximum phase variation and its rate of change with respect to time depends on the reflection coefficient of the terrain. An upper bound of this reflection coefficient is determined by using Huygen's principle. The maximum and expected values of the phase fluctuations and their time derivatives have been estimated for various statistical properties of the ground.

An analysis for determining the expected level of the received signal in a microwave ground link in the presence of two and three independent tropospheric multipaths by using the principles of random walk is also included in the paper.

Tropospheric Motions Observed in Rapid Beam-Swinging Experiments†—A. T. Waterman, Jr., *Stanford Electronics Laboratories, Stanford University*—Through the use of a phased array, a narrow antenna beam can be swung rapidly and in quick succession through a limited sector. This technique has been employed in microwave transhorizon propagation experiments‡ to observe rapid changes in atmospheric structure. A 0.5-degree receiving-antenna beam is swung through a 4.2-degree azimuthal sector facing in the direction of the distant, broad-beam transmitter at a rate of 10 times per second. The received signal takes on a variety of forms, some indicating multiple discrete angles of arrival and some just one, some showing rapid changes with time and others altering more slowly.

* D. S. Bugnolo, "Correlation Function and Power Spectrum of Scatter Propagation Links for Arbitrary Inputs," *Columbia University Research Rep., AFORS TN-58-463, ASTI 158 270*.

† The research reported in this paper was made possible through the U. S. Signal Corps under Contract DA36(039)sc-73151.

‡ Reported by the author at the URSI Spring Meeting, Washington, D. C.; April 26, 1958.

Further measurements of this nature are reported, with particular emphasis on their implications as to atmospheric motions.

Power Spectra of Temperature, Humidity and Refractive Index from Tethered Balloon Measurements—E. E. Gossard, *U. S. Navy Electronics Laboratory*—Measurements of fluctuations of temperature, humidity, and refractive index taken by tethered balloon are described and compared with aircraft refractometer data. Point spectra are computed at 500-feet intervals up to an altitude of 3000 feet MSL. Spectra taken under stable and unstable conditions are compared, and the various proposed spectral power laws (3/2, 5/3, 7/3, 9/3) are discussed. Ensemble data taken with a microwave refractometer in an SNB-5 aircraft are described, and spectra taken within stable layers are compared with those taken under unstable conditions.

Transhorizon UHF Radio Field Characteristics as a Function of the Meteorological Scale of Influence—W. F. Moler, *U. S. Navy Electronics Laboratory*—Results of correlation between transhorizon radio signal characteristics and meteorological parameters are presented.

Median signal strengths for periods of the order of days are best correlated with the macrosynoptic meteorology of the middle and upper troposphere. The superposition of time-dependent mesoscale synoptic regimes upon a nearly constant macroscale regime may result in fades or signal enhancement of the order of hours or minutes.

A mesoscale streamline analysis of airflow over Southern California coastal waters shows that minor cyclonic or anticyclonic eddies which have strong effects upon scattered propagation radio fields may develop in a macroscale homogeneous air mass. The effects of the eddies upon radio fields appear to be independent of their location over the radio link, indicating the possibility of multiple scattering events as the propagation mechanism rather than single scattering at midpath.

Radar Terrain Cross Section at Microwave Frequencies—D. R. Bianco and C. S. Morris, *Applied Physics Laboratory, The Johns Hopkins University*—An experimental study is being made of the radar cross section of various terrain types such as grassland, trees, cropland, and sand.

The system utilizes a 1000-cps modulated klystron, phase-sensitive lock-in detector, and separate receiving and transmitting antennas at X , K_u , and K_a band frequencies.

The power returned from the terrain is measured relative to that returned from a calibrated standard Luneberg lens reflector. This is accomplished by reading the settings on attenuators which are adjusted manually so as to cause the power received from the terrain to equal that received from the Luneberg lens reflector. This technique completely avoids the difficulties inherent in measuring absolute power.

The results will be presented and preliminary interpretation in terms of theoretical models discussed.

Precipitation Static on Modern Aircraft—P. W. Couch, *Communication and Navigation Laboratory, Wright Air Development Center*—Aircraft frequently encounter strong

low- and medium-frequency radio interference when flying through precipitation. Radio reception aboard the aircraft is often completely masked or badly degraded at frequencies below 30 mc; VHF reception is occasionally affected. The noise is broadband with a continuous spectrum, and produces a loud hissing noise, very similar to shot-effect noise, in the receiver output. Because it appears when flying through precipitation, the noise has been termed "precipitation static" in the United States and England; in Germany it has been termed "hissing static."

Three different processes can contribute to the total noise. The basic phenomenon underlying all of these processes is the acquisition of electric charge by precipitation particles when they are struck by the frontal surfaces of an aircraft. Current flow charges the airframe to a voltage sufficient to establish discharge currents in equilibrium with the charging current. The process by which charge is transferred from a highly electrified conductor to a surrounding gas, corona, is responsible for most of the noise encountered on older types of aircraft, and is also the source of much of the noise on jet aircraft. Modern aircraft frequently employ antennas mounted underneath exterior surfaces of dielectric material. When these substances are exposed to particle impact, charge deposited on the insulating surface accumulates until flashover to the airframe occurs. This process, called "streaming," produces strong pulses at fairly low repetition rates, which can couple noise into antennas underneath, or close to, the dielectric surface. Antennas underneath dielectric surfaces are also exposed to the electric field of charged particles on the dielectric surface. If the surface is exposed to particle impact, the very abrupt change in particle charge and voltage at impact can induce noise pulses in the antenna. Interference generated in this fashion has been termed "particle impact noise." The magnitude is much smaller than noise from antenna corona and from streaming, and the intensity decreases more rapidly with increasing frequency.

Relation of speed to charging, discharging, and noise levels, and the effectiveness of corrective measures, will be discussed in this paper.

On the Electrostatic Theory of Lightning Discharges—H. W. Kasemir, *U. S. Army Signal Engineering Laboratories*—The lightning channel is substituted for by a very thin prolonged spheroid. For any given field pattern of the thundercloud the charge distribution along the lightning channel and the field distortion are calculated. Very simple approximative formulas are derived for the channel capacity, the charge distribution, the displacement, and the net charge destroyed by a lightning stroke.

The different field variations on the ground are discussed. It will be shown that the electromagnetic theory of transients on long transmission lines can be applied to the main stroke of the cloud-to-ground discharge. In this way, characteristic features of this discharge mechanism like the speed of the traveling wave or reflections on branch points or the top of the lightning

stroke can be calculated from the geometrical dimension of the lightning and vice versa.

Amplitude Probability Distribution Measurements of Atmospheric Radio Noise from 13 KC to 20 MC—W. Q. Crichtlow, C. J. Roubique, and W. M. Beery, *National Bureau of Standards*—A method for converting the three moments of atmospheric radio noise measured by the ARN-2 recorder into an amplitude probability distribution was needed. In order to obtain data from which to develop an empirically derived graphical method, a distribution meter was constructed which when used in conjunction with the ARN-2 recorder allows simultaneous measurements to be made of the three moments (average power, average voltage, and average logarithm of the voltage) and the amplitude probability distribution over the range of 13 to 20 mc. The percentage of the time any level is exceeded is read directly, for a 100-db range of levels in steps of 2 db or more. The time duration of each statistical sample may be automatically preset within one second over a range of one second to one hour.

Representative distributions at eight frequencies are presented, with a discussion of their characteristics.

A Graphical Method of Obtaining Amplitude-Probability Distributions from Statistical Moments of Atmospheric Radio Noise—W. Q. Crichtlow and A. D. Spaulding, *National Bureau of Standards*—Methods of converting the three statistical moments of atmospheric radio noise measured by the ARN-2 recorder (average power, average voltage, and average logarithm of the voltage) into amplitude-probability distributions have been investigated. Using available data, an empirically derived graphical method was developed which has proven to be quite accurate.

This graphical method and its development are presented along with representative predicted and measured distributions at eight frequencies.

Some Unusual Features of the Tornado Oscillator that Accompanied the Blackwell Tornado—H. L. Jones, *Oklahoma State University*—New information has been obtained relative to the tornado oscillator. The data obtained from the tornado oscillator of the Blackwell tornado of May 25, 1955 are being reexamined in order to evaluate the number of surges per second during the actual periods of activity of the oscillator. Since each individual surge resulted in a directional pip on the 150-kc static direction finder, the directional pips from the Blackwell oscillator can be readily identified from the film records.

In some instances the surge rates were found to be greater than 40 directional pips per second. The results from these studies may provide possible clues to the fundamental nature of the tornado oscillator.

Recent Results from the Whistler-West IGY Program—R. A. Helliwell, J. H. Crary, R. L. Smith, and W. T. Kreiss, *Radio Propagation Laboratory, Stanford University*—Synoptic data from ten IGY whistler stations located in the Pacific area are beginning to come in. A preliminary analysis of some of the data shows the following interesting features:

- 1) On occasion, whistlers observed simultaneously at Stanford and Seattle appear to trigger bursts of strong chorus observed only at Seattle.
- 2) "Nose" whistlers have been observed at Stanford with nose frequencies ranging from 6 to 35 kc.
- 3) Whistlers have been observed simultaneously at stations separated as much as 4100 km.
- 4) Pure-toned whistler components are usually observed only at one station.
- 5) The low frequency cutoff of whistlers appears to vary with time of day.
- 6) Whistlers with echoes up to 20 kc have been observed, indicating that round-trip observation of whistler-mode signals from VLF stations should be possible.

These results will be illustrated and discussed.

Propagation of Electromagnetic Waves Along a Columnar Ionic Irregularity—F. H. Northover, *Carleton University, Canada*—Recent studies lend support to the theory that whistling atmospherics are caused by lightning flashes, the electromagnetic energy radiated by these being guided along discrete columnar ionic irregularities which follow approximately the lines of force of the earth's magnetic field. The present paper examines the type of waves which can be guided by such columns, both for columns with a central ionic surplus and for columns with a central ionic deficiency. It is found that guiding can take place over well-defined frequency ranges and that there is a low frequency cutoff for the former type of column. It appears necessary to suppose the coexistence of both types of column in order to explain by this means the relatively wide band of frequencies that are observed in the whistling atmospherics.

Effect of Antenna Beamwidth and Upper-Air Wind Velocity on Fading of 4 KMC Waves Propagated Beyond the Horizon—D. C. Hogg and L. R. Lowry, *Bell Telephone Laboratories*—Measurements and a simple theory of the short-term fading of microwaves propagated beyond the horizon are discussed. The results show that the rate of fading is governed mainly by the horizontal beamwidths of the antennas employed and by the horizontal drift winds in the atmosphere. A formula for the fading rate is calculated on the basis of the Doppler shift introduced by horizontal drift of numerous small layers randomly positioned throughout the atmosphere.

$$R = \frac{1.27}{\lambda} V_n \frac{\beta_t \beta_e \beta_r}{\sqrt{\beta_e^2 \beta_r^2 + \beta_t^2 \beta_r^2 + \beta_t^2 \beta_e^2}} c/s$$

where V_n is the component of the drift wind normal to the path; β_t , β_r are the horizontal beamwidths of the antennas; and β_e is the effective horizontal scattering angle of the atmosphere. This formula is found to agree well with measurements using antenna beamwidths of various sizes. Calculations using upper-air wind data obtained by the U. S. Weather Bureau in the above formula compare favorably with the experimental data.

* This work was supported in part by AF Contract 18(600)-572.

Comparison of Short-Term Fading at 4110 and 460 MC in Propagation Beyond the Horizon—D. C. Hogg and L. R. Lowry, *Bell Telephone Laboratories*—The rate of fading of signals propagated over a 171-mile path at 4110 mc is compared with that of signals propagated simultaneously at 460 mc. Antennas with approximately the same beamwidths at the two frequencies were employed. It is found that the ratio of the fading rates at the two frequencies at times is about nine times the ratio of the radio frequencies. However, often the ratio of the fading rates is 40 or 50. The high ratios usually occur during the early hours of the morning and are caused by very slow fading at 460 mc during these periods.

The ratio of fading rates is found to be correlated with the ratio of the median received powers at the two frequencies.

These results are interpreted in terms of the formation of large "wavy" layers during the early morning hours when the atmosphere is believed to be most stable.

Propagation into the Twilight Region by Guided Modes Contained in the Normal Air by Partial Reflections—T. J. Carroll and R. M. Ring, *Air Force Cambridge Research Center*—The whole set of modes guided around the earth by partial reflections contained in the gravitationally stratified inhomogeneous air of the troposphere and stratosphere supplies a simple understanding of twilight region propagation. Twilight fields, though weak and fading, are omnipresent and useful, and have low attenuation rates which make them observable many hundreds of miles beyond the horizon. Beyond the horizon, groups of modes corresponding to radiation inclined to the earth at somewhat different elevation angles within the antenna beams must be considered as phase incoherent, because of inevitable small perturbations of the phases and amplitudes of received modal fields, after guided propagation over long paths by air of refractivity which can never be considered to be completely static in time to more than about three significant figures. Within, near, and just beyond the horizon, these same guided modes contained in the air by partial reflection sum coherently to the same fields as given by classical 4/3 airless earth theory. In the twilight region beyond the horizon, the inevitable gradual onset of phase incoherence among the modes propagated by the real air is responsible for the continual fading of the resultant field, and an average level somewhat above the field of the single mode of maximum contribution by partial reflection, with take-off and arrival angle corresponding to the lowest lobe of the vertical polar diagram. The partially reflected ray from the postulated "escape height into free space" aloft is negligible especially for paths where this ray lies well outside the antenna beams. Transition from classical airless earth or completely coherent mode representations to the incoherent set of partially reflected modes responsible for the twilight region occurs a surprisingly short distance beyond the horizon.

Spectral Analysis of Dual Frequency Multirange Beyond-the-Horizon Microwave

† This work was supported in part by AF Contract 18(600)-572.

Scattered Fields—N. R. Ortwein, *U. S. Navy Electronics Laboratory*—Power spectra of *X*-band and *L*-band signals on three overwater beyond-the-horizon microwave paths are presented. Dependence on range, time, antenna aperture size, and frequency is shown. Spectra of off-axis scattered fields during synchronous beamswinging experiments are presented. Temporal and spatial auto- and cross-correlation functions, probability distributions, and fading rates which have been obtained are also discussed.

Dual-Frequency Multirange Overwater Measurements of Beyond-the-Horizon Microwave Scattered Field Strength—R. U. F. Hopkins, *U. S. Navy Electronics Laboratory*

—Tropospheric scatter propagation links using *X* band and *L* band were operated simultaneously on three overwater paths at ranges of 48, 144, and 190 miles. Experiments consisting of synchronized narrow-beam beamswinging, aperture comparison, and space correlation were performed at both frequencies and at three ranges. The results of the measurements of rapidly fading mean field strengths averaged over one minute samples are discussed. Methods of measurement and signal processing are also described.

Sweep-Frequency Studies in Beyond-the-Horizon Propagation—W. H. Kummer, *Bell Telephone Laboratories*—One of the questions in beyond-the-horizon propagation is the useful bandwidth of the propagating medium.

To study this problem, a frequency-sweep experiment was performed over a 171-mile experimental circuit. A 4.11-kmc transmitter was modulated at a 1000-cps rate over a 15-mc band. The receiver was swept nonsynchronously over the same band at a 30-cps rate. The resultant pulses were displayed on an oscilloscope and photographed at the rate of one frame per second.

The experiment used a 28-foot transmitting antenna and 8-, 28-, and 60-foot receiving antennas.

Sequences of selected sweep-frequency pictures will be shown for various antenna combinations and atmospheric structures.

The selective fading characteristics and bandwidth will be discussed.

Reciprocity and Scattering by Rough Surfaces—W. S. Ament, *Naval Research Laboratory*—Let a $y=0$ plane separate vacuum in $y>0$ from a granular, statistically described medium in $y<0$. The statistical problem is to estimate the specular reflection coefficient R and differential scattering cross section σ per unit area of $y=0$, source and observer being in $y>0$. Assuming that electromagnetic reciprocity holds for any fixed configuration of the material in $y<0$, we first obtain statistical reciprocity theorems for R and σ . In the standard self-consistent formulation of the problem, we then show that reciprocity is satisfied by the partial fields due to individual granules; this leads to approximate quasivariational expressions for σ guaranteeing its statistical reciprocity. We give sample results for 1) $y<0$ containing parallel, tilted, randomly spaced plates for two polarizations, 2) scalar waves and $y<0$ containing random isotropic scatterers. Some approximate results for case 2 are compared with the

exact results of Chandrasekhar's "Radiative Equilibrium," and compatibilities with requirements of the first two laws of thermodynamics are discussed. Finally, it is heuristically argued that short wavelength reflection and backscatter become independent of polarization in the grazing limit.

Early Results from the Equatorial Close-Spaced Chain of Vertical Sounding Stations

—R. W. Knecht and D. W. Schlitt, *National Bureau of Standards*—In order to study better the nature and extent of the ionospheric anomalies which occur in the magnetic equatorial zone, for the IGY a chain of five vertical sounding stations has been established.

Comparisons are made of 1) monthly median f_0F_2 at the chain stations, 2) electron density profiles along the chain, 3) occurrence of equatorial spread-*F* echoes, and 4) occurrence of equatorial-type sporadic *E* (E_{s-q}). Also the time of occurrence of equatorial E_s and its relation to lunar phase is shown.

Both the monthly median f_0F_2 and the electron density profiles show horizontal gradients of ion density across the magnetic equator in the late evening. The observed gradients are equivalent to a 2° to 3° layer tilt with the low end being to the north.

The frequency of occurrence of equatorial spread *F* and of equatorial E_s , and the strength of the equatorial E_s as indicated by f_0E_s were used to give measures of the width of the equatorial zone. Spread *F* gives a zone of 20° in dip centered at the dip equator. Both E_s parameters give a zone symmetrical about the dip equator 14° in width, which is about 400 miles in the north-south direction.

It is also found that the time in the morning when E_{s-q} first begins to be observed continuously at Huancayo seems to show a relation to lunar phase, E_{s-q} occurring earliest just prior to new and full moon.

Study of Vertical Drift in the *F* Region from True Height Profiles*—S. Chandra, J. J. Gibbons, and E. R. Schmerling, *Ionosphere Research Laboratory, The Pennsylvania State University*—The $W-f$ records of July and August, 1957 from four IGY stations (Washington, Panama, Huancayo, and Talaria) have been analyzed and presented in the form of diurnal plots of N at fixed real heights by Schmerling. The records exhibit large variations of N during night hours, indicating that the control is almost entirely by drift, and not by attachment. With this assumption the continuity equation can be integrated to give an expression for the vertical drift, v , which depends on measurable properties of the N curves, but contains a constant of integration v_0 which cannot be directly determined from the data. Assumption of a constant v gradient allows a determination of v_0 . In this case drift velocities of the order of $+15$ to -15 m/sec have so far been deduced.

Some Effects of Strong Blast Waves Upon the Ionosphere—F. B. Daniels and

A. K. Harris, *U. S. Army Signal Research and Development Laboratory*—The blast wave initiated by a nuclear detonation apparently causes a number of ionospheric phenomena that have been observed with a vertical-incidence ionosphere recorder. The phenomena include: 1) a signal return that has the characteristics of sporadic *E* but that moves upward through the *E* region at sonic velocity; 2) disturbances in both the *E* and *F* regions above the blast apparently associated with the shock front; and 3) disturbances in the *F* region, observed at some distance from the blast, the nature of which is greatly influenced by the direction of travel relative to the geomagnetic field, and exhibiting two distinct velocities.

Examples of some of these effects will be presented, including sequences of ionograms shown as a motion picture. Possible explanations will be given.

Rocket Studies of Arctic Ionosphere—

J. C. Seddon and J. E. Jackson, *U. S. Naval Research Laboratory*—Preliminary results are presented of ionospheric research conducted with Aerobee-Hi rockets fired at Fort Churchill, Manitoba, Canada. The electron density profiles are shown for three firings, a summer day, a winter day, and a winter night. The daytime profiles are quite similar to those measured over New Mexico at lat. 33° N. The one winter night flight showed very little ionization (less than 20,000 el/cc) up to 165 km. Above 190 km, spread *F* caused the data to be so complex that only qualitative statements can be made. Differential absorption was also measured on the two daytime flights during polar blackout conditions. The region between 60 and 70 km accounted for the bulk of the absorption at 7.75 mc. It was possible to compute in the *D* region the frequency of occurrence of electron collisions with neutral particles, with the surprising result that the collisions were a factor of three less than has been believed previously.

A Versatile Computer Program for Obtaining Refractive Indices and Polarizations from the Appleton-Hartree Equations†—E. A. Mechtly, L. M. Meixsell, and J. J. Gibbons, *Ionosphere Research Laboratory, The Pennsylvania State University*—J. M. Kelso (1951, Ionosphere Research Laboratory Report No. 24) has computed refractive indexes and polarizations at a fixed frequency of 150 kc and fixed geomagnetic latitude of $19^\circ 8'$ over a range of values of electron densities and collision frequencies by means of an IBM computer.

C. Ross and C. S. Fluke (1953, Wright Air Development Center Technical Report 53-96) have tabulated more extensive calculations of refractive indexes and polarizations over ranges of frequency as well, but also for the most part, at fixed geomagnetic conditions, by means of the OARAC computer.

The need has arisen for a computer program which will perform essentially the same computations as those of Kelso and

* The research reported in this paper has been sponsored by the U.S.A. National Committee for the IGY under Proj. No. 6.9 and by the Geophysics Research Directorate of the Air Force Cambridge Research Center, Air Research and Development Command, under Contract AF19(604)-1304, and in part by the Research Projects Office of the Army Ballistic Missile Agency, under Contract DA-36-061-ORD-577.

† The research reported in this paper has been sponsored by the Geophysics Research Directorate of the Air Force Cambridge Research Center, Air Research and Development Command, under Contract AF19(604)-1304, and in part by the Research Projects Office of the Army Ballistic Missile Agency, under Contract DA-36-061-ORD-577.

Ross-Fluke, but with the additional provision for variations in the geomagnetic conditions. Such a program has been prepared for the Pennsylvania State University digital computer PENNSTAC.

Another feature of the new program is a selective routine for extracting the square root of a complex number. This selective routine provides much greater accuracy than any of the possible fixed methods.

Comparisons of computations made on PENNSTAC with the Kelso and Ross-Fluke tables are made. Applications of the new program are outlined.

Coefficients for the Rapid Reduction of $h'-f$ Records to $N-h$ Profiles without Computing Aids*—C. A. Ventrice and E. R. Schmerling, *Ionosphere Research Laboratory, The Pennsylvania State University*—Tables of coefficients are presented by means of which $h'-f$ records may be readily reduced to electron density-height profiles without the use of computing aids. The ordinary ray trace is utilized. No special assumptions concerning profile slopes are made. Account is taken of the earth's magnetic field but collisions are neglected. The tables presented are for any station whose magnetic dip angles do not exceed 80°.

The sensitivity of these coefficients to magnetic dip angle and gyrofrequency is discussed. Sample $h'-f$ records are reduced by means of the coefficients and the results are compared with those from the Budden matrix method.

Prediction of Lower Frequency Limits for F -Layer Oblique Transmissions by Direct Ray and by Pedersen Ray—B. Fulton, O. Sandoz, and E. Warren, *Defence Research Telecommunications Establishment, Canada*—The sharp decrease in received signal strength at the low frequency end of direct ray trace and Pedersen ray trace of oblique transmission records is explained as due to reflections at lower heights in both cases. Either the up-going ray or the down-going ray from the F layer can be reflected from the E layer if the frequency of the ray is less than or equal to the MUF of the E layer for the region of entry and angle of incidence. A slider constructed on this principle, and satisfying the geometry of the oblique path, has been used on vertical ionograms to predict the cutoff of the direct ray. The calculated diurnal variation corresponds closely to the observed values for one-hop Ottawa-Saskatoon transmission and three-hop Ottawa-Slough transmission. CRPL LUF predictions are presented for comparison of the two methods.

In the case of the Pedersen ray trace, certain "high-angle" reflections are not possible because of previous "low-angle" reflections. Those "high-angle" reflections which are obscured depend on the height and density distribution of the F layer, and the transmission distance. A slider was obtained from theoretical considerations and was superimposed on vertical ionograms. The predicted oblique frequencies agree well with

observed values taken from the Ottawa-Slough records.

The Oblique Propagation of Long and Very Long Waves—Abnormal Phenomena Associated with Great Geomagnetic Storms—J. S. Belrose, *Defence Research Telecommunications Establishment, Canada*—During and after great magnetic storms the diurnal variations of the phase and amplitude of the skywave, of long and very long waves, are markedly abnormal. The *primary storm effect*, during the greatest intensity of the geomagnetic storm, shows in the radio data as an ionization storm in the nighttime lowest ionosphere. The radio waves show rapid, large, irregular fluctuations of amplitude and phase. The reflection conditions start to return to normal, after cessation of the magnetic fluctuations, until 3-4 days after the start of the storm when the nocturnal ionization in the lowest ionosphere is markedly enhanced. This anomaly can last for a period of 1-6 nights, with a gradual return to normal. An outstanding feature of this *after effect* is the "calmness" of the earth's magnetic field throughout the period which shows the greatest radio effects. The radio observations indicate that a change in the atmosphere, such as an increase in the negative ion content, must occur during this time.

Geometric-Analytic Theory of Transition in Electrical Engineering—E. F. Bolinder, *Electromagnetic Radiation Laboratory, Air Force Cambridge Research Center*—A geometric-analytic theory of transition is presented and applied to circuit theory. A transition from one state to another is represented in a complex plane by two points which, by the variation of a parameter, approach each other, coalesce, and then separate along trajectories perpendicular to the original trajectories.

Three analogous cases are treated:

- 1) movements of fixed points in the complex reflection coefficient plane by varying the frequency,
- 2) movements of saddle-points in the complex frequency plane by varying the time,
- 3) movements of poles in the complex frequency plane by varying the frequency.

In the analytic treatment the linear fractional transformation or Möbius transformation is used, which makes conformal graphical methods applicable in the geometric treatment. Such a method is, for example, the isometric circle method.

By stereographically mapping the complex plane on the Riemann sphere, it is shown that a transition can be represented in three dimensions by the movements of two straight lines, each being the polar of the other with respect to the sphere. The transition takes place when both lines are perpendicular and tangent to the sphere at a point corresponding to the transition point.

Inductive Probability in Radar and Communications—L. S. Schwartz, *College of Engineering, New York University*—In the classical approach to radar and communication problems a model for the long-term

statistics of the signal and the noise are assumed, and probabilities of error are computed for given decision parameters. This might be called the method of direct estimation of error probability. The assumptions and the resulting probabilities of error determine the integration time and the information rate consistent with a specified reliability of operation. The effectiveness of this method is dependent on how closely the actual and the assumed states of prior information agree. An alternate approach is to take observations and from the observations obtain an estimate of the probability of error for decision parameters which vary in response to changing conditions of operation. This might be called the method of indirect estimation of error probability. This estimate is then used to control the number of integrations and the information rate. To do this also requires certain prior information such as some knowledge concerning the degree of independence of the signal and the noise and concerning essential distinguishing features. This latter prior information will, however, be insufficient in general to compute probabilities of error. Therefore, the indirect method should be used where adequate prior information is unavailable.

Carnap has developed a system of inductive probability involving logical relations between propositions which seems well suited to the indirect estimation of error probabilities. This paper applies Carnap's concept of probability to the problem of controlling the number of integrations in radar and to adjusting decision threshold settings in communication systems, in accordance with observed data. The consequences to detection probability and information rate are examined. An illustrative application is made to radar and to a decision feedback communication system.†

Capacity of Channels with Memory—G. H. Myers, *Bell Telephone Laboratories*—Communications channels with memory are encountered in many practical problems, and are usually more difficult to analyze than than memoryless systems. Considerable interest has been aroused in the literature by such cases. The theoretical work by Feinstein, Khinchin, and Wolfowitz concerning the basic nature of such channels is analyzed. Methods for actually calculating channel capacity in these cases, such as those proposed by Muroga, Bellman, and Kalaba are presented, along with some recent work by the author on channels which have memory of previous outputs as well as of previous inputs.

Analytic expressions for the various entropies encountered in such channels, as well as the form of the capacity equation and methods for computing the capacity, are discussed.

On the Identity of Absolute Capacity and Ergodic Capacity of a Discrete Stationary Channel with Finite Memory—S. S. L. Chang, *College of Engineering, New York University*—In their investigations on the foundations of information theory, Khin-

† R. Carnap, "Logical Foundations of Probability," University of Chicago Press, Chicago, Ill.; 1950.

† B. Harris, A. Hauptschein, and L. S. Schwartz, "Optimum decision feedback systems," 1957 IRE NATIONAL CONVENTION RECORD, pt. 2, pp. 3-10.

* The research reported in this paper has been sponsored by the U.S.A. National Committee for the IGY under Project No. 6.9 and by the Geophysical Research Directorate of the Air Force Cambridge Research Center, Air Research and Development Command, under Contract AF19(604)-1304.

chin* and Feinstein have shown that for a stationary channel with finite memory, a set of signaling alphabets can be transmitted with as little error probability as desired at a rate up to the ergodic capacity† of the channel. Both authors expressed the opinion that the question is still unanswered whether information can be transmitted essentially error free at a rate larger than the ergodic capacity C_e .

The above question is answered in the negative by proving the following statement which obviously contradicts the definition of ergodic capacity: "If, from whatever source a set of N signals of length n can be generated such that either a) the set is transmitted error free and $N > 2^{nC_e}$, or b) as n approaches infinity, N approaches 2^{nC_e} , $C > C_e$, and the error probability approaches zero, holds, an ergodic source can be constructed with a higher rate of transmission through the channel than C_e ."

Some Practical Aspects of Signal-Compression Coding—A. E. Laemmel, *Microwave Research Institute, Polytechnic Institute of Brooklyn*—Most of the studies of digital codes in communication systems have dealt with the reduction of errors. While the fundamental principle of using message redundancy to reduce required channel capacity has been understood for some time, several subsidiary problems seem to have limited the application of these ideas to practice. It is the purpose of this paper to review what is known of compression coding itself, and also of the following related problems: prevention of increased susceptibility to channel errors, economy of coding apparatus, methods for message analysis to find the required redundancies, and the synchronization of coder and decoder.

On Synthesis of Information Networks—R. Ash, *Columbia University*—Consider the following problem. Given 1) a number of information channels, each with a specified capacity of information flow, and 2) a number of relay stations (or junctions). Find a topological arrangement of the channels (or elements of a connected graph with the specified weights) such that the maximum flow of information between any two junctions exceeds a specified constant. This problem is shown to be closely related to the synthesis problem of a linear connected graph with a specified cut set matrix. A synthesis procedure is demonstrated with examples.

The problem proposed in this paper is related to the work done by Elias, Feinstein, and Shannon.‡ However, the latter paper is concerned with the analysis of information networks, while the present paper indicates a method of synthesis for a certain class of networks.

Proofs of Some Network Theorems by Topological Formulas—S. L. Hakimi and W.

* A. I. Khinchin, "Mathematical Foundations of Information Theory" (English translation by R. A. Silverman and M. D. Friedman), Dover Publications, Inc., New York, N.Y.; 1957.

† A. Feinstein, "Foundations of Information Theory," McGraw-Hill Book Co., Inc., New York, N.Y.; 1958.

‡ Maximum rate of transmission taking over all ergodic inputs.

§ P. Elias, A. Feinstein, and C. E. Shannon, "A note on the maximum flow through a network," IRE TRANS. ON INFORMATION THEORY, vol. IT-2, pp. 117-119; December, 1956.

Mayeda, *University of Illinois*—The elementary transformation of the trees of a network is introduced to obtain the necessary and sufficient condition so that a polynomial in a network function may have missing powers. It is shown that the numerator of the transfer function is a polynomial which cannot have more than two successive missing coefficients, unless there are some factor cancellations with the denominator of the transfer function. This result is useful in topological synthesis where one must decide on the minimum number of vertices and geometry of the network. Furthermore it is shown that in transfer function synthesis sometimes surplus factors (*i.e.*, common factors of the numerator and denominator) are necessary. Using the topological formulas, an alternative and simple derivation of Fialkow and Gerst coefficient condition is obtained. Finally, frequency and magnitude scaling from a topological point of view are discussed. The object of the paper is to suggest the usefulness of network topology and especially topological formulas in a variety of problems related to network synthesis.

Angular Scintillations of Cassiopeia—B. Nichols and J. L. Rosson, *Cornell University*—Since November, 1957, measurements of the angular scintillations of the Cassiopeia radio source have been made at Ithaca, N. Y., at a frequency of 53 mc. Continuous observations have been made using traveling-wave antennas arranged as phase-switched interferometers on both North-South and East-West baselines, with 50 wavelength separations. The antennas are fixed but so designed that Cassiopeia remains in the antenna beam continuously. Angular measurements are made using a servo system which varies a time-delay unit so as to keep the source at an interferometer null.

Using the North-South interferometer system near lower culmination of the source, variations greater than 1.3 degrees of arc have been observed, with a maximum rate of change of 2.5 minutes of arc per second of time. Using the East-West interferometer system near upper culmination of the source, variations as high as 10 minutes of arc have been observed with a maximum rate of change of 0.4 minute of arc per second of time.

The amplitude of the interferometer pattern exhibits long-time decreases that cannot be attributed to the measuring system or to absorption in the ionosphere. These are undoubtedly due to the loss of phase correlation of the signals received at the two interferometer antennas. The decreases in amplitude are centered about lower culmination and are correlated with large variations in the angle of arrival.

Observations of the Zenith Angle Dependence of Radio Star Scintillations at Manchester, England and College, Alaska—C. G. Little, *Geophysical Institute, University of Alaska*—Observations of the zenith angle dependence of the scintillations of the Cygnus and Cassiopeia radio sources at Manchester, England and College, Alaska are discussed. The following effects are deduced from the data: 1) a marked increase in scintillation activity with magnetic latitude, 2) a decrease in the diurnal variation of scintillation activity with increasing magnetic latitude, 3) a dependence of the scintillation activity upon magnetic time, 4) an elongation of the irregularities along the magnetic lines of force, and 5) a reduction of the intensity of the scintillation activity of the Cassiopeia source, relative to the Cygnus source, owing to the larger angular size of the former. Some information on the magnitude of these different effects at the two sites is presented.

Comparison of Phase and Amplitude Radio-Star Scintillations with Other Ionospheric Phenomena—R. S. Lawrence, *National Bureau of Standards*—Simultaneous phase and amplitude measurements of Cygnus-A, made principally at 53 and 108 mc, show that the fluctuations in apparent position are usually, but not always, uncorrelated with those in apparent source amplitude.

The scintillations observed at Boulder are compared with ionograms taken simultaneously at Ellsworth, Neb. Ellsworth lies beneath a point where the line of sight from Boulder to Cygnus-A penetrates the 100-km level. In the comparison particular attention is given to spread *F* and sporadic *E*. The depth and rate of nighttime scintillations increase with both these phenomena and also with the minimum frequency at which the *F* region can be observed, but the correlation is far from perfect.

The relationship of these observations to the problem of determining the height of origin of scintillations is discussed.

Incoherent Scattering of Radio Waves by Free Electrons with Applications to Space Exploration by Radar—W. E. Gordon, *Cornell University*—Free electrons in an ionized medium scatter radio waves weakly. Under certain conditions only incoherent scattering exists. A powerful radar can detect the incoherent backscatter from the free electrons in and above the earth's ionosphere. The received signal is spread in frequency by the Doppler shifts associated with the thermal motion of the electrons.

On the basis of incoherent backscatter by free electrons a powerful radar, but one whose components are presently within the state of the art, is capable of

- 1) measuring electron density and electron temperature as a function of height and time at all levels in the earth's ionosphere and to heights of one or more earth's radii;
- 2) measuring auroral ionization;
- 3) detecting transient streams of charged particles coming from outer space;
- 4) exploring the existence of a ring current.

The instrument is capable of

- 1) obtaining radar echoes from the sun, Venus, and Mars, and possibly from Jupiter and Mercury;

¶ The research reported in this paper was sponsored by the Rome Air Development Center under Contract AF30(635)-2886 with Cornell University.

|| The analysis described in this paper was sponsored by the Rome Air Development Center of the Air Research and Development Command under Contract AF30(635)-2887.

** Now at the National Bureau of Standards, Boulder Laboratories, Boulder, Colo.

2) receiving from certain parts of remote space hitherto-undetected sources of radiation at meter wavelengths.

A Theory of Electrostatic Fields in a Nonhomogeneous, Nonisotropic Conducting Medium, with Application to the Ionosphere—D. Farley, Jr., *Cornell University*—A theory is developed to describe quantitatively the idea that, in an ionized gas subject to an imposed magnetic field, the lines of magnetic flux are approximately equipotential lines. With the ionosphere in mind, the case in which the gas is stratified perpendicular to the magnetic field is considered. The analysis shows that the variation of conductivity with height in the ionosphere strongly affects the electrostatic equations, in some cases more than the nonisotropy due to the magnetic field.

With a view towards elucidating the phenomena of spread-*F* and radio star scintillation, small-scale electrostatic fields are considered. For a reasonable model of the ionosphere, it is shown that it is possible, under certain conditions, for a horizontal electric field one kilometer or larger in extent, at a height of about 120 kilometers or greater, to produce a similar localized electric field in the *F* region not appreciably reduced in strength. The height of the source is a very important factor. The strength of the field in the *F* region may be reduced by as much as a factor of ten, in some cases, if the height of the source is reduced by 10 kilometers.

Evidence for a 200-MC Ionospheric Forward Scatter Mode Associated with the Earth's Magnetic Field*—J. L. Heritage, S. Weisbrod, and W. J. Fay, *Smyth Research Associates*—In July, 1958, two experiments were carried out to study the gross features of an ionospheric scatter mode observed at 200 mc in the southwestern United States. The transmitter is pulsed, high-powered, and transmits during alternate one-minute periods on one of two pencil beams, differing in azimuth by 5 degrees. The direction of transmission is southeast to northwest, and the hot spots, or areas of strong illumination in the *E* layer, are about 850 km from the transmitter.

Contours representing specular reflection from earth magnetic field lines passing through the hot spots were calculated. In the first experiment one mobile receiver was positioned on the specular contour for each beam. Both receivers were well south of the great circle paths. As the beams were switched, the level of the scatter signal changed in antiphase at the two receivers, suggesting that the scattered energy is fairly sharply peaked about the specular contour. The scatter signal was characterized by rapid fading, absence of a clear height-gain function at the receiver, and broad angle of arrival in azimuth.

The second experiment used one receiver on the great circle path and the second on one of the specular magnetic field contours. No scatter-type signals were observed on the great circle while the station located on the

magnetic contour showed the usual rapid fading scatter signals.

The Simultaneous Observation of Meteor Echoes over a 1250-KM Path at Two VHF Frequencies†—M. L. Meeks, J. C. James, and J. B. Berry, *Georgia Institute of Technology*—Simultaneous transmissions at 49 and 74 mc, originating at Walpole, Mass., were received at a site near Columbia, S. C., via scattering from meteor trails (and also by ionospheric scatter at 49 mc). Two entirely separate receiving systems were used on each frequency, and the four receiver outputs, together with the simultaneous differences in the two signals on each frequency, were recorded on a six-channel Edin recorder. The meteor-signal rates were compared for various combinations of antenna heights on each frequency, and the shapes of the recorded bursts were compared at these frequencies. No large effects of antenna height on average signal rate were observed even though the terrain in front of the receiving antenna was sufficiently flat and uncluttered to permit the formation of well-defined interference lobes. Height differences in the antennas, however, did decorrelate the peak amplitudes of the echoes from underdense trails. The decay time-constants were observed to be 2.2 times greater at the lower frequency as predicted by theory.

Wave Propagation Through Ionized Gases—F. J. Tischer, *The Ohio State University*—The theory of wave propagation through nonhomogeneous ionized gas is reviewed and plasma resonance discussed. Plasma resonance affects the wave propagation particularly in the case of small irregularities of ionized gas. The resonance effects cause scattering of the passing wave energy. Scattering cross sections are calculated and discussed for a number of interesting cases.

A Surface Wave Antenna Paradox—F. J. Zucker, *Air Force Cambridge Research Center*, and A. F. Kay, *Technical Research Group, Inc.*—Antenna engineers calculate the radiation pattern of a surface wave antenna by integrating the tangential field component of the surface wave over the length of the antenna. This results in a $\sin x/x$ -type pattern, which is perturbed by direct radiation from the feed. (Method I.)

An alternative method would be to start with an infinitely long antenna and, following Sommerfeld, calculate the direct feed radiation and the surface wave excited by the source. If the antenna is now made finite in length, the terminal discontinuity will diffract the incoming surface wave, the resulting radiation field interfering with that from the feed to produce the total antenna pattern. (Method II.)

We choose the simple two-dimensional case of a reactive strip embedded in an infinite ground plane, excited by a line source located above its center. Assuming equal excitation efficiencies of the source, the two methods should result in identical patterns.

This turns out not to be so. The two methods in fact imply entirely different mechanisms of surface wave antenna radiation, and lead to contradictory design principles for such antennas.

To resolve the apparent paradox, we show that turbulence in the surface field near the feed, which Method I neglects, plays an important part in forming the antenna pattern. This neglect accounts for the discrepancy between the two methods.

If, as is usually the case, the surface wave antenna is excited at one end instead of in the center, Method II needs to be modified. We indicate the nature of this modification, and also show why Method I, in spite of its serious shortcomings, nevertheless yields certain results that are useful in engineering design.

Four-Dimensional Antenna Systems—H. E. Shanks and R. W. Bickmore, *Hughes Aircraft Company*—This paper describes an entirely new and fundamental technique which has wide application to many fields of the antenna art as well as important system implications. It is the object of these concepts to provide an additional degree of freedom to the antenna operation which results in a greatly enhanced information handling capacity. In addition this technique allows synthesis of antenna radiation characteristics which might be unobtainable by conventional methods.

The essence of this philosophy is the utilization of the time domain as an additional variable with which to control antenna radiation characteristics. One way to accomplish this is by periodically time modulating one or more of the antenna parameters (aperture excitation, aperture shapes, frequency, phase distribution, aperture size, etc.) in a prescribed way. The result of this modulation is a radiation pattern whose characteristics are periodically changing as a function of time. By virtue of the periodic nature of the pattern fluctuations, an infinite number of independent information channels are available corresponding to the harmonic frequency components of the modulated patterns. Since each harmonic will, in general, have a different space factor associated with it, proper data processing can be utilized to provide simultaneous operation of a single antenna in a variety of modes.

The general theory is presented and is applied to such typical applications as: Simultaneous Scanning (Radar-Vision), Multi-Pattern Operation, Simultaneous Lobing, and Sidelobe Suppression. Mathematical details are discussed as well as important practical considerations, such as: system requirements, countermeasure capability, error analysis and possible physical configurations. Preliminary experimental results, verifying the general theory, are also presented.

A Reciprocity Relation for Nonperiodic Fields—G. Gouba, *Signal Engineering Laboratories*—A reciprocity relation will be derived which is applicable to electromagnetic fields of any time dependence. This relation formulates cross-correlation properties between two arbitrary fields $E_1(t), H_1(t)$ and $E_2(-t), H_2(-t)$ within a space free of sources. If both fields have the same time dependence factor $e^{j\omega t}$ the relation reduces to the well-known Lorentz reciprocity theorem. The relation may therefore be considered as a generalization of this theorem to nonperiodic fields. The generalized theorem

* This work was carried out under the sponsorship of Rome Air Development Center, Air Research and Development Command, Griffiss Air Force Base, N. Y., under Contract No. AF30(602)-1624.

† The research described in this paper has been supported by the Air Force Cambridge Research Center under Contract No. AF19(604)-1593.

is also applicable to fields of movable sources. Some applications will be discussed.

The Far Fields Excited by a Point Source in a Dissipationless Passive Anisotropic Uniform Waveguide—A. D. Bresler, *Microwave Research Institute, Polytechnic Institute of Brooklyn*—It is shown that when a point source is introduced into any dissipationless passive uniform waveguide at a point whose axial coordinate is $z=z^1$, then the far fields, $|z-z^1| \rightarrow \infty$, excited by this source will consist only of some superposition of propagating modes (*i.e.*, modes characterized by real propagation constants). If, as is often the case in anisotropic waveguides, the direction of the net power flow associated with a propagating mode is opposite to its direction of (phase) propagation, then it is shown that this mode contributes to the far field only in that direction for which the power flow associated with the mode is directed away from the source. The proof given is based on the known properties of the frequency dependence of the physical parameters of any linear passive system in which the causality restriction is satisfied.

The Calculation of Reflector Antenna Polarized Radiation—L. E. Raburn, *General*

Electric Company—A procedure is described for calculating the cross-polarized as well as the direct-polarized directive patterns of paraboloid reflector antennas. The two orthogonal components of the illumination field radiated by the primary feed are first assumed or measured. These components are assumed to propagate from a phase center point to the reflector surface and then into the aperture with new values which are calculated by simple trigonometric equations. The far-field patterns are then calculated by integration of these aperture plane fields. A practical example is given which employs integration by a limited number of elemental area-moments.

High-Frequency Diffraction of Electromagnetic Waves by a Circular Aperture in an Infinite Plane Conducting Screen—S. R. Seshadri and T. T. Wu, *Gordon McKay Laboratory of Applied Science, Harvard University*—The scattering of plane electromagnetic waves of wave number k by a circular aperture of radius a in an infinitely conducting plane screen of zero thickness and infinite extent is considered. An exact solution to this problem was obtained by the method of separation of variables of the

wave equation in oblate spheroidal coordinates. But the solution in the form of a series of eigenfunctions converges slowly at high frequencies. In this paper, the high frequency problem is treated in an alternate way and the asymptotic series for the transmission cross section is found up to the order $(ka)^{-5/2}$, for the case of normal incidence.

The formulation is based on the integral equation for the current induced on the shadow side of the screen. In this formulation the geometrical optics part separates out in a natural way in the expression for the transmission cross section. Two simultaneous integral equations are obtained for the two components of the current on the shadow side of the screen. The radial and the angular components of the current have simple dependencies on the angle variable and the integrals occurring in the kernels of the integral equations are approximated by an asymptotic evaluation with respect to the angle variable. The resulting simultaneous integral equations for the components of the current involve only the radial coordinate and are of the Wiener-Hopf type. These are solved by an iterative procedure using the Fourier transform.

Abstracts of Papers from the Region Three Technical Meeting

November 17-18, 1958—Atlanta, Ga.

ORGANIZED BY THE IRE HUNTSVILLE SECTION, CENTRAL FLORIDA SECTION, AND ATLANTA SECTION

MISSILE INSTRUMENTATION AND CONTROL I

Inertial Guidance of Ballistic Missiles, J. S. Farrior, *Army Ballistic Missile Agency*—A fantastically accurate, relatively simple, and entirely self-contained apparatus is being used to guide both long and short range ballistic missiles. This ingenious device, the Inertial Guidance System, contains precision instruments known as "accelerometers" which measure the missile accelerations in accurately known directions permitting on-board computation of the instantaneous velocity and distance traveled. Using this data, it is possible to derive path guidance signals in yaw and pitch and also thrust cutoff signals.

Telemetry Techniques for Satellite Vehicles, O. B. King, *Army Ballistic Missile Agency*—Data transmission systems for satellite vehicles involve the same factors associated with any communication link. In addition a number of additional parameters become of prime importance. In many instances a number of these requirements conflict directly. The paper outlines these problems and discusses techniques which have been evolved to provide workable solutions. To illustrate the practicality of these approaches representative component designs developed for satellite applications are described. In conclusion probable future trends are enumerated.

Spatial Attitude Control of Explorer I, F. Digesu, *Army Ballistic Missile Agency*—This report gives a derivation of the Euler equations governing the motion of the Jupiter C top (with its gyroscopic moments in pitch and yaw due to the rotating solid propellant 2nd, 3rd, and 4th stages) from the time of separation of the Redstone booster until firing of the solid stages for orbital injection of Explorer I at apex.

The derived equations are then used to show how Guidance and Control Laboratory designed a conventional control system which tilted and held the top unit in the prescribed firing direction for ignition at Stage II.

Also, a brief description of the computer set-up used in the Flight Simulation study of the in-flight dynamics of the top unit and the control system is given.

Finally, a comparison between predicted and actual (telemetered) flight control dynamics is offered as justification of the design philosophy followed.

The Importance of the Systems Concept in Missile Systems, S. L. Johnston, *Army Rocket and Guided Missile Agency*—The advent of the guided missile system, with its merger of many technical fields which formerly functioned separately, required that a new look be given to the interrelationships between these fields. Composition of a guided missile system is discussed and some of the interrelationships are considered, with principal attention being given to the guidance subsystem. Goals for the optimization of a guided missile are cited to show that no subsystem can be considered as a separate isolated item.

MISSILE INSTRUMENTATION AND CONTROL II

Performance of Copper Mandrel Potentiometers in AC Operational Amplifiers, H. H. Hosenstein, *Army Ballistic Missile Agency*—In ac analog computers which use suppressed carrier amplitude modulation, the gain setting of the operational amplifiers can be accomplished by means of a precision variable feedback resistance. If this variable feedback resistance consists of a multturn copper mandrel potentiometer, considerable phase errors result from the distributed capacity between resistance winding and copper mandrel. This paper presents an analysis of this effect, based on transmission line theory.

A simple method of phase error compensation is presented whereby the potential of the copper mandrel is held close to one-third the potential of the potentiometer slider with respect to the beginning of the resistance winding. A figure of merit of compensation is established. The stability of the operational amplifier with phase error compensation is discussed. Practical circuit configurations employing phase error compensation are presented.

By means of the modulation-equivalent method of analysis (reference 2), the effect of the distributed capacity of the copper mandrel potentiometer upon the amplitude and phase of the modulating signals is derived from the modulation-equivalent direct and quadrature transfer functions.

An Approach to the Data Transmission Problems of Ballistic Missiles, W. O. Frost, *Army Ballistic Missile Agency*—The paper begins with a brief description of some of the outstanding problems encountered in missile-to-ground data links. Some of the factors which make the problems different, and in most cases more difficult than other applications of telemetry, are mentioned.

The discussion then proceeds to the approach to these problems taken in the R and D versions of the Redstone and Jupiter Missiles. An account of the telemetry systems developed for these missiles is given with system and hardware descriptions. The paper concludes with a comparison of the old and new systems with emphasis on the miniaturization and other improvements that have resulted from state of the art advances and experience with the previous systems.

Transistor Circuits Alter Frequency Response of Magnetic Amplifiers, J. C. Taylor and C. L. Wyman, *Army Ballistic Missile Agency*—One of the most serious limitations of full-wave magnetic amplifiers is their relatively long time constant associated with the control winding. Furthermore, the variance of time constant with gain is so large that convenient compensating methods are quite difficult to employ. This problem has often led to the use of high-gain transistor (reference 1) or vacuum tube preamplifiers preceding the magnetic amplifier or one or more stages of half-wave amplifiers (reference 2), which are considerably more inefficient and are generally lower gain amplifiers.

This paper describes a simple and convenient means of employing transistors to shape the dynamic response of self-saturating magnetic amplifiers without disturbing the dc gain or adding additional drift problems. Thereby, the range of application of the efficient high-gain full-wave magnetic amplifiers is greatly extended. It should be mentioned that the techniques employed are general and are not limited to a given type of magnetic amplifier.

Operation Gaslight, D. D. Woodbridge and R. V. Hembree, *Army Ballistic Missile Agency*—The first recovery of a scaled Army Ballistic Missile Agency Jupiter nose cone was accomplished in August, 1957. A recovery fleet supplied by the Navy was in an excellent position to observe the nose cone as it re-entered the atmosphere. A member of ABMA's scientific staff was stationed on each ship to observe re-entry phenomena and the recovery operation.

In addition to these visual observations, a Navy photographer succeeded in capturing a few motion picture frames of the body, heated to incandescence, as it plunged through the atmosphere. Analyses of the reports of observers and the motion picture film indicated the practicality of a more extensive radiation measurement program of future re-entry tests.

The outstanding success of the August test with the Jupiter-C launched, scaled nose cone prompted the decision to proceed at once to recovery of a full scale Jupiter nose cone.

A Tracking Comb Filter for the Detection of Pulsed Signals in Noise, W. H. Todd, *Army Rocket and Guided Missile Agency*—A filter termed a "comb" filter has been utilized to effect an improvement in the signal-to-noise ratio in the detection of pulsed signals in noise. The "comb" filter, whose transfer function resembles the "teeth" of a comb, reproduced the steady state pulse train by passing the energy represented by the spectral lines of a repetitive pulse while providing zero transmission for other frequencies. However, if the received signal contains information in the form of phase variations, it is necessary that the filter be active or self-tuning. Such a filter, termed a tracking comb filter, has been mechanized and investigated in the laboratory.

The heart of the tracking comb filter is the phase lock loop which will detect and track a relatively weak, narrow-band signal in the presence of wide-band noise. The constant amplitude outputs of the active elements are weighted and summed to produce the output pulse. Noise at the input results in phase jitter of the reconstituted pulses. Jitter is investigated in terms of input signal-to-noise ratios.

An Experiment for Electron Density Determination by a Rocket Method, E. A. Mechtly, *Ionosphere Res. Lab., Pennsylvania State University*—Ionospheric sounding by the usual method of reflecting radio pulses from the ionosphere has revealed the electron density maxima of the D , E , F_1 , and F_2 regions, their gross structures, and their periodic variations. Because sounding pulses experience changes over

their entire path through the ionosphere and not only at specific heights, however, the information in reflected echoes reveals integrated effects from which only gross ionospheric structure can be deduced.

With the use of rockets, measurements at well-defined heights and determination of the details of ionospheric structure become possible.

Seddon and Jackson of the Naval Research Laboratory are currently probing the ionosphere with Aerobee rockets. The NRL experiment is limited, however, by the performance characteristics of the Aerobee.

The weight carrying capacity, stability, and altitude of more recently developed rockets offer advantages in their use as vehicles for ionospheric probes. The Ionosphere Research Laboratory is preparing instruments to probe the ionosphere. The object of this paper is to outline the technical aspects of the proposed experiments.

IONOSPHERIC PROPAGATION

Review of Radio Propagation Research Programs at the M.I.T. Lincoln Laboratory, J. H. Chisholm, M.I.T. Lincoln Laboratory—An extensive program of radio propagation research has been conducted over the past seven years by the M.I.T. Lincoln Laboratory with particular emphasis on the radio propagation factors related to the development of communications and radar systems for air defense. These propagation programs have been in the following general areas: 1) Studies of the communications capacity of tropospheric scattering at UHF and SHF over paths ranging from 200 to 830 miles in length. 2) Studies of the communications capacity of ionospheric scattering at VHF for both ground point-to-point and air-ground applications over ranges 1000 to 2000 miles. 3) Studies of the influence of auroral phenomena at VHF, utilizing radar backscatter and lunar reflections. 4) Studies of the reflections from meteor trails in the UHF band. 5) Studies of radio refraction in the earth's atmosphere. The results of these programs are discussed in relation to system applications and current theoretical models.

The Frontier of Space—The Ionosphere, A. H. Waynick, Pennsylvania State University—A summarization of the factors involved in ionospheric region formation and the current state of knowledge concerning the more important of these is attempted in this paper. The parameters considered include: effective solar radiations, their penetration into the earth's atmosphere, the neutral atmosphere and electron density-height profiles. Brief statements are made concerning future research needs in this field.

The Prediction of Meteor Echo Rates, M. L. Meeks, Georgia Institute of Technology—The meteor-echo rate has been observed to vary with the time of day, and this diurnal pattern, furthermore, changes slowly from month to month. In general the meteor rate is highest during the early morning hours and lowest in the late afternoon. However, the details of the diurnal pattern of rate variation depend on

parameters such as the geographical position of the meteor-scatter path, the antenna patterns, and the season.

The observed diurnal variations in meteor rate for several meteor-scatter paths have been predicted satisfactorily by representing the distribution of sporadic meteor radiants by means of a small number of point radiants. These computations, of course, can be made for meteor showers as well, and good agreement has been found with rate data taken during showers.

Radio Astronomy at Air Force Cambridge Research Center, J. P. Castelli, AF Cambridge Research Center—The radio astronomy section of the Propagation Laboratory of AF Cambridge Research Center has made atmospheric absorption, refraction, and scintillation measurements during the summers of 1956, 1957, and 1958 at 3.2 cm, 8.7 mm, 6.4 cm, and 10 cm using the sun as a signal source. Equipment used has been the "Dicke" type radiometer using superhet receiver at X and KA bands, and a traveling-wave tube tuned radio frequency receiver at C and S bands. A small radar altazimuth antenna mount, with relatively small dishes, and the drift technique for data recording were used in making the measurements.

Ionospheric Ray Tracing with Analog Computer, M. S. Wong, AF Cambridge Research Center—The equations of ray paths in the ionosphere, as given by Hamiltonian optics, are solved by an electronic differential analyzer. This computer has input-function devices capable of accommodating variations with height and horizontal distance of the electron-number density, and accommodating the earth's dipole magnetic field.

Ray patterns are obtained showing the spatial distribution of rays emitted from a radio transmitter, including cases when the rays are at arbitrary orientations with respect to the earth's magnetic field. Emphasis is on anomalous situations, for example those giving rise to extremely far reaching rays, and others giving rise to diminished ray density in some spatial regions. Results on deviations of initial angles and angles of arrival of the rays are also given by the computer.

The point of view is taken that the geometry of a system of rays, in a ray pattern, has an invariant meaning irrespective of whether the medium in which the rays occur is homogeneous or inhomogeneous. Caustics, cusps, and foci occurring in the ray patterns under ionospheric situations can be established in ray patterns in a homogeneous atmosphere with suitable conductive boundaries. The electromagnetic wave equations for this case of homogeneous atmosphere can be solved, and results obtained for the radio field intensity near caustics, cusps, and foci. These same results can be taken to apply, in a wave theoretically consistent way, for the corresponding entities occurring in the inhomogeneous, anisotropic ionosphere (where the wave equations are beyond solution by analytical methods). Also, the ray-tracing results can be wave theoretically supplemented where the reflection coefficient is under unity.

MISSILE RANGE ACTIVITIES

Management of Navy Technical Programs on a Tri-Service Range, R. F. Sellars, AF Missile Test Center—This paper is designed to point out types of management necessary in support of Navy technical programs on a tri-service missile range such as the AF Missile Test Center. It discusses cases in which conflicting administrative and technical management problems have been resolved satisfactorily. It gives an unclassified review of initial difficulties encountered in starting Navy missile programs, and how these difficulties were solved on the missile test range. Conclusions are drawn as to the most effective types of technical management to be followed in working with other military services on a joint missile range.

Telemetry Tomorrow, C. H. Hoeppner, Radiation Inc.—Recent advances in technology, the video-frequency magnetic tape recorder, the 60-foot automatic tracking antenna, the phase-locked discriminator, and solid-state pulse code modulation converters have opened new horizons in telemetry for both aircraft and missile testing. The trend of Telemetry Tomorrow is to place more sophisticated and extensive equipment on the ground and less in the vehicle. Always, there is the requirement for more channels at greater accuracies but this is being tempered with the realization that in many cases the data channel is not required all of the time and that many measurements do not require high accuracy. Greater versatility of telemetry is becoming apparent and a wider variety of equipment is being required. Pulse-code modulation telemetry is a reality and the choice of standard systems is imminent. A discussion of pulse-code modulation telemetry standards is treated in some detail.

Education and Training of Personnel for Nuclear Industry, J. Weil, University of Florida—(Abstract not available.)

Test Operations at the Atlantic Missile Range, P. T. Cooper, AF Missile Test Center—This will be an unclassified side presentation of missile test activities at the Atlantic Missile Range. Information will be given concerning the configuration of the test range, including the Cape Canaveral launching complex area, down range instrumentation stations and picket ships, and airborne recording stations. The various range instrumentation sites are needed for the tracking of test vehicles and acquisition of data from them. Instrumentation includes radar, telemetry, timing, optical, and CW tracking systems. The instrumentation sites are connected by elaborate networks of submarine cable, radio, and microwave communication circuits. In addition, various technical problems and features surrounding actual test operations will be outlined, as well as operational procedures, coordination between the various activities, etc. The need for and use of special equipment for range safety will be discussed.

Contributors

Robert E. Collin (M'54) was born in Donalda, Alberta, Can., on October 24, 1928. He received the B.S. degree in engineering physics from the University of Saskatchewan, Can., in 1951. The following two and a half years were spent in graduate work at Imperial College, London, England, from which he received the Ph.D. degree and the Diploma of Imperial College. Upon returning to

Canada, he worked for four years at the Canadian Armament Research and Development Establishment. In February, 1958, Dr. Collin joined the professorial staff of the Electrical Engineering Department at Case Institute of Technology. He is a member of Sigma Xi.

◆

A. A. De Carvalho Fernandes (M'47) was born on October 11, 1920, in Reigada, Portugal. He graduated from the school of electrical engineering at the Technical University of Lisbon, in 1943, and remained there as an instructor in electrical engineering. He became "professor catedrático" of applied electronics in July, 1956. He has simultaneously worked on the technical staff of Standard Eléctrica, an associated company of ITT. He became chief engineer in September, 1949, technical director in September, 1954, and managing director in May, 1957.

Mr. Fernandes has published several papers on transmission lines and antennas, and a book on rhombic antenna arrays.

◆

Peter Foldes (M'58) was born in Budapest, Hungary, on April 8, 1928. He received the B.S. degree in electrical engineering from the Technical University of Budapest in 1950. From 1950 to 1956 he was a research engineer at the Hungarian Telecommunication Research Institute and from 1953-1956, on a part-time basis, was also a lecturer on antennas at the Technical University of

Budapest. In 1957 he joined RCA Victor Co., Ltd., Montreal, Can. His work has been mostly in the field of antenna, propagation, and system engineering studies.

Mr. Foldes is a member of the American Institute of Electrical Engineers.

◆

J. R. Johler (A'47-M'55-SM'55) was born in Scranton, Pa., February 23, 1919. He received the B.A. degree from American

University, Washington, D. C., in 1941, and the B.S. degree in engineering from George Washington University, Washington, D. C., in 1950, with major study in physics and electrical engineering. He also attended the Graduate School of the National Bureau of Standards and the University of Colorado in Boulder.

From 1942 to 1946 he was associated with the Ballistic Research Laboratory of the Aberdeen Proving Ground, Aberdeen, Md., and was primarily concerned with the computational and engineering details of exterior ballistics. From 1944 to 1946 he was on military leave on active duty in the U. S. Navy, during which time he attended the Radio Materiel School of the Naval Research Laboratory in Washington, D. C.

In 1946 he was employed by the National Bureau of Standards, first in Washington, D. C., and later at Boulder, Colo., as physicist, radio engineer, electronic engineer, and supervisory electronic scientist in the field of radio wave propagation. He was concerned with instrumentation and measurement of radio noise of natural origin, especially in the VHF band, and radio astronomy and the measurement of cosmic radio noise, having been in large measure responsible for the design and development of certain specialized equipment for the measurement of atmospheric radio noise. Since 1953 he has been primarily concerned with radio navigation systems evaluation, low and very-low frequency radio wave propagation, and sferics. He was responsible from 1953 to 1955 for the theoretical prediction of the performance of certain pulse-type radio navigation systems.

Mr. Johler is now a project leader in the radio navigation systems section of the Central Radio Propagation Laboratory, Radio Propagation Engineering Division, Boulder, Colo., and is responsible for the solution of various theoretical problems which develop as a result of low and very-low frequency systems evaluation studies.

◆

Alan F. Kay (M'55) was born in Newark, N. J., in 1925. He received the B.S. degree from the Massachusetts Institute of Tech-

nology in 1948, and the Ph.D. degree from Harvard University in 1951, both in mathematics. Since then he has worked on microwave and antenna problems.

In 1957 he was appointed secretary to the corporation of Technical Research Group, where he has been employed for the last five years. He assisted in the founding of the microwave and antenna laboratory at TRG which was recently relocated in

Somerville, Mass.

Dr. Kay is a member of SIAM and AMS.

◆

Irvin W. Kay was born on April 19, 1924, in Savannah, Ga. He received the B.A. degree in 1948, the M.S. degree in 1949, and the Ph.D. degree in 1953, from New York University, New York, N. Y.

He taught mathematics and physics in the Bell Laboratories training program; undergraduate mathematics at New York University, and mathematics in the graduate division of Adelphi College, Garden City, Long Island, N. Y.

Since 1953, Mr. Kay has held the position of research associate at the Electromagnetic Division of the Institute of Mathematical Sciences, New York University, and in addition, in September, 1958, became an assistant professor of mathematics at the University.

◆

Ronald King was born in Williams-town, Mass., in 1905. He received the A.B. degree in 1927, and the S.M. degree in 1929

from the University of Rochester, Rochester, N. Y., where he majored in physics. He was awarded the Ph.D. degree by the University of Wisconsin, Madison, in 1932 after having done graduate work at the University of Munich, Germany, and Cornell University, Ithaca, N. Y.

He served as teaching and research assistant at the University of Wisconsin in



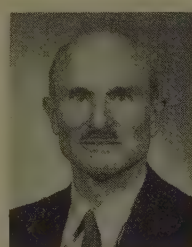
R. E. COLLIN



J. R. JOHLER



I. W. KAY



R. KING

He served as teaching and research assistant at the University of Wisconsin in

A. FERNANDES

associated company of ITT. He became chief engineer in September, 1949, technical director in September, 1954, and managing director in May, 1957.

Mr. Fernandes has published several papers on transmission lines and antennas, and a book on rhombic antenna arrays.



P. FOLDES

1932-1934 and as instructor and assistant professor of physics at Lafayette College, Easton, Pa., in 1934-1937. The year 1937-1938 was spent in Germany as a Guggenheim Fellow. In 1938 he joined the faculty of Harvard University, Cambridge, Mass., where he advanced to the rank of professor in 1946. He is now Gordon McKay Professor of applied physics at Harvard University. In 1958 he studied and traveled abroad as Guggenheim Fellow.

Dr. King is the author of "Electromagnetic Engineering," "Transmission-Line Theory," and "Theory of Linear Antennas." He is coauthor of "Transmission Lines, Antennas, and Wave Guides." His research has been primarily in the field of antennas, transmission lines, and microwave circuits.

He is a Fellow of the American Physical Society and the American Academy of Arts and Sciences, and a member of the American Association of University Professors and the American Association for the Advancement of Science. He is a member of Phi Beta Kappa and Sigma Xi.

Harold Staras (M'50-SM'53) was born in New York, N. Y., on December 24, 1922. He received the B.S. degree in physics from the College of the City of New York in January, 1944, and then joined the staff of the National Advisory Committee for Aeronautics at Langley Field, Va., as a junior physicist. In 1945, he entered active military duty with the Air Corps, his major assignment being that of a counter-intelligence officer in Germany. He returned to full-time graduate study at N.Y.U. in 1947, and obtained the M.S. degree in physics in 1948.

From 1948 to 1954, he was on the staff of the National Bureau of Standards where he was engaged in the study and analysis of the vagaries of tropospheric propagation phenomena. During this time he continued with his graduate studies in physics on a part-time basis, receiving his Ph.D. degree from the University of Maryland in 1955.

In 1954, Dr. Staras joined the Advanced Development Section of RCA, Camden, N. J., where his efforts were directed to the study, analysis, and system design of scatter circuits in many parts of the world. He was also involved in the analysis of tracking radar performance in the presence of scintillating targets and ground clutter. In July, 1956, he transferred to the RCA Research Laboratories in Princeton, N. J., where, in addition to continuing research in propagation phenomena, directed mostly to space communication problems, he is also engaged in information theory considerations of optimum modulation techniques for various applications, e.g., bandwidth compression and minimizing required signal-to-noise ratios.

Dr. Staras is a member of the IRE Wave Propagation Committee, the American Physical Society, Sigma Xi, the U. S. National Committee of URSI Commission II, and Study Group V of the U. S. Preparatory Committee of CCIR. He is also a lecturer in mathematics and physics at LaSalle College, Philadelphia, Pa.



H. STARAS

in Laramie, the Junior College of Northeast Colorado in Sterling, and the Junior College of Southeast Colorado in Lamar.

Since 1953, Mrs. Walters has been employed as mathematician at the National Bureau of Standards, Central Radio Propagation Laboratories, Boulder, Colo.



A. D. Wheelon (M'56-SM'58) was born in Moline, Ill., on January 18, 1929. He received the B.S. degree in engineering science from Stanford University, Stanford, Calif., in 1949. Until 1952, when he received the Ph.D. degree in physics, he was a teaching fellow in the Physics Department of M.I.T., Cambridge, Mass., as well as a research assistant in the Research Laboratory of Electronics.



A. D. WHEELON

He is now a senior member of the technical staff of Space Technology Laboratories Inc., where he is manager of the applied physics department. He is working on ballistic missiles, space vehicles, and radiowave propagation. His research has been directed to tropospheric and ionospheric scatter propagation and the associated problems of turbulence theory, line-of-sight phase and amplitude instabilities, applied mathematics, and orbital analysis for earth satellites.

Dr. Wheelon is a consultant to the director of the National Bureau of Standards Boulder Laboratories, and a lecturer in the Engineering Department of the University of California at Los Angeles.

He is a member of the American Physical Society, URSI Commission II, and Sigma Xi.



James Y. Wong (S'46-A'53-M'56-SM'58) was born in Elm Creek, Manitoba, Can., on November 21, 1926. He received the B.S. degree in electrical engineering from the University of Manitoba in 1948 and the M.S. and Ph.D. degrees in electrical engineering from the University of Illinois, Urbana, in 1949 and 1952, respectively.



J. Y. WONG

From 1950 to 1952

Dr. Wong was a research assistant in the University of Illinois Antenna Laboratory, where he was engaged in aircraft antenna research. Since 1952 he has been a research scientist in the Antenna Group of the Microwave Section, National Research Council, Ottawa, Can.

Dr. Wong is a member of Eta Kappa Nu, and Sigma Xi.



L. C. WALTERS

Hans J. Schmitt (A'58) was born in Dortmund, Germany, on August 3, 1930. He received the degree of Dipl. Phys. from the University of Goettingen, Germany, in 1954. This was followed by research work in microwave techniques, for which he received the Dr.rer.nat. degree in 1955. After one year as research assistant at the University of Goettingen, where he carried out research in dielectric materials, he became associated with Harvard University, Cambridge, Mass., as research fellow, working on scattering problems and antenna theory.

H. J. SCHMITT

Dr. Schmitt is a member of Sigma Xi.



Lillie C. Walters (SM'57) was born November 18, 1911, in Butte, Mont. She received the B.A. and M.A. degrees in mathematics in 1933 and 1948, respectively, from the University of Colorado, Boulder, Colo. She was an instructor in applied mathematics at the University of Colorado from 1945 to 1953. Prior to this she taught mathematics at the University of Wyoming

For Information Concerning ADVERTISING RATES

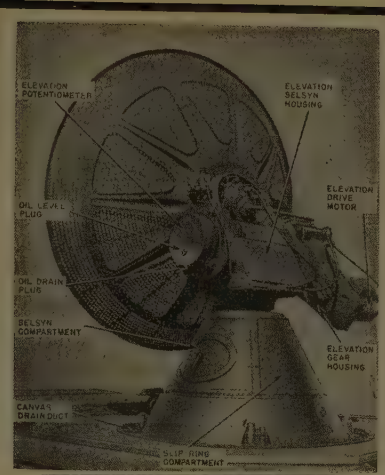
Contact

MR. DELMER C. PORTS
Jansky and Bailey, Inc.
1339 Wisconsin Ave., N.W.

Washington 7, D. C.

Telephone:

Federal 3-4800



ANTENNA PEDESTAL SCR 584—MP 61B

Full azimuth and elevation sweeps. 360 degrees in azimuth, 210 degrees in elevation. Accurate to 1 mil. over system. Complete for full tracking response. Includes pedestal drives, selsyns, potentiometers, drive motors, control amplifiers. Excellent used condition. This is the first time these pedestals have been available for purchase. Limited quantity in stock for immediate shipment. Ideal for antenna pattern ranges, radar systems, radio astronomy, any project requiring accurate response in elevation and azimuth.

Complete description in McGraw-Hill Radiation Laboratory Series, Volume 1, page 284 and page 209, and Volume 26, page 233.

We have a complete, as new, SCR-584 Radar System in stock for immediate delivery. Call us for details. P. J. Plishner

RADIO RESEARCH
INSTRUMENT CO.

550
FIFTH AVE.
NEW YORK
JUDSON
6-4691

AVAILABLE BACK ISSUES OF IRE TRANSACTIONS ON ANTENNAS AND PROPAGATION

Publication	Prices		
	Group Members	IRE Members	Non- Members*
AP-1, No. 1, July, 1953	\$1.20	\$1.80	\$3.60
AP-1, No. 2, October, 1953	\$1.20	\$1.80	\$3.60
AP-2, No. 1, January, 1954	\$1.35	\$2.00	\$4.05
AP-2, No. 2, April, 1954	\$2.00	\$3.00	\$6.00
AP-2, No. 3, July, 1954	\$1.50	\$2.25	\$4.50
AP-3, No. 4, October, 1954	\$1.50	\$2.25	\$4.50
AP-3, No. 1, January, 1955	\$1.60	\$2.40	\$4.80
AP-3, No. 2, April, 1955	\$1.60	\$2.40	\$4.80
AP-4, No. 4, October, 1956	\$2.10	\$3.15	\$6.30
AP-5, No. 1, January, 1957	\$3.20	\$4.80	\$9.60
AP-5, No. 2, April, 1957	\$1.75	\$2.60	\$5.25
AP-5, No. 3, July, 1957	\$2.00	\$3.00	\$6.00
AP-5, No. 4, October, 1957	\$1.70	\$2.25	\$5.10
AP-6, No. 1, January, 1958	\$3.85	\$5.80	\$11.55
AP-6, No. 2, April, 1958	\$1.15	\$1.75	\$3.45
AP-6, No. 3, July, 1958	\$2.40	\$3.60	\$7.20
AP-6, No. 4, October, 1958	\$1.50	\$2.25	\$4.50

* Colleges, Universities, Subscription Agencies, and all Libraries, may purchase at IRE Member rate.

microwave engineers

- The Hughes Research and Development Laboratories are engaged in basic and applied research and development programs in a wide variety of fields, including antennas, radomes, microwave and storage tubes, masers, ferrite devices, microwave circuitry, instrumentation, and other fields.

One of the several interesting problems is the design of feedback loops for locking the local oscillator klystron to an available reference signal. The requirements—good stability and low noise in a very trying environment.

Your inquiry is invited.
Please write Mr. John Bailey.

the West's leader in advanced electronics

HUGHES

RESEARCH & DEVELOPMENT

LABORATORIES

Hughes Aircraft Co., Culver City, Calif.

INSTITUTIONAL LISTINGS

The IRE Professional Group on Antennas and Propagation is grateful for the assistance given by the firms listed below, and invites application for Institutional Listing from other firms interested in the field of Antennas and Propagation.

ANDREW CORPORATION, 363 E. 75th St., Chicago 19, Ill.
Antennas, Antenna Systems, Transmission Lines, Development and Production.

ANTLAB, INC., 6330 Proprietors Rd., Worthington, Ohio
Antenna Pattern Range Systems—Recorders & Mounts.

BLAINE ELECTRONETICS, INC., 14757 Keswick St., Van Nuys, Calif.
Antennas, Paraboloids, Scale Models, Antenna Radiation Pattern Measurement Towers.

COMMUNICATION PRODUCTS COMPANY, INC., Marlboro, N. J.
Fixed Station and Vehicular Antennas and Associated Cable Systems

DEVELOPMENTAL ENGINEERING CORP., 1001 Conn. Ave. N.W., Washington, D. C. and Leesburg, Va.
Research, Development, Installation of Antennas and Antenna Equipment for Super Power Stations.

DORNE AND MARGOLIN, INC., 29 New York Ave., Westbury, L. I., N. Y.
Research, Development, and Manufacture of Airborne Antennas and Systems

THE GABRIEL LABORATORIES, Div. of the Gabriel Co., 135 Crescent Road, Needham Heights 94, Mass.
Research and Development of Antenna Equipment for Government and Industry.

HUGHES AIRCRAFT COMPANY, Culver City, Calif.
Research, Development, Mfr.: Radar, Missiles, Antennas, Radomes, Tubes, Solid State Physics, Computers.

I-T-E CIRCUIT BREAKER CO., Special Products Div., 601 E. Erie Ave., Philadelphia 34, Pa.
Design, Development and Manufacture of Antennas, and Related Equipment.

JANSKY & BAILEY, INC., 1339 Wisconsin Ave. N.W., Washington 7, D. C.
Radio & Electronic Engineering; Antenna Research & Propagation Measurements; Systems Design & Evaluation.

MARK PRODUCTS CO., 6412 W. Lincoln Ave., Morton Grove, Ill.
Multi Element Grid Parabolas, Antennas for Two-Way Communications, R & D.

THE RAMO-WOOLDRIDGE CORPORATION, Los Angeles 45, Calif.

TRANSCO PRODUCTS, INC., 12210 Nebraska Ave., Los Angeles 25, Calif.
Res., Design, Dev., & Mfr. of Antenna Systems & Components for Missile, Aircraft & Ground Installations.

WHEELER LABORATORIES, INC., 122 Cutter Mill Road, Great Neck, N. Y.
Consulting Services, Research and Development, Microwave Antennas and Waveguide Components.

WIND TURBINE COMPANY, West Chester, Pa.
Complete Antenna Systems and Towers

The charge for an Institutional Listing is \$25.00 per issue or \$75.00 for four consecutive issues. Application may be made to the Technical Secretary, The Institute of Radio Engineers, 1 East 79th Street, New York 21, N.Y.